

Middlesex University Research Repository

An open access repository of

Middlesex University research

<http://eprints.mdx.ac.uk>

Alpendurada, Francisco Diogo (2013) Cardiovascular magnetic resonance of the right ventricle.
PhD thesis, Middlesex University. [Thesis]

Final accepted version (with author's formatting)

This version is available at: <https://eprints.mdx.ac.uk/12211/>

Copyright:

Middlesex University Research Repository makes the University's research available electronically.

Copyright and moral rights to this work are retained by the author and/or other copyright owners unless otherwise stated. The work is supplied on the understanding that any use for commercial gain is strictly forbidden. A copy may be downloaded for personal, non-commercial, research or study without prior permission and without charge.

Works, including theses and research projects, may not be reproduced in any format or medium, or extensive quotations taken from them, or their content changed in any way, without first obtaining permission in writing from the copyright holder(s). They may not be sold or exploited commercially in any format or medium without the prior written permission of the copyright holder(s).

Full bibliographic details must be given when referring to, or quoting from full items including the author's name, the title of the work, publication details where relevant (place, publisher, date), pagination, and for theses or dissertations the awarding institution, the degree type awarded, and the date of the award.

If you believe that any material held in the repository infringes copyright law, please contact the Repository Team at Middlesex University via the following email address:

eprints@mdx.ac.uk

The item will be removed from the repository while any claim is being investigated.

See also repository copyright: re-use policy: <http://eprints.mdx.ac.uk/policies.html#copy>

Middlesex University Research Repository:

an open access repository of
Middlesex University research

<http://eprints.mdx.ac.uk>

Alpendurada, Francisco Diogo, 2013. Cardiovascular magnetic resonance of the right ventricle. Available from Middlesex University's Research Repository.

Copyright:

Middlesex University Research Repository makes the University's research available electronically.

Copyright and moral rights to this thesis/research project are retained by the author and/or other copyright owners. The work is supplied on the understanding that any use for commercial gain is strictly forbidden. A copy may be downloaded for personal, non-commercial, research or study without prior permission and without charge. Any use of the thesis/research project for private study or research must be properly acknowledged with reference to the work's full bibliographic details.

This thesis/research project may not be reproduced in any format or medium, or extensive quotations taken from it, or its content changed in any way, without first obtaining permission in writing from the copyright holder(s).

If you believe that any material held in the repository infringes copyright law, please contact the Repository Team at Middlesex University via the following email address:

eprints@mdx.ac.uk

The item will be removed from the repository while any claim is being investigated.

CARDIOVASCULAR MAGNETIC RESONANCE OF THE RIGHT VENTRICLE

FRANCISCO DIOGO ALPENDURADA

MIDDLESEX UNIVERSITY

ROYAL BROMPTON HOSPITAL

PHD THESIS

SEPTEMBER 2013

ABSTRACT

Introduction: Whilst most of the attention has been devoted to the left ventricle in cardiovascular disease, the right ventricle has been somewhat neglected. In the last decades, there has been a renewal of interest in the right ventricle, in part driven by advances in cardiovascular imaging.

Methods: Cardiovascular magnetic resonance is arguably the best imaging modality for the study of the right ventricle. In this research thesis, cardiovascular magnetic resonance was used as the primary research tool to assess the right ventricle in different conditions and settings.

Results: This thesis encompasses five studies that have been published as peer-reviewed articles. The results of these studies were the following: 1) Right ventricular dilatation and dysfunction was found in a group of patients with Marfan syndrome, further supporting the existence of a Marfan-related cardiomyopathy; 2) In thalassaemia major, right ventricular volumes and ejection fraction differed from healthy controls, and new reference ranges based on patients without iron overload were derived; 3) Myocardial iron loading in thalassaemia major was associated with progressive right ventricular dysfunction; 4) Right ventricular dysfunction due to myocardial siderosis was reversible with effective iron chelation therapy, and; 5) In advanced heart failure, right ventricular function was a predictor of response and outcomes in patients undergoing cardiac resynchronization therapy.

Conclusion: The right ventricle is an essential component of the circulatory system, and should be more widely evaluated in patients with cardiopulmonary disease.

TABLE OF CONTENTS

CHAPTER 1	SUMMARY AND OBJECTIVES	1
------------------	-------------------------------	----------

INTRODUCTION

CHAPTER 2	THE RIGHT VENTRICLE	4
2.1	HISTORICAL BACKGROUND	4
2.2	ANATOMY	7
2.2.1	Location	7
2.2.2	Structure	8
2.2.3	Myofibre architecture	10
2.2.4	Distinctive anatomical features	11
2.3	PHYSIOLOGY	12
2.3.1	Embriology	12
2.3.2	Mechanics	14
2.3.3	Haemodynamics	14
2.3.4	Cardiodynamics	15
2.3.5	Ventricular interdependence	16
2.3.6	Perfusion	17
2.4	PATHOPHYSIOLOGY	17
2.4.1	Pressure overload	18
2.4.2	Volume overload	19
2.4.3	Ischaemia and infarction	20
2.4.4	Cardiomyopathies	20
2.4.5	Regulation of right ventricular function	21
2.4.6	Consequences of right ventricular failure	22
2.4.7	Arrhythmias and sudden death	23
2.5	IMAGING OF THE RIGHT VENTRICLE	23
2.5.1	Contrast angiography	24
2.5.2	Echocardiography	26
2.5.3	Nuclear imaging	29
2.5.4	Computed tomography	32
2.5.5	Magnetic resonance	34
2.5.6	Multimodality imaging	36

CHAPTER 3	CARDIOVASCULAR MAGNETIC RESONANCE (CMR)	39
3.1	PRINCIPLES OF MAGNETIC RESONANCE IMAGING	39
3.1.1	Magnetic resonance system components	39
3.1.2	Origin of magnetic resonance signals	41
3.1.3	T1, T2 and T2* relaxation	43
3.1.4	Magnetic resonance echoes	45
3.1.5	Image creation	46
3.1.6	Image formation	49
3.1.7	Image contrast	50
3.2	BASIC PULSE SEQUENCES	52
3.2.1	Spin echo sequences	52
3.2.2	Gradient echo sequences	53
3.3	CARDIOVASCULAR MAGNETIC RESONANCE	56
3.3.1	Synchronising with the cardiac cycle	56
3.3.2	Dealing with respiratory motion	57
3.3.3	Fast imaging techniques	57
3.3.4	Fast spin echo	59
3.3.5	Cine imaging	59
3.3.6	Perfusion imaging	61
3.3.7	Angiography	62
3.4	CLINICAL APPLICATIONS OF CMR	64
3.4.1	Volumes and function	64
3.4.2	Coronary artery disease	65
3.4.3	Cardiomyopathies	68
3.4.4	Valvular heart disease	72
3.4.5	Pericardial disease	73
3.4.6	Congenital heart disease	73
3.4.7	Cardiac masses	74
3.4.8	Great vessels	74
3.4.9	Pulmonary hypertension	76
3.4.10	Limitations	77
3.4.11	Conclusions	77

METHODS

CHAPTER 4	METHODS	79
------------------	----------------	-----------

4.1	RIGHT VENTRICULAR VOLUMES	80
4.2	FLOW MEASUREMENTS	87
4.3	T2* GRADIENT ECHO	91
4.4	LATE GADOLINIUM ENHANCEMENT	95

RESULTS

CHAPTER 5	EVIDENCE FOR MARFAN CARDIOMYOPATHY	100
5.1	ABSTRACT	100
5.2	INTRODUCTION	101
5.3	METHODS	102
5.3.1	Study population	102
5.3.2	Magnetic resonance	103
5.3.3	Ventricular volumes and mass	103
5.3.4	Aortic dimensions	104
5.3.5	Valve disease	105
5.3.6	Other parameters	105
5.3.7	Statistical analysis	106
5.4	RESULTS	106
5.4.1	Study population	106
5.4.2	Left ventricle	106
5.4.3	Right ventricle	109
5.4.4	Aorta	109
5.5.5	Valves	110
5.4.6	Medication	111
5.5	DISCUSSION	111
5.5.1	Left ventricle	112
5.5.2	Right ventricle	113
5.5.3	Aorta	114
5.5.4	Valves	114
5.5.5	Medication	115
5.5.6	Limitations	115

5.6	CONCLUSION	116
CHAPTER 6	RELATION OF MYOCARDIAL T2* TO RIGHT VENTRICULAR FUNCTION IN THALASSAEMIA MAJOR	118
6.1	ABSTRACT	118
6.2	INTRODUCTION	119
6.3	METHODS	120
6.3.1	Study population	120
6.3.2	Magnetic resonance	122
6.3.3	CMR analysis	122
6.3.4	Statistical analysis	123
6.4	RESULTS	125
6.5	DISCUSSION	128
6.5.1	Limitations	131
6.6	CONCLUSION	132
CHAPTER 7	RIGHT VENTRICULAR VOLUMES AND FUNCTION IN THALASSAEMIA MAJOR PATIENTS	134
7.1	ABSTRACT	134
7.2	INTRODUCTION	135
7.3	METHODS	136
7.3.1	Study population	136
7.3.2	Cardiovascular magnetic resonance	137
7.3.3	CMR analysis	137
7.3.4	Haemoglobin measurements	139
7.3.5	Statistical analysis	139
7.4	RESULTS	140
7.4.1	Patient population	140
7.4.2	Right ventricular parameters	141
7.4.3	Correlation with haemoglobin levels	143
7.5	DISCUSSION	144

7.5.1	Limitations	147
7.6	CONCLUSION	147
CHAPTER 8	EFFECTS OF COMBINED DEFERIPRONE WITH DEFEROXAMINE ON RIGHT VENTRICULAR FUNCTION IN THALASSAEMIA MAJOR	149
8.1	ABSTRACT	149
8.2	INTRODUCTION	150
8.3	METHODS	151
8.3.1	Study population	151
8.3.2	Cardiovascular magnetic resonance	152
8.3.3	Echocardiography	153
8.3.4	Biochemistry	154
8.3.5	Statistical analysis	154
8.4	RESULTS	155
8.4.1	RCT trial in mild to moderate cardiac siderosis	155
8.4.2	Longitudinal open-label study in severe cardiac siderosis	158
8.4.3	Entire study cohort	161
8.5	DISCUSSION	162
8.5.1	Limitations	164
8.6	CONCLUSION	165
CHAPTER 9	RIGHT VENTRICULAR DYSFUNCTION IS A PREDICTOR OF NON-RESPONSE AND CLINICAL OUTCOME FOLLOWING CARDIAC RESYNCHRONIZATION THERAPY	166
9.1	ABSTRACT	166
9.2	INTRODUCTION	167
9.3	METHODS	168
9.3.1	Study population	168
9.3.2	Imaging	168
9.3.3	Outcomes	171
9.3.4	Statistical analysis	171
9.4	RESULTS	172

9.4.1	Patients	172
9.4.2	Left ventricle	173
9.4.3	Right ventricle	174
9.4.4	Myocardial fibrosis	175
9.4.5	Follow-up	177
9.4.6	Response to therapy	177
9.5	DISCUSSION	180
9.5.1	Previous work	181
9.5.2	Tricuspid annular plane systolic excursion	182
9.5.3	Pulmonary hypertension	183
9.5.4	Myocardial fibrosis	183
9.5.5	Atrial fibrillation	184
9.5.6	Response	185
9.5.7	Limitations	186
9.6	CONCLUSION	186

DISCUSSION

CHAPTER 10	DISCUSSION	188
10.1	MARFAN SYNDROME	189
10.1.1	Overview	189
10.1.2	Present work	193
10.1.3	Future work	195
10.2	THALASSAEMIA MAJOR	197
10.2.1	Overview	197
10.2.2	Present work	202
10.2.3	Future work	204
10.3	CARDIAC RESYNCHRONIZATION THERAPY	205
10.3.1	Overview	205
10.3.2	Present work	209
10.3.3	Future work	211
10.4	ORIGINAL CONTRIBUTION TO RESEARCH	213
10.4.1	Marfan syndrome	213
10.4.2	Thalassaemia major	214
10.4.3	Cardiac resynchronization therapy	215

CHAPTER 11	CONCLUSION	217
-------------------	-------------------	------------

APPENDIX

CHAPTER 12	APPENDIX	219
12.1	PUBLICATIONS ARISING FROM THIS WORK	219
12.1.1	Peer reviewed research papers	219
12.1.2	Abstracts	220
12.1.3	Invited presentations	223
12.2	PERSONAL CONTRIBUTION TO RESEARCH	223
12.3	CRITICAL DEVELOPMENT REVIEW AS A RESEARCHER	223
12.4	SUPERVISION	224
12.5	LIST OF ABBREVIATIONS	225
12.6	REFERENCES	228

CHAPTER 1: SUMMARY AND OBJECTIVES

Lying at the centre of the human body, the heart is responsible for the continuous movement of blood around the circulatory system, supplying oxygen and nutrients to the body's 75 trillion cells. The heart is considered by many as a remarkable piece of engineering. Weighing approximately 300 grams, it will beat more than 2.5 billion times and will pump nearly 6.5 million litres of blood during an average lifetime. Despite a relatively small power output ranging from 1-5 watts, it does the most physical work of any muscle during a lifetime. Its muscle fibres are organized in such a way that a 15% shortening of individual myocytes will translate into the ejection of 70% of the total blood content. It can also increase its output up to 5 times if necessary to respond to the body needs.

The human heart is comprised of 4 chambers, the left and right atria, and the left and right ventricles. Blood enters the heart through the atria and is pumped out by the ventricles. During ontogenesis, the heart has been divided into left and right sides to accommodate 2 parallel circulations: the left side receives oxygenated blood from the lungs and expels through the aorta to the systemic arteries, whilst the right side receives deoxygenated blood from the systemic veins and expels to the pulmonary vasculature, where the blood is oxygenated by the lungs.

Most of the attention has been devoted to the left side of the heart, particularly the left ventricle. It is usually the largest and heaviest chamber of the heart because it has to pump blood to the entire body against a high vascular resistance in order to keep adequate perfusion to the tissues. As a consequence of the higher haemodynamic stress, it is also more vulnerable to pathology, in particular hypertension, coronary artery and valve disease, the commonest causes of heart disease in the Western world.

For a long time, the right ventricle has been somewhat neglected. As opposed to the left ventricle, it is connected to a smaller and lower resistance pulmonary vascular system. Indeed, early animal experiments suggested that life can be maintained without a functioning right ventricle, which is corroborated in humans by palliative surgeries in congenital heart disease where the systemic venous blood bypasses the right ventricle into the lungs. However, it comes at a cost of increased peripheral venous pressure as well as low cardiac output, either of which can result in morbidity and mortality. Interest in the right ventricle has been revived in the last decades, during which several reports showed the right ventricle to have a major impact in congenital heart disease and pulmonary vascular disease, conditions where the right side of the heart is predominantly affected. Much of this renewal was fostered by the development of cardiac imaging, which enables direct visualization of the beating heart. Of all the available imaging modalities, cardiovascular magnetic resonance is arguably the ideal technique to assess the right ventricle. This technique provides excellent image quality at a good temporal resolution, and is currently considered the reference for assessing cardiac morphology and function. In addition, by exploring different tissue properties, it allows in vivo characterization of the myocardium as validated by histology without the need for invasive biopsy procedures. Magnetic resonance is also safe to humans as it does not involve ionizing radiation. For these reasons, cardiovascular magnetic resonance (CMR) is considered the imaging modality of choice to assess the right ventricle, representing a unique research opportunity for this rather overlooked structure.

By using CMR as the primary research modality, the aim of this thesis was to investigate the role of the right ventricle in the physiology, physiopathology, diagnosis and prognosis of different conditions and in different settings. The core of the thesis relates to works that have already been published by peer-reviewed journals. **Chapter 5** examines the existence of a primary cardiomyopathy associated with Marfan syndrome, a connective tissue disease where

the cardiovascular system is frequently involved. The following chapters describe the right ventricle in thalassaemia major, an inherited haemoglobin disorder requiring lifelong blood transfusions that results in excessive iron accumulation with direct toxicity to the heart. **Chapter 6** addresses right ventricular function according to the relative iron concentrations, while **Chapter 7** documents the normal expected ranges for right ventricular measurements in patients with thalassaemia major, and **Chapter 8** evaluates the response of right ventricular function to different chelation therapies. Finally, **Chapter 9** looks at the prognostic value of the right ventricle in patients with heart failure undergoing cardiac resynchronization therapy. A diagram with the structure of the public works can be appreciated below (figure 1.1).

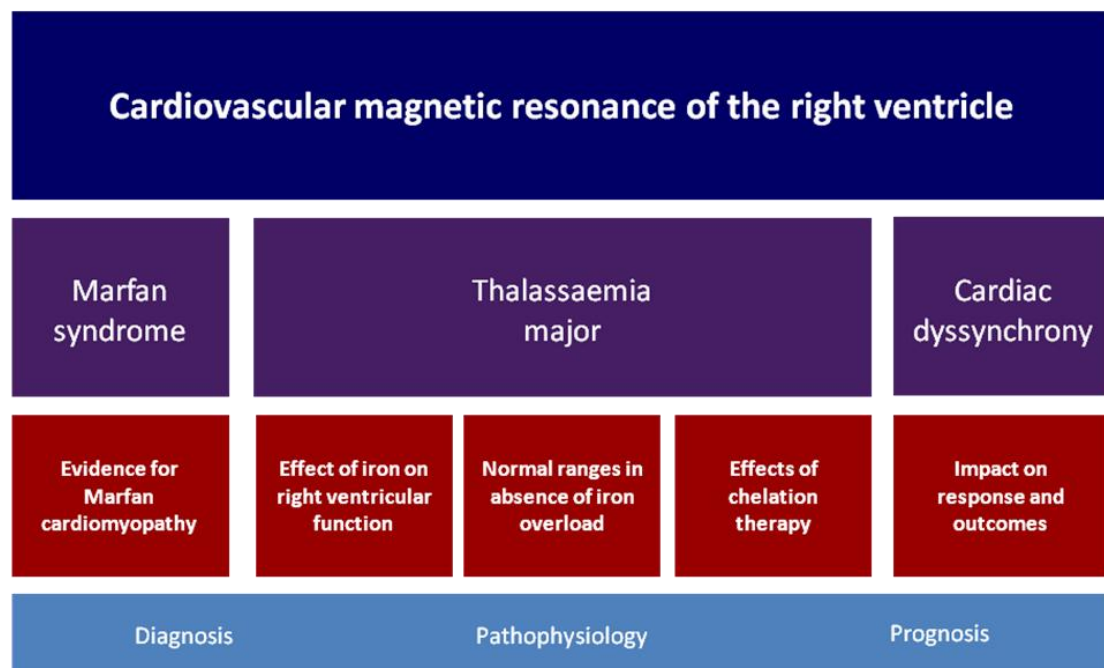


Figure 1.1. Thesis organisation. The diagram is an overview of the thesis, with pathologies displayed in purple, and works displayed in red.

CHAPTER 2: THE RIGHT VENTRICLE

2.1. HISTORICAL BACKGROUND

The brilliant proof by William Harvey (1578-1657) of the continuous circulation of blood within a contained system was the 17th century's most significant achievement in physiology and medicine [Lyons 1997]. It was Harvey who worked out most of the problems and is responsible for the present understanding of the blood's circulation (figure 2.1). Through an experimental approach, he defied previous conceptions established since the Classical era, and faced many criticisms so that his seminal work, "De Motu Cordis", took 12 years to be published. Contrary to the conventional knowledge until then, he demonstrated that the heart acts as a pump, and by observing the valves in the right ventricle, he concluded that blood could only flow in one direction. Harvey later demonstrated that there is no communication between the right and the left ventricle as previously defended by the Galenic school (figure 2.2). Supported by quantitative data on the daily cardiac output, it became obvious to him that the blood had to circulate in a closed system. What Harvey couldn't prove was how the blood flows from the pulmonary arteries to the veins, where he assumed the existence of porosities. It was later that Marcelo Malpighi (1628-94), with the development of the microscope, who discovered the capillary vessels; and Antonie van Leeuwenhoek (1632-1732), by observing blood flow therein, who established the basis of the pulmonary circulation [Snellen 1984, Lyons 1997].

The history of the heart and circulation evolved from anatomy to physiology (*anatomia animata* as coined by Harvey) in the 17th century, and then to pathology in the 18th and 19th centuries [Snellen 1984]. By then, the study of the heart was often confounded with the study of the left ventricle (LV), the dominant chamber of the heart, and the one most affected by

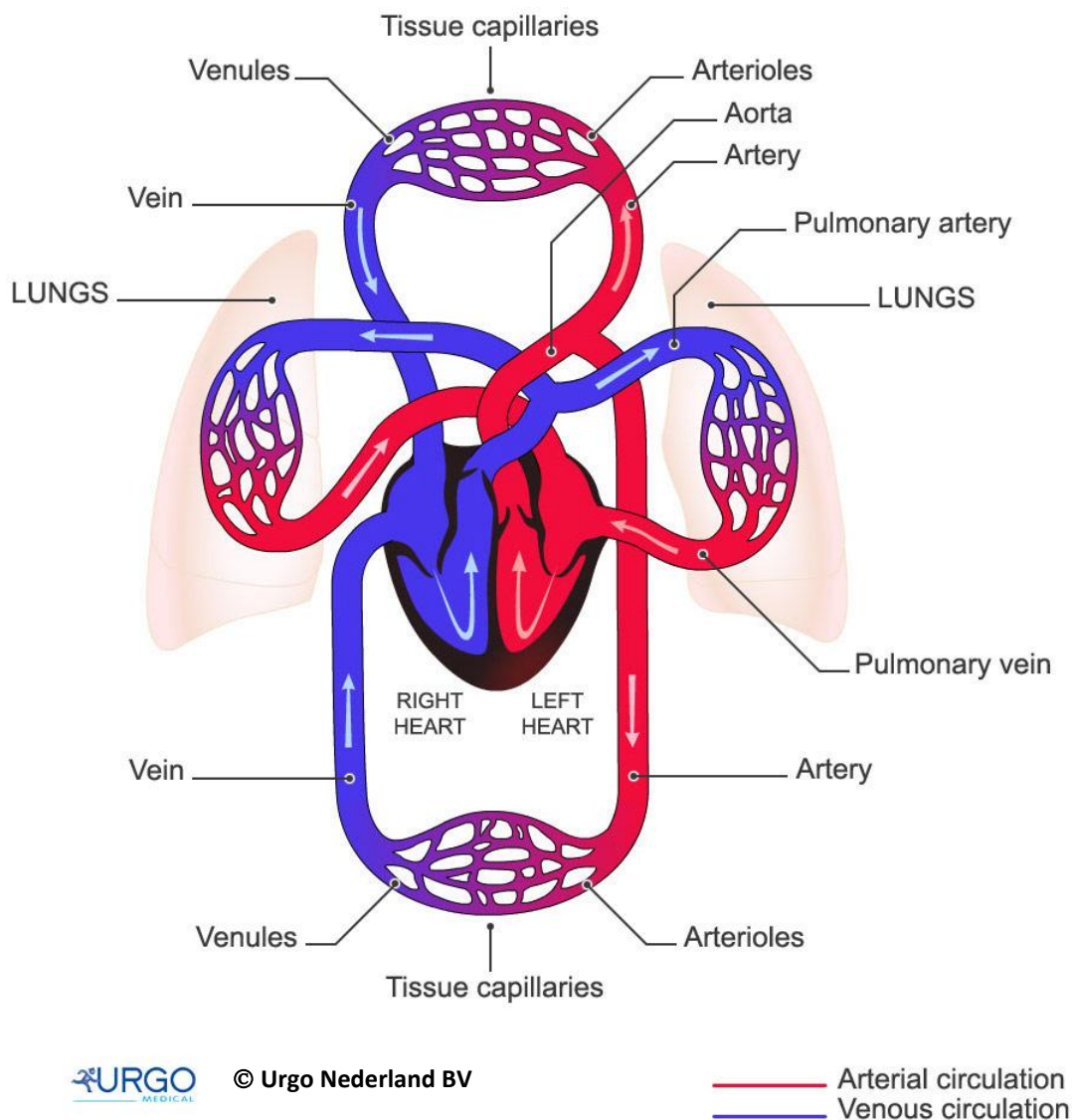


Figure 2.1. Diagram of the circulatory system.

pathology. The development of instruments like the sphygmograph to measure arterial pulse pressures (Marey in the mid 19th century), arterial catheterization to measure LV pressures (Chaveau in the late 19th century), and the electrocardiogram to measure electrical activity (Einthoven in the early 20th century), also contributed to a better understanding of the LV [Snellen 1984]. In the first half of the 20th century, the study of the right ventricle (RV) was limited to a small group of investigators who were intrigued by the hypothesis that human

circulation could function adequately without RV contractile function [Lee 1992, Haddad 2008a]. This perception originated from studies using open-pericardium dog models which showed that cauterization of the RV lateral wall did not result in a reduction of cardiac output or an increase in systemic venous pressure [Starr 1943, Kagan 1952, Haddad 2008b]. Moreover, many surgical procedures for congenital heart disease culminated in a circulation devoid of a subpulmonary ventricle, though it is clear that such circulations are far from normal [Sheehan 2008]. From the early 1950s through the 1970s, cardiac surgeons recognized the importance of the RV as they evaluated procedures to palliate right heart hypoplasia [Haddad 2008a]. In 1982, Goldstein and colleagues reported that RV myocardial infarction (RVMI) in a closed-pericardium dog model would lead to significant haemodynamic compromise [Goldstein 1982]. Since then, the RV has been recognized as a determinant of clinical symptoms, morbidity and mortality in heart failure [Di Salvo 1995, Juillière 1997, de Groote 1998, La Vecchia 1999, Ghio 2001]. The importance of the RV has also been emphasised as a prognosticator in a number of conditions besides heart failure [Sheehan 2008], such as coronary artery disease [Polak 1983, Shah 1986, Mehta 2001, Zornoff 2002], chronic obstructive pulmonary disease [Marti 2006, Almagro 2006], pulmonary hypertension [D'Alonzo 1991, Sitbon 2002], pulmonary embolism [Kreit 2004], and congenital heart disease [Gatzoulis 1995, Graham 2000, Roos-Hesselink 2004].

In 2006, a report from the National Heart, Lung, and Blood Institute (U.S.) recognised that the relevance of the RV in health and disease has historically lagged behind that of the LV [Voelkel 2006]. Given the pivotal importance in a wide spectrum of cardiovascular diseases, this group identified the RV as a high priority for cardiovascular research and for funding by the National Institutes of Health [Voelkel 2006].

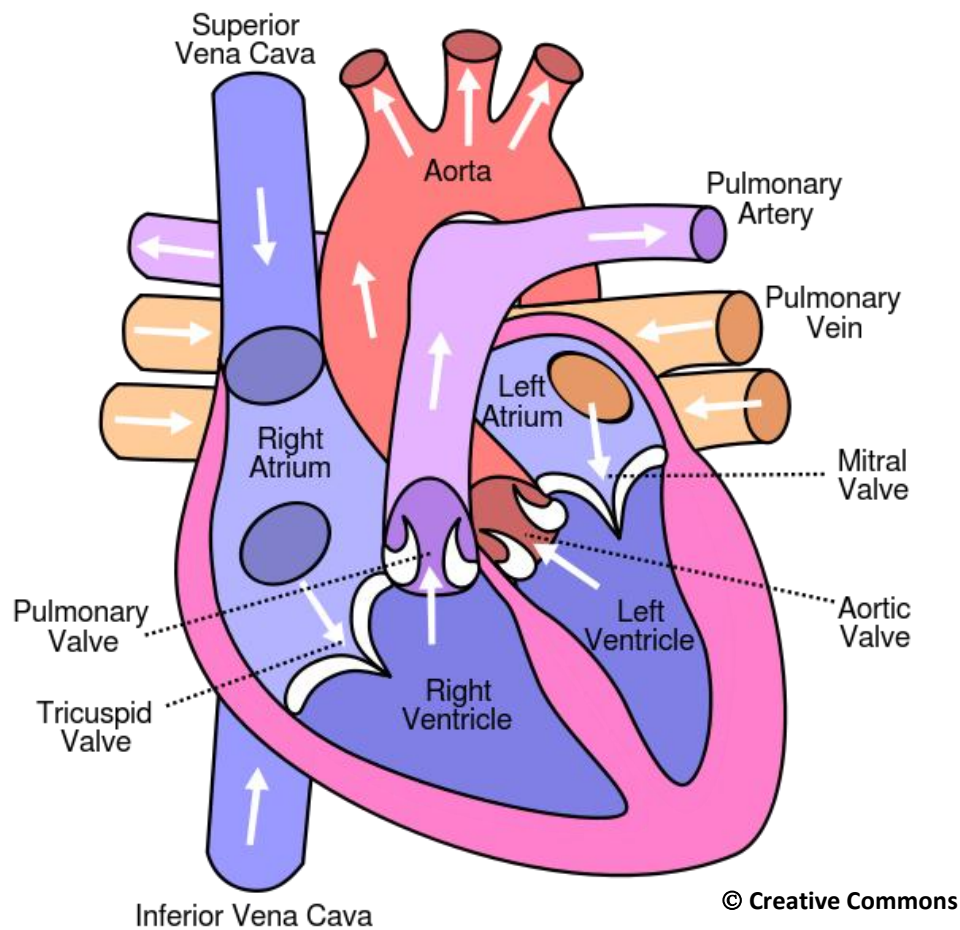


Figure 2.2. Diagram of the heart.

2.2. ANATOMY

2.2.1. Location

The RV is the most anteriorly situated cardiac chamber in the normal heart as it lies immediately behind the sternum [Ho 2006]. Alongside the anterior border, the RV also marks the inferior border of the cardiac silhouette. In contrast to the near conical shape of the LV, the RV is more triangular in shape when viewed from the front (figure 2.3). The pulmonary valve marks the superior margin of the RV while the tricuspid valve marks its right margin (figure 2.3). The apex of the RV is frequently inferior to that of the left. Viewed from the

diaphragmatic aspect of the heart, the right and left ventricles lie side by side (figure 2.3). In cross section the cavity appears like a crescent wrapping around a circular LV. Thus, the curvature of the ventricular septum places the right ventricular outflow tract antero-superiorly to that of the left ventricle's resulting in a characteristic "cross over" relationship between right and left ventricular outflows [Ho 2006].

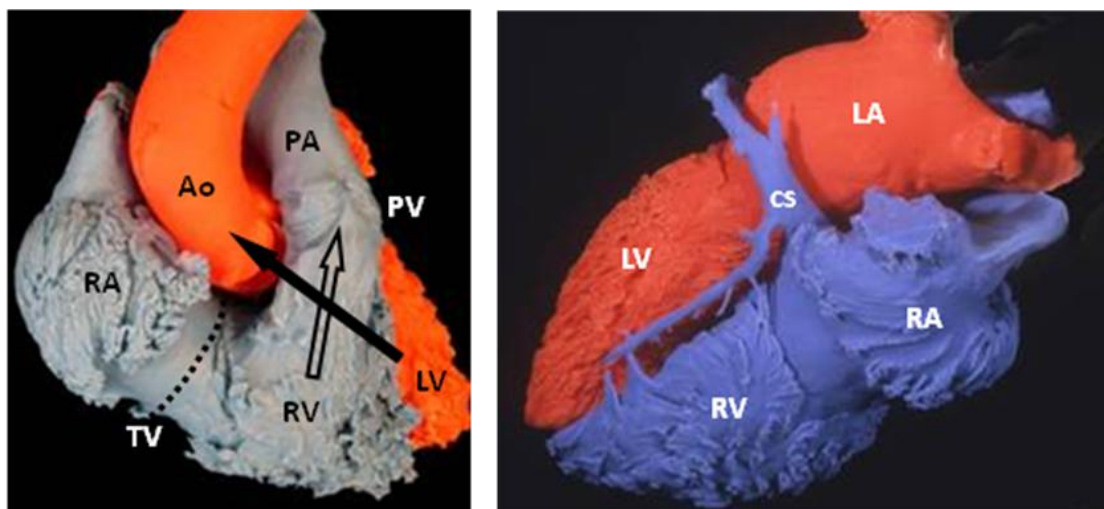


Figure 2.3. Endocast of a normal heart. Left panel, Anterior view. Right panel, Inferior (or diaphragmatic) view. RA- Right atrium; TV- tricuspid valve; RV- Right ventricle; PV- pulmonary valve; PA- Pulmonary artery; Ao- Aorta; LV- Left ventricle. The coronary sinus (CS) drains the coronary venous system into the right atrium. Courtesy of Professor Siew Yen Ho.

2.2.2. Structure

The RV can be described in three components [Goor 1975]: 1) the inlet, or sinus, which contains the tricuspid valve, chordae tendineae, and papillary muscles; 2) the trabeculated apical myocardium, and; 3) the infundibulum, or conus, which corresponds to the smooth myocardial outflow region (figure 2.4) [Haddad 2008a].

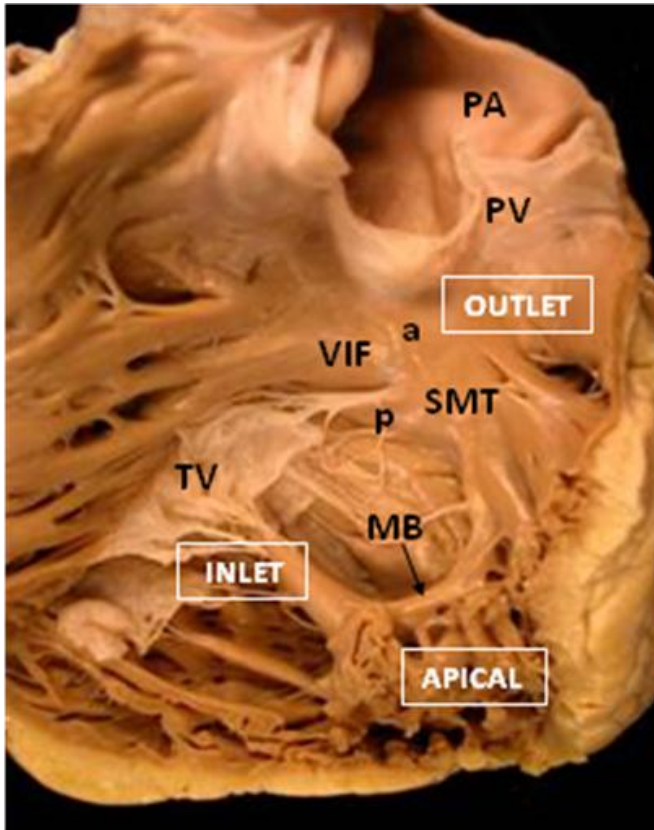


Figure 2.4. Anatomical dissection of the RV, exposing the inlet, apical myocardium, and outlet.

The septal aspect of the RV is displayed to show the septo-marginal trabeculation (SMT) with its anterior (a) and posterior (p) arms embracing the ventriculo-infundibular fold (VIF). The moderator band (MB) crosses the ventricular cavity as a distinct bundle. Other abbreviations as in figure 2.3. Reproduced with permission from Ho 2006.

The pulmonary valve is separated from the tricuspid valve by a muscular fold, the ventriculo-infundibular fold. At its septal margin, the fold forms the supraventricular crest, which divides the inlet from the outlet portion of the RV [Ho 2006]. The fold continues superiorly into the right ventricular outlet. The antero-superior wall of the right ventricle completes the muscular tube known as the subpulmonary infundibulum that leads to the pulmonary valve. The infundibulum lifts the pulmonary valve clear of the ventricular septum (figure 2.4) [Ho 2006].

On the septal aspect of the right ventricle is a characteristic muscle band termed the septomarginal trabeculation (figure 2.4). In some hearts it can be seen clearly as a Y shaped strap that cradles the supraventricular crest between its arms [Ho 2006]. The medial papillary muscle inserts to the posterior arm, whilst the anterior arm blends into the subpulmonary infundibulum [Ho 2006]. The moderator band, another marker for the morphologically right

ventricle, takes off from the body of the Y to cross to the parietal wall carrying within it a fascicle of the right bundle branch of the atrioventricular conduction system (figure 2.4) [Farb 1992, Ho 2006]. The insertion of the medial papillary muscle is the landmark for the more proximal portion of the right bundle branch [Ho 2006].

2.2.3. Myofibre architecture

The muscular fibres of the RV form the parietal (or free) wall and the right side of the interventricular septum. The RV free wall is formed by 2 layers of myofibres: 1) the superficial or subepicardial myofibres are arranged more or less circumferentially in a direction that is parallel to the atrioventricular groove and encircle the subpulmonary infundibulum; 2) the deep myofibres are aligned longitudinally from apex to base (figure 2.5) [Ho 2006]. In the normal heart, the thickness of the RV free wall is in the range of only 3-5 mm, and the RV mass is approximately one-sixth to one-fourth of that of the LV [Foale 1986, Sandstede 2000, Maceira 2006a, Jurcut 2010]. In contrast, the thicker LV wall contains epicardial myofibres arranged in a longitudinal left handed helix, endocardial fibres arranged in a longitudinal right hand helix, and predominantly circular myofibres in between [Ho 2006, Sengupta 2006]. This arrangement contributes to the more complex movement of the LV, which includes torsion, translation, rotation, and thickening [Dell'Italia 1991, Ho 2006]. The continuity between the superficial muscle fibres of the RV and LV functionally binds the ventricles together and represents the anatomical basis of RV wall traction caused by LV contraction. This continuity also contributes, along with the interventricular septum and pericardium, to the interdependence between both ventricles [Dell'Italia 1991, Haddad 2008a].

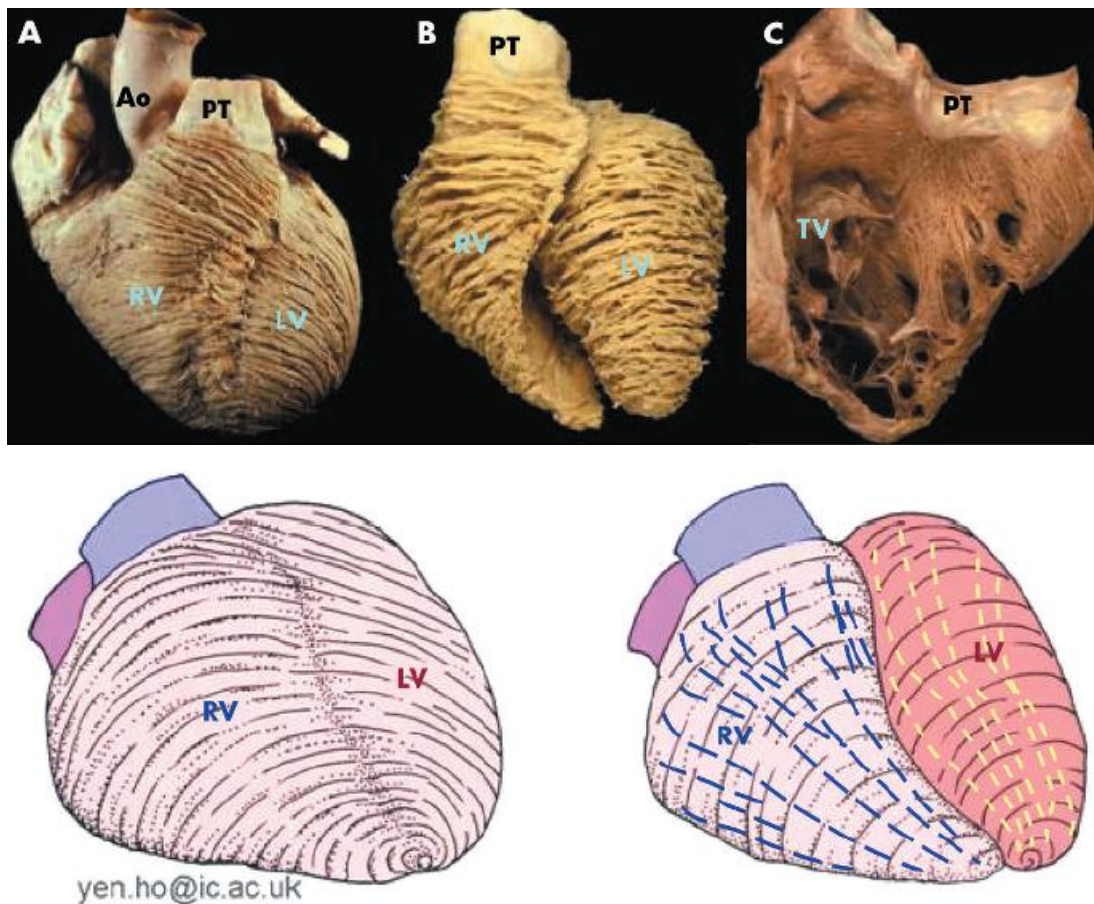


Figure 2.5. Myofibre architecture elicited by sequential dissections. Panel A, Normal heart showing oblique arrangement of the subepicardial fibres. Panel B, Myofibres lying deeper retain the circumferential arrangement in the RV but change from oblique to circumferential in the LV. Panel C, The right ventricle is opened to show the longitudinally arranged subendocardial myofibres. The lower panels depict in simplistic fashion the ventricular subepicardial myofibres (left) and the subendocardial myofibres (right) of the normal heart. Abbreviations as in figure 2.3. Reproduced with permission from Ho 2006.

2.2.4. Distinctive anatomical features

Although the RV is usually located on the right side of the heart and connects with the pulmonary circulation, the anatomical RV is defined by its structure rather than by its position or connections [Haddad 2008a]. The morphological features that best differentiate the

anatomical RV from the LV include the following: 1) the more apical hingeline of the septal leaflet of the tricuspid valve relative to the anterior leaflet of the mitral valve; 2) the trileaflet configuration of the tricuspid valve with papillary muscle attachments to the septum; 3) the presence of a moderator band; 4) the presence of coarse trabeculations around the whole circumference as opposed to the lack of trabeculations on the septal side of the LV, and; 5) a lack of fibrous continuity between its inlet and outflow valves, patent in the form of the ventriculo-infundibular fold (table 2.1) [Haddad 2008a].

2.3. PHYSIOLOGY

2.3.1. Embryology

The RV differs substantially from the LV in its morphology, structure, and physiology (table 2.1). These differences are present from the very early embryological origin of both ventricles [Mertens 2010]. Whilst LV myocardial precursor cells originate from the primary heart field in the anterior plate mesoderm, RV precursor cells originate from the secondary heart field [Zaffran 2004, Rochais 2009]. During foetal life, the lungs are not functional as the oxygen is delivered by the placenta. The RV pumps most of its blood to the systemic circulation via the ductus arteriosus [Rudolph 1970, Hopkins 2002], thus contributing for most of the total cardiac output [Rudolph 2010]. RV and LV free wall thickness and force development are equal throughout foetal life, and the interventricular septum is midline and flat throughout the cardiac cycle [Rudolph 1970, Haddad 2008a]. After birth, the LV becomes the systemic ventricle, whereas the RV becomes the subpulmonary ventricle, supporting the low impedance pulmonary circulation [Mertens 2010]. RV hypertrophy regresses, and the heart remodels to the typical postnatal shape with a crescentic RV and an elliptic LV [Haddad 2008a]. Once this adaptation has occurred, the RV loses its capacity to revert to its foetal

phenotype and is limited in its ability to respond to abnormal hemodynamic loading, especially to increased pressure loading [Bogaard 2009, Mertens 2010]. The different embryological origins of the right and left ventricles may explain the different expression of genes involved in adaptive remodelling [Mertens 2010], as molecular changes in the RV myocardium induced by pressure loading differ from those in the LV myocardium [Mital 2006, Urashima 2008, Kaufman 2008].

Table 2.1. Comparison between the left and right ventricles.

	Left ventricle	Right ventricle
Embryology	Primary heart field	Secondary heart field
Components	Inflow and myocardium, no infundibulum	Inflow, trabeculated myocardium, infundibulum
Anatomical features		
Morphological valve	Bileaflet (mitral) valve	Trileaflet (tricuspid) valve with more apical hingeline
Trabeculations	Septum free of trabeculations	Coarse trabeculations Moderator band
Inlet-outlet valves	Fibrous continuity	Muscular interposition
Myofibre arrangement		
Subepicardium	Oblique	Circumferential
Mesocardium	Circumferential	-
Subendocardium	Oblique	Longitudinal
Volumetry		
EDV, mL/m²	78 ± 9 (60-95)	78±11 (57-99)
ESV, mL/m²	26 ± 5 (16-36)	27±7 (13-41)
EF (%)	67 ± 5 (58-76)	66±6 (54-78)
Mass	69 ± 8 (53-84)	31±6 (19-43)
Haemodynamics		
Pressures, mmHg	130/8 (90–140)/(5–12)	25/4 (15–30)/(1–7)
Elastance (E_{max}), mmHg/mL	5.48 ± 1.23	1.30 ± 0.84
SVR vs. PVR, dyne.s.cm⁵	1100 (700–1600)	70 (20–130)

EDV- end-diastolic volume; ESV- end-systolic volume; EF- ejection fraction; SVR- systemic vascular resistance; PVR- pulmonary vascular resistance.

2.3.2. Mechanics

The primary function of the RV is to pump the systemic venous return into the pulmonary vasculature. The stroke volume of the RV is similar to the LV but at about 25% of the stroke work because of the low resistance of the pulmonary vasculature [Dell'Italia 1991, Voelkel 2006]. Therefore, by virtue of the Laplace relationship, the RV is more thin-walled and compliant. The higher compliance of the RV [Leyton 1971, Gaasch 1975] probably explains why the RV volumes are slightly higher than the LV volumes, and why the RV ejection fraction is slightly lower than the LV ejection fraction, as the stroke volume is roughly the same under normal physiological conditions [Lorenz 1999, Maceira 2006a]. RV contraction is sequential, starting with the contraction of the inlet and trabeculated myocardium and ending with the contraction of the infundibulum (approximately 25 to 50 ms apart) [Dell'Italia 1991, Haddad 2008a]. The RV contracts by 3 separate mechanisms: 1) contraction of the longitudinal fibres, which shortens the long axis and draws the tricuspid annulus towards the apex; 2) inward movement of the free wall, which produces a bellows effect, and; 3) traction on the free wall at the attachment points secondary to LV contraction [Jiang 1994, Haddad 2008a]. As most myocytes lie in the longitudinal orientation in the subendocardial layer, longitudinal shortening is a greater contributor to the stroke volume than radial shortening [Kukulski 2000, Petitjean 2005].

2.3.3. Haemodynamics

Under normal conditions, the RV is coupled to a low impedance pulmonary vascular system. Compared to the systemic circulation, pulmonary circulation has greater arterial distensibility and lower vascular resistance [Dell'Italia 1991, Haddad 2008a]. Hence, RV pressures are significantly lower than LV pressures. RV pressure tracings show an early peaking and a rapidly

declining pressure in contrast to the rounded contour of LV pressure tracing [Dell'Italia 1988a]. RV isovolumic contraction time is shorter because RV systolic pressure rapidly exceeds the low pulmonary artery diastolic pressure. A careful study of hemodynamic tracings and flow dynamics also reveals that end-systolic flow may continue even in the presence of a negative ventricular-arterial pressure gradient [Dell'Italia 1988a]. This interval, which is referred to as the hangout interval, is most likely explained by the momentum of blood in the outflow tract [Dell'Italia 1988a, Haddad 2008a].

2.3.4. Cardiodynamics

RV systolic function is a reflection of preload, contractility, and afterload. RV performance is also influenced by heart rhythm, synchrony of ventricular contraction, and ventricular interdependence [Feneley 1985, Dell'Italia 1990, Goldstein 1990, Santamore 1998]. RV afterload represents the load that the RV has to overcome during ejection. Compared to the LV, the RV demonstrates a heightened sensitivity to afterload changes [MacNee 1994, Chin 2005]. In clinical practice, pulmonary artery systolic pressure and pulmonary vascular resistance (PVR) are the most commonly used indices of afterload. On the other hand, RV preload represents the load present before contraction. Within physiological limits, an increase in myocyte stretching due to an increase in preload improves myocardial contraction on the basis of the Frank-Starling mechanism. But beyond the physiological range, excessive RV volume load can compress the LV and impair the global ventricular function through the mechanism of ventricular interdependence [Chin 2005]. The diastolic filling period is also an important determinant of ventricular preload. RV filling normally starts before and finishes after the filling of the LV. RV isovolumic relaxation time is shorter, and RV filling velocities are lower. The respiratory variations in RV filling velocities are, however, more pronounced [Yu

1996]. Many factors influence RV filling, including heart rate, intravascular volume status, ventricular relaxation, ventricular chamber compliance, passive and active atrial characteristics, LV filling, and pericardial constraint [Burgess 2002, Haddad 2008a].

2.3.5. Ventricular interdependence

The RV is linked to the LV in several ways: by a shared wall (the septum), by mutually encircling epicardial fibres, by attachment of the RV free wall to the anterior and posterior septum, and by sharing the pericardial space [Voelkel 2006]. Consequently, it is impossible to consider abnormalities of the RV in isolation, and vice versa [Haddad 2008a]. Ventricular interdependence refers to the concept that size, shape, and compliance of one ventricle may affect the size, shape, and pressure-volume relationship of the other ventricle through direct mechanical interactions [Santamore 1998]. Ventricular interdependence is mediated mainly through the interventricular septum, but the pericardium may also play a role during diastole [Feneley 1985, Santamore 1998]. Experimental animal studies showed that approximately 20% to 40% of RV systolic pressure and volume outflow results from LV contraction [Damiano 1991, Hoffman 1994, Santamore 1998]. The evidence for ventricular interdependence is well established and based on experimental and clinical studies [Taylor 1967, Santamore 1998]. In acute RV pressure or volume overload states, dilatation of the RV shifts the interventricular septum towards the left, alters LV geometry, and increases pericardial constraint. As a consequence, the decreased distensibility shifts the LV diastolic pressure-volume curve upward, which potentially leads to decreased LV preload and a low cardiac output state [Brookes 1999]. Conversely, LV volume or pressure overload has also been shown to shift upward the RV diastolic pressure-volume relationship and to redistribute RV filling into late diastole [Taylor 1967, Santamore 1998, Haddad 2008a].

2.3.6. Perfusion

The blood supply of the RV varies according to the dominance of the coronary system. In a right-dominant system, which is found in about 80% of the population, the right coronary artery (RCA) supplies most of the RV [McGill HC Jr 1968]. The lateral wall of the RV is supplied by the marginal branches of the RCA. The left anterior descending coronary artery (LAD) supplies the anterior free wall and superior two thirds of the septum, while the posterior descending artery of the RCA supplies the inferior free wall and inferior third of the septum [Voelkel 2006]. The infundibulum derives its supply from the conal artery, which has a separate ostial origin from the RCA in 30% of cases [McGill HC Jr 1968, Farrer-Brown 1968]. Whilst coronary flow to the LV and interventricular septum occurs only in diastole, coronary artery flow to the RV free wall occurs during both systole and diastole [Kinch 1994]. This explains the relative resistance of the RV to irreversible ischemic injury, alongside its lower oxygen consumption [Kusachi 1982], more extensive collateral system from the left coronary arteries [Goldstein 2002], and ability to increase oxygen extraction [Haupt 1983, Haddad 2008a].

2.4. PATHOPHYSIOLOGY

RV failure is a complex clinical syndrome that can result from any structural or functional cardiovascular disorder that impairs the ability of the RV to fill or to eject blood [Haddad 2008b]. The cardinal manifestations of RV failure are: 1) fluid retention, which may lead to peripheral oedema, ascites, and anasarca; 2) decreased systolic reserve or low cardiac output, which may lead to exercise intolerance and fatigue, and; 3) atrial or ventricular arrhythmias. RV dysfunction, on the other hand, refers to abnormalities of filling or contraction without

reference to signs or symptoms of heart failure [Haddad 2008b]. Numerous mechanisms can be responsible for RV dysfunction. These include pressure or volume overload, ischaemia, intrinsic myocardial disease, or pericardial constraint (table 2.2).

Table 2.2. Causes of right ventricular dysfunction.

2.4.1. Pressure overload	2.4.2. Volume overload	2.4.3. Myocardial ischaemia
Pulmonary hypertension	Valve disease	Myocardial infarction
Idiopathic	Tricuspid regurgitation	
Pulmonary embolism	Pulmonary regurgitation	2.4.4. Cardiomyopathies
Lung disease	Congenital heart disease	Uhl's anomaly
Congenital heart disease	Atrial septal defect	ARVC
Tetralogy of Fallot	Anomalous venous return	
Pulmonary stenosis	Ebstein's anomaly	Other causes
Double-chambered RV	Coronary artery fistula	Constrictive pericarditis
Systemic RV		Mechanical ventilation
Left heart failure		Vena cava stenosis

2.4.1. Pressure overload

RV pressure overload can be due to fixed pulmonary valve stenosis or dynamic right ventricular outflow tract obstruction, or even occur in less frequent forms of congenital heart

disease such as transposition of the great arteries [Haddad 2008b]. However, the commonest cause of RV pressure overload is pulmonary hypertension [Simonneau 2009]. An initial adaptive response of myocardial hypertrophy is followed by progressive contractile dysfunction [Dias 2002]. Chamber dilatation ensues to allow compensatory preload and maintain stroke volume despite a reduced ejection fraction. As contractile weakening progresses, decompensated RV failure occurs, characterized by rising filling pressures, diastolic dysfunction, and diminishing cardiac output, which can be further compounded by tricuspid regurgitation due to annular dilatation and poor leaflet coaptation [Louie 1995, Voelkel 2006]. Pressure overload of the RV may also lead to RV ischemia, which may further aggravate ventricular dysfunction [Chin 2005, Haddad 2008b]. In pulmonary hypertension, RV function is the most important determinant of survival, even when accounting for the pulmonary artery pressures [D'Alonzo 1991, Sandoval 1994, Sitbon 2002, McLaughlin 2005, Chin 2005].

2.4.2. Volume overload

In general, the thin-walled RV adapts better to volume overload than to pressure overload. In atrial septal defect and tricuspid regurgitation, the RV may tolerate volume overload for a long time without a significant decrease in RV systolic function [Davlouros 2006]. Even when Eisenmenger's physiology (pulmonary vascular disease caused by a large pre-existing left-to-right shunt) is well established, the outlook for these patients is better than for those with idiopathic pulmonary arterial hypertension [Hopkins 1996], perhaps due to preconditioning or retention of the foetal right heart phenotype mediated by embryonic adaptive mechanisms [Hopkins 2002, Hopkins 2005, Voelkel 2006]. Compared to volume-overload states, histological changes are more pronounced in RV pressure-overload states as demonstrated by

the increased density of myocardial connective tissue both seen in animal and human studies [Marino 1985, Kasimir 2004]. Recent studies, however, have suggested that longstanding volume overload may also lead to an increase in morbidity and mortality [Messika-Zeitoun 2004, Davlouros 2006].

2.4.3. Ischaemia and infarction

RV myocardial infarction (MI) usually occurs after occlusion of the RCA proximal to the major RV branches in the context of an inferior MI [Bowers 2002]. It may also occur in anterior MIs as the anterior part of the RV free wall is supplied by collaterals from the LAD [Kakouros 2010]. RV involvement is present in about 50% of LV inferior infarctions and about 10% of LV anterior infarctions [O'Rourke 2004], and is associated with an increased risk of arrhythmias, heart failure and shock [Pfisterer 1986, Mehta 2001, Chockalingam 2005, Hamon 2008]. Although arrhythmias and haemodynamic compromise associated with acute RV ischaemia lead to early mortality [Zehender 1993], in the longer term most patients improve spontaneously, even in the absence of reperfusion of the infarct related artery [Bowers 1998, Yasuda 1990]. Recovery can be explained by the intrinsic resilience of the RV to infarction [Laster 1993], as demonstrated by the more favourable oxygen and metabolic supply-demand profile [O'Rourke 2004].

2.4.4. Cardiomyopathies

Primary myocardial diseases can be associated with globally or regionally decreased RV performance. Arrhythmogenic RV cardiomyopathy (ARVC) and Uhl's anomaly are the classic examples of cardiomyopathies with predominant RV involvement [Hoch 1992, Lindstrom 2001]. However, most cardiomyopathies present with biventricular or predominant LV

involvement [La Vecchia 1999]. Cardiomyopathies affecting the LV may impact RV function by increased LV filling pressures leading to pulmonary hypertension, or by ventricular interaction with an exaggerated displacement of the septum to the right, impairing both filling and contraction of the RV [Haddad 2008b]. Indeed, LV dysfunction, either ischaemic or non-ischaemic in origin, is one of the commonest causes of pulmonary hypertension and RV dysfunction [Hoeper 2009].

2.4.5. Regulation of right ventricular function

Numerous studies describe the roles of the autonomic and renin-angiotensin-aldosterone systems, endothelin, natriuretic peptides and cytokines in the regulation of RV function [Kiely 1996, Mulder 1997, Nagaya 2000]. Although activation and modulation of these neuro-hormonal and cytokine pathways are important to regulate RV function according to the varying loading conditions and metabolic needs, persistent upregulation can be detrimental in the long term and contribute to RV dysfunction. In the failing RV, excessive sympathetic stimulation may adversely affect ventricular remodelling and survival [Fan 1987, Bolger 2002]. Activation of the renin-angiotensin-aldosterone system may also contribute to fluid retention and ventricular remodelling [Kiely 1996]. Endothelin system activation is an important feature in pulmonary vascular disease and RV dysfunction [Ueno 1999, Channick 2001, Bolger 2002]. In patients with pulmonary hypertension and congenital heart disease, elevated endothelin-1 levels are associated with decreased exercise capacity and impaired ventricular function [Channick 2001, Bolger 2002]. Conversely, pharmacological modulation of the renin-angiotensin-aldosterone and endothelin systems has resulted in improvements in exercise capacity, pulmonary vascular resistance, and reverse ventricular remodelling in pulmonary arterial hypertension [Mulder 1997, Channick 2001, Rouleau 2001]. B-type natriuretic peptide

levels may increase in RV pressure or volume overload states such as pulmonary hypertension, pulmonary embolism, cor pulmonale, and congenital heart disease [Nagaya 2000, Bolger 2002], and are associated with increased mortality in patients with idiopathic pulmonary hypertension [Nagaya 2000].

2.4.6. Consequences of right ventricular failure

Many factors may contribute to the low cardiac output in patients with RV failure, including RV systolic dysfunction, ventricular interdependence, arrhythmias, and suboptimal preload [Haddad 2008b]. The resulting hypotension may further aggravate RV dysfunction by inducing coronary hypoperfusion and RV ischaemia [O'Rourke 2004]. Ventricular interdependence plays an important role in the pathophysiology of RV failure, especially in the acute setting. RV volume or pressure overload causes a leftward shift of the septum, changing LV geometry; RV dysfunction may also increase the constraining effect on the pericardium [Santamore 1998]. These changes contribute to a low cardiac output state by reducing LV distensibility and preload. RV diastolic dysfunction impairs RV filling and increases diastolic RV and right atrial pressures [Haddad 2008b]. RV failure may also cause tricuspid regurgitation, which may beget RV volume overload, decreased cardiac output, and increased right atrial pressures [Voelkel 2006]. These combined effects may lead to fluid retention and congestive hepatopathy, as well as cardiac cirrhosis in more advanced cases. Increased pressures in the right atrium may also lead to right-to-left shunting through a patent foramen ovale and result in hypoxemia [Haddad 2008b]. Protein-losing enteropathy due to extremely elevated systemic venous pressures is occasionally seen after the Fontan procedure, in constrictive pericarditis, in severe tricuspid regurgitation, and RV failure. This condition may result in profound hypoproteinemia, malnutrition, and immunological deficiencies [Feldt 1996, Haddad 2008b].

2.4.7. Arrhythmias and sudden death

Persistent RV dysfunction may lead to atrial tachyarrhythmias due to increased right atrial filling pressures and subsequent neuro-hormonal activation with adverse remodelling. Atrial tachyarrhythmias are common in patients with RV dysfunction, and often lead to hemodynamic instability in severe RV failure [Haddad 2008b]. Many studies have demonstrated that atrial flutter or atrial fibrillation portend a poorer prognosis in patients with RVMI, pulmonary hypertension, and congenital heart disease [Goldstein 1990, O'Rourke 2004, Tongers 2007, Walsh 2007]. Ventricular tachycardia arising from the RV occurs in pulmonary hypertension, congenital heart disease, RVMI, ARVC, and idiopathic RV outflow tract tachycardia [Hoch 1992, Walsh 2007]. Sudden death in patients with RV disease is often caused by arrhythmias (either tachycardia or bradycardia). Other important causes of sudden death include pulmonary embolism and mechanical complications associated with RVMI [Haddad 2008b].

2.5. IMAGING OF THE RIGHT VENTRICLE

The development of imaging has made a huge impact in medicine by enabling in vivo visualization of different organs and systems. Several techniques using different fundamental principles (X-ray, scintigraphy, ultrasound and magnetic resonance) are currently used to aid with the diagnosis and define the management of a wide spectrum of diseases. Cardiac imaging historically took longer to establish because the heart is an organ in perpetual motion, requiring ECG-gating and relatively high temporal resolution to acquire images from the desired phases of the cardiac cycle.

This section approaches the different imaging modalities for the evaluation of the RV. Despite significant improvements in cardiac imaging, assessment of the RV still faces many challenges. These include: 1) the complex geometry of the RV, with a triangular appearance in the sagittal plane and a crescentic shape in the coronal plane; 2) the thin wall of the RV, which makes it difficult to visualize and differentiate from the surrounding structures; 3) the limited definition of the RV endocardial surface caused by the heavily trabeculated myocardium; 4) the retrosternal position of the RV, which limits echocardiographic image acquisition, and; 5) the marked load dependence of indices of RV function [Haddad 2008a, Mertens 2010].

2.5.1. Contrast angiography

The oldest method for assessing the RV is conventional X-ray contrast angiography. By direct injection of a radiopaque contrast agent via right heart catheterization, digital radiographic images can be obtained in one or several projections (figure 2.6) [Greyson 2011]. Contrast angiography provides detail about the RV morphology and function, abnormal shunts, and valve stenosis or incompetence [Greil 2008]. A major limitation is that a two-dimensional (2D) projection of a complex three-dimensional (3D) structure can be difficult to interpret and quantify [Greyson 2011]. Although multiple slice methods and rotational angiography with 3D reconstruction have shown promising results [Sheehan 2004, Orlov 2011], RV angiography has now been superseded by alternative non-invasive methods yielding more accurate and reproducible data on RV volumes and function [Kjaergaard 2006, Greil 2008].

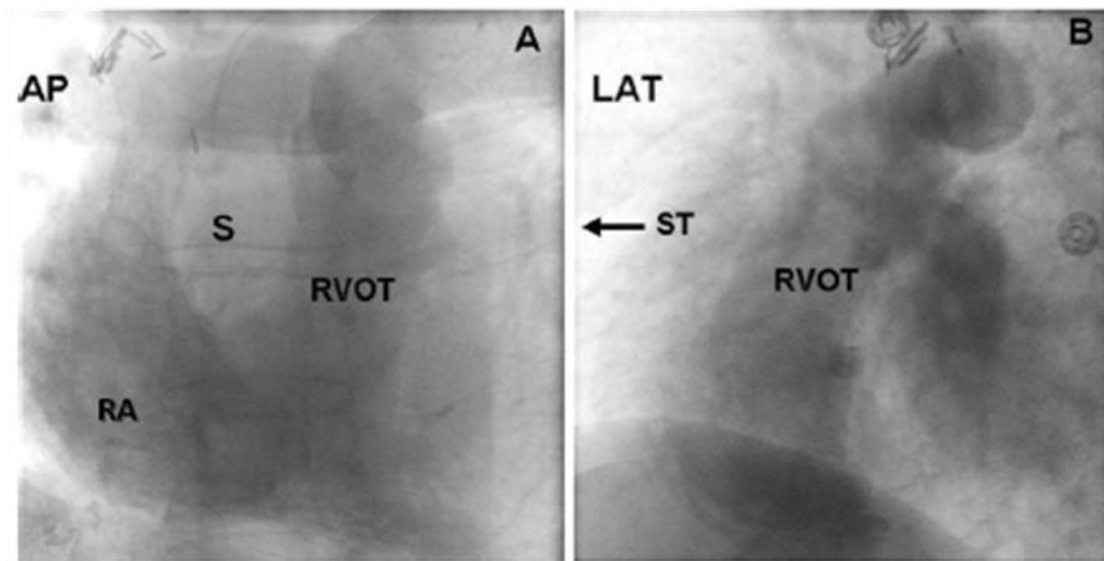


Figure 2.6. Contrast angiogram of the right ventricle. Panel A, Antero-posterior view (AP). Panel B, Lateral view (LAT). RA- right atrium; RVOT- right ventricular outflow tract; S- spine; ST- sternum. Reproduced with permission from Orlov 2011.

The current advantage of right heart catheterization is that haemodynamic data can be obtained at the same time as image data are acquired [Greyson 2011]. Right heart catheterization remains the gold standard for quantifying pulmonary haemodynamics and assessing right heart function through direct measurement of right atrial pressure, cardiac output, and pulmonary artery pressures [Greyson 2011]. Pulmonary vascular resistance and response to vasodilators are critical to identify the aetiology and potential therapies for right heart failure due to pulmonary hypertension [Greyson 2011]. Pressure-volume curve analysis using conductance catheters can quantify various determinants of RV function such as the first derivative of RV pressure (dP/dt), RV elastance, ventricular compliance, and stroke work (figure 2.7) [Haddad 2008a, Bleeker 2006a]. Maximum ventricular elastance is considered by many investigators as the best index of contractility because it appears to be the least load dependent parameter of RV performance [Starling 1987, Dell'Italia 1988b, Vogel 2002]. However, some studies have outlined limitations in the RV time-elastance model, such as

nonlinearity, variability in slope values, and afterload dependency [Kass 1988]. Moreover, when compared with LV conductance studies, RV conductance studies are technically more challenging owing to the difficulty in obtaining reliable ventricular volumes [Haddad 2008a, Champion 2009, Hein 2009]. Because invasive techniques are time consuming and entail some element of risk, the role of conductance catheterization is currently restricted to research, as most clinicians depend on other imaging modalities to assess the RV [Greyson 2011].

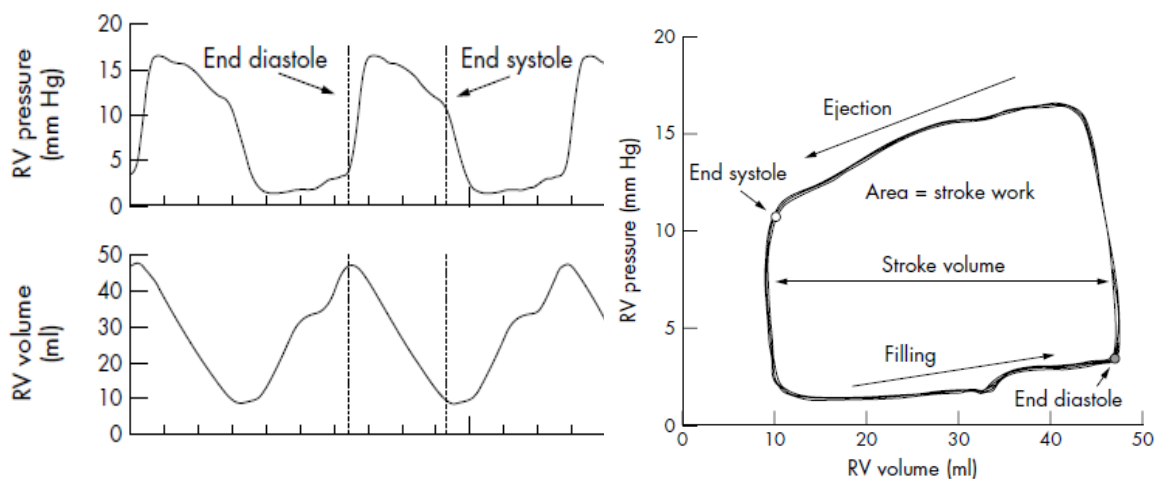


Figure 2.7. Left panel, RV pressure-volume signals obtained by conductance catheter. Right panel, RV pressure-volume curves generated by conductance catheter over successive cardiac cycles. Reproduced with permission from Bleeker 2006a.

2.5.2. Echocardiography

Echocardiography relies on the emission and reflection of ultrasounds (defined as sound pressure waves with frequencies above the human hearing, i.e. >20 kHz). Probes made of pyzoelectrical crystals convert alternate energy currents into ultrasound beams that obey to

the common laws of reflection and refraction as they pass through different media or tissues. Ultrasound waves reflected by the target tissues can then be detected and characterized by the ultrasound probe. The entering energy waves are converted into voltage signals, which in turn are rendered into echocardiographic images [Armstrong 2009]. Echocardiography provides comprehensive information of the heart without any known side effects to man. The technique is non-invasive, relatively inexpensive, portable, and widely available [Selton-Suty 2009]. As a result, echocardiography is currently the primary imaging modality for the morphological and functional assessment of the RV (figure 2.8) [Greil 2008, Horton 2009, Rudski 2010]. Velocities can be determined using the Doppler principle, allowing for quantification of RV diastolic function, valve disease and shunts, and estimation of pulmonary artery, right ventricular and right atrial pressures [Yu 1996, Lee 2007]. However, the technique is hindered by limited views due to the retrosternal position of the RV and lung interference (bone and air are not good conductors of ultrasound). Furthermore, the acoustic window and image quality can be quite variable from patient to patient, and the image acquisition is very operator dependent [Jurcut 2010, Mangion 2010].

Initial echocardiographic markers of RV size and function were based on conventional 2D and Doppler techniques [Miller 2004], and included simple measurements such as RV dimensions, percent fractional area change (%FAC), tricuspid annular plane systolic excursion (TAPSE), and the ejection isovolume index (Tei index). These parameters correlate with reference techniques [Kaul 1984, Tei 1995], and have demonstrated prognostic value [Yeo 1998, Ghio 2010]. However, none of these surrogate markers has achieved the same reference status as RVEF [Mertens 2010], and are of limited interest in pathologies like repaired tetralogy of Fallot or ARVC, where regional function not always corresponds to global function [Morcos 2009].

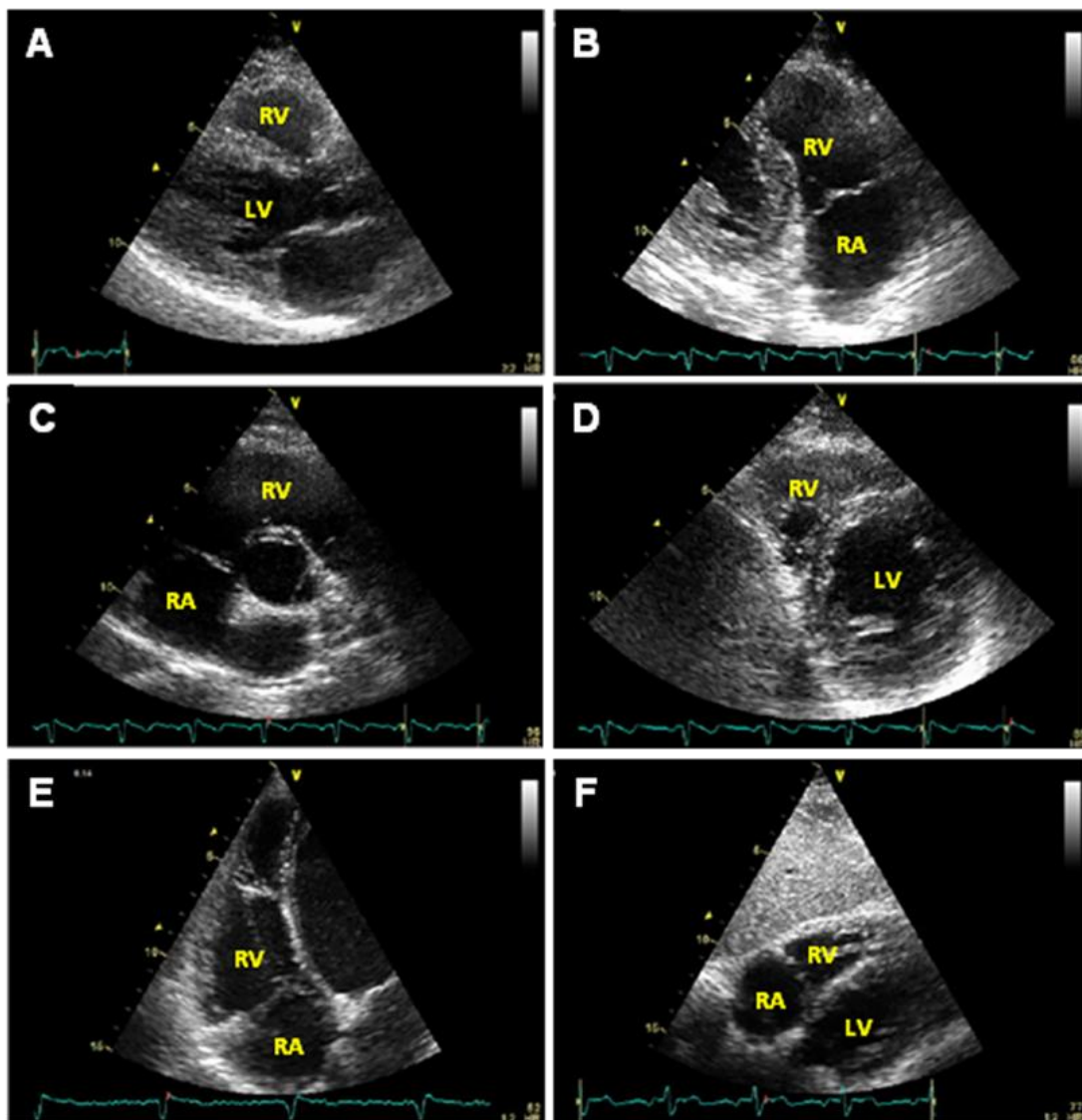


Figure 2.8. Echocardiographic planes of the right ventricle. Panel A, Parasternal LV long-axis. Panel B, Parasternal RV long-axis. Panel C, Short-axis at aortic valve level. Panel D, Short-axis at mid-ventricular level. Panel E, Apical four-chamber of the right ventricle. Panel F, Subcostal four-chamber view. LV- left ventricle; RA- right atrium; RV- right ventricle. Reproduced with permission from Selton-Suty 2009.

Novel markers of RV function employ tissue Doppler to assess local tricuspid plane velocities (tricuspid annular velocity and isovolumic contraction) and regional myocardial deformation [Vogel 2002, Lee 2007]. The latter can be evaluated by strain and speckle tracking [D'Hooge 2000, La Gerche 2010], which appear relatively operator and load independent [Bijnens 2009],

and have already provided with new insights onto RV mechanics [Meris 2010, Yang 2010]. Myocardial strain and strain rate imaging are promising techniques in the assessment of RV function, but solid data on the reliability of these technically challenging approaches are still lacking. Therefore, the potential clinical use of RV Doppler imaging still needs to be defined [Mertens 2010].

More recently, 3D echocardiography has become available owing to the development of rotating ultrasound transducers. Multiple planes can be acquired at the same time and rendered into 3D images. Despite overcoming the 2D limitation on relying in simple geometrical assumptions for the RV [van der Zwaan 2011], 3D echocardiography is still dependent on adequate acoustic windows and appropriate endocardial delineation [Mertens 2010, Greyson 2011]. Comparison studies have shown 20-40% smaller RV volumes by 3D echocardiography and only moderate correlation against CMR [Kjaergaard 2006, Khoo 2009, Leibundgut 2010, van de Zwann 2010]. As volume underestimation occurs in both systole and diastole, RVEF by 3D echocardiography correlates well with CMR [Niemann 2007, Khoo 2009, Leibundgut 2010, van de Zwann 2010, Grapsa 2010], showing only slightly lower values on a recent meta-analysis [Shimada 2010].

2.5.3. Nuclear imaging

Nuclear imaging techniques are based on the signal emitted by radioactive agents. The primary application of nuclear imaging in cardiology is myocardial perfusion, where the role to evaluate myocardial ischaemia and viability is well established [Faber 2010]. An additional application of nuclear imaging is the study of left and right ventricular size and function. As a count-based technique, radionuclide angiography is free of geometric assumptions, making it suitable for evaluating the RV [Ramani 2010]. Changes in radiotracer counts over time are

measured by a gamma camera. The blood volume is proportional to the number of counts recorded per unit of time, which is used for direct volumetric assessment of the cardiac chambers [Ramani 2010]. Using ECG-gating, end-diastolic and end-systolic counts can be used to assess ventricular volumes and derive ejection fraction. Determination of RVEF by nuclear imaging is reliable, reproducible, and shown to have diagnostic and prognostic relevance across many cardiac conditions [Reduto 1978, Johnson 1979, Di Salvo 1995, Kawut 2005, van Wolferen 2007, Rich 2010].

Radionuclide angiography can be completed with either first-pass [Friedman 2006] or equilibrium [Corbett 2006] techniques. First-pass radionuclide angiography (FPRNA) uses dynamic image acquisition immediately following radionuclide bolus injection, and acquires counts from the RV before the isotope transits to the pulmonary circulation [Ramani 2010, Greyson 2011]. FPRNA thus enables short acquisition times (about 30s) without significant overlap with overwhelming structures. However, the first-pass technique is limited by lower count densities [Jain 1992], and the quality of the study is highly dependent on the experience of the operator. These shortcomings can be magnified when significant arrhythmias, RV dysfunction or tricuspid regurgitation are present [Ramani 2010]. The limitations described above contributed to FPRNA's gradual decline in popularity, as only few nuclear laboratories are able to reliably perform this study [Ramani 2010]. In equilibrium radionuclide angiography (ERNA), blood is labelled with a radioisotope to increase its circulatory half-life, and equilibrium images are acquired over a longer period of time, hence increasing the total number of counts acquired [Maddahi 1979, Greyson 2011]. There is a strong correlation between RVEF determined by ERNA and FPRNA [Rezai 1991], though the correlation appears slightly better for FPRNA when compared to CMR [Johnson 1995]. Calculation of RVEF via planar ERNA can be problematic due to overlap of right ventricular with right atrial activity [Ramani 2010], and is currently not recommended for measuring RV function [Corbett 2006].

ERNA has been refined with single photon emission computed tomography (SPECT) to provide 3D spatial information, allowing adjacent structures to be more easily separated (figure 2.9) [Greyson 2011]. Studies comparing the accuracy of SPECT ERNA to validated techniques, including FPRNA and CMR, have however yielded mixed results [Daou 2004, Nichols 2002, Slart 2003, Daou 2007, Sibille 2011]. Although SPECT ERNA appears a promising technique for assessing RVEF, more studies are needed for clinical validation [Ramani 2010].

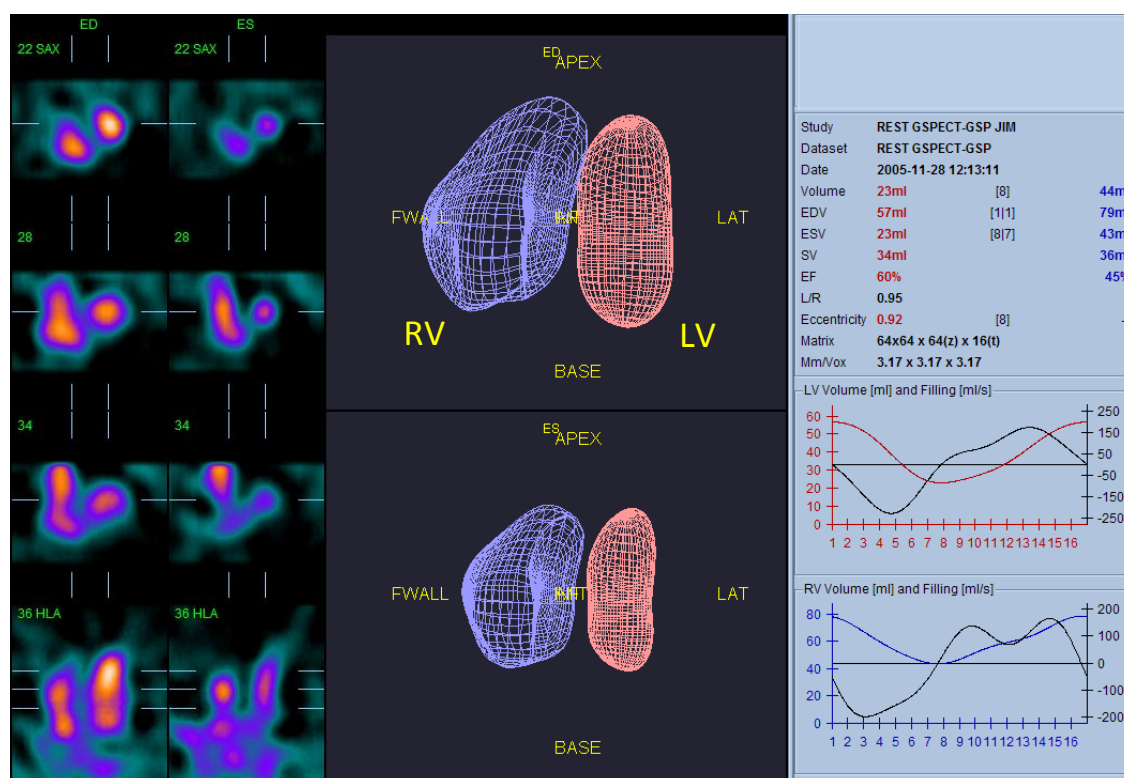


Figure 2.9. SPECT equilibrium radionuclide angiography. Radiotracers counts (left panel) are used to generate 3D ventricular models in end-diastole (upper middle panel) and end-systole (lower middle panel). Time-volume curves of the left and right ventricles display volumes and ejection fraction (right panel). LV- left ventricle; RV- right ventricle; FWALL- free wall; LAT- lateral. Courtesy of Dr Eliana Reyes.

Nuclear perfusion imaging may be potentially useful in assessing myocardial ischaemia of the RV [DePuey 1991, Abuhid 2007], particularly in patients with RV hypertrophy, where the increased coronary blood flow leads to increased radiotracer uptake and thus better RV visualization [Khaja 1979, Rabinovitch 1981, Rich 2010]. Reports suggest that RVH is a determinant of RVMI after inferior MI [Kopelman 1985, Forman 1987], and that inadequate myocardial perfusion in RVH contributes to RV dysfunction in pulmonary hypertension [Gomez 2001, Greyson 2011]. However, assessment of RV myocardial perfusion has been somewhat limited in the general population, in part due to inconsistent visualization of the thin-walled RV [Ramani 2010], and also because interventional therapy for coronary artery disease of the RV free wall is not commonly employed [Greyson 2011].

2.5.4. Computed tomography

Whilst commonly used in the evaluation of the pulmonary parenchyma and vascular system, computed tomography (CT) can provide complementary information on the right side of the heart. Simple RV measurements and indices can be obtained during investigation of lung disease [Dupont 2011]. RV enlargement, as defined by increased RV/LV dimensional ratio, and RV dysfunction, as defined by ventricular septal bowing to the left, have been validated against echocardiography [Contractor 2002], and able to predict adverse outcomes in patients with acute pulmonary embolism [Aaroz 2003, Quiroz 2004, Schoepf 2004]. However, these parameters appear to be unreliable [Aaroz 2007], and are not routinely used for the management of pulmonary conditions.

CT differs from other X-ray techniques because X-ray transmission is registered under a large number of projection angles. The signal received by the detectors is computer processed, enabling reconstruction of 2D trans-axial tomographic images where signal intensity reflects

tissue attenuation properties [Geleijns 2005]. CT of the heart was only made possible after the introduction of ECG-gated acquisitions. However, it was the prospect of evaluating coronary artery disease, the most prevalent cardiac disease, that substantial improvements in CT performance have been accomplished. The new generation multidetector CT scanners (MDCT) with increased spatial-temporal resolution and extended coverage can generate 3D coronary angiograms with excellent image quality. As the whole heart is also covered, reliable information about the cardiac chambers thus became possible, usually with acquisition times of only a few seconds (figure 2.10). When CT data are retrospectively referenced to the recorded ECG signal, images can be reconstructed at the desired time points of the cardiac cycle [Halliburton 2012]. End-diastolic and end-systolic frames are then selected, from which ventricular volumes, EF and myocardial mass are derived [Bruzzi 2006a, Bruzzi 2006b]. Since the implementation of MDCTs in 2004, several authors have validated its use for estimation of RV size and function in comparison with echocardiography [Dogan 2006], nuclear imaging [Kim 2005, Coche 2005], and the gold standard CMR [Plumhans 2008, Nicol 2009, Guo 2010, Gao 2012, Maffei 2012]. Despite being regarded as accurate and reproducible for estimation of RV volumes and mass, CT is not routinely used for RV assessment. Like conventional angiography, CT is hampered by the amount of radiation delivered and iodinated contrast injection involved [Dupont 2011]. In addition, the temporal resolution of CT is still lower than other techniques, limiting its sensitivity for detecting and evaluating regional wall motion abnormalities [Fischbach 2007]. Nevertheless, the use of cardiac CT for the RV is expected to rise in the future, as continuous improvements in hardware and software capabilities will increase the temporal resolution and reduce the radiation burden. CT is likely to become an attractive option for the evaluation of the right ventricular-pulmonary unit.

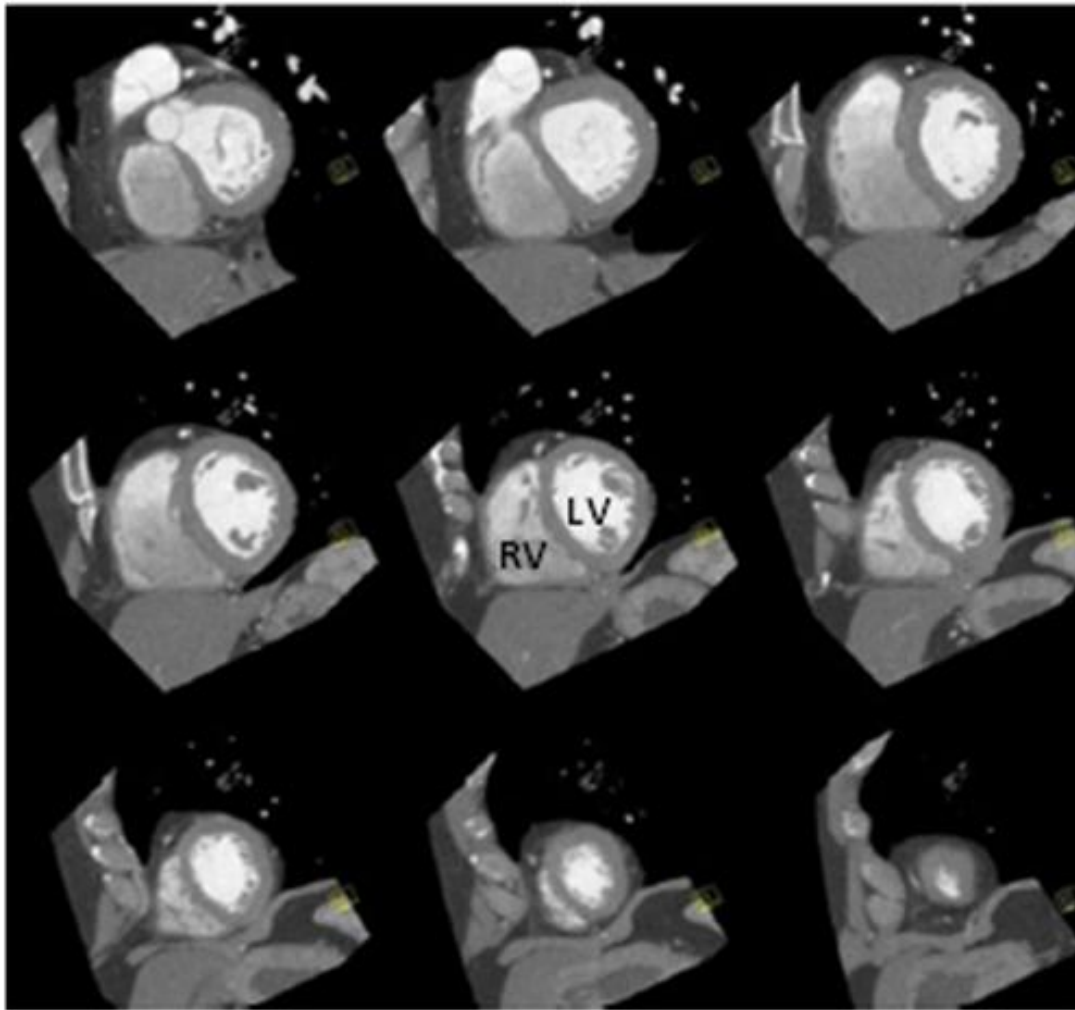


Figure 2.10. Computed tomography short-axis reconstruction of the left and right ventricles from base to apex. LV- left ventricle; RV- right ventricle. Reproduced from with permission from Maffei 2012.

2.5.5. Magnetic resonance

Cardiovascular magnetic resonance (CMR) provides comprehensive evaluation of the heart by exploring the magnetic relaxation properties of the tissues (figure 2.11). CMR is a safe technique, thus enabling serial evaluation without the need for iodinate contrast agents or exposing patients to ionizing radiation [Dupont 2011]. Other advantages include the ability for in vivo tissue characterization, and good spatial and temporal resolution regardless of patient body habitus, orientation or position of the heart [Greyson 2011].

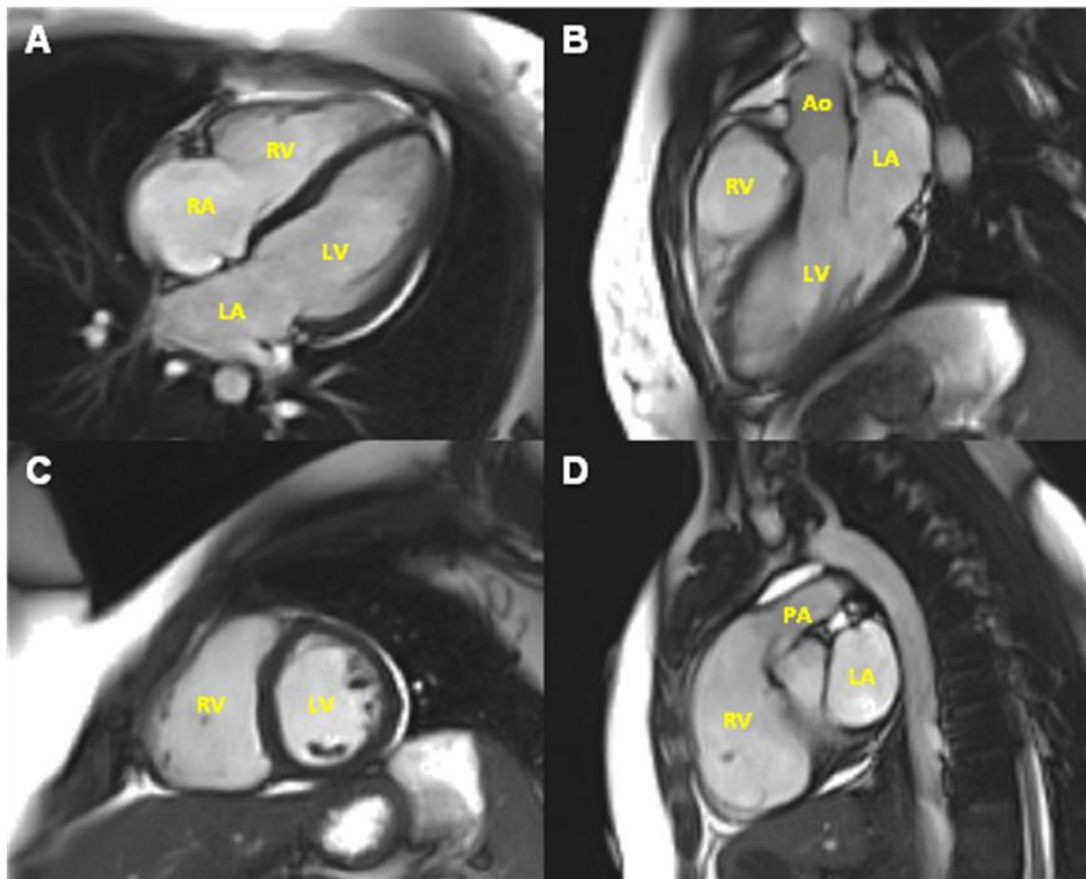


Figure 2.11. Examples of cardiovascular magnetic resonance planes covering the right ventricle. Panel A, Four-chamber view. Panel B, Left ventricular outflow tract view. Panel C, Short-axis view at mid-ventricular level. Panel D, Right ventricular outflow tract view. Ao- aorta; LA- left atrium; LV- left ventricle; PA- pulmonary artery; RA-right atrium; RV-right ventricle.

CMR allows accurate and reproducible calculation of RV volumes, ejection fraction, myocardial wall thickness and mass [Mogelvang 1988, Katz 1993, Helbing 1995, Grothues 2004]. When compared to other imaging modalities, CMR is considered the most reliable method for measuring RV volumes and ejection fraction [Sugeng 2010], and is currently regarded as the reference for validation of other techniques [Dupont 2011, Greyson 2011]. Using phase-contrast velocity mapping, CMR can estimate cardiac output, peak velocities, regurgitant fractions and shunts, which are useful in the assessment of valvular and congenital

heart disease [Kilner 2007]. Moreover, tissue characterization using different sequences and gadolinium chelated contrast agents can reveal tissue characteristics such as the presence of fat or fibrosis in the RV myocardium without the need for invasive cardiac biopsy [Molinari 1995, Sato 1995].

Despite the increasing role in the evaluation of the RV, wider application of CMR is hindered by the high costs, limited availability and specialised training, restricting its use to experienced centres. Caution should be undertaken with metallic implants, and electronic devices are usually regarded as contraindications to the technique. Other drawbacks include long scan times (particularly troublesome in patients with claustrophobia) and the frequent need for gadolinium (relative contraindication in patients with severe renal dysfunction).

Detailed information on magnetic resonance physics, image acquisition and clinical applications to the cardiovascular system will be provided in the following chapter.

2.5.6. Multimodality imaging

The use of cardiovascular imaging has increased significantly over time. There are two main reasons behind this trend: 1) a steady rise in cardiovascular pathology due to an ageing population and prolonged survival as a result of better treatment, and; 2) technological advances leading to new imaging applications, initially in the research setting, and later translated into the routine clinical practice. As described in the previous sections, each and every individual imaging modality has its own merits, caveats and applications (table 2.3). Hence the combined use of different modalities has the potential to provide additional and complementary information, and thereby improve diagnostic accuracy, risk stratification, and individual management. These propositions are the cornerstones for the use of multimodality imaging, which will be briefly discussed for the RV.

Echocardiography is traditionally the initial method of choice for patients with suspected or confirmed RV disease. As opposed to other imaging modalities, it is portable, readily available, and relatively inexpensive. It permits comprehensive evaluation of RV morphology, systolic and diastolic function, as well as estimating RV and pulmonary haemodynamics [Mertens 2010]. However, the parameters measured by echocardiography are hampered by the high variability and lack of clinical validation. Hence, in most echocardiographic laboratories, the most frequently used technique to estimate RV function is subjective visual assessment [Mertens 2010].

CMR is being increasingly used as a standard tool for the evaluation of RV structure and function [Haddad 2008a]. It is the most accurate method for assessing RV morphology, global and regional function, and has the additional ability of evaluating the tissue characteristics of the myocardium. In addition, flow studies can be used to assess cardiac output, valve function and shunts. Because of its limited availability, CMR is usually indicated when echocardiographic windows are limited, or when more reliable information on the RV is required.

Right cardiac catheterization enables direct pressure measurements and precise haemodynamic assessment of the RV and pulmonary vascular system [Bleeker 2006a]. Conventional contrast angiography is sometimes performed during catheterization, but is seldom used today due to the limited 2D planar information, use of ionization radiation and iodinated contrast agents. This technique is invasive and only convened when pulmonary or RV haemodynamic information is important for decision making.

Radionuclide angiography had been used in the past for quantification of RV ejection fraction and cardiac shunts. However, its popularity has decreased over the years due to the low spatial resolution and high radiation burden. Nuclear imaging has been replaced by more

precise and radiation-free techniques, and is nowadays rarely used for evaluation of the RV [Greil 2008].

Despite the high spatial resolution, CT is limited by the low temporal resolution and exposure to radiation, and is only considered for the assessment of RV when there are contra-indications to all other imaging modalities [Greil 2008]. Nevertheless, thoracic CT is widely used in the evaluation of thoracic disorders, some of which have potential repercussions on the right side of the heart [Dupont 2011].

Table 2.3. Comparison of the available imaging modalities.

	Angio	Echo	Nuclear	CMR	CT
Image quality	++	++	+	+++	+++
Temporal resolution	++	+++	+	++	+
Availability	++	+++	++	+	+
Cost	+++	+	++	+++	++
Radiation	+	0	+	0	+
General applications	++	+++	+	+++	+
RV applications	++	++	+	+++	+

Angio- X-ray angiography; Echo- echocardiography; Nuclear- nuclear imaging; CMR- cardiovascular magnetic resonance; CT- computed tomography; RV- right ventricle.

CHAPTER 3: CARDIOVASCULAR MAGNETIC RESONANCE

Since the acquisition of the first magnetic resonance (MR) signal in 1952 by Herman Carr, and the first MR images in the early 1970s by the Nobel laureates Paul Lauterbur and Sir Peter Mansfield, magnetic resonance imaging (MRI) has progressed enormously to become a popular technique in the medical community. MRI is most useful in the evaluation of the nervous and musculoskeletal systems, but can be applied to the cardiovascular system as well. This chapter comprises the basic principles of MRI, image acquisition of the moving heart, and general applications to the cardiovascular system.

3.1. PRINCIPLES OF MAGNETIC RESONANCE IMAGING

3.1.1. Magnetic resonance system components

An MRI system comprises three main electromagnetic components: 1) a set of main magnet coils; 2) three gradient coils; and 3) a radiofrequency transmitter coil (figure 3.1) [Ridgway 2010]. The main magnet coils generate a strong, constant and homogeneous magnetic field. The strength of the magnetic field is measured in units of Tesla (T), with 1 Tesla corresponding to approximately 20,000 times the earth's magnetic field. Nominal field strengths range from 0.5T to 3.0T for commercially available clinical MR systems, with the commonest field strength for cardiac imaging being 1.5T [Ridgway 2010]. Gradient magnetic fields superimposed onto the main magnetic field can be rapidly switched on and off by three gradient coils mounted inside the main magnet. The gradient coils can change the position of the magnetic field along the x, y, and z directions, with the z axis conventioned to be parallel to the direction of the main magnetic field. A small radiofrequency (rf) magnetic field can be emitted by the rf

transmitter coil located inside the gradient coils. The rf pulse waves are in the MHz range, and are responsible for generating the MR signal.

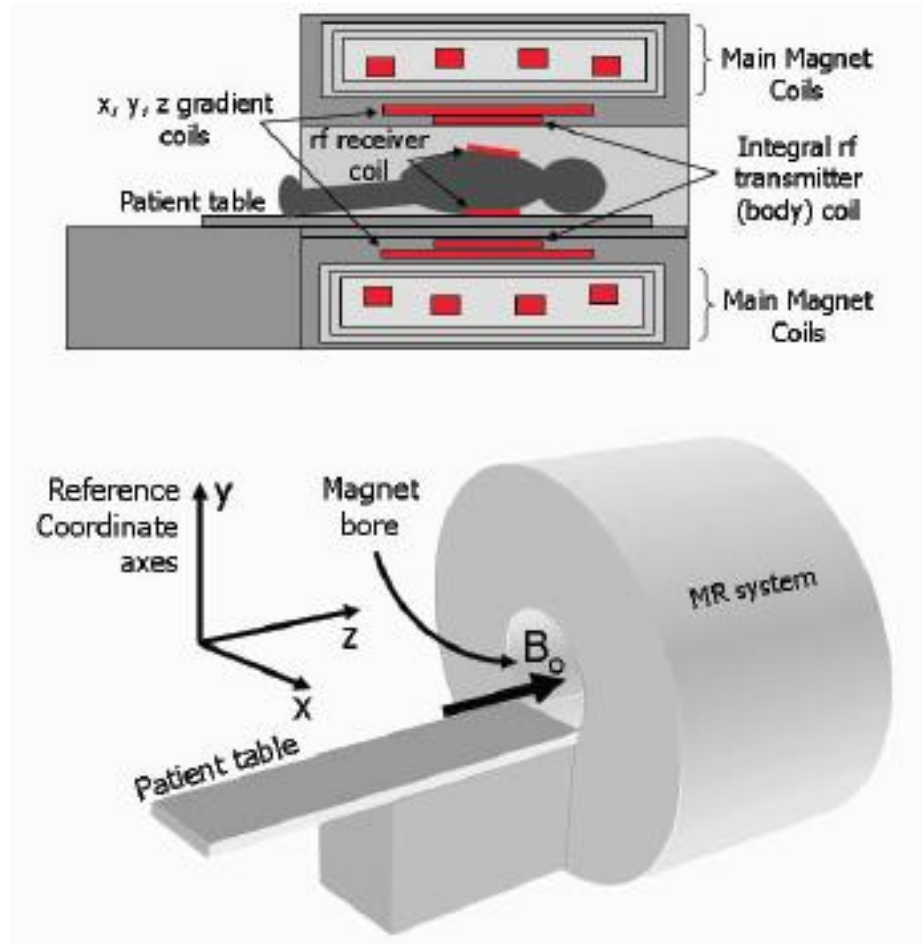


Figure 3.1. Top panel, Diagram showing the relative locations of the main magnet coils, gradient coils, rf transmitter body coil and rf receiver coils. Bottom panel, Arrangement of a typical MR system showing the magnet bore and the reference coordinate axes with the static B_0 field direction along the horizontal z axis. Reproduced with permission from Ridgway 2010.

Each component produces a different type of magnetic field which, when applied in combination to a patient, generates spatially localised and encoded MR signals that are used to create the MR images. For cardiac imaging, a separate rf receiver coil is tailored to maximise the signal from the heart [Ridgway 2010].

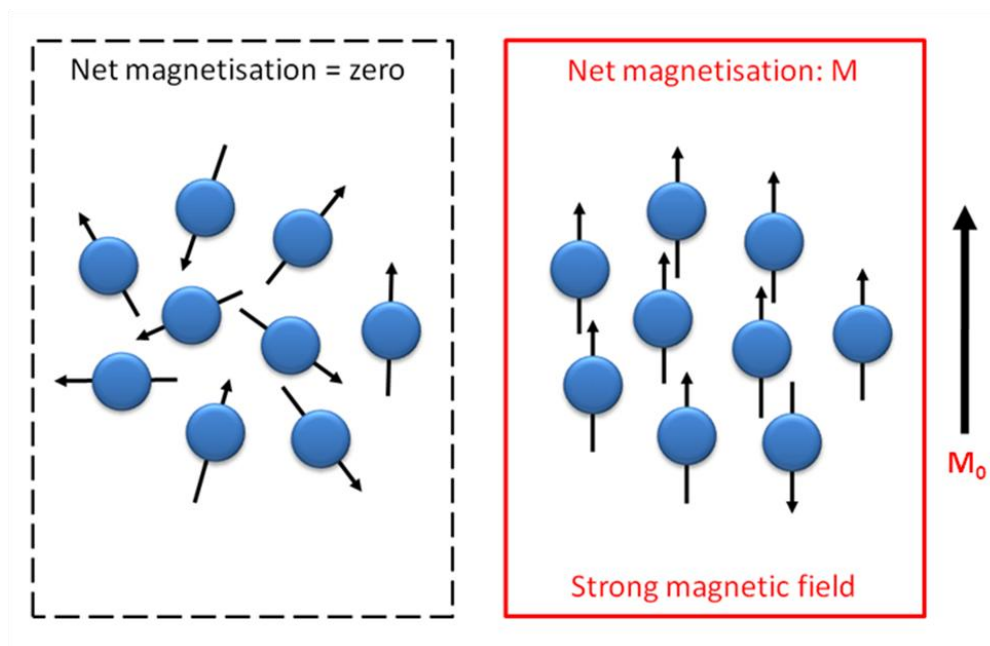


Figure 3.2. Each hydrogen proton possesses a magnetic moment (vector). Under normal conditions, the magnetic moments are randomly orientated and the net magnetisation vector is zero. When the protons are placed within a strong magnetic field, they usually align with axis of the main magnetic field, resulting in the net magnetisation vector M_0 at equilibrium. Courtesy of Dr John-Paul Carpenter.

3.1.2. Origin of magnetic resonance signals

Only elements with unpaired atoms show magnetic properties, some of which can be explored for research by MR-spectroscopy (e.g. ^{13}C , ^{19}F , ^{23}Na , ^{31}P). However, hydrogen (^1H) is the one used in clinical MRI due to its abundance in the human body and high MR signal [Schild 1990]. Hydrogen nuclei (single protons) possess an intrinsic property known as nuclear spin that gives rise to a small magnetic field known as a magnetic moment [Ridgway 2010]. Normally the magnetic moments are randomly oriented but in the presence of an external magnetic field, they behave as small magnets and tend to align with the main magnetic field (figure 3.2). In order to generate a MR signal, an rf pulse is used to deliver energy to the population of protons. When the rf pulse is switched on, the net magnetisation vector M_0 begins to move away from the z axis and starts rotating around the x and y axis. The rf pulse is

switched off once the angle of precession has reached a prescribed value. This is known as the flip angle of the rf pulse [Ridgway JCMR 2010]. The net magnetisation vector can be split into two components (figure 3.3). One component is parallel to the z-axis, and is known as the longitudinal component or M_z . The other component lies at right angles to the z axis within the plane of the x and y axes and is known as the transverse component or M_{xy} . The transverse component rotates at a particular frequency, the Larmor frequency, which is proportional to the strength of the magnetic field [Dymarkowski 2005]. As it rotates, it generates its own small, oscillating magnetic field, which is detected as an MR signal by the rf receiver coil [Ridgway 2010].

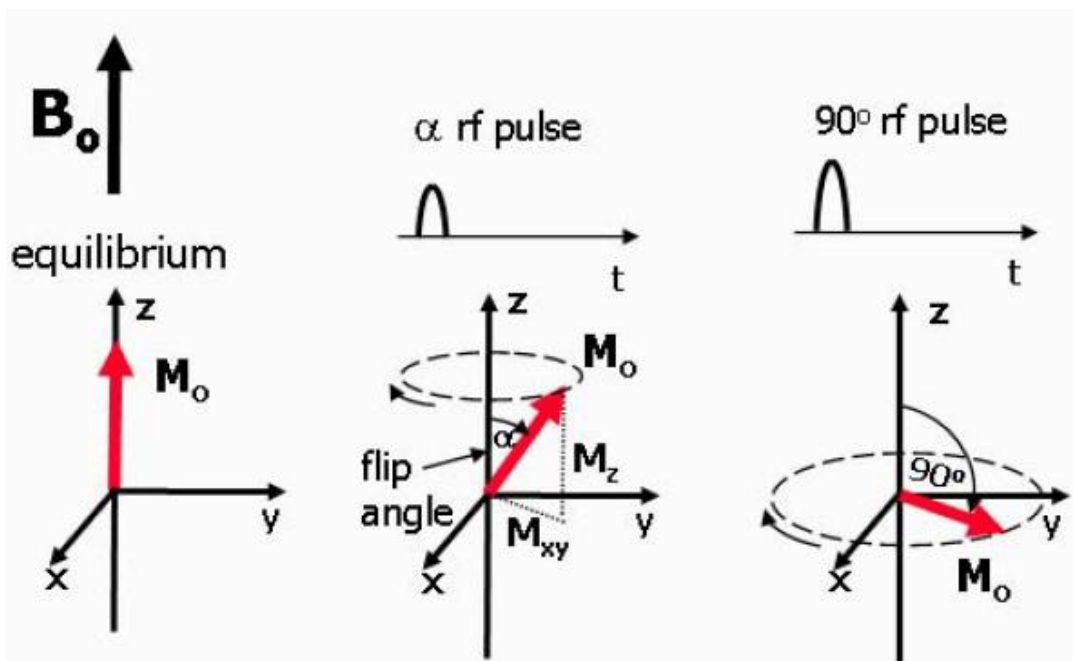


Figure 3.3. rf pulses and magnetisation. Left panel, At equilibrium the net magnetisation M_0 is aligned with the bore magnetic field (B_0). Middle panel, When an rf pulse is applied, M_0 makes an angle with the z-axis, known as the flip angle (α), and rotates around the axis (curved arrow). At any instant the magnetisation can be split into two components, M_z and M_{xy} . The rotating M_{xy} component generates the MR signal. Right panel, The maximum detectable signal amplitude occurs after a 90° flip angle tilts the magnetisation vector to the transverse plane. Reproduced with permission from Ridgway 2010.

3.1.3. T1, T2 and T2* (T2-star) relaxation

As soon as the rf pulse is switched off, the excited spins start to return back to their original low energy state at equilibrium. This process is known as relaxation [Ridgway 2010]. There are two simultaneous but distinct relaxation processes that relate to the two components of net magnetisation. The first relaxation process occurs along the longitudinal (z) axis as the magnetic moment loses energy. Longitudinal relaxation is an exponential process and can be measured by the time constant T1 (figure 3.4).

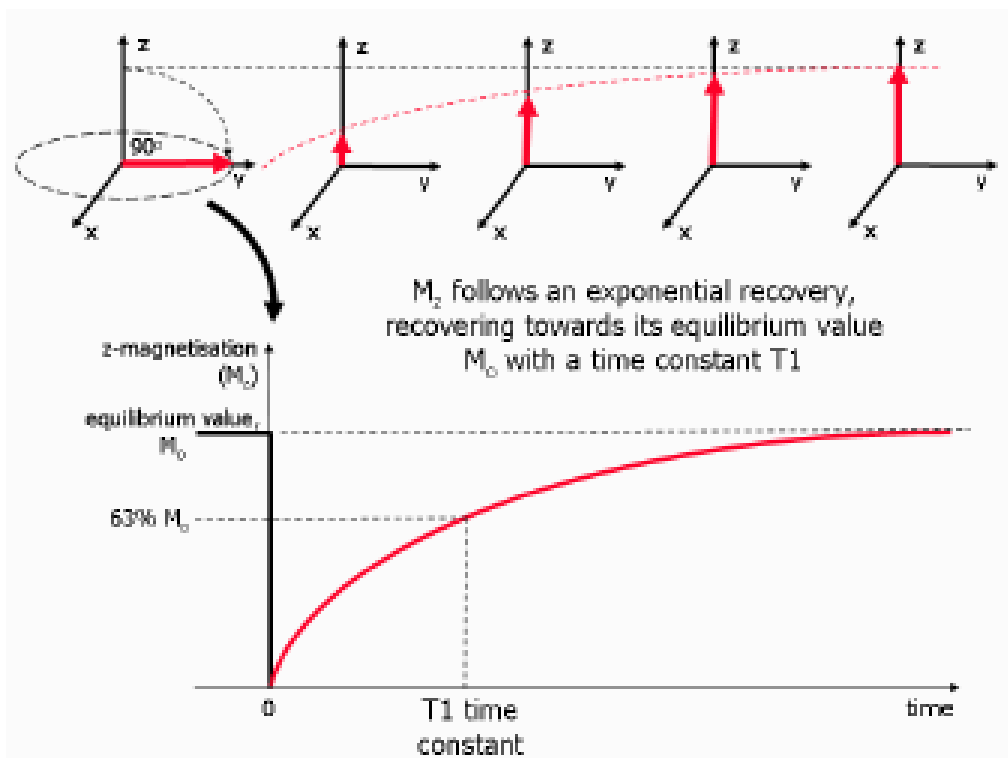


Figure 3.4. T1 relaxation. After application of a 90° rf pulse, the z component of magnetisation (M_z) is reduced to zero, but then recovers gradually back to equilibrium. The recovery of M_z is an exponential process with a time constant T1. This is the time when magnetization has recovered to 63% of its value at equilibrium. Reproduced with permission from Ridgway 2010.

The second relaxation process occurs in the transverse (xy) plane. While precessing at different frequencies, the spins become out of phase and cancel each other out, causing a

decay of the observed MR signal [Schild 1990]. There are two causes for the loss of phase coherence. The first cause is related to the magnetic interaction between neighbouring protons. This is an irreversible process with an exponential decay curve that can be measured by the time constant T_2 (figure 3.5.). The second cause for transverse relaxation is reversible as it is due to local inhomogeneities of the magnetic field. The combined effect of T_2 relaxation and magnetic field non-uniformities is called T_2^* relaxation, which corresponds to the actual decay of MR signal also known as free induction decay (FID) [Ridgway 2010].

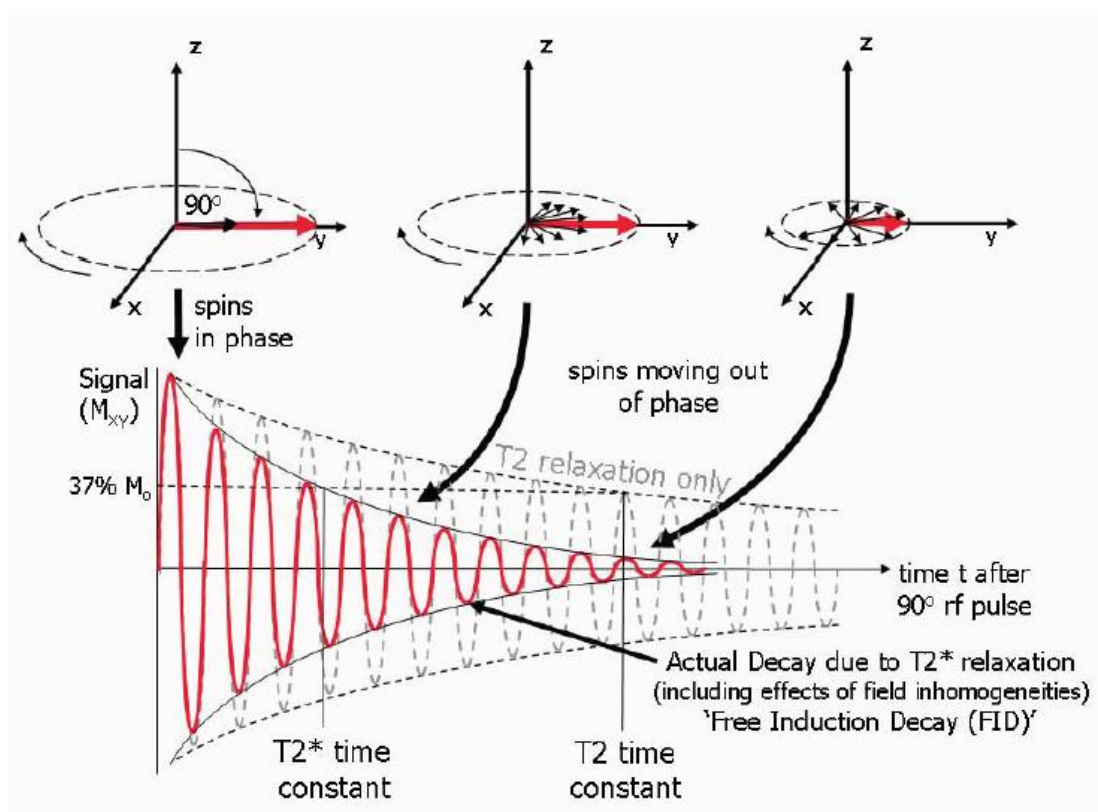


Figure 3.5. T_2 and T_2^* relaxation. After a 90° rf pulse is applied, the net magnetisation vector (red arrow) is at maximum amplitude as the proton magnetic moments rotate in phase. The detected signal decays as the spins move out of phase with one another (small black arrows). The resultant decaying signal is known as the free induction decay (FID), and corresponds to the T_2^* relaxation. T_2 relaxation is observed when magnetic field inhomogeneities are neutralized by 180° refocusing pulses. Both T_2 and T_2^* are exponential processes with time constants T_2 and T_2^* respectively. This is the time when magnetization has decayed to 37% of its initial value after the 90° rf pulse. Reproduced with permission from Ridgway 2010.

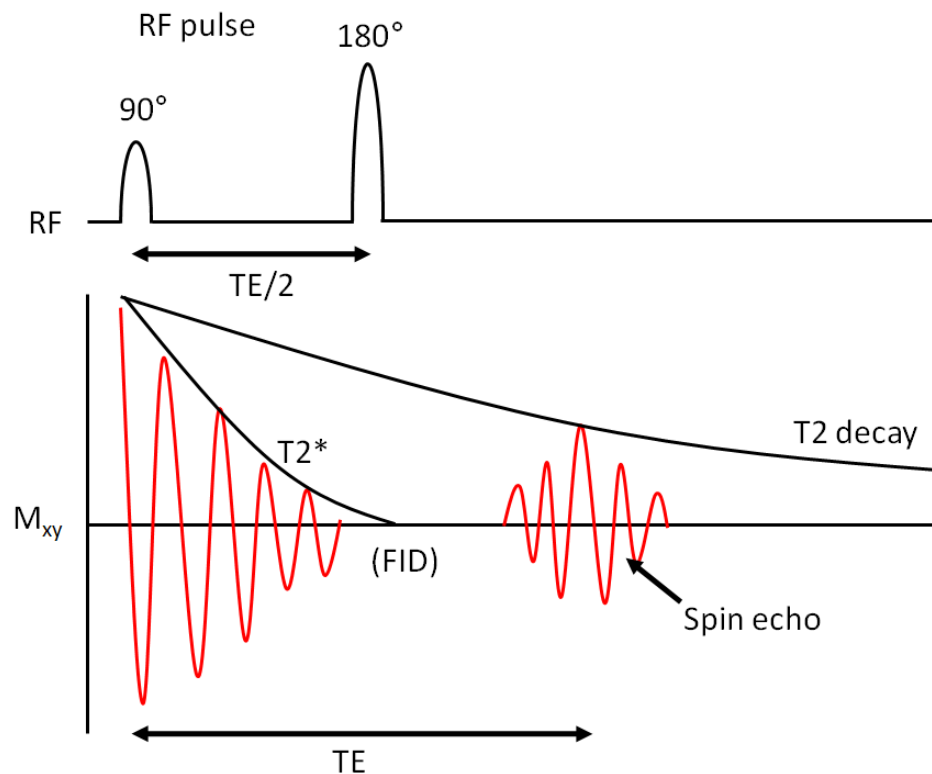


Figure 3.6. Spin echo. After the initial 90° pulse, free induction decay occurs (T_2^* decay). A subsequent 180° pulse rephases the spins resulting in a spin echo. The 180° pulse is only able to correct the dephasing caused by field inhomogeneities while the dephasing due to spin-spin interactions remains. The peak amplitude of the spin echo consequently exhibits exponential decay governed by T_2 relaxation. RF pulse- radiofrequency pulse; TE- echo time; M_{xy} - magnetization in transverse plane; FID- field induction decay. Courtesy of Dr John-Paul Carpenter.

3.1.4. Magnetic resonance echoes

Whilst the FID can be detected as an MR signal, for MRI it is more common to acquire the MR signal in the form of an echo [Ridgway 2010]. The echoes used for MRI can be divided into spin echoes and gradient echoes. Spin echoes are generated by the application of 180° refocusing rf pulses after a 90° excitation pulse (figure 3.6). The initial 90° excitation pulse tilts the spins into the transverse plane and into the same phase (in phase). After the rf pulse, the spins start to move out of phase with a consequent loss of signal as represented by the FID. By

application of a 180° refocusing pulse, the protons reverse their spin direction and come back into phase reaching the maximum signal at the echo time, TE. For the spin de-phasing caused by the field inhomogeneities to be completely reverted, the 180° pulse must be applied at half the echo time, TE/2. The resulting echo is called spin echo [Schild 1990]. Gradient echoes are generated by the controlled application of magnetic field gradients. When a magnetic field gradient is switched on it causes proton spins to de-phase rapidly along the direction of the gradient. The de-phasing caused by one magnetic field gradient can however be re-phased by applying a second magnetic field gradient with an equal amplitude and for the same amount of time but in the opposite direction. The corresponding signal after re-phasing is known as a gradient echo [Ridgway 2010].

3.1.5. Image creation

The MR echo signals produced above can be localized and spatially encoded by applying magnetic field gradients [Ridgway 2010]. A cross-sectional 2D image can be built in any particular plane by using a combination of rf pulses and gradient magnetic fields in 3 steps as described below.

Step 1 - Slice selection

First, the resonance of protons is confined to a slice of tissue. This is done by applying a gradient magnetic field at the same time as the rf excitation pulse is transmitted (figure 3.7). The frequency of the slice select rf pulse corresponds to the Larmor frequency at a chosen point along the direction of the applied gradient. Only the protons precessing at the rf pulse frequency will become excited, thereby defining a slice of tissue which will be sampled for image acquisition. This process is known as slice selection and the orientation of the slice is determined by the slice selection gradient, G_s [Ridgway 2010].

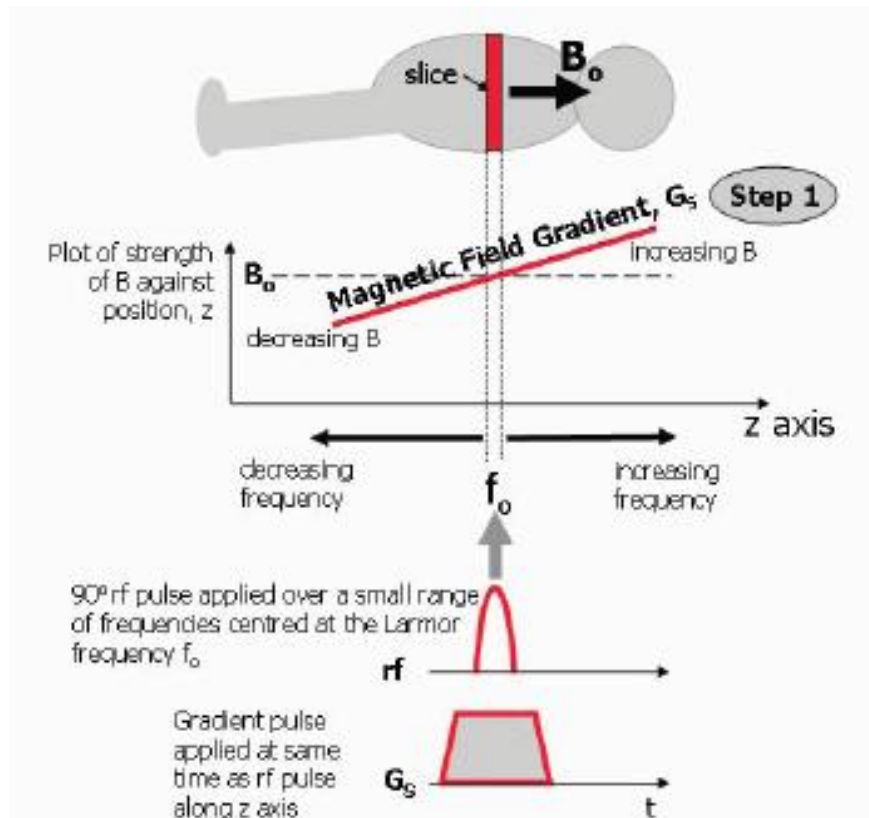


Figure 3.7. Slice selection. A slice selection gradient, G_s , is applied at the same time as the rf pulse. Only spins precessing at the rf pulse frequency will be excited, thereby forming a slice of tissue that will be sampled for image acquisition. Reproduced with permission from Ridgway 2010.

Step 2 - Phase encoding

Following slice selection, a phase encoding gradient, G_p , is applied in a perpendicular direction for a specified period of time. This causes the protons to rotate at different frequencies according to their position along the gradient. When the gradient is turned off, the protons will have changed their relative phase by an amount depending on their position along the gradient (figure 3.8). This process is known as phase encoding and the direction of the applied gradient is known as the phase encoding direction [Ridgway 2010].

Step 3 - Frequency encoding

Following the phase encoding gradient, a frequency encoding gradient, G_f , is applied at right angles to the previous gradients, causing the protons to rotate at different frequencies

according to their relative position along that direction gradient. This gradient is applied for longer, during which the MR signal is being digitally sampled. The signal is comprised of a range of frequencies, corresponding to the Larmor frequencies of the magnetic moments at their different locations along the gradient (figure 3.8). This process is known as frequency encoding, and the direction of the applied gradient defines the frequency encoding (or readout) direction [Ridgway 2010].

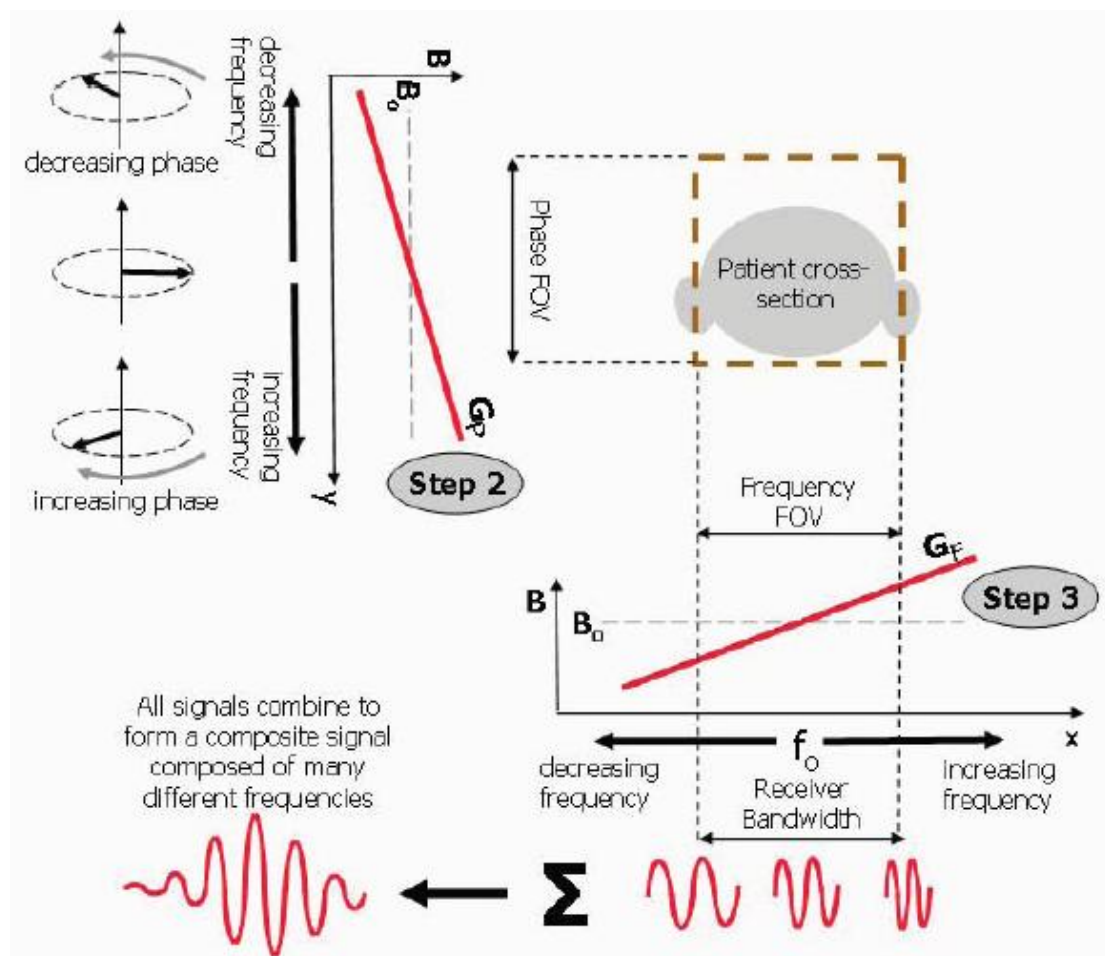


Figure 3.8. Phase and frequency encoding. The phase encoding gradient is transiently applied in one image direction (in this case, the y direction), leaving a phase shift relative to the proton position along the G_p direction. The frequency encoding gradient is then applied in the other direction of the image plane (in this case, the x direction), during which the MR echo signal is measured. The individual frequencies from the combined MR signal are used to locate the MR signal along the G_f direction. FOV- field of view; B_0 - bore magnetic field; f_0 - resonance frequency. Reproduced with permission from Ridgway 2010.

In summary, to localise the MR signal in three dimensions, three separate magnetic field gradients are applied in a three step process. The ability to define an arbitrary slice at any plane and position is a key strength of MRI, especially for cardiac applications where oblique views are usually needed for acquiring the standard views of the heart [Ridgway 2010].

3.1.6. Image reconstruction

Following slice selection and excitation of the region of interest, the MR signal is collected by the receiver coils into an abstract platform called k-space [Mezrich 1995]. The spatial frequencies are displayed in two orthogonal directions, with the x axis corresponding to the gradient frequency direction and the y axis corresponding to the gradient phase direction. After the phase encoding step, the data is sampled along the x axis in the frequency or readout direction, thereby filling a line of k-space. If several phase encoding steps are repeated successively over time, several lines of k-space will be filled to form the k-space matrix (figure 3.9) [Ridgway 2010]. The k-space is thus defined by the space covered by the phase and frequency encoding data, where the brightness of each point is proportional to the signal amplitude at a particular spatial frequency [Moratal 2008]. Every point in the raw data matrix contains part of the information for the complete image matrix. Conversely, a specific point in the image matrix may have contributions from every single point in the raw data matrix. The Fourier transform is a mathematical tool used to decode the combined time dependent MR signal into its different frequency components. By means of the Fourier transform, the system can allocate the MR signal by phase and frequency onto a specific location, which will then result in the final MRI image (figure 3.9) [Schild 1990].

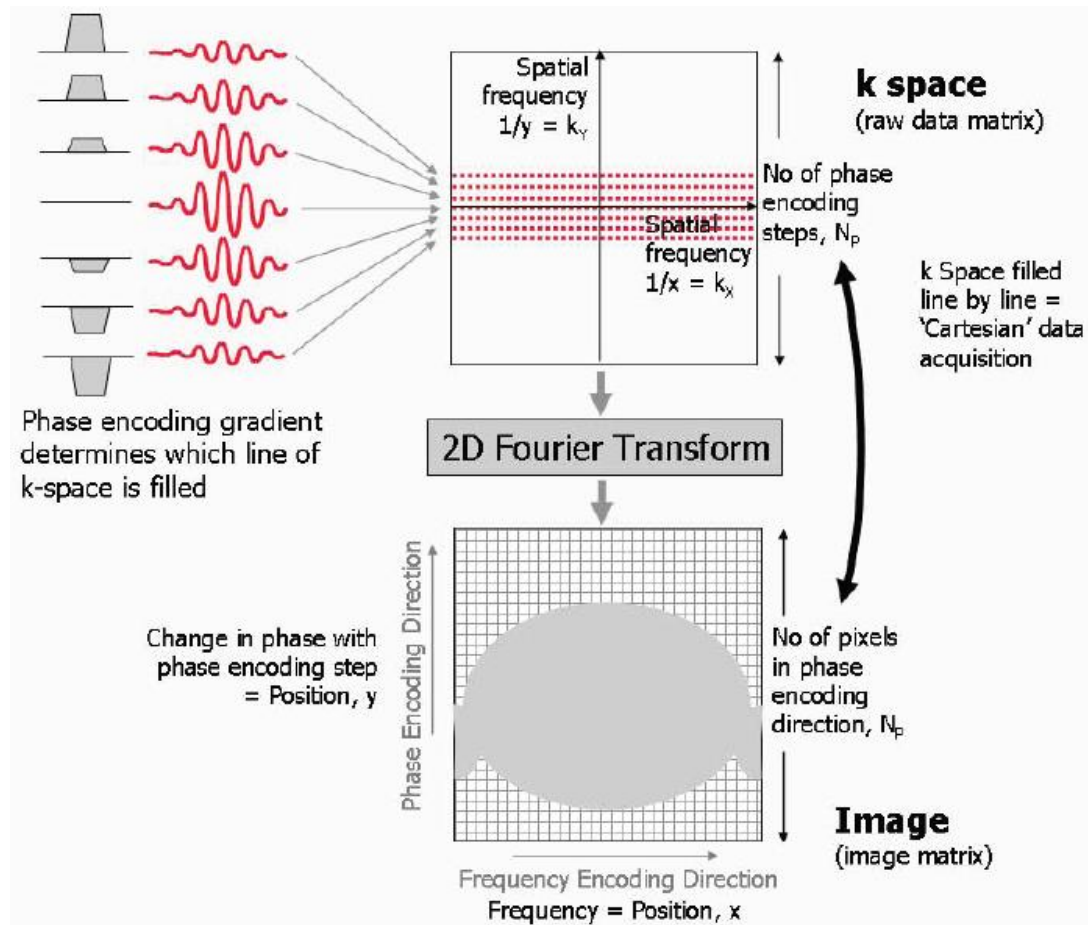


Figure 3.9. Image reconstruction, k-space and image space. The MR signals derived from each phase encoding step are stored in a raw data matrix (k-space). A 2D Fourier transformation of the matrix results in the reconstruction of the image. The number of phase encoding steps determines the number of pixels in the image along the phase encoding direction. Reproduced with permission from Ridgway 2010.

3.1.7. Image contrast

One of the most important strengths of MRI over other imaging modalities is the ability to generate contrast between tissues, as particular tissues have specific MR relaxation properties [Ridgway 2010]. The closely bound hydrogen protons in lipid molecules have precession rates close to the Larmor frequency which are favourable for energy exchange. Hence fat has a short T1 relaxation time. On the other hand, hydrogen protons in free water molecules have a much faster precession rate which is unfavourable for energy exchange. Therefore free water

has a long T1 relaxation time [Ridgway 2010]. T2 relaxation is related to the amount of spin-spin interaction. Free water contains small molecules moving rapidly and far apart. Therefore spin-spin interactions are less frequent and the T2 relaxation is slow, leading to long T2 relaxation times. Water molecules bound to large molecules in soft or liquid tissues are slowed down and more likely to interact, leading to shorter T2 relaxation times [Ridgway 2010]. Hydrogen protons in fat and other solid tissues will generally de-phase more quickly than in liquids, leading to even shorter T2 relaxation times [Constable 1992].

The relaxation properties of any particular tissue can be manipulated by different pulse sequence parameters in order to achieve T1 and T2 contrast or weighting. As each particular tissue has its own relaxation properties, the combined use of different weightings and sequences will constitute the basis for tissue characterization, which is one of the distinctive features of MRI (table 3.1).

Table 3.1. Signal characteristics of different types of tissues according to pulse sequences.

	T1	T2	T2*	SSFP	EG	LG
Fat	↑	↔	↔	↑	↔	↔
Water	↓	↑	↑	↑	↓	↓
Myocardium [†]	↔	↔	↔	↔	↑	0
Thrombus	~	~	↓	↔	↓	↓
Blood	↑	↑	↔	↑	↑	~
Fibrosis	↓	↓	↓	↓	↓	↑
Calcium	↓	↓	↓	↓	↓	↓
Air	0	0	0	0	0	0

↑ high signal; ↔ intermediate signal; ↓ low signal; ~ variable signal; 0- no signal

[†]Normal myocardium; SSFP- steady state free precession; EG- early phase after gadolinium injection; LG- late phase after gadolinium injection.

3.2. BASIC PULSE SEQUENCES

A pulse sequence is defined as a set of radiofrequency pulses and magnetic gradients used to produce an MR signal. Two of the most important modifiable parameters of a sequence are the repetition time, TR, and the echo time, TE. The time between each excitation pulse is called repetition time. Each repetition corresponds to a phase encoding step and a frequency encoding measurement. The time between repetitions is the most important factor for image acquisition time [Balaban 2010]. The echo time is the time interval between the excitation pulse and the resulting echo, which is normally arranged to coincide with the data sampling. Depending on the type of MR echo generated, pulse sequences can be divided into spin echo (SE) and gradient echo (GE) sequences, which will be briefly described below.

Pulse sequences are frequently accompanied by pulse modifiers or prepulses, which consist of rf pulses or gradients applied in front of a standard MR sequence to manipulate the net magnetisation. Prepulses are often used for contrast enhancement, artefact reduction and tissue labelling.

3.2.1. Spin echo sequences

The 90° excitation pulse combined with a 180° refocusing pulse used by the SE sequences give the largest possible echo signal at TE while neutralizing field inhomogeneities at the same time. Spin echo techniques are therefore suited for anatomical imaging when the primary goal is to achieve images with high signal-to-noise ratio and reduced sensitivity to artefacts related to magnetic field inhomogeneities (figure 3.11) [Ridgway 2010]. However, the inherently slow scanning times only allow images to be acquired in part of the cardiac cycle. Hence dynamic imaging is not possible with SE sequences.

The parameter choice for T1-weighted spin echo is a short TR and a short TE. T1 weighted images are characterised by bright signal from fat and low signal from fluid. Therefore T1

weighted SE sequences are useful for anatomical imaging where contrast is required between fat, muscle and fluid. The parameter choice for T2-weighted spin echo is a long TR and a long TE. Tissues with short T2 relaxation return low signal, while tissues with a long T2 return high signal. T2-weighted SE images are useful for the depiction of fluid collections and myocardial oedema which will appear with bright signal [Ridgway 2010].

A particular feature of SE sequences is the intrinsic black blood contrast due to moving blood through the image slice [Herfkens 1983]. Since the 90° and 180° pulses are slice selective, any moving blood not stimulated by both pulses will not produce a SE signal, thus resulting in a signal void. This black blood effect can be optimized by specific dark blood preparation pulses. SE sequences hence provide consistently high contrast between the blood pool and the surrounding heart and blood vessel walls [Simonetti 1996].

3.2.2. Gradient echo sequences

The concept of GE imaging was only possible after the introduction of more powerful MR systems. Key differences to SE sequences include a single rf pulse with a low flip angle (between 15-60°) for slice selection, and use of gradients instead of time-consuming rf pulses for echo generation. These factors significantly shorten the acquisition times by reducing the repetition and echo times. Several images can be acquired throughout the cardiac cycle, expanding the role of CMR from still frame anatomical imaging to functional cine imaging. GE sequences are used where imaging speed is more important than image quality, as the absence of the 180° refocusing pulse leads to signal loss in the setting of magnetic susceptibility effects [Ridgway 2010]. The two main types of gradient echo pulse sequences used for cardiac imaging are called spoiled GE and balanced steady state free precession (bSSFP) [Boyle 2006].

3.2.2.1. Spoiled gradient echo

The TR values used in GE sequences are much shorter than the T2 relaxation times of blood and myocardium. This means that unless the residual transverse magnetisation generated by each rf pulse is destroyed after it has been sampled, it would still exist when the next rf pulse is applied. In spoiled gradient echo, the remnant signal is de-phased (or spoiled) by a spoiler gradient after each readout period so that its contribution to the subsequent TR periods is suppressed [Zur 1991]. Spoiled GE sequences tend to be T1-weighted because of the short TR required for rapid imaging, and also because the long TE signals with T2* information are destroyed by the spoiler gradients [Westbrook 2005]. However, T2* weighting is still possible with spoiled GE by increasing the TR and TE to relatively long values, while keeping the flip angle low. For T2* weighted GE, the image contrast is strongly influenced by the presence of magnetic susceptibility effects and can be used to detect the presence of iron in tissues [Anderson 2001]. The main cardiac applications for spoiled GE sequences are contrast imaging, flow imaging, and myocardial iron imaging, all of which will be discussed in more detail in the methods chapter.

3.2.2.2. Balanced steady state free precession

These sequences are designed to ensure that the transverse magnetisation is not spoiled but actually brought back into phase when the next rf pulse is applied. The residual magnetisation is carried over to the next repetition and superimposed onto the transverse magnetisation generated by the subsequent rf pulses [Ridgway 2010]. After several repetitions, a steady state is established where the signal from successive repetition periods is combined to give a much greater signal [Scheffler 2003]. Balanced SSFP is a special type of SSFP sequence where applied gradients are compensated by gradients with opposite polarity (rewinder gradients), speeding up the rephasing process and ensuring the highest amount of signal during the

steady state [Westbrook 2005]. The increased signal allows for a shorter TE and TR compared to spoiled GE sequences and improved imaging efficiency [Ridgway 2010]. The contrast behaviour of bSSFP is unique because the rf pulse is applied exactly between the echo times attenuating the T_2^* effects of the transverse residual magnetisation [Westbrook 2005]. bSSFP contrast is related to a complex T_2/T_1 ratio, with fat and fluid appearing brighter than any other tissue [Dymarkowski 2005]. The intrinsic high contrast between the blood and the myocardium is the distinctive feature of bSSFP, which has become the standard imaging sequence for the functional assessment of the heart (figure 3.10). The key differences between GE and SE techniques are summarised in table 3.2.

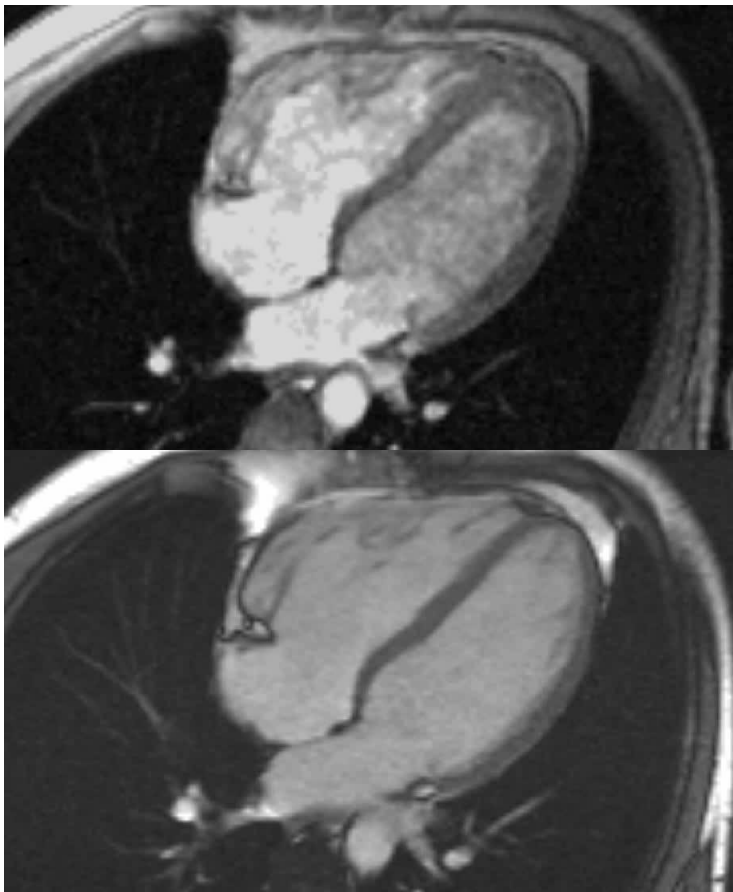


Figure 3.10. Four-chamber view of a normal heart at end-diastole as acquired by a spoiled gradient echo sequence (top panel) and a balanced steady state free precession sequence (bottom panel). Cine imaging initially relied on spoiled gradient echo, but was later replaced by steady state free precession, which ensures better image quality and superior delineation of the myocardial borders.

Table 3.2. Summary of key differences between spin echo and gradient echo sequences.

	Spin echo	Gradient echo (spoiled)	Gradient echo (bSSFP)
Flip angle	90°	5-40°	50-70°
Refocusing pulse	Yes	No	No
Contrast weighting	T1, T2	T1, T2*	T2/T1 ratio
Short TR (for T1 weighting)	400-800ms	3-400ms†	3-5ms
Short TE (for T1 weighting)	6-25ms	1-3ms	1-3ms
Long TE (for T2/T2* weighting)	60-100ms	7-15ms	N/A
Long TR (for T2/T2* weighting)	1500-2500ms	100ms†	N/A
Shortest practical TR	200ms	2-5ms	2-5ms
Susceptibility to iron	No	Yes	Yes
Signal from flowing blood	Dark (spin washout)	Bright (inflow enhancement)	Bright (T2/T1 contrast)

bSSFP- balanced steady state free precession; TE-echo time; TR- repetition time; †depends on flip angle. Reproduced with permission from Ridgway 2010.

3.3. CARDIOVASCULAR MAGNETIC RESONANCE

3.3.1. Synchronising with the cardiac cycle

For routine CMR, cardiac synchronization with the electrical activity is required for both pulse sequence and signal acquisition. ECG monitoring can be achieved by application of MR compatible electrodes. The ECG tracing is transmitted by a wireless system to the CMR console for processing. Computer software is programmed to detect the R wave of the QRS complex, which marks the electrical systole and the beginning of the cardiac cycle [Lanzer 1985]. Based on the ECG information, images of the beating heart can either be obtained at a

single time point (still imaging) or at multiple time points throughout the cardiac cycle (cine imaging) [Ridgway 2010].

3.3.2. Dealing with respiratory motion

Besides the intrinsic cardiac motion, CMR has to deal with the external cardiac motion that occurs during the respiratory cycle. Respiratory gating techniques were designed to address the respiratory motion. Continuous rf pulses track the position of the diaphragm relative to the chest in the respiratory cycle. Image acquisition is then set up for a stable moment of the respiratory cycle (usually end-expiration), and only data in the specified image window is processed for image formation [Ridgway 2010]. Respiratory gating was originally used for conventional sequences lasting several minutes. Nowadays it is only used for high-definition coronary angiograms, since conventional pulse sequences have largely been abandoned in favour of fast imaging techniques, which will be discussed below. Fast imaging has mitigated respiratory motion artefacts as most images are now acquired within a single breath-hold.

3.3.3. Fast imaging techniques

Conventional pulse sequences only acquire one line of k-space per TR. As a result, it will take several minutes to acquire a single SE image dataset or a single GE cine dataset. To overcome this limitation, fast pulse sequences were designed to acquire several lines of k-space per TR, thus reducing significantly the imaging acquisition times [Reeder 2000]. Other methods exploring the particular geometry of the k-space have also been developed to shorten the acquisition times. Since the k-space is symmetrical, filling just over one half of the k-space is possible without any significant loss of information [Plein 2001, Lee 2002]. More refined methods such as parallel imaging techniques explore the geometrical arrangement of multi-

array receiver coils to compensate the undersampling of the k-space [van der Brink 2003, Glockner 2005]. The introduction of fast imaging was an important landmark in the history of CMR, as image datasets previously taking minutes now only need seconds to acquire [Edelman 1990]. Further refinements have allowed the possibility of single-shot imaging (one image acquired per heart beat), or even real time cine imaging (though at the expense of temporal and spatial resolution) [Setser 2000].

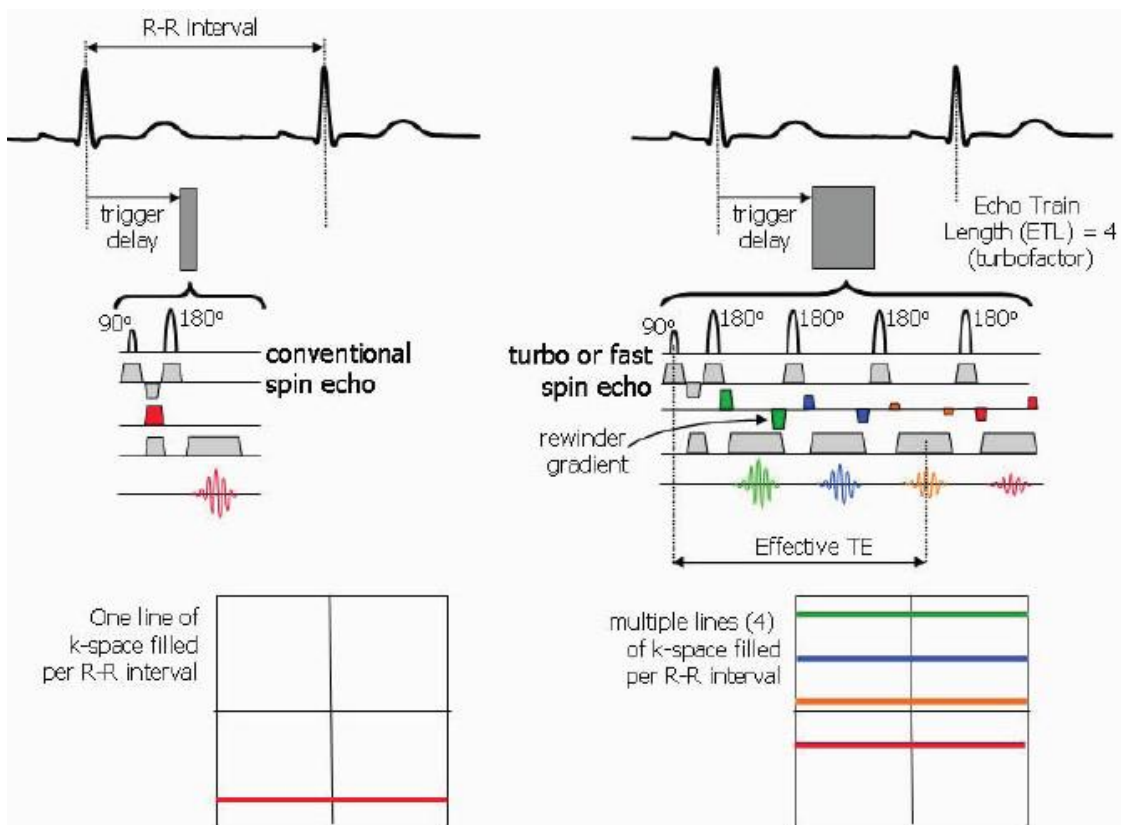


Figure 3.11. Conventional spin echo vs. fast spin echo. Conventional spin echo sequence (left) only applies a single 180° to generate a single spin echo and a single line of k-space per R-R interval. Fast spin echo pulse sequence (right) applies multiple 180° pulses following the 90° pulse to generate multiple spin echoes. In this example, four 180° pulses are applied to generate four spin echoes (echo train length or turbofactor = 4), resulting in a four-fold acceleration in scan time. Reproduced with permission from Ridgway 2010.

3.3.4. Fast spin echo

As mentioned before, conventional SE sequences only acquire one SE and one line of k-space per repetition time. Fast SE sequences [Henning 1986, Listerud 1992] generate multiple echoes by applying multiple 180° pulses after the initial 90° pulse (figure 3.11). Each time a SE becomes de-phased, a further 180° refocusing pulse is applied, generating a further SE. Each formed echo is used to fill a new line of k-space by applying a different amount of phase encoding to each echo prior to data sampling (figure 3.11) [Ridgway 2010]. The number of echoes acquired per excitation pulse is known as the echo train length. Typically echo train lengths of 16 to 64 are used, resulting in a 16 to 64 fold acceleration in scan time, which will usually fall within a breath-hold period. Fast spin echo is today the standard pulse sequence for anatomical imaging [Ridgway 2010].

3.3.5. Cine imaging

Cine imaging can be accomplished by using GE pulse sequences with very short repetition times. It involves data acquisition at multiple time points, known as cardiac phases, throughout the cardiac cycle [Ridgway 2010]. Data acquired within each cardiac phase fill a separate k-space, resulting in the reconstruction of a separate image corresponding to a separate cardiac phase. The combined images can then be displayed as a movie, thus enabling functional assessment of the heart [Ridgway 2010].

For retrospective ECG gating, the traditional method used for cine imaging, data are acquired continuously over several heart beats. Synchronisation pulses are recorded when coincident with the R-wave. The MR signal data from this and subsequent repetitions are then allocated to the corresponding time points in the cardiac cycle at the end of the entire k-space acquisition (figure 3.12) [Lenz 1989]. The use of retrospective gating is essential for applications such as valve and flow imaging.

While retrospective gating is the preferred acquisition modality since the entire cardiac cycle can be displayed in a continuous cine loop, image quality can be significantly degraded in the presence of arrhythmias. Prospective ECG triggering is used to commence data acquisition immediately after the QRS complex. Data is acquired for multiple consecutive cardiac phases until nearly at the end of the cardiac cycle. Data acquisition is then stopped until the synchronisation pulse from the next R-wave is received. The consequence is that there is a 'blind spot' where no data is acquired at the end of the cardiac cycle while the system waits for the next trigger pulse (figure 3.12). Prospective gating is useful to reduce artefacts from arrhythmias. However, this approach is limited when imaging of late diastole is important.

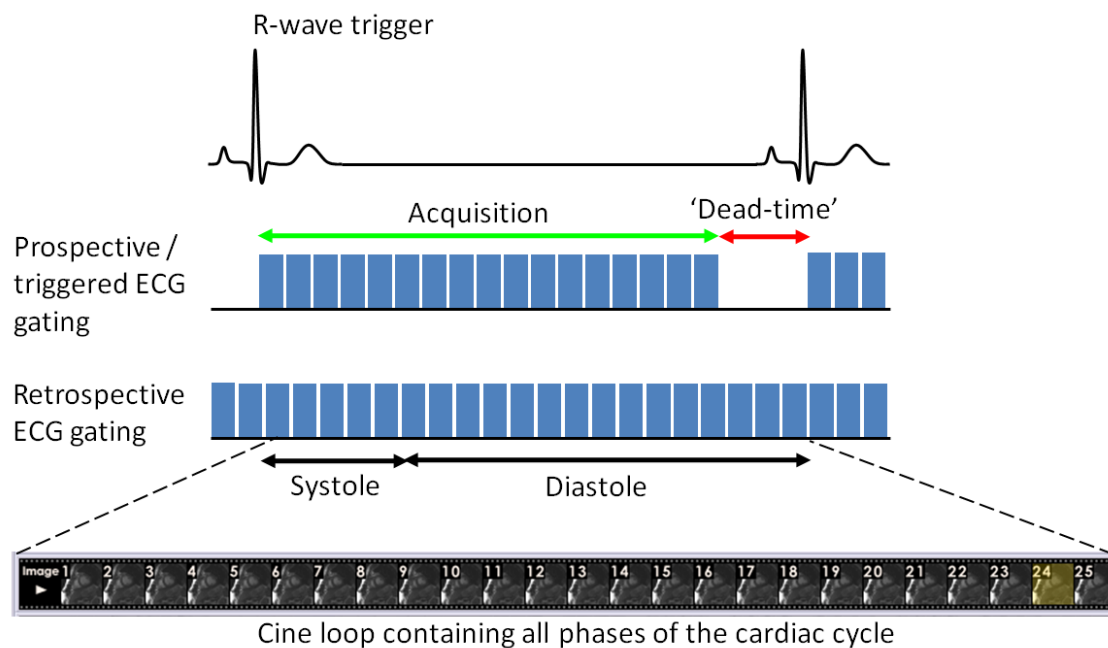


Figure 3.12. Cine imaging. Data divided into cardiac phases (blue blocks) to form individual images (bottom row). In retrospective gating, there is continuous data acquisition prior to allocation into cardiac phases. In prospective gating, data acquisition commences at the R-wave trigger and ends before the end of the cardiac cycle. Courtesy of Dr John-Paul Carpenter.

3.3.6. Perfusion imaging

Myocardial perfusion imaging is routinely used in coronary artery disease to assess the blood flow in the myocardium [Manning 1991]. It requires ultra fast imaging techniques able to acquire several images of the myocardium (usually 3-5 short-axis slices) per cardiac cycle while a gadolinium based contrast agent transits through the coronary arteries (figure 3.13).

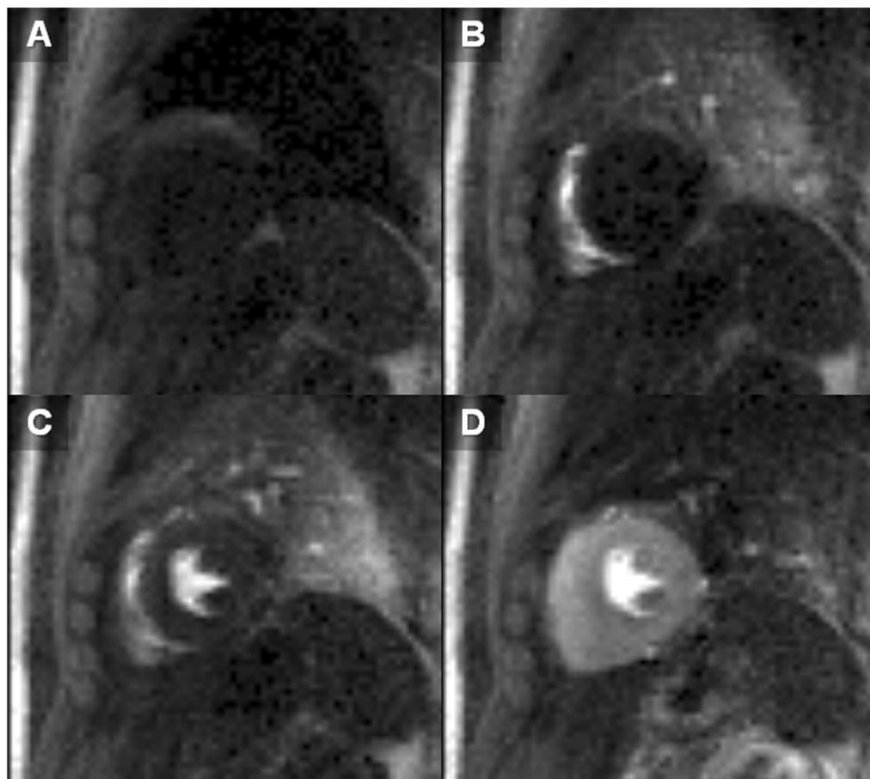


Figure 3.13. Sequential perfusion images. Continuous images of the heart after contrast injection in a peripheral vein. The saturation prepulse minimises the signal from the region of interest at mid-ventricular level (panel A). Contrast bolus circulates in the right ventricle and pulmonary vessels (panel B), before arriving to the left ventricle (panel C) and coronary arteries (panel D). The myocardial signal enhancement is fairly homogenous, suggesting balanced circulation and absence of significant coronary artery disease.

The single shot images are usually presented as a movie where the resulting myocardial signal correlates with the coronary blood flow and gadolinium concentration in the myocardium.

Regional imbalances in contrast concentration under maximal pharmacological dilatation may reveal areas of hypoperfusion indicating myocardial ischaemia. The sequences normally employed for perfusion images are based on spoiled gradient echo, balanced steady state free precession, and hybrid-echo planar imaging (efficient method of filling k-space via a combination of radiofrequency pulses and gradients). T1-weighting and a saturation recovery preparation pulse (for signal reduction of the background tissue) are necessary to maximise the effect of the contrast agent [Kellman 2007, Biglands 2012].

3.3.7. Angiography

Vessel imaging is another common indication for CMR. As opposed to the previously described techniques which rely on acquisition of single slices to form 2D images, magnetic resonance angiography (MRA) involves acquisition of a volume to acquire 3D images. Three-dimensional acquisition is more suitable for vessel imaging because of the high isotropic spatial resolution, but it comes at the expense of more information and longer acquisition times. MRA can either be performed with or without contrast agents.

Contrast-enhanced magnetic resonance angiography (CE-MRA) is the most frequently used technique to delineate the lumen of the blood vessels. The standard pulse sequence for CE-MRA is a spoiled GE with extremely short TR and TE for fast acquisition and T1 weighting [Biglands 2012]. A bolus of gadolinium based contrast agent is injected and the angiogram is acquired during the first passage of the bolus through the vessels of interest [Prince 1993, Sivananthan 1993]. The vessels of interest will appear as bright structures in the angiogram, as the strong T1 weighting yields high contrast between the blood containing gadolinium and the surrounding tissues. The very short TR also results in saturation of the background tissue signal, which significantly improves the quality of the angiograms [Biglands 2012].

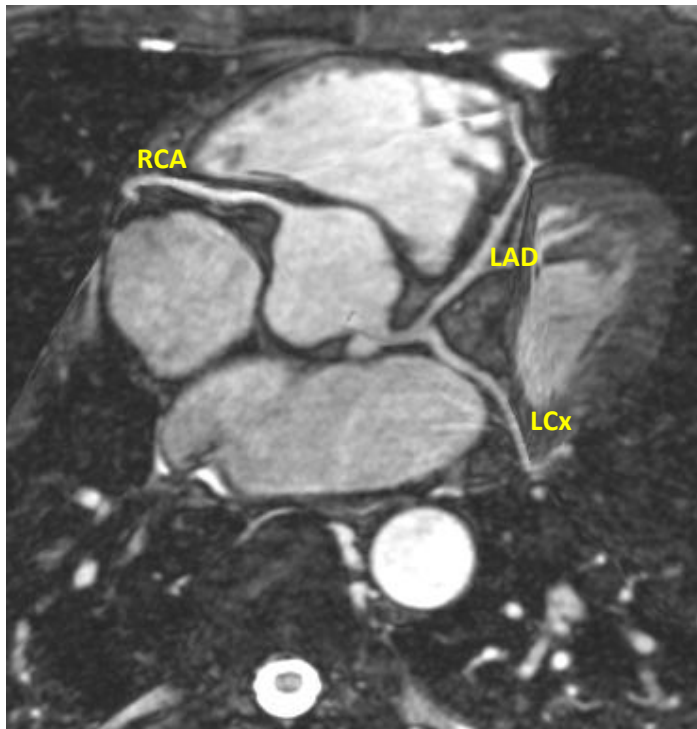


Figure 3.14. Three-dimensional steady state free precession coronary angiogram.

The example is of a curvilinear planar reconstruction showing normal origin and course of the main coronary arteries. LAD- left anterior descending artery; LCx- left circumflex artery; RCA- right coronary artery. Courtesy of Dr Jennifer Keegan.

Despite the fast acquisition times, CE-MRA is not suitable to assess the coronary arteries due to the cardiac motion artefacts. Visualization of the small and tortuous coronary arteries is only accomplished by high-resolution 3D SSFP sequences that acquire information of the entire heart and coronary vessels [Weber 2003]. Because of the long acquisition time, breath-hold acquisitions are not possible. Respiratory motion is therefore compensated by respiratory navigators, while the influence of cardiac motion is minimised by synchronizing the ECG with mid diastole [Biglands 2012]. Two preparation pulses are used to optimize contrast: a frequency selective fat suppression pulse aimed to remove the fat signal surrounding the coronary arteries; a T2 preparation pulse to suppress signal from the venous blood and the myocardium as their T2 relaxation values are shorter than the arterial blood (figure 3.14) [Stuber 1999, Botnar 1999]. Three-dimensional SSFP angiogram does not require gadolinium based contrast agents, and has been increasingly used outside the heart when there is a contra-indication to gadolinium.

3.4. CLINICAL APPLICATIONS OF CARDIOVASCULAR MAGNETIC RESONANCE

In the physics section, several properties of MRI were described: 1) MR signal can be spatially localised to any part of the body; 2) Gradients operating in all three-dimensions render image acquisition in any plane or position; 3) Multiple sequences can elicit different tissue properties. These features underline the versatility of CMR for the anatomical and functional assessment of the heart and great vessels. This section encompasses a basic description of the wide and ever increasing range of applications of CMR. A more comprehensive CMR review can be found elsewhere [Pennell 2010].

3.4.1. Volumes and function

Evaluation of ventricular volumes and mass has major implications for the diagnosis, prognosis, and management of cardiac conditions. CMR is frequently used for this purpose, since its measurements have shown to be accurate in post-mortem studies [Rehr 1985, Jauhiainen 1998, Lorenz 1999, Heusch 1999], and reproducible when compared to the other imaging techniques [Grothues 2002, Grothues 2004]. CMR is actually the most reliable method for volume assessment, and is frequently used as the benchmark for validation of other imaging modalities [Hoffmann 2005]. Thus, CMR can provide valuable information when the results of other imaging modalities are conflicting or inconclusive. In addition, changes over time are more robustly detected and clinical decisions can be taken more confidently. The intrinsic low variability heralds a considerable advantage in research, where smaller sample sizes can be used to achieve statistical significance, saving time on recruitment and reducing costs accordingly [Bellenger 2000]. Ejection fraction (derived from the end-diastolic and end-systolic volumes) is the parameter measured by CMR to assess systolic function.

Diastolic function can be also assessed by CMR, but is not usually performed as echocardiography remains the preferred approach [Paelinck 2002, Rathil 2008].

3.4.2. Coronary artery disease

Coronary artery disease (CAD) is the commonest cause of cardiac disease. CMR is established in the evaluation of ischaemia, infarction and viability, which will be detailed below. CMR can also detect myocardial infarct complications such as extension to the RV, ventricular thrombi, and differentiate aneurysms from pseudoaneurysms. However, coronary angiography by CMR is not recommended for the evaluation of coronary artery stenosis, and its role is limited to the diagnosis of congenital coronary artery anomalies.

3.4.2.1. Myocardial Ischaemia - Stress CMR

CMR evaluates ischaemia either by assessing regional function with inotropes like dobutamine or by assessing first pass perfusion with vasodilators like adenosine. Dobutamine stress CMR is well validated for identifying ischaemia induced wall motion abnormalities in CAD [Nandalur 2007]. Diagnostic results are excellent and superior to dobutamine stress echocardiography [Nagel 1999], providing an attractive alternative to echocardiography when the acoustic window is poor. The prognostic role of dobutamine CMR has also been defined [Jahnke 2007a].

3.4.2.2. Myocardial Ischaemia - Perfusion CMR

First-pass myocardial perfusion is the most popular CMR method for evaluating myocardial ischaemia (figure 3.15). Diagnostic accuracy has been validated against the anatomical standard X-ray angiography [Hamon 2010], and the functional significance has been correlated with fractional flow reserve, the new reference for haemodynamic assessment of coronary stenosis [Rieber 2006, Watkins 2009, Lockie 2011]. Recent comparative studies have

suggested superiority of perfusion CMR over the established SPECT techniques [Schwitter 2008, Greenwood 2012, Schwitter 2012a, Schwitter 2012b]. The use of perfusion CMR is therefore expected to rise in the future, not only due to the superior results, but also because CMR is safer and more comprehensive than SPECT. Perfusion CMR also yields prognostic information, which is useful for risk stratification of patients with suspected or confirmed CAD [Ingkanisorn 2006, Jahnke 2007a].

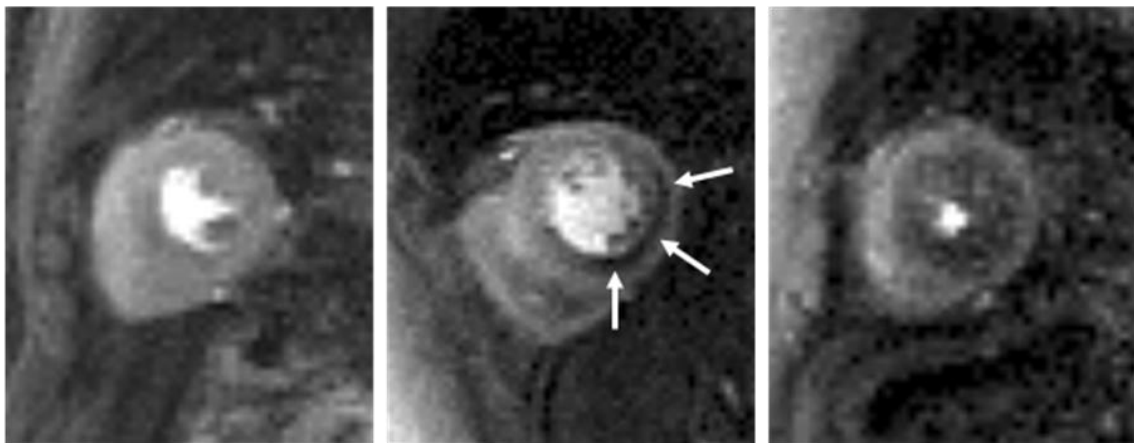


Figure 3.15. Adenosine stress first-pass perfusion. Left panel, Homogeneous signal enhancement of the LV indicating normal perfusion. Middle panel, Inducible perfusion defect in the inferior walls (arrows) suggesting ischaemia in the right coronary artery territory. Right panel, Widespread circumferential inducible perfusion defect of the subendocardium and mesocardium typical of hypertrophic cardiomyopathy.

3.4.2.3. Infarction and viability

Myocardial infarctions (MIs) depicted by gadolinium-enhanced CMR show a remarkable correlation with histological findings due to the high spatial resolution and contrast-to-noise ratio (figure 3.16) [Kim 1999, Wagner 2003]. CMR has been shown to identify small MIs even when wall motion and perfusion by nuclear imaging is normal (figure 3.16) [Wagner 2003, Klein 2002, Ibrahim 2007]. This has important implications, because the presence of a MI,

whatever its size, is a strong and independent prognosticator in CAD [Kwong 2006]. Hence the superior resolution makes CMR the best technique in discriminating viable from non-viable myocardium. Myocardial viability estimated by CMR became a simple and effective way to predict recovery of function following acute MI and after revascularization [Kim 2000, Beek 2003]. The likelihood of functional recovery appears better discriminated by CMR when compared to nuclear imaging techniques [Gutberlet 2005, Kühl 2006].

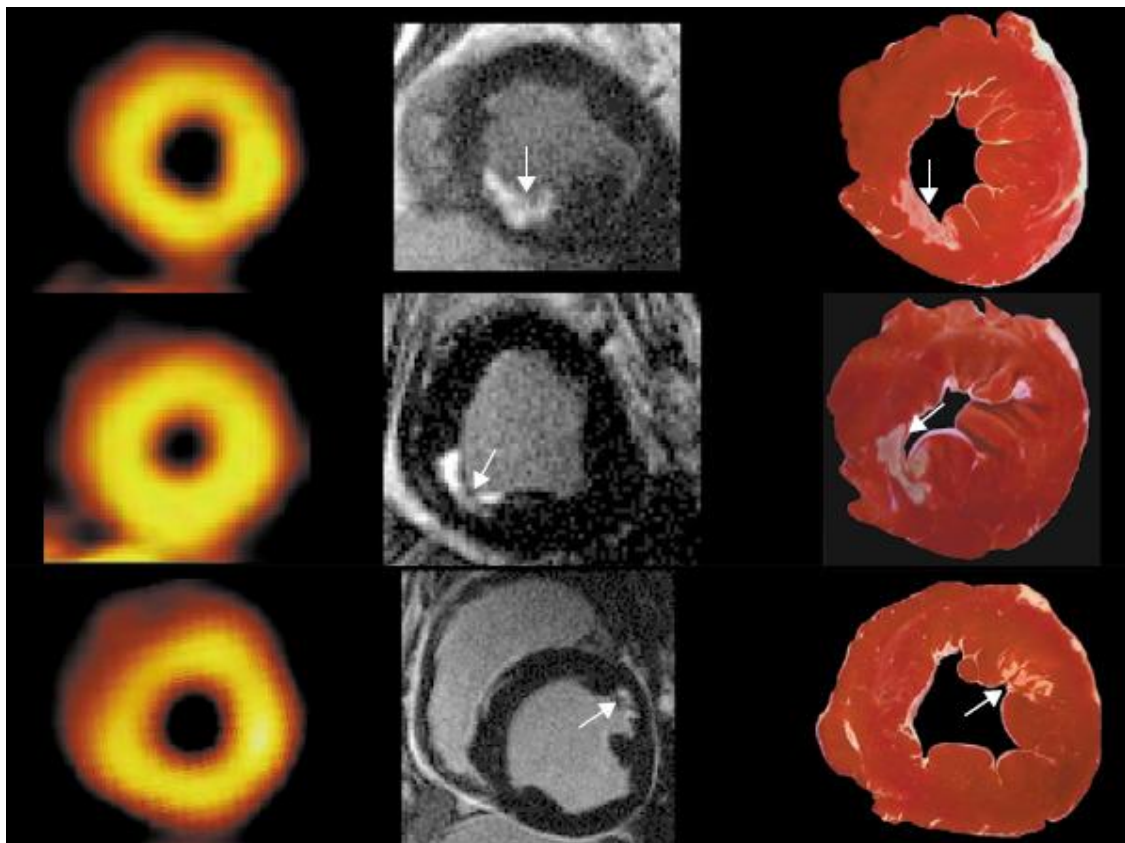


Figure 3.16. Comparison of 99mTc-sestamibi SPECT (left panel), contrast-enhanced CMR (middle panel), and histological specimens (right) in animal models with myocardial infarction. In these examples, CMR is able to visualise small infarcts (arrows) confirmed by histology which were undetected by SPECT. Reproduced with permission from Wagner 2003.

3.4.2.4. Right ventricular infarction

Extension of MI to the RV portends a significant increase in hospital mortality [Zehender 1993, Bueno 1997]. Like in the LV, RV myocardial infarction (RVMI) is more easily detected by CMR than by conventional diagnostic techniques [Kumar 2006]. In addition, the presence of RVMI by CMR is a sign of irreversible injury and persistent RV dysfunction [Kumar 2006, Masci 2010]. These findings may be useful for risk stratification because both the extent of RVMI and RV dysfunction measured by CMR have shown to independently predict adverse events in patients presenting with MI [Larose 2007, Miszalski-Jamka 2010, Grothoff 2012].

3.4.2.5. Coronary arteries

Imaging of the coronary arteries is one of the greatest challenges for CMR due to their small size and constant motion throughout the cardiac and respiratory cycles. Despite the promising results for the detection of CAD published over a decade ago [Kim 2001], this technique is still limited by the low resolution and high propensity to motion artefacts due to the long acquisition times when compared to the standard X-ray angiography [Sakuma 2006, Kato 2010], or even non-invasive CT angiography [Hamdan 2011]. Thus, the role of radiation free CMR coronary angiography is currently limited to the assessment of congenital coronary anomalies and coronary aneurysms [Chiribiri 2011].

3.4.3. Cardiomyopathies

Cardiomyopathies are a heterogeneous group of diseases of the myocardium associated with architectural abnormalities and mechanical dysfunction. Our understanding of these diseases has been facilitated by the use of CMR with late gadolinium enhancement (LGE), which correlates with histological findings and thus permits in vivo characterization of the myocardium. Hence, CMR is frequently used in the diagnostic evaluation of heart failure

[McCrohon 2003, Casolo 2006], and in the characterization of specific types of cardiomyopathies [Mahrholdt 2005], which will be briefly described below.

3.4.3.1. Dilated cardiomyopathy

Dilated cardiomyopathy (DCM) is defined as dilatation and dysfunction of the LV due to primary myocardial disease. CMR offers reliable diagnosis of increased ventricular volumes and reduced ejection fraction which can be normalized to body surface area, gender and age. Mid-wall fibrosis, present in up to 30% of DCM patients [McCrohon 2003], is a predictor of adverse outcomes, and independent of more conventional risk markers such as LVEF [Assomull 2006, Wu 2008]. RV involvement is also present in about 30% of patients and has been associated with worse outcomes in recent CMR studies (Bourantas 2011, Gulati et al, submitted data).

3.4.3.2. Myocarditis

Diagnosis of myocarditis can be challenging as symptoms, ECG changes and troponin rises are variable and often non-specific. LGE demonstrating areas of myocardial injury can be seen in up to 95% of cases confirmed by histopathology [Mahrholdt 2004]. Characteristic patterns of LGE affect the septal mid-wall and subepicardial lateral wall. LGE also appears to predict adverse remodelling and long term outcomes after an acute episode of myocarditis [Mahrholdt 2006, Grün 2012].

3.4.3.3. Hypertrophic Cardiomyopathy

Hypertrophic cardiomyopathy (HCM) is thought to be the commonest inherited cardiomyopathy with a prevalence of 1/500 individuals. CMR is helpful in confirming or excluding HCM, especially in the apical and lateral walls, which are often poorly visualized by echocardiography [Moon 2004, Rickers 2005]. Although the LV is predominantly affected, involvement of the RV is present in one-third of patients, and useful to establish a final

diagnosis [Maron 2007]. The presence of patchy mid-wall LGE and widespread perfusion defects are typical of HCM, helping to differentiate from other forms of left ventricular hypertrophy (figure 3.15 and 3.17) [Petersen 2007]. LGE is present in about two-thirds of HCM patients, and has been associated with risk factors for sudden cardiac death, adverse remodelling and outcomes [Moon 2003a, Adabag 2008, O'Hanlon 2010]. LV mass index appears to be a more sensitive indicator of risk of death than peak wall thickness [Olivotto 2008], and may be used in the future as a potential prognostic marker.

3.4.3.4. Arrhythmogenic right ventricular cardiomyopathy (ARVC)

ARVC is one of the commonest causes of sudden cardiac death in the young [Basso 2009]. CMR is useful in the diagnosis of ARVC due to the superior depiction of the right ventricle [Sen-Chowdhry 2004]. The possibility of tissue characterization allows detection of fibro-fatty replacement, which is the histological hallmark of this condition [Tandri 2003, Tandri 2005]. Diagnosis accuracy appears to be high, especially when genotypic evaluation is available [Sen-Chowdhry 2006]. Although this condition is traditionally associated with the RV involvement, recent CMR studies have documented phenotypes with biventricular and predominant LV involvement [Sen-Chowdhry 2007, Sen-Chowdhry 2008]. Hence, CMR is an important modality in the assessment of ARVC and should be considered in all patients presenting with tachyarrhythmias of RV origin.

3.4.3.5. Secondary Cardiomyopathies

The heart can be affected by a number of systemic conditions, such as sarcoidosis, amyloidosis, Anderson-Fabry and other metabolic storage disorders, Chagas disease, muscular dystrophies, and iron-overload cardiomyopathy. These patients are usually referred to CMR when there is suspected cardiac involvement, although sometimes these conditions are incidentally diagnosed in the evaluation of unexplained heart failure or left ventricular hypertrophy. LGE imaging is extremely helpful in this setting, where infiltration or fibrosis

depicted by LGE shows good correlation with endomyocardial biopsy [Smedema 2005, Vogelsberg 2008]. Moreover, the presence and extent of LGE is usually associated with more advanced forms of cardiomyopathy [Moon 2003b, Rochitte 2005, Silva 2007]. Thus, LGE can detect the presence of cardiac involvement in these conditions, obviating the need for invasive cardiac biopsies.

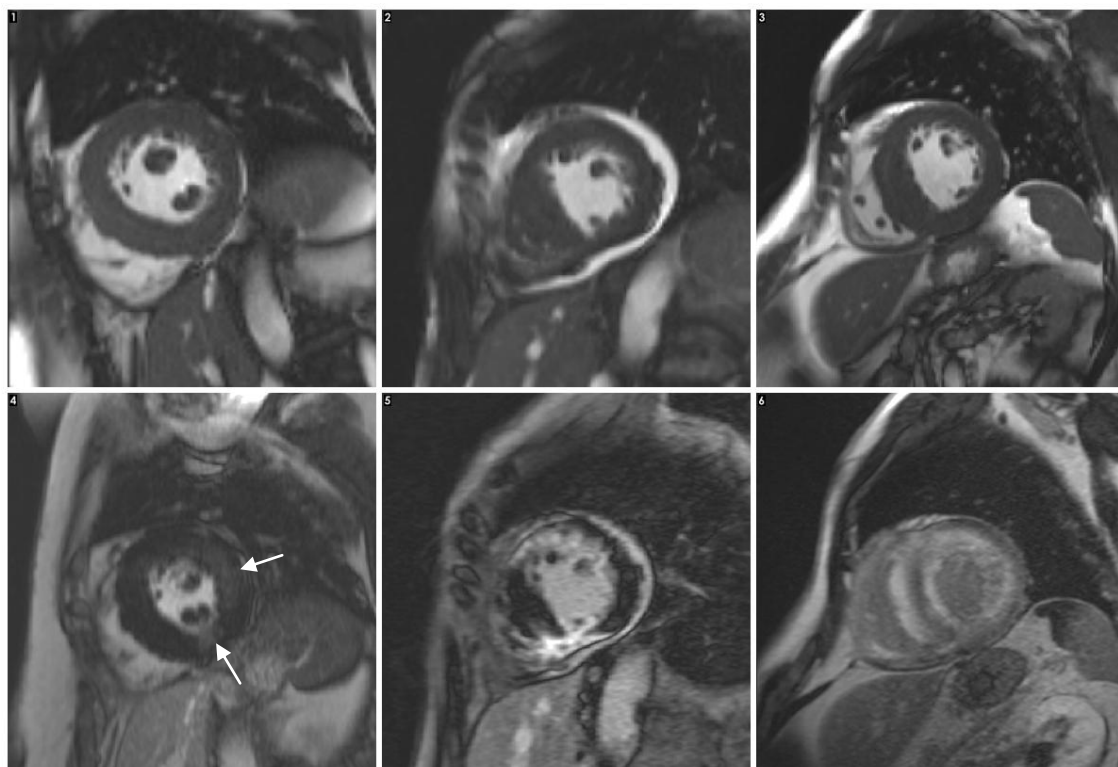


Figure 3.17. Diagnostic evaluation of left ventricular hypertrophy. Top row shows SSFP images, and the bottom row shows LGE images. Left panels, Severe concentric hypertrophy associated with mild LGE in the inferior and lateral walls (consistent with hypertensive heart disease). Middle panels, Severe asymmetrical hypertrophy associated with extensive patchy LGE of the insertions points (typical of hypertrophic cardiomyopathy). Right panels, Severe asymmetrical hypertrophy with diffuse LGE (more pronounced in subendocardium and subepicardium) and dark blood pool (pathognomic of cardiac amyloidosis).

Iron overload cardiomyopathy is the peculiar condition in this group of systemic diseases because diagnosis by CMR is not based on the presence of LGE [Kirk 2011], but rather by documentation of iron deposition in the myocardium. This is possible by assessment of T2* relaxation, which is inversely related to tissue iron concentration [Carpenter 2011]. CMR has the unique ability of investigating iron deposition and ventricular function at the same time [Anderson 2001], and has contributed to the significant decline in mortality from iron-overload cardiomyopathy in the United Kingdom [Modell 2008].

3.4.4. Valvular heart disease

Whilst echocardiography is the first line imaging modality for valve disease, CMR can be an option when transthoracic acoustic windows are poor and a transoesophageal approach is undesirable, or when results of echocardiography and catheterization are conflicting [Cawley 2009]. Direct visualization of all valves and accurate flow measurements, either by volumetric or flow mapping methods, are important components of this technique [Christiansen 2011]. Valve stenosis quantification by planimetry or peak flow velocity is technically possible for all valves. Direct planimetry of the aortic and mitral valves is reproducible and comparable with both echocardiographic and cardiac catheterization estimations [Lin 2004, Kupfahl 2004, Djavidani 2005, Reant 2006]. Assessment of valve regurgitation by flow mapping or planimetry of the regurgitant orifice is feasible and accurate for the aortic and pulmonary valves [Debl 2007, Kilner 2007]. For the mitral and tricuspid valves, regurgitation can be quantified by combining ventricular volumetric analysis with velocity mapping data [Chan 2008, Masci 2008]. Volumetric analysis is considered to be the reference standard, which is extremely useful for the follow-up and management of regurgitant lesions [Maurer 2006]. Although

rarely used for the diagnosis of endocarditis, CMR can be helpful in assessing myocardial extension and to defining surgical intervention.

3.4.5. Pericardial disease

CMR can complement the information given by echocardiography in the evaluation of the pericardium [Dawson 2011]. Pericardial effusions can be easily visualized and differentiated from mediastinal fat or pleural effusions. Moreover, CMR has the advantage of assessing complex or loculated effusions and determining fluid content. Signs of cardiac tamponade, such as chamber collapse or exaggerated respiratory flattening of the ventricular septum, can also be assessed. Pericardial thickening and inflammation can be characterized and quantified for the evaluation of pericarditis [Taylor 2006]. Adherence of the myocardium to the pericardium and signs of ventricular interdependence can be additionally assessed for diagnosis of constrictive pericarditis [Kojima 1999, Giorgi 2003]. The combined use of LGE can differentiate constrictive pericarditis from restrictive cardiomyopathy. CMR can also predict the response to medical therapy in constrictive pericarditis as well as planning for surgical therapy [Feng 2011]. Pericardial cysts are easily recognized and usually preclude the need of an invasive diagnostic procedure.

3.4.6. Congenital heart disease

A growing application of CMR is in congenital heart disease (CHD), which reflects the increasing number of patients surviving into adulthood due to advances in medical care and surgical interventions. CMR is most useful in complex CHD, where echocardiography is limited by the intrinsically abnormal cardiac arrangements and distorted thoracic anatomy. Advantages of CMR over echocardiography include a wider field of view allowing visualization

of all thoracic structures, more accurate ventricular assessment, and more precise flow measurements. CMR is frequently indicated to assess structures not clearly visualized by echocardiography, such as the RV and the pulmonary vessels. Moreover, the pulmonary and aortic flow ratio (Q_p/Q_s) measured by flow mapping can confidently quantify any particular shunt. Patients with CHD often have right-sided cardiac disease, which has a negative impact on long-term outcomes [Warnes 2009]. By determining the severity of the congenital lesions and quantifying their impact on the RV, CMR can be particularly useful in the planning and timing for both palliative and corrective surgical procedures [Therrien 2001, Buechel 2005, Oosterhof 2007].

3.4.7. Cardiac masses

The possibility of 3D imaging and tissue characterization makes CMR one of the most important techniques in the evaluation of suspected or confirmed cardiac masses [Butany 2005, Fieno 2006, Burke 2008]. CMR is particularly helpful in determining the relationship of the mass with adjacent intra-cardiac and extra-cardiac structures. The use of multiple sequences, coupled with the use of gadolinium, provides information on tissue composition, vascularity, necrosis and fibrosis, and may point towards a specific diagnosis, or help with the clinical management [Srichai 2006, Hoffmann 2003, Fussen 2011]. Thus, CMR yields important information for the diagnosis, management, and follow-up of cardiac masses.

3.4.8. Great vessels

CMR is well established for the evaluation of a wide range of vascular diseases. Contrast enhanced magnetic resonance angiography (figure 3.18) can visualize the lumen of the aorta

and major branches [Neimatallah 1999] with similar diagnostic accuracy [Nienaber 1993] and superior cost-effectiveness compared to conventional angiography [Berry 2002].



Figure 3.18. Aortic coarctation. Shaded surface display of contrast-enhanced angiogram of the thoracic aorta showing severe aortic coarctation (red arrow) with extensive collateral circulation (white arrows). Courtesy of Professor Raad Mohiaddin.

Besides angiography, the wide variety of soft tissue contrast available to CMR can be applied to assess features of the vessel wall such as thrombus, hematoma, inflammation, and atherosclerosis [Nienaber 1995, Bogaert 1997, Choe 1999]. Velocity mapping can be used to assess blood flow, providing additional functional information [Cigarroa 1993, Mohiaddin 1994]. The versatility of CMR has made an important imaging modality for the evaluation of the thoracic and abdominal aorta disease, where the lack of radiation or the need of iodinated

contrast agents is an advantage for serial follow-up studies. Angiography of the pulmonary arteries is possible, but does not appear as accurate as CT angiography, especially for the smaller peripheral pulmonary arteries [Gupta 1999]. Of growing interest is pulmonary venous angiography prior to ablation of atrial fibrillation, which combined with evaluation of atrial fibrosis may predict arrhythmia free survival [Peters 2009].

3.4.9. Pulmonary hypertension

This entity comprises a heterogeneous group of conditions leading to increased pulmonary vascular resistance and pulmonary artery pressure [Simonneau 2009]. CMR can be helpful for the diagnosis of some of these conditions, especially those of cardiac origin. Nonetheless, CMR is most used for assessing the consequences of pulmonary hypertension on the RV, since the pulmonary vascular system and the RV work as a functional unit [Champion 2009]. It has been demonstrated that CMR measurements of RV structure and function correlate with disease severity and prognosis of pulmonary hypertension [van Wolferen 2007]. CMR can also monitor response to treatment, as several studies reported the positive effects of medical [Roeleveld 2004, van Wolferen 2006] and surgical therapy [Kasimir 2004, Reesink 2007] on RV structure and function [Bradlow 2012]. Several haemodynamic markers of pulmonary hypertension have been proposed based on flow imaging [Kondo 1992, Mousseau 1999, Reiter 2008, Nogami 2009] and distensibility of the pulmonary arteries [Bogren 1989, Laffon 2001]. However, the lack of validation of these indices hinders CMR in measuring pulmonary artery pressures [Roeleveld 2005], which are routinely assessed by Doppler echocardiography or right heart catheterization.

3.4.10. Limitations

Despite providing the most comprehensive information, CMR is an expensive technique and not readily available in most institutions. Image acquisition is technically challenging and image interpretation requires adequate training. In CMR studies, scans times are relatively long, patients have to lie flat, and monitors or other electronic devices inside the magnet room have to be MR-compatible. Therefore, CMR is not suitable for the very unstable patient and should be avoided in these patients if other studies can give similar information. Claustrophobia can be problematic, but with reassurance and rarely the use of mild sedation, only 1% of patients are unable to tolerate the scan [Francis 2000]. Despite pacemakers and implantable electronic devices being regarded as contra-indications, CMR can potentially be safely performed in experienced centres when appropriate precautions are taken [Nazarian 2006, Naehle 2009]. Nevertheless, a new generation of electronic devices has been specifically designed to be MR-compatible, as a result of the growing need for MRI scans. With the possible exception of intracerebral devices, metallic implants are usually safe. Further information on safety can be found in specific statements [Levine 2007] or in dedicated websites (e.g. www.mrisafety.com). Finally, in patients with end-stage renal failure, gadolinium based contrast agents should be used with caution due to the potential risk of nephrogenic systemic fibrosis [Perazella 2008], although this has been greatly mitigated by the advent of the more stable contrast agents using cyclic chelation molecules.

3.4.11. Conclusions

CMR currently offers the most comprehensive cardiovascular information of all imaging techniques. Extensive research in the last decade has validated this technique in several clinical settings and supports its use in daily practice. However, lack of availability, medical

training and cost constrains a more widespread use of this technique. Further studies, in particular prospective multi-centre trials, are needed to embrace CMR in routine clinical management. Thus, future challenges for CMR include the development of strategies that will allow health care systems to benefit from the increased diagnostic accuracy, improved risk assessment and therapeutic decision making [Alpendurada 2009a].

CHAPTER 4: METHODS

The methods employed in each published work are summarized in table 4.1. All papers involved calculation of RV volumes and ejection fraction. RV mass was also calculated in two papers on thalassaemia major (TM). These parameters were compared with LV volumes, ejection fraction and mass in most papers. More specific sequences were used in addition to the information provided by the standard steady state free precession cine images. Phase contrast gradient echo sequences allowed flow quantification in Marfan syndrome. T2* gradient echo images were used to determine iron concentration in TM. Finally, contrast imaging with gadolinium was acquired to assess myocardial fibrosis and infarction in the Marfan and CRT populations. General considerations about the methods used are discussed below. More detailed descriptions (including study design and statistical analysis) can be found in the published articles from chapters 5 to 9.

Table 4.1. Methods used in the works according to pathology.

	Marfan	TM	CRT
Volumes	X	X	X
Flows	X		
T2*		X	
LGE	X		X

TM- thalassaemia major; CRT- cardiac resynchronization therapy; LGE- late gadolinium enhancement.

4.1. RIGHT VENTRICULAR VOLUMES

Under ideal conditions, RV contractile function would be determined through use of high-fidelity pressure catheters, continuous measurement of RV pressure-volume curves, and manipulation of loading conditions using vasoactive drugs or balloon occluders placed in the vena cavae [Dell'Italia 1988b, Redington 1988]. Because these methods are technically challenging, simpler non-invasive measurements are more commonly employed. Despite providing useful clinical information, these simpler measurements may not directly reflect underlying RV performance and may be misleading in abnormal loading conditions [Greyson 2008].

$$EF = \frac{SV}{EDV} = \frac{EDV-ESV}{EDV}$$

Figure 4.1. Mathematical equation of ejection fraction. Ejection fraction is the volumetric fraction of blood ejected by the ventricle per heart beat. EF- ejection fraction; SV- stroke volume; EDV- end-diastolic volume; ESV- end-systolic volume.

Among all indices of RV function, ejection fraction (EF) is the most established one in the medical community, because its concept is simple, easy to apply, and available to all imaging modalities (figure 4.1). Despite the reported influences by loading conditions, EF has been extensively validated for diagnostic and prognostic purposes [Carabello 2002]. In the available consensus statements, EF is the only specified marker for the diagnosis and classification of heart failure [McMurray 2012], and the only performance marker used for the clinical management of coronary and valvular heart disease [Antman 2008, Bonow 2008, Anderson 2011, McMurray 2012]. It is noteworthy that the EF mentioned in these documents is for the

LV. Conversely, EF of the RV is hardly mentioned in any of the guidelines, even in those where the RV assumes a dominant role, such as in congenital heart and pulmonary vascular disease [Warnes 2008, Galiè 2009, Baumgartner 2010]. This also applies to other markers of RV function, which are not mentioned in the guidelines at all. There are two main reasons why RV measurements are under-represented in the consensus documents. The first reason relates to the lack of validation by large multicentre trials. This is especially true for congenital and pulmonary vascular disease, which comprise uncommon and heterogeneous conditions. Despite the foreseeable challenges in patient recruitment, further studies are still needed to define optimal RV cut-offs for the diagnosis and management of these conditions. The second reason relates to the fact that RV measurements tend to be more variable [Caudron 2012]. As opposed to the elliptical LV, the shape of the RV is much more complex and cannot rely on one- or two-dimensional geometrical assumptions [Pfluger 2010]. In addition, the heavily trabeculated RV myocardium with a relatively thin free wall poses a special challenge for all imaging techniques. For CMR, these limitations are minimised by the 3D visualization of the heart and superior image quality. Thus, CMR is valued as the most accurate and reproducible technique for the assessment of the RV [Longmore 1985, Jauhainen 1998, Mertens 2010]. As CMR scanners are becoming increasingly more available, it is likely that the current and ongoing research will strengthen the use of CMR derived measurements. RV volumes and EF measured by CMR are therefore expected to become more recognized in the guidelines and integrated in the clinical care pathways.

Estimation of ventricular volumes in this thesis comprised acquisition of a contiguous stack of short-axis cines from base to apex. The cine sequence used was the steady state free precession, which permits good temporal and spatial resolution and excellent contrast between the blood and the myocardium. Typical parameters of the cine sequence are presented in table 4.2. Ventricular volumes and mass were determined by planimetry for each

slice and summed for the whole ventricle by using a semi-automated analysis software CMR tools (Cardiovascular Imaging Solution, London, UK), an in-house developed programme (figures 5.1, 7.1, and 9.1). Volume analysis follows three steps. Firstly, both LV and RV epicardial and endocardial borders were delineated in the short-axis slices at end-diastole and end-systole. Then, thresholding of the blood pool was adjusted in order to include the papillary muscles and trabeculations in the ventricular mass calculation. Finally, tracking of the mitral and tricuspid valve planes in both end-diastole and end-systole ensured that any blood signal from atria was excluded from the ventricular volume calculation. Any blood pool signal above the aortic and pulmonary valves was also excluded from the ventricular volume using the endocardial contour definitions. The final results represented the sum of the volumes of each individual slice based on the Simpson's rule, bearing in mind that the myocardial mass was derived from the myocardial volumes multiplied by the density of the myocardium ($\times 1.05\text{g/mL}$). LV and RV parameters were indexed to body surface area (BSA) as determined by the Mosteller formula [Mosteller 1987].

There are some technical considerations that are worth being mentioned, as there is still no consensus on how RV analysis should be performed.

a) Slice thickness

Although the traditional CMR cine images are displayed in 2D pixels, the original signal information is actually made of 3D anisotropic voxels, where the slice thickness is substantially larger than the in-plane dimensions. By increasing the slice thickness, a larger amount of protons will be excited, thereby increasing the signal-to-noise ratio of the 2D image. Typical in-plane diameters were around 2.0-2.5mm in our studies, whereas the slice thickness was about 7mm. The interval between slices was 10mm, meaning that there was a 3mm uncovered gap between the slices. This 7mm slice thickness/3mm slice gap approach was

comparable to 6mm slice thickness/4mm gap and with 7mm slice thickness/no gap protocols for determining volumes, ejection fraction and mass [Hogan 2007]. Thus the 7mm slice thickness/3mm slice gap approach is feasible, with the additional advantage of allowing for a lower number of slice acquisitions and shorter acquisition times. Although the findings of the above study refer to the LV, similar results are expected for the RV.

Newer 3D high resolution data acquisition techniques have the potential to permit full volumetric coverage of the ventricles with high image quality [Greil 2007]. Algorithms have been developed to acquire a single dataset with high 3D isotropic resolution and full biventricular coverage within one breath-hold [Jahnke 2007b]. These new techniques enable accurate assessment of LV and RV parameters when compared to standard multiple breath-hold acquisition, and may be used in the future allowing for significant reductions in scanning acquisition times.

b) Slice orientation

Volume measurement in the short-axis stack can be challenging, especially for the basal slices, where it is difficult to differentiate the atrial from the ventricular borders due to the through plane motion occurring during the cardiac cycle. This is especially true for the RV, where longitudinal motion plays an important role towards RV contraction. It has been suggested that orientating the ventricular acquisition axially [Alfakih 2003, Fratz 2009] or perpendicularly to the long-axis of the RV [Strugnell 2005] would circumvent these problems (figure 4.2) [Bradlow 2012]. Whilst these approaches appear to improve interobserver variability compared with the conventional short-axis planimetry measurements, they have not been adopted more widely. Short-axis acquisition is still more popular because it allows for better assessment of the ventricular wall morphology and regional function. Short-axis

measurements have also been more extensively validated regarding reference values [Maceira 2006, Kawut 2011].

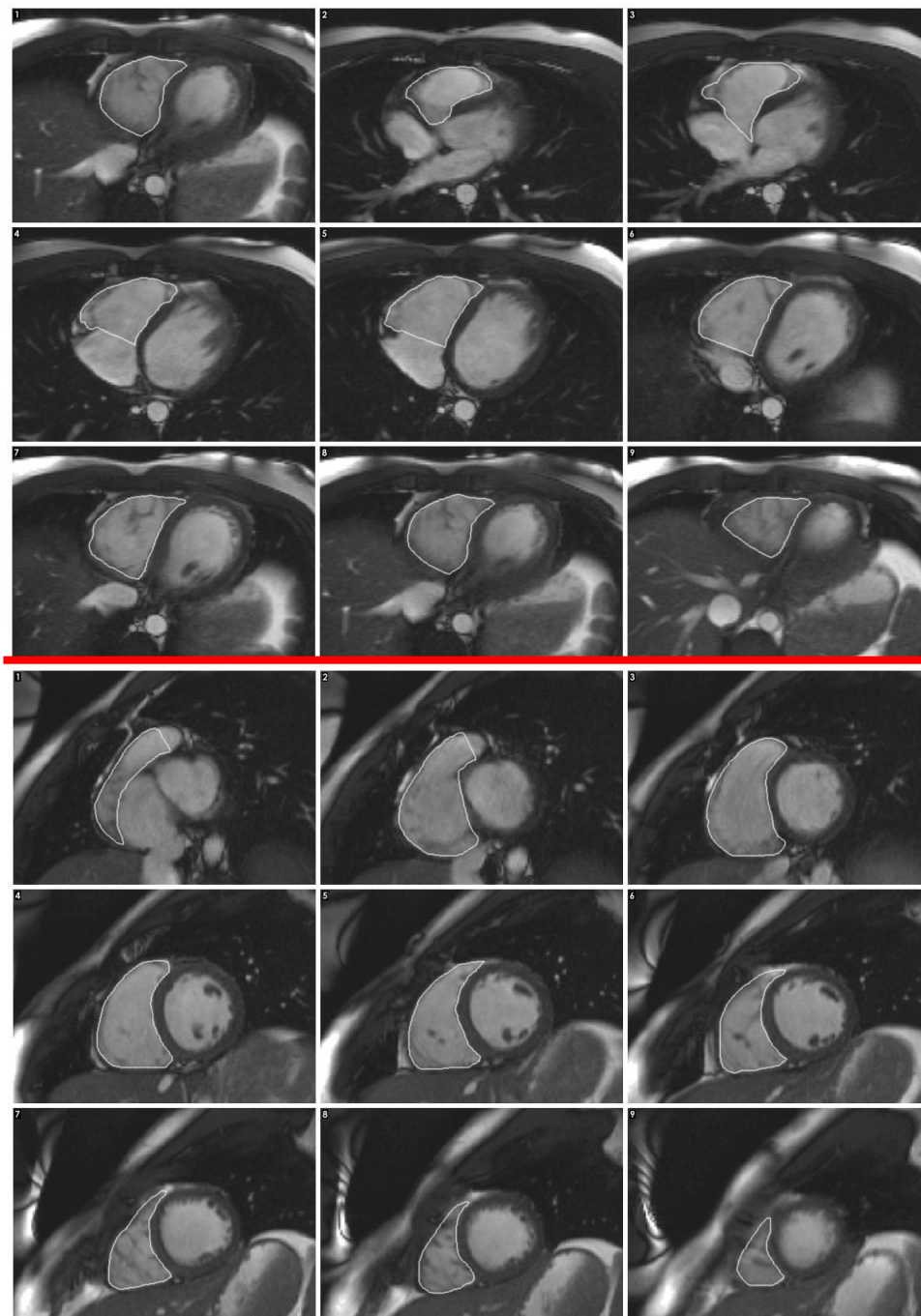


Figure 4.2. Manual planimetry of a normal right ventricle at end-diastole. The top panel shows the trans-axial orientation, while the bottom panel shows the short-axis orientation.

c) Valve plane

Trans-axial acquisition appears more reproducible to the short-axis acquisition because the tricuspid valve can be easily delineated, therefore separating the RA and RV cavities more accurately. This important limitation of the short-axis acquisition can be overcome by defining and tracking the tricuspid and pulmonary valve planes. Commercially available software can delineate the valve planes in the long-axis views, and integrate the spatial information into the volumetric acquisition, thereby excluding the volumes corresponding to the RA, and only obtaining the volumes pertaining to the RV. This is of critical importance for the RV, especially because of its characteristic morphology with a triangular shape and a broad base. Short-axis image acquisition corrected for the valve planes has been shown to have good intraobserver and interobserver variability [Maceira 2006], a finding that was further substantiated by this thesis. Therefore, either the trans-axial or the short-axis approach (preferably with valve correction) can be used for volumetric analysis, as long as the operator is experienced and the method validated.

d) Trabeculations

For volume measurements, there is controversy on whether the trabeculae and papillary muscles should be included in the RV cavity or in the RV myocardium (figure 4.3). This may be relevant for certain conditions where volumes are pivotal to define the optimal surgical timing [Buechel 2005, Oosterhof 2007]. Inclusion of trabeculae in the calculation of RV volumes results in faster analysis and higher volumes, whereas excluding trabeculations results in longer processing times and lower volumes [Winter 2008]. Nonetheless, it is still not known which method is more reproducible as previous publications on the subject showed different results [Winter 2008, Bradlow 2010]. Manual planimetry offers better control over delineation than semi-automated analysis, reflected in improved interobserver reproducibility [Bradlow

2010]. However, it is time consuming and not entirely appropriate in the routine clinical setting [Bradlow 2012].

In our centre, the papillary muscles and trabeculae are included in the total RV mass. However, RV mass is not routinely performed in the clinical setting because measurements can be highly variable [Bradlow 2010]. Combined volumetric assessment is usually performed by semi-automated analysis and takes around 10 minutes to complete.

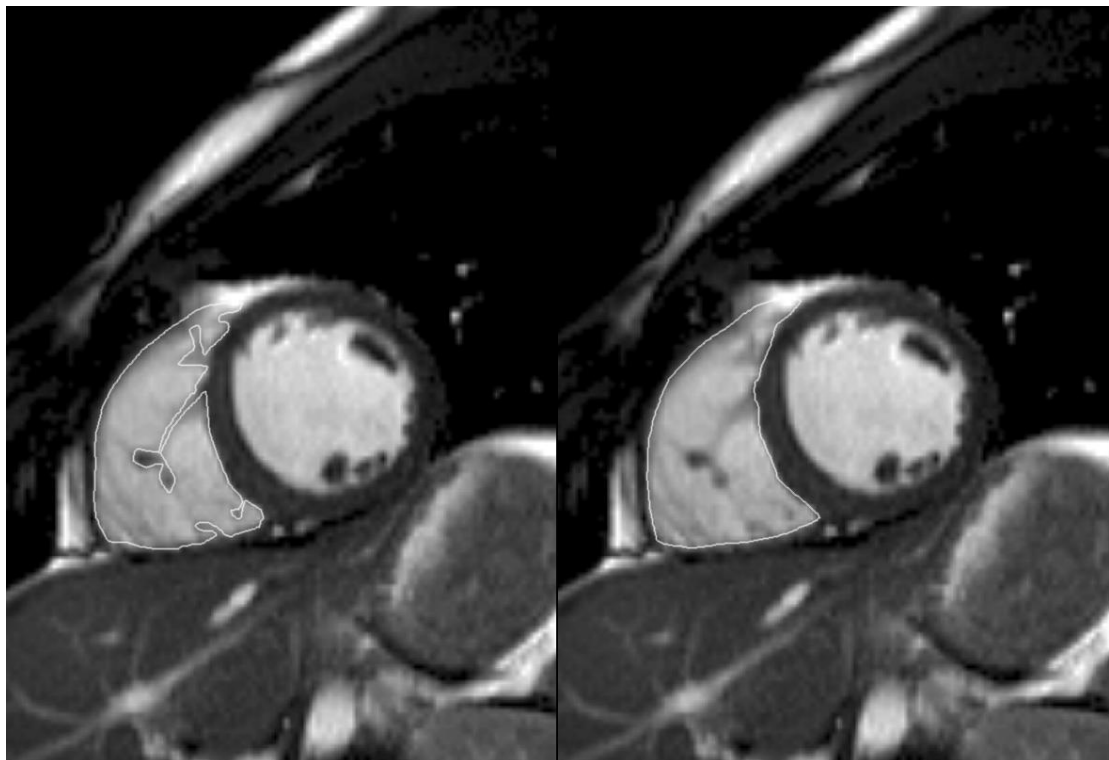


Figure 4.3. Manual planimetry of a normal right ventricle at a mid-ventricular slice. The left panel includes trabeculations, whilst the right panel excludes trabeculations for the final right ventricular volumes.

Table 4.2. Basic properties of the sequences used in the thesis.

	Volumes	Flows	T2*	LGE
Sequence	Steady state free precession	Spoiled gradient echo	Spoiled gradient echo	Spoiled gradient echo
Modifier	-	Opposite gradient pulses in the velocity encoding direction	-	180° inversion recovery prepulse
Field of view read	300-400mm	300-400mm	400mm	300-400mm
Field of view phase	60-75%	60-75%	50-75%	60-75%
TR (ms)	40.2	61.1	101	700
TE (ms)	1.1	3.1	2.6-16.7	3.2
Base resolution	192	256	256	256
Phase resolution	100%	50%	50%	60%
Slice thickness	7mm	6mm	10mm	8mm
Flip angle	70°	25°	35°	20°
Bandwidth, Hz/pixel	930	391	810	230
Phases/cycle	25	25	-	-

4.2. FLOW MEASUREMENTS

Imaging of blood flow within the heart and blood vessels was one of the first MRI developments for the cardiovascular system [Nayler 1986]. Since initial validation and application reports [Firmin 1987, Underwood 1987], flow imaging has evolved over the years owing to improved hardware and software performance, and is now an established application for the evaluation of vascular, valvular and congenital heart disease [Firmin 2010, Myerson 2012].

Velocity imaging is based on a modified spoiled gradient echo sequence with two opposing gradient pulses separated by a time offset. These additional gradients are known as velocity-encoding gradients and are responsible for the phase contrast. For protons in a static tissue, the effects of these two gradients will cancel out each other, and hence the phase of the spins will remain the same. Conversely, if the protons are moving between the velocity-encoding gradients, they will leave a phase shift that is proportional to the velocity along the direction of the applied gradients [Gatehouse 2005]. The resulting image is called velocity-sensitive phase image. A reference phase image is acquired at the same time to remove uncontrolled phase errors due to magnetic field inhomogeneities and to ensure that only velocity phase shifts in the desired direction are detected [Biglands 2012]. Subtracting the reference phase image from the velocity-sensitive phase image makes the phase-contrast velocity image [Gatehouse 2005]. The resulting image acts as a velocity map, where signal intensity of each individual pixel reflects tissue velocity rather than tissue composition. Velocity maps are generally displayed using a grey scale. Stationary tissue will appear as mid-grey pixels (zero-value velocity), with increasing positive velocities appearing as brighter pixels (towards white), and increasing negative velocities appearing as darker pixels (towards black) [Biglands 2012].

Flow measurements by CMR are accurate and extremely reliable because of the consistent image quality and multiplanar acquisition [Kondo 1991]. Image planes can be perfectly aligned with the flows, and the measured velocity can be defined along any desired of the three gradient directions. Flows can be calculated by delineating a region of interest around the lumen of the blood vessel along all frames of the cardiac cycle. Each pixel within the region of interest contains information about the instant velocity at a particular point of the vessel and at a particular time of the cardiac cycle. The sum of the pixels in the dominant signal (positive or negative) will permit calculation of the forward and backward flows. Regurgitant fraction can be estimated by dividing the backward flow by the total forward flow. The output through

a vessel can also be quantified by dividing the net forward flow by the estimated R-R interval used for image acquisition. Finally, flow curves can be displayed by deriving the integral of all the pixel information along the cardiac cycle (figure 4.4).

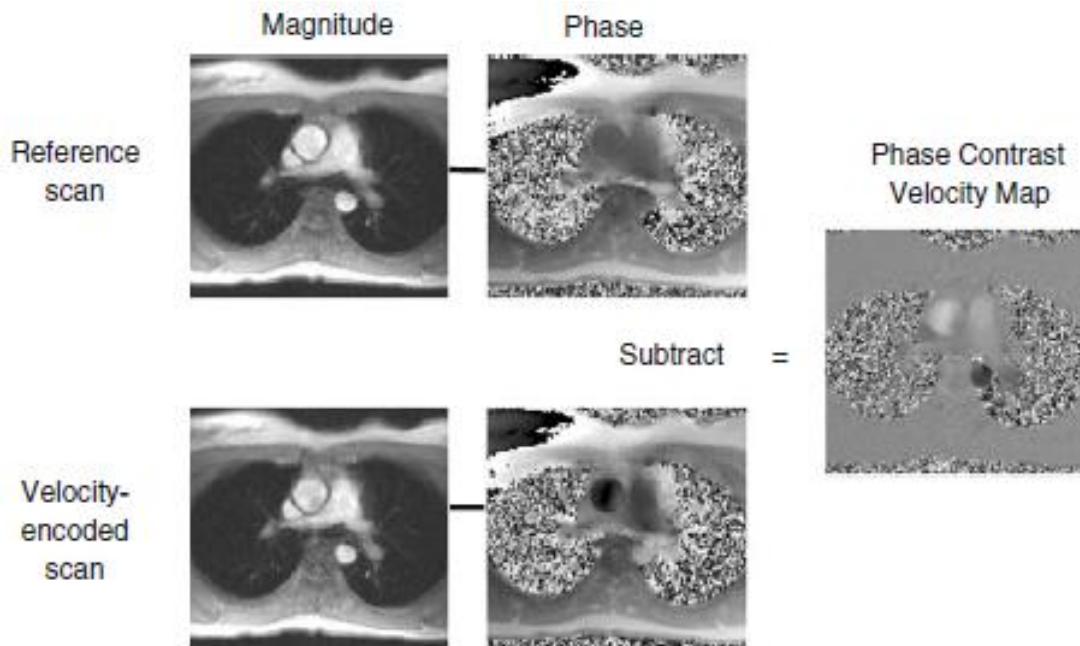


Figure 4.4. Flow imaging acquisition. Magnitude and phase images are reconstructed from the reference scan (top row) and also from the velocity-sensitive scan (bottom row). The phase images are subtracted to make the phase contrast velocity image. Reproduced with permission from Gatehouse 2005.

The basic principles described above about flow image acquisition and quantification have been successfully applied into clinical practice. Phase contrast velocity mapping of volume flow over the great arteries theoretically provides the most accurate measurements of cardiac output [Kilner 2007], shunt flow [Petersen 2002, Colletti 2005], and aortic or pulmonary regurgitation [Rebergen 1993, Gelfand 2006]. Aortic and pulmonary flow data when combined with left and right ventricular volume measurements can estimate the severity of mitral and

tricuspid regurgitation, respectively [Hundley 1995, Kon 2004, Gelfand 2006]. In addition, the peak velocity within the flow column can be measured for quantification of valvular and non-valvular stenoses [Caruthers 2003, Lin 2004].

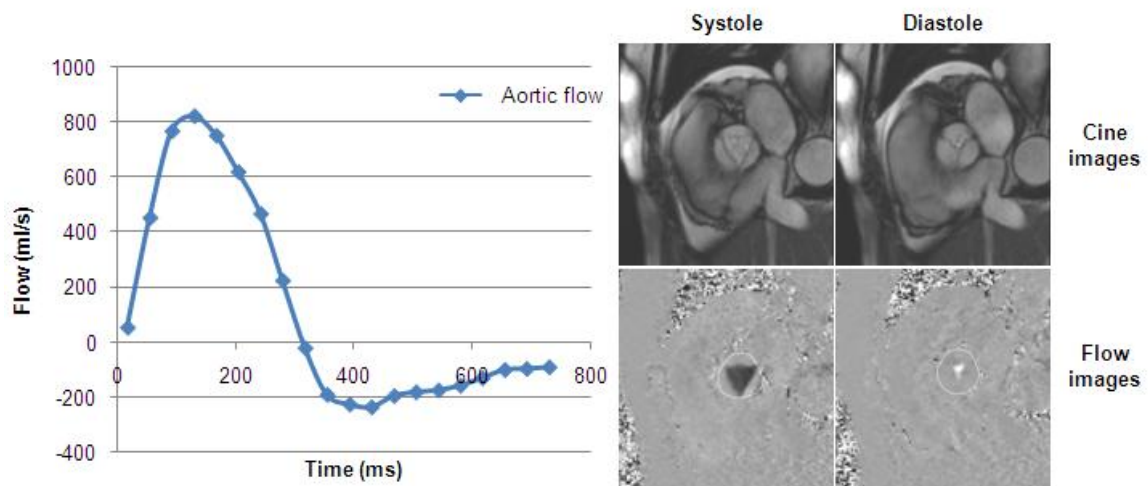


Figure 4.5. Flow imaging of the aortic valve in a patient with aortic regurgitation. Aortic flow curves are derived from flow images. Corresponding cine images in mid-systole and mid-diastole are displayed for reference.

Phase contrast imaging was used to estimate the severity of aortic and mitral regurgitation in the Marfan article. Typical parameters for this sequence are displayed in table 4.2. Aortic regurgitation was quantified from the through plane images over the aortic root close to the level of the sinotubular junction, while mitral regurgitation was quantified from the difference of total LV stroke volume minus the aortic forward flow thus giving the regurgitant volume through the mitral valve [Kilner 2007]. Tricuspid and pulmonary regurgitation were not displayed in the article because there were no cases of significant right-sided valve disease.

4.3. T2* GRADIENT ECHO

The story of the T2* imaging is an extraordinary example on how a limitation in magnetic resonance imaging can turn into a valuable application. To ensure optimal image quality, the magnetic field has to be as homogeneous as possible. Metal implants, such as stents, clips or wires can disrupt the local magnetic fields and produce artefacts. These artefacts depend on the type of metal and pulse sequences used, and can compromise the diagnostic quality of the study. At a microscopic level, metal deposits in tissues can also alter the local magnetic fields and cause signal loss [Stark 1991]. By creating pulse sequences most vulnerable to magnetic susceptibility artefacts, it was hypothesised that iron could be detected in tissues and eventually quantified. This was the rationale behind the development of T2* imaging for the evaluation of iron loading [Anderson 2001]. Ten years on, the substantial evidence collected has established T2* as the technique of choice for assessing iron in the heart [Wood 2009, Carpenter 2011].

T2* relaxation refers to the decay of transverse magnetisation caused by a combination of spin-spin interaction and magnetic field inhomogeneity. This type of relaxation is only seen with gradient echo sequences because transverse relaxation caused by magnetic field inhomogeneities is eliminated by the refocusing pulse on spin echo sequences [Chavhan 2009]. Gradient echo sequences can be made predominantly T2* weighted by using a low flip angle, a long repetition time, and a long echo time [Nitz 1999].

Magnetic field inhomogeneities from susceptibility differences among tissues and materials may occur at macroscopic and microscopic levels. Macroscopic inhomogeneity can be induced by deoxyhaemoglobin in veins, by air-tissue interfaces, and by metallic implants. Causes of microscopic inhomogeneity include paramagnetic contrast agents, blood products, and iron deposits [Chavhan 2009]. Interaction between iron and adjacent protons causes dephasing of transverse magnetisation in iron laden tissues, leading to signal loss on gradient echo images

[Gossuin 2004, Chavhan 2009]. This effect was found to be concentration dependent [Alústiza 2004, Wood 2008]. Thus, $T2^*$ is inversely related to the iron concentration in tissues, with increasing concentrations of iron particles resulting in faster $T2^*$ relaxation times and shorter $T2^*$ values.

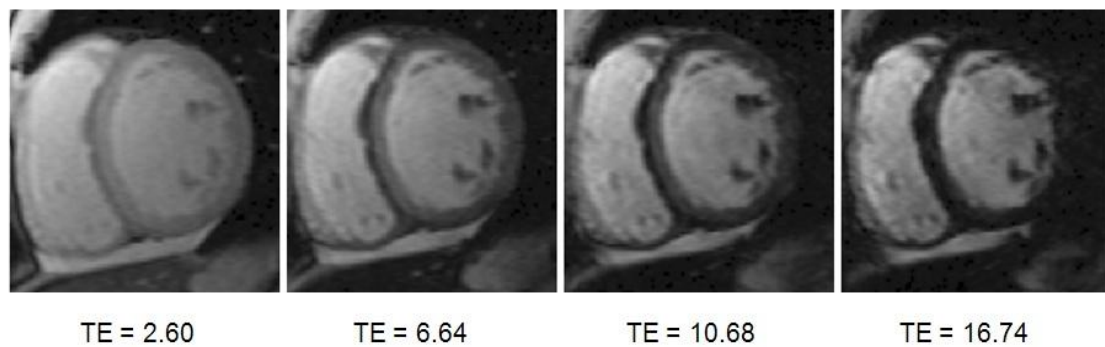


Figure 4.6. Images of a mid-ventricular short-axis slice at increasing echo times (TE) after an initial rf pulse. The myocardium becomes progressively darker as $T2^*$ decay occurs. Courtesy of Dr John-Paul Carpenter.

The original $T2^*$ method for determining iron concentration consisted on the acquisition of several images of the same short-axis slice at different echo times (figure 4.6). The signal intensity of each image would then be plotted against time, generating a curve from which a $T2^*$ value could be calculated (figure 4.7) [Anderson 2001]. $T2^*$ measurements are accurate in determining iron concentrations and have been validated against liver biopsies [Anderson 2001, St Pierre 2005], and animal and human hearts [Wood 2005, Ghugre 2006a]. More recently, $T2^*$ CMR has been calibrated against iron concentration in ex-vivo human hearts [Carpenter 2011].

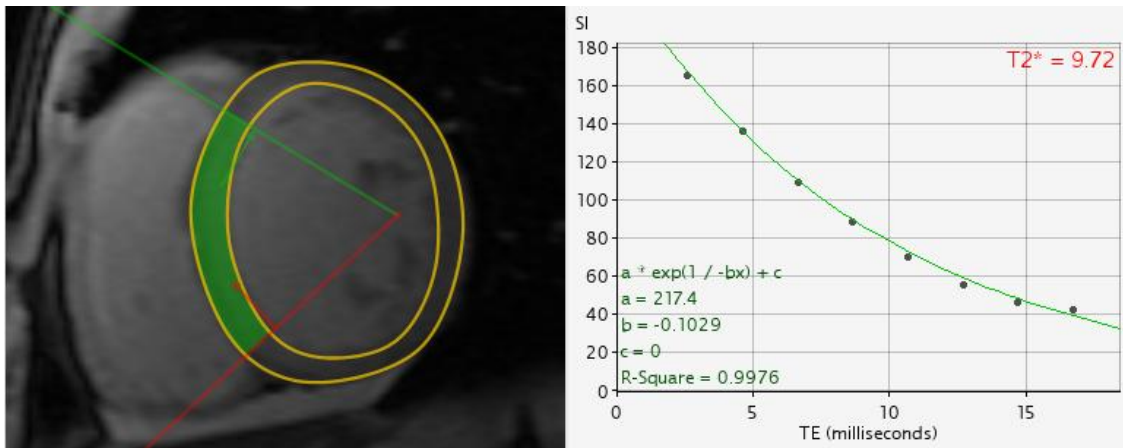


Figure 4.7. T2* calculation. Left panel, An optimal region of interest is chosen in the interventricular septum of a mid-ventricular slice. Right panel, The signal intensity is plotted for each echo time. A mono-exponential trendline is fitted to derive a T2* value of 9.72ms, which indicates severe cardiac iron loading. Courtesy of Dr John-Paul Carpenter.

With the development of newer scanners with faster gradients, refinements to the original method have resulted in a multi-echo sequence able to acquire several images within a single breath-hold [Westwood 2003a]. This new sequence, which is in use today, has significantly reduced the acquisition time as well as minimising motion or position artefacts. T2* has shown to be reliable and robust, demonstrating good intraobserver, interobserver, interstudy and interscanner reproducibility [Westwood 2003a, Westwood 2003b, Tanner 2006, He 2007, Kirk 2010].

From initial experience, the lower limit of normal for myocardial T2* was determined at 20ms. This value was derived from the lower 95% confidence interval for healthy volunteers [Anderson 2001]. Although in retrospect it would have been more appropriate to describe the logarithmic variable T2* as geometric mean and coefficient of variability, the 20ms cut-off is easy to remember and has been adopted worldwide. Values above 20ms thus represent normality, whilst values below 20ms represent myocardial iron loading. With increasing iron

overload, there is an increased risk of complications. A cross-sectional report showed that most patients presenting with heart failure had $T2^*$ values below 10ms [Tanner 2005]. The same value of 10ms was strongly predictive of arrhythmia and heart failure in a subsequent longitudinal study [Kirk 2009]. As a result of these clinical observations, a risk scale has been proposed, with $T2^*$ levels >20 ms indicating low risk, $T2^*$ 10-20 ms indicating intermediate risk, and $T2^*$ levels <10 ms indicating high risk of cardiac complications [Kirk 2009].

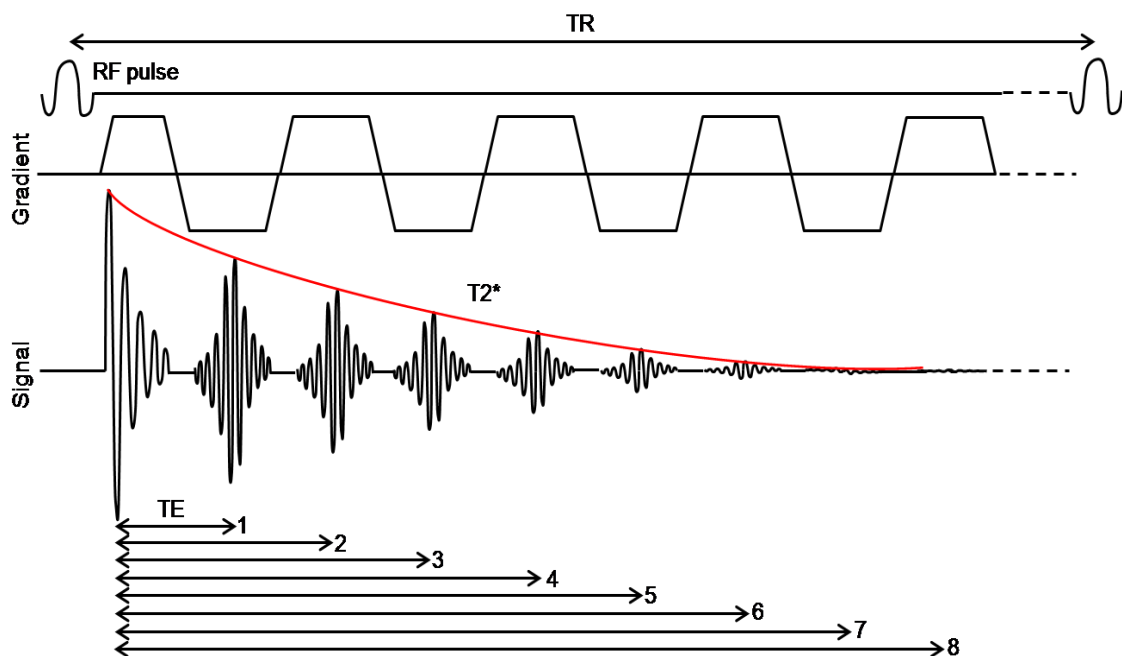


Figure 4.8. Single breath-hold multiecho $T2^*$ sequence. A series of continuous dephasing and rephasing gradients generate a train of multiple echoes. Courtesy of Dr Gill Smith.

The $T2^*$ method used in this thesis was based on the modified single breath-hold spoiled gradient echo sequence with multiple echo times [Westwood 2003a]. A short-axis mid-ventricular slice was acquired immediately after the R wave trigger to minimise blood flow and myocardial motion artefact (table 4.2). This sequence generated a series of eight images with a range of equally spaced echo times from 2.6 to 16.7 ms (figure 4.8) [Westwood 2003a].

From this single breath-hold sequence, a series of images at different echo times after the initial rf pulse was generated. Myocardial $T2^*$ was measured from a full-thickness region of interest in the interventricular septum (routinely chosen to avoid contamination artefacts from the cardiac veins, liver, and lungs). $T2^*$ decay was calculated using a semi-automated analysis software (Thalassaemiatools, Cardiovascular Imaging Solutions, London, UK). For $T2^*$ analysis, the mean signal intensity of each image was plotted against the echo time. The $T2^*$ value was then calculated from the resulting exponential decay curve. To correct for background noise, a truncation method was used as previously described (figure 6.5) [He 2008].

As mentioned above, measurements of myocardial $T2^*$ were restricted to the interventricular septum, as the LV and RV free walls are affected by in vivo artefacts arising from the deoxygenated blood in the coronary veins and from interfaces between the myocardium and the chest wall, lungs, diaphragm and liver. Some authors have questioned the septal approach to estimate whole-heart iron, and suggested that global $T2^*$ measurements of the LV could be a better indicator of myocardial iron burden [Pepe 2006a, Positano 2009]. However, a recent calibration study concluded that both iron and $T2^*$ measured in the mid-septum are highly representative of their respective global myocardial values, thus supporting the routine use of septal $T2^*$ in the assessment of global myocardial iron loading [Carpenter 2011].

4.4. LATE GADOLINIUM ENHANCEMENT

The advent of gadolinium based contrast agents (GBCAs) was arguably one of the most important breakthroughs in CMR. Gadolinium (Gd^{3+}) is a rare metal in the lanthanide series with seven unpaired electrons in the outer shell, the most of any element. In an MRI environment, local field interactions between the unpaired electrons of the Gd^{3+} ion and the

hydrogen nuclei within adjacent water molecules will cause a shortening in both the T1 and T2 times of the surrounding tissues [Biglands 2012]. This unique paramagnetic property was the background for the use of gadolinium in MRI. Because gadolinium is toxic in its free form, it has to be bound to a chelating agent for clinical use. These agents are small enough to leak through the capillaries from the vascular into the extracellular space, but not through the cell membranes into the intracellular space [Biglands 2012]. In the normal myocardium, where the myocardial cells are tightly bound together, gadolinium is barely seen because the extracellular space is small and the contrast wash-out relatively rapid. Conversely, when there is myocardial cell death or an increase of the interstitial space from any cause, the extracellular volume of distribution expands allowing for the gadolinium to accumulate (figure 4.9). Accumulation of GBCAs in the diseased myocardium is best imaged by CMR at least 10 min after injection, and is therefore termed late gadolinium enhancement (LGE) [Alpendurada 2008a].

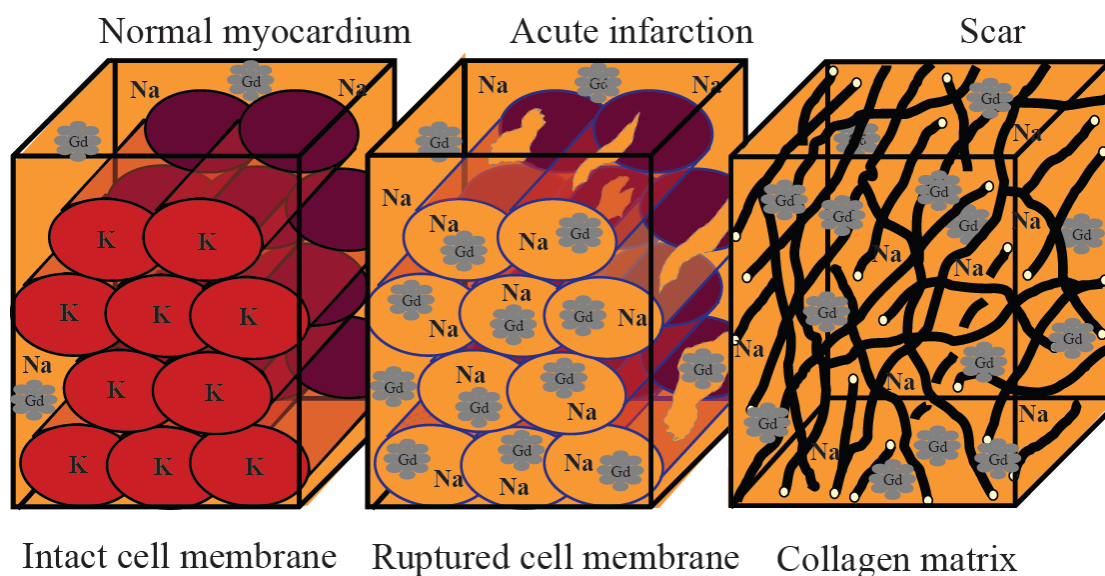


Figure 4.9. Distribution of gadolinium in the normal and abnormal myocardium. Reproduced with permission from Kim 2003.

Experimental animal studies showed a remarkable correlation between LGE images and histology for myocardial infarction [Kim 1999, Simonetti 2001]. Subsequent reports confirmed the superior ability of CMR to detect myocardial infarcts when compared to other imaging modalities [Wagner 2003, Ibrahim 2007]. The use of gadolinium was later extended to the diagnosis of heart failure, where two distinct patterns of enhancement have emerged: subendocardial enhancement patterns were associated with myocardial infarcts and coronary artery disease, whereas mid-wall and subepicardial enhancement patterns were typically associated with myocardial fibrosis in cardiomyopathies [McCrohon 2003, Soriano 2005]. Attention then turned to individual cardiomyopathies, where particular patterns of LGE were found in certain heart conditions [Maceira 2005, Smedema 2005, Mahrholdt 2005]. After the initial diagnostic and histological validation, more recent works have demonstrated the prognostic value of LGE in predicting adverse events such as arrhythmias, heart failure and death [Assomull 2006, Adabag 2008, Wu 2008, Iles 2011]. In summary, this technique allows for direct interrogation of the myocardium without the need of invasive procedures, and has become the diagnostic method of choice in a wide range of myocardial conditions [Hundley 2010]. However, further prognostic studies are necessary to document the role of LGE techniques for risk stratification and clinical decision making.

Like all the landmark studies described above, the LGE protocol in this thesis stems from the original concept developed by Simonetti and co-workers. Post-contrast imaging is based on a T1-weighted fast spoiled gradient echo sequence with a 180° inversion recovery prepulse [Simonetti 2001]. Importantly, the time between the inversion recovery pulse and the image acquisition, which is called inversion time (TI), is specifically chosen to null the signal of the normal myocardium after contrast administration (figure 4.10). Tissues containing gadolinium will have shorter relaxation times and hence will appear bright in a T1 weighted sequence when compared to the dark remote myocardium. This constitutes the principle of gadolinium

enhancement. Optimal conditions to observe this effect are with gadolinium doses of 0.1-0.2 mmol/kg given intravenously and an ideal time of 10 minutes after injection to maximise the contrast between the abnormal and normal myocardium and the ventricular cavities.

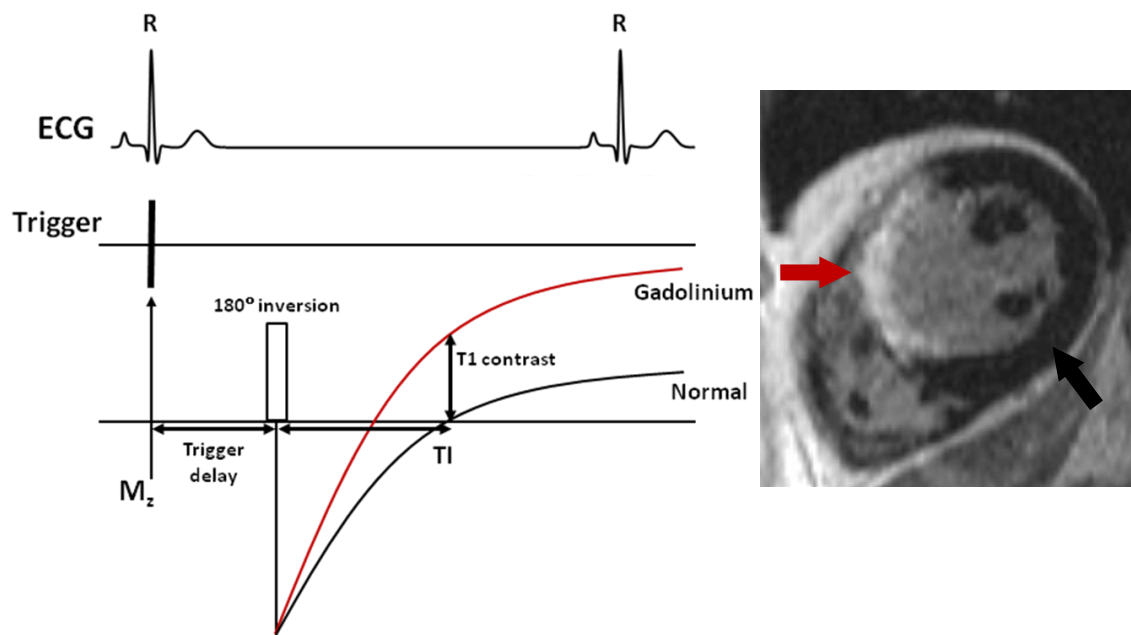


Figure 4.10. Inversion recovery and gadolinium enhancement. Inversion-recovery sequences use a 180° prepulse to invert the net magnetisation vector (M_z). At optimal inversion time (TI), normal myocardial signal will be nulled (black line and arrow), while myocardium containing gadolinium will have shorter T1 relaxation and return high signal (red line and arrow).

Contrast imaging was performed in two of the studies in this thesis (figure 4.1). Typical parameters are displayed in table 4.2. Image acquisition was set up for mid-late diastole to minimise cardiac motion artefacts, while the TI was manually adjusted between 300-440ms to suppress the signal from the normal myocardium. For the Marfan study, LGE was deemed positive if present in two short-axis images at different phase encoding directions plus a cross-cut long-axis image [Assomull 2006]. For the cardiac resynchronization therapy study, in

addition to the qualitative analysis described above, gadolinium enhancement was measured by a customised software (Qmass, Medis, Leiden, the Netherlands). Gadolinium quantification was based on the LGE short-axis images and relied on the following steps. Firstly, the LV epicardial and endocardial borders were manually traced for each short-axis slice from base to apex. Secondly, a region of interest averaging 50mm^2 was defined within an area of normal myocardium. Thirdly, a separate region of interest was defined from the most enhanced area [O'Hanlon 2010]. Myocardial enhancement was identified by the "full width at half maximum" (FWHM) criterion, where areas with signal intensity $>50\%$ of the maximum signal intensity were classified as enhanced [Amado 2004]. The extent of myocardial enhancement was finally quantified and displayed as a percentage of the LV mass. Although LGE measurements are known to be reproducible [Mahrholdt 2002], there is still no consensus about the best method for LGE quantification [Welinder 2011, Vermes 2013]. The FWHM criterion for LGE quantification was chosen for this thesis because it appears to be the closest one to manual planimetry from personal experience.

CHAPTER 5: EVIDENCE FOR MARFAN CARDIOMYOPATHY

5.1. ABSTRACT

Aim: Marfan syndrome is an inherited connective tissue disease which frequently involves the cardiovascular system. The heart can be affected since valvular regurgitation is a common complication. However, there is still debate whether a primary cardiomyopathy exists. Our aim was to evaluate the existence of a Marfan-related cardiomyopathy using cardiovascular magnetic resonance.

Methods and results: We retrospectively evaluated 68 consecutive adult patients with no cardiovascular surgery or significant valvular regurgitation. Left ventricular (LV) and right ventricular (RV) volumes, ejection fraction (EF) and mass were estimated and compared with published data on a healthy control population. Patients were also assessed for heart failure, aortic dimensions and valve disease. One quarter (25.0%) of Marfan patients had reduced LVEF, with 25.0% having increased LV end-diastolic and 30.8% having increased end-systolic volumes. The RVEF was reduced in 10.3%, with increased RV end-diastolic volumes in 11.8% and increased end-systolic volumes in 13.2%. On univariate analysis, no association was found between reduced LVEF and age, gender, indexed aortic dimensions, presence of mitral valve prolapse or valve regurgitation.

Conclusion: This study supports the existence of a primary cardiomyopathy in a subgroup of Marfan patients. The biventricular enlargement and dysfunction is usually mild, asymptomatic, and independent from other cardiovascular manifestations. Further studies are needed to assess underlying causes and natural history of this condition. Routine monitoring and treatment in Marfan syndrome may need to be tailored not only to prevent aortic root expansion but also to support myocardial function.

5.2. INTRODUCTION

Marfan syndrome (MFS) is a systemic connective tissue disease involving the skeletal, ocular, and cardiovascular systems [Pyeritz 1979]. This autosomal dominant disorder is caused by mutations of the gene encoding fibrillin-1, a glycoprotein component of elastic fibres that has important structural and regulatory roles in the extracellular matrix [Ramirez 2007]. The clinical diagnosis is based on the presence of major and minor criteria in different organ systems, as defined by the revised Ghent criteria [De Paepe 1996]. MFS is one of the commonest inherited connective tissue diseases, with an estimated prevalence of 1 in 5,000 individuals worldwide [Judge 2005].

Cardiovascular manifestations are common in MFS, and constitute the main cause of mortality, usually by aortic dissection and related complications [Silverman 1995a]. Aortic dilatation typically involves the aortic root and proximal ascending aorta with effacement of the sinotubular junction. Other aortic segments and branches can also be affected in more severe forms of the disease. The heart is frequently involved as aortic dilatation with secondary aortic regurgitation, and mitral valve prolapse with associated mitral regurgitation are common manifestations. However, there is still a debate whether a primary cardiomyopathy exists, since fibrillin-1 is also present in the myocardium [Vracco 1990]. At present there is no published data in animal models, and no robust evidence available in humans, with conflicting data from studies on myocardial performance.

Since the first case report published 25 years ago [Fujiseki 1985], there has been an increasing interest in evaluating the possibility of a cardiomyopathy in patients with MFS. Echocardiography has been used as the primary imaging modality in these studies. Although more recent echocardiographic data have shown impairment in diastolic and systolic function

using Doppler imaging, there is no clear evidence of myocardial dysfunction based on the measurement of left ventricular ejection fraction [Roman 1989, Savolainen 1994, Chatrath 2003, Meijboom 2005, De Backer 2006, Das 2006, Rybczynski 2007, Kiotsekoglou 2008, Kiotsekoglou 2009a].

Ejection fraction (EF), the percentage of chamber volume ejected in systole, is the most important and most commonly used marker of left ventricular (LV) function. It is a powerful prognostic factor across all groups of cardiac disease, and is commonly used for risk stratification and decision making [Antman 2004, Bonow 2008, Hunt 2009].

Cardiovascular magnetic resonance (CMR) has emerged as an important modality in the evaluation of cardiac disease. It provides accurate and reproducible estimation of ventricular volumes and ejection fraction and it is now considered the “gold standard” for these measurements [Grothues 2002, Grothues 2004]. Therefore the aim of this study was to investigate the existence of a primary cardiomyopathy in the Marfan population using CMR.

5.3. METHODS

5.3.1. Study population

We reviewed 150 consecutive Marfan patients referred for their first cardiovascular magnetic resonance (CMR) study in our institution between 2003 and 2008. All patients had a diagnosis based on the revised Ghent criteria. From this original cohort, we excluded 45 patients with a history of aortic or cardiac surgery and 21 patients with significant aortic or mitral regurgitation on CMR or echocardiography. We also excluded 9 patients under the age of 18 years old because reference volumes and EF are not available for this population, and 7 patients whose CMR study was incomplete. Thus, a cohort of 68 adult patients without

previous cardiovascular surgery or significant valvular regurgitation was available for analysis. As this study involved a retrospective review of patient medical records, individual patient consent was not required by our Ethics Committee who approved the study.

5.3.2. Magnetic resonance

All studies were performed on Sonata or Avanto 1.5T scanners (Siemens, Erlangen, Germany). The standard protocol included: (1) multislice anatomical imaging in 3 planes (trans-axial, coronal, and sagittal oblique); (2) long-axis cines (2-chamber, 4-chamber, left ventricular outflow tract [LVOT] and respective cross-cut); (3) aortic valve cines, and aortic flow images when aortic regurgitation was present; (4) short-axis view of both ventricles from atrio-ventricular level to the apex. The cine images were acquired using a steady-state free precession (SSFP) sequence following a standard protocol [Maceira 2006a, Maceira 2006b], whereas the flow images were acquired using a modified phase-contrast gradient-echo sequence [Chai 2005].

5.3.3. Ventricular volumes and mass

Left and right ventricular volumes at end-diastole and end-systole, as well as left ventricular mass, were determined using a semi-automated analysis software (CMR tools, Cardiovascular Imaging Solutions, London, UK) - figure 5.1. The resulting values were then normalised to age, gender and body surface area (BSA), and compared with published reference ranges in a normal population of 120 individuals where the same methodology was used [Maceira 2006a, Maceira 2006b]. Individual values for each patient were considered to be abnormal if they fell outside the 95% confidence interval (CI) for the normal population; patients were considered

to have cardiomyopathy if the LVEF was below the lower 95% CI for corresponding gender and age decile.

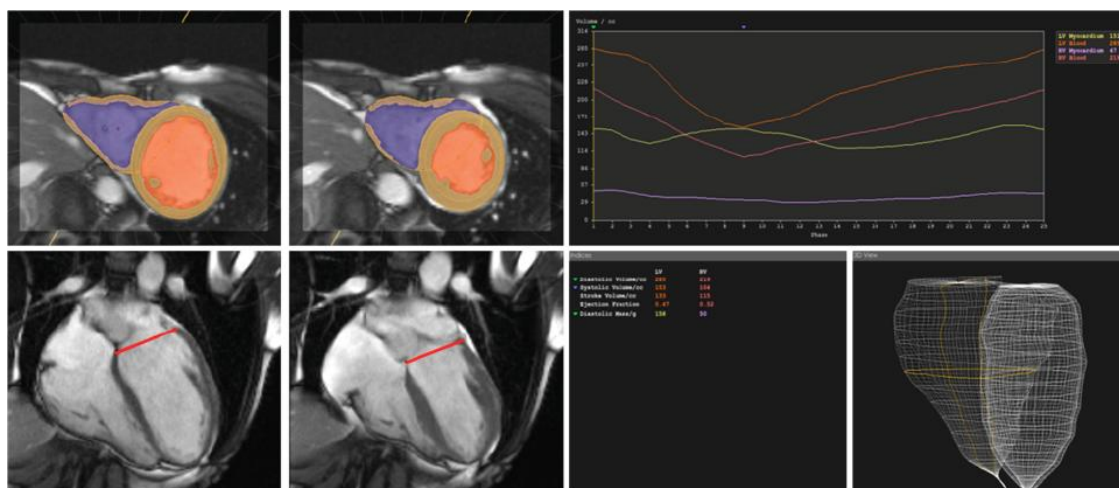


Figure 5.1. Software used for ventricular volume and mass measurements. Left panel: mid-ventricular short-axis and four-chamber views at end-diastole and end-systole. Highlighted areas represent the ventricular cavities and myocardium. Mitral valve plane (solid line) confines the LV in end-diastole and end-systole. Right panel: Volume curves throughout cardiac cycle. In the graph above, LV and RV volume curves are presented. In the table below, LV and RV dimensions and EF are shown.

5.3.4. Aortic dimensions

Aortic root measurements were intra-luminal and taken at end-diastole using SSFP cine images: the aortic annulus was measured from the sagittal and coronal LVOT and LVOT views and the average diameter was used; the sinus of Valsalva was measured from the aortic valve and LVOT views and the average cusp-cusp diameter was used. These values were compared with recently published reference values for the aortic root using CMR [Burman 2008].

Ascending aorta at right pulmonary artery level, aortic arch, and descending aorta at pulmonary artery level measurements were taken from multi-slice spin-echo and SSFP sequences, since these are considered the most reproducible techniques to measure the thoracic aorta at these levels.

5.3.5. Valve disease

The four cardiac valves were evaluated in all patients. Valvular regurgitation was graded by experienced observers, and was based on regurgitation fraction by flow mapping and regurgitant volumes by stroke volume difference between the left and right ventricles. Patients with more than mild aortic or mitral regurgitation (defined as regurgitant fraction > 15%) were excluded from further evaluation [Gelfand 2006]. Echocardiographic data was collected if performed within 6 months of the CMR study. Fifty-four patients who fulfilled this criterion had their studies reviewed by blinded experienced observers. None of these 54 patients had more than mild aortic or mitral regurgitation, in concordance with their CMR findings. Mitral valve prolapse (MVP) was defined as systolic displacement of one or both leaflets >2mm from the mitral annulus plane in the LVOT view, as per current criteria [Bonow 2008].

5.3.6. Other parameters

Heart rate (HR) was recorded at the time of the study. Blood pressure (BP) and cardiovascular medications (to prevent aortic expansion) were obtained from patient's medical records. None of these patients were known to have hypertension or coronary artery disease.

5.3.7. Statistical analysis

Continuous variables are presented as mean \pm SD, while categorical variables are presented as percentages. Relationship between pairs of continuous variables was expressed by the Pearson correlation and two sample t-test. Association between categorical variables was determined by using the chi-square test. Statistical significance was set at $p < 0.05$. All statistical analysis was performed using SPSS 15.0 software (SPSS Inc., Chicago, Illinois).

5.4. RESULTS

5.4.1. Study population

The population demographics are presented in table 5.1. The final cohort of 68 patients had a mean age of 33.9 ± 11.9 years (range: 18-71) and a slight male predominance (60.3%). All patients were in sinus rhythm at the time of the study. One patient had symptomatic heart failure (NYHA II) at the time of the study; no late gadolinium enhancement was seen. One other patient was admitted one year after the baseline study with a Takotsubo-like syndrome and cardiogenic shock which resolved on medical therapy; the coronary arteries were unobstructed. Both patients were included in the analysis as they were clinically stable at the time of scanning.

5.4.2. Left ventricle

In 25% of patients the LVEF was reduced when compared with our healthy control population (figures 5.2 and 5.3). The mean LVEF of this group with reduced LVEF was $53.8 \pm 3.1\%$ (vs. $65.2 \pm 4.5\%$ patients with normal EF). The reduction of LVEF was less than 10% below the lower

reference value for age and gender in all except one patient. LV end-diastolic (ED) and end-systolic (ES) indexed volumes were also increased in a significant proportion of patients (25.0% and 30.9%, respectively) - figure 5.4, while LV mass index was only increased in a minority of patients (2.9%).

Table 5.1. Patient characteristics according to the presence or absence of reduced LVEF.

	Total (n = 68)	Normal EF (n = 51/75.0%)	Reduced EF (n = 17/25.0%)	P
Age (years)	33.9 ± 11.9	34.9 ± 11.4	30.7 ± 13.0	0.21
Gender (male)	41 (60.3%)	28 (54.9%)	13 (76.4%)	0.16
Height (m)	1.88 ± 0.11	1.87 ± 0.10	1.91 ± 0.13	0.28
Weight (kg)	78.9 ± 17.1	76.8 ± 14.1	85.2 ± 23.1	0.08
Body surface area (m ²)	2.04 ± 0.25	2.01 ± 0.28	2.13 ± 0.32	0.09
Heart rate (b.p.m.)	64.3 ± 12.5	64.0 ± 12.0	65.1 ± 14.3	0.75
Systolic BP (mmHg)	116.8 ± 11.9	117.1 ± 12.1	115.5 ± 11.9	0.68
Heart failure	2 (2.9%)	0 (0.0%)	2 (11.8%)	NS
LVEDV (mL)	181.1 ± 48.1	171.1 ± 39.9	211.1 ± 59.6	0.03
LVEDV index (mL/m ²)	88.9 ± 21.7	85.1 ± 17.7	100.5 ± 28.4	0.01
LVESV (mL)	70.1 ± 27.4	60.3 ± 18.0	99.8 ± 30.0	<0.001
LVESV index (mL/m ²)	34.4 ± 12.6	30.0 ± 8.3	47.5 ± 14.3	<0.001
LVEF (%)	62.1 ± 6.9	65.2 ± 4.5	52.8 ± 3.1	N/A
LV mass (g)	137.9 ± 34.2	132.3 ± 32.4	154.7 ± 35.0	0.02
LV mass index (g/m ²)	67.3 ± 12.7	65.3 ± 12.0	73.0 ± 13.4	0.03
RVEDV (mL)	176.1 ± 44.1	169.4 ± 40.1	196.2 ± 50.5	0.03
RVEDV index (mL/m ²)	86.4 ± 19.1	84.2 ± 17.4	93.1 ± 22.9	0.1
RVESV (mL)	74.7 ± 25.0	67.2 ± 18.2	97.0 ± 29.3	0.001
RVESV index (mL/m ²)	36.4 ± 10.7	33.4 ± 8.2	45.7 ± 12.1	0.001
RVEF (%)	58.1 ± 6.5	60.6 ± 5.0	50.8 ± 5.1	<0.001
Aortic annulus (mm)	27.4 ± 3.4	26.7 ± 3.3	29.3 ± 2.8	0.006
Annulus index (mm/m ²)	13.5 ± 1.8	13.4 ± 1.5	14.1 ± 2.3	0.26
Aortic sinus (mm)	44.6 ± 6.0	43.8 ± 6.4	46.8 ± 4.0	0.07
Sinus index (mm/m ²)	22.0 ± 3.3	21.9 ± 3.1	22.5 ± 4.0	0.52
Ascending aorta (mm)	30.7 ± 5.6	29.8 ± 4.9	33.1 ± 6.8	0.04
Ascending index (mm/m ²)	15.1 ± 2.8	14.9 ± 2.3	15.9 ± 3.9	0.34
Aortic arch (mm)	22.4 ± 3.4	22.1 ± 3.5	23.2 ± 3.2	0.22
Arch index (mm/m ²)	11.1 ± 1.8	11.4 ± 1.7	11.2 ± 2.1	0.81
Descending aorta (mm)	22.2 ± 3.7	21.8 ± 3.6	23.5 ± 3.9	0.1
Descending index (mm/m ²)	10.9 ± 1.6	10.8 ± 1.5	11.2 ± 1.9	0.46
Mitral valve prolapse	25 (36.8%)	18 (35.3%)	7 (41.2%)	0.66
Beta blocker	37 (54.4%)	30 (58.8%)	7 (41.2%)	0.21
ACE inhibitor	2 (2.9%)	2 (3.9%)	0 (0.0%)	NS
Angiotensin II inhibitor	4 (5.9%)	3 (5.9%)	1 (5.9%)	NS

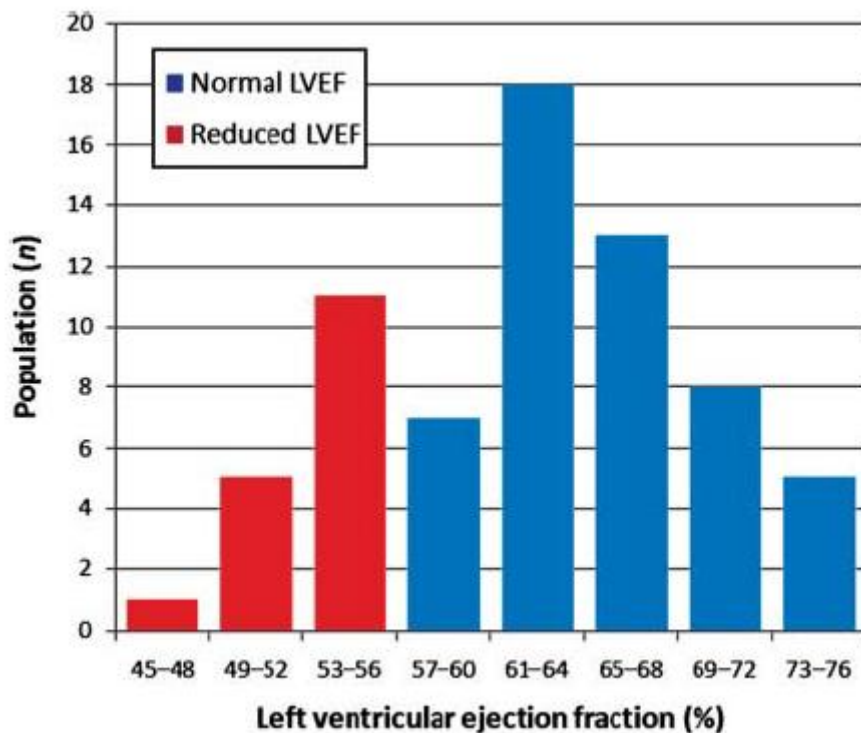


Figure 5.2. Distribution of LVEF in the entire study population. Patients with reduced LVEF are presented in red, whereas patients with normal LVEF are presented in blue.

Patients were divided in two groups (with reduced EF and normal EF) and their demographics are shown in table 5.1. There was no significant difference in age or gender between both groups. Although there was no association between height and reduced EF, there was a trend for an association between reduced EF and an increased weight and BSA.

Patients with reduced LVEF had a significantly increased indexed LVEDV, LVESV and mass when compared with the group of patients with normal LVEF. No association regarding symptoms, heart rate, blood pressure, medication, and reduced LVEF was found.

There was a strong positive correlation between LV mass and LVEDV ($r=0.56$, $p<0.01$), and a significant negative correlation between HR and LVEDV ($r=-0.49$ LV, $p<0.01$); no correlation was found between HR or SBP and LVEF when regarded as continuous variables ($r=-0.03$, $p=0.81$; and $r=-0.07$, $p=0.61$ respectively).

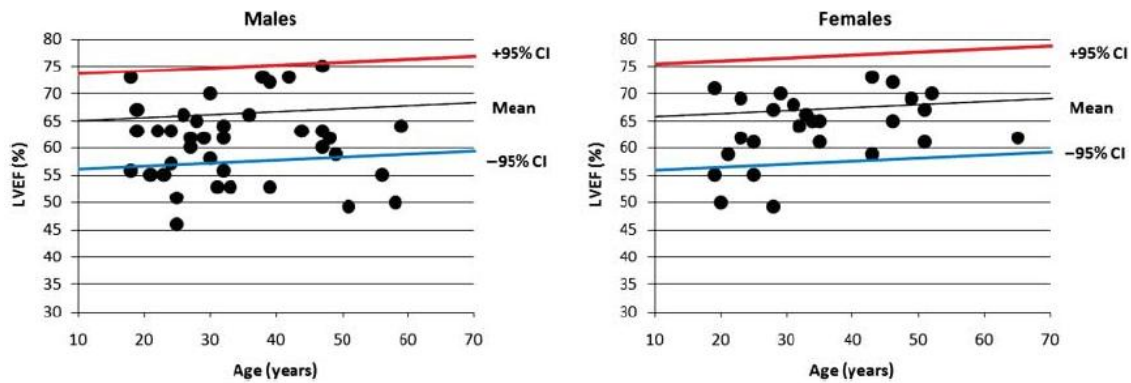


Figure 5.3. Distribution of individual LVEF across the study population according to age and gender (left panel for males, right panel for females). The red and blue lines represent the upper and lower 95% confidence interval, respectively.

5.4.3. Right ventricle

RVEF was reduced in 10.3% of patients and indexed RVEDV and RVESV were increased in 11.8% and 13.2%, respectively (figure 5.4). Patients with reduced LVEF had a significantly reduced RVEF, a trend for an increased RVEDV, and a significantly increased RVESV when compared with the group of patients with normal LVEF. All patients with RV systolic impairment had also LV systolic impairment, and no patients with normal LVEF had reduced RVEF. All these patients with reduced RVEF had only mild systolic impairment.

5.4.4. Aorta

The aortic annulus was dilated in 55.9% (n=38) and the aortic sinus was dilated in 86.7% (n=59) of the study population. Patients with reduced LVEF had significantly larger aortic annulus (29.3 ± 2.8 vs. 26.7 ± 3.3 mm, $p=0.006$) and ascending aorta (33.1 ± 6.8 vs. 29.8 ± 4.9 mm, $p=0.04$), and a trend for a larger aortic sinus (46.8 ± 4.0 vs. 43.8 ± 6.4 mm, $p=0.07$). However,

after adjusting the aortic diameters to body surface area there was no significant difference in indexed aortic dimensions between the groups with normal and reduced LVEF (table 5.1).

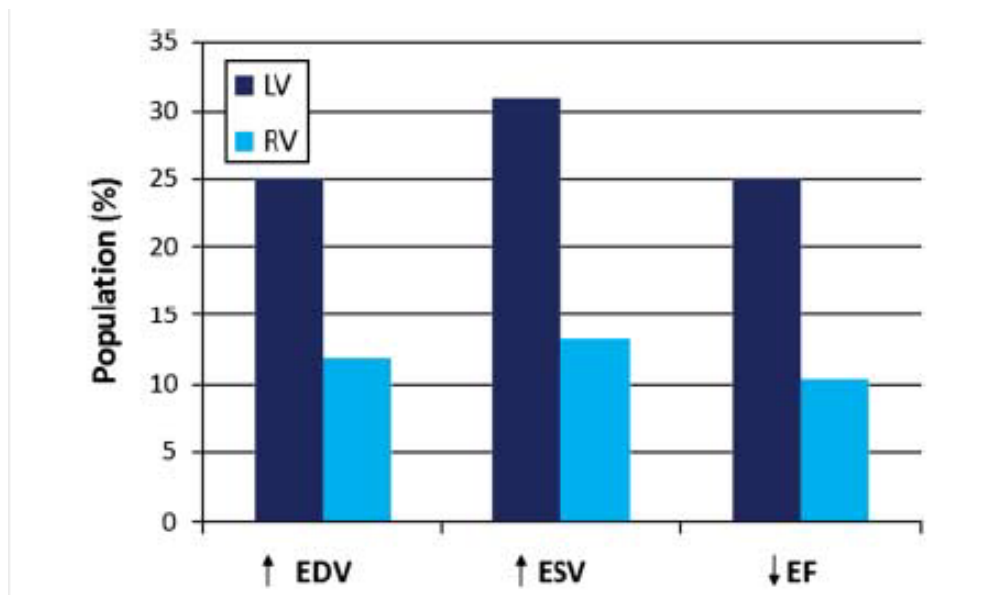


Figure 5.4. Percentage of patients with increased LV and RV end-diastolic volume (EDV), end-systolic volume (ESV), and reduced ejection fraction (EF).

5.4.5. Valves

The aortic valve was tricuspid in all except one patient, and mitral valve prolapse was present in 25 patients (36.8%). No patients had valvular stenosis or significant valvular regurgitation at rest. Mild aortic or mitral regurgitation was found in 27 patients (39.7%). Of these, 20 patients had aortic regurgitation, 3 patients had mitral regurgitation, and 4 patients had combined aortic and mitral regurgitation. Patients with mild left-sided valvular regurgitation had a small but significant increase in LVEDV and LVESV, and a trend for increased mass when compared with patients without left-sided valvular regurgitation. However, there was no significant difference between these 2 groups regarding LVEF, RV volumes and RVEF (table 5.2). In addition, no association between MVP and reduced EF was found.

Table 5.2. Patient characteristics according to the presence of aortic or mitral regurgitation.

	Total (n = 68)	No valvular regurgitation (n = 41/60.3%)	Mild valvular regurgitation (n = 27/29.7%)	P
LVEDV index (mL/m ²)	88.9 ± 21.7	83.0 ± 15.4	98.0 ± 26.6	0.01
LVESV index (mL/m ²)	34.4 ± 12.6	30.9 ± 8.6	39.6 ± 15.8	0.01
LVEF (%)	62.1 ± 6.9	63.2 ± 6.1	60.5 ± 7.7	0.12
LV mass index (g/m ²)	67.3 ± 12.7	65.0 ± 11.5	70.6 ± 13.9	0.08
RVEDV index (mL/m ²)	86.4 ± 19.1	84.0 ± 16.6	90.1 ± 22.3	0.2
RVESV index (mL/m ²)	36.4 ± 10.7	34.9 ± 9.3	38.8 ± 12.3	0.14
RVEF (%)	58.1 ± 6.5	58.6 ± 6.2	57.4 ± 7.1	0.51

Data are mean (SD). P-values are from t-test.

5.4.6. Medication

Beta-blockers, angiotensin-converting enzyme (ACE) inhibitors and angiotensin receptor blockers (ARB) were part of the regular medication in 54.4%, 2.9%, and 5.9% of the patients, respectively. There was no significant association between the use of beta-blockers and the group with reduced EF, and the number of patients on ACE inhibitors and ARBs was too small to perform a meaningful statistical analysis (table 5.1). However, when assessing the cohort according to medication status, we found that patients on medication had significantly higher LVEF than the patients who were not on any medication (63.7%±6.9% vs. 59.7±6.4%, p=0.02).

5.5. DISCUSSION

This study is the largest cohort of Marfan patients evaluated by CMR for the existence of a Marfan cardiomyopathy. Our main findings are: (1) a significant proportion of patients have reduced ejection fraction, suggesting impaired systolic function and an underlying cardiomyopathy; (2) this systolic impairment is usually mild (<10% below the lower limit of normal) and asymptomatic; (3) patients with impaired LV systolic function had higher incidence of RV dysfunction, as manifested by reduced RVEF; (4) the impairment in systolic

function was independent of classic CV manifestations of the disease and medication regime at the time of the study.

5.5.1. Left ventricle

The definition of cardiomyopathy is complex and an ever-evolving challenge [Elliott 2008]. For this group of patients, we used reduction of LVEF below the 95% CI for the normal population to define cardiomyopathy, since LVEDV was also influenced by heart rate and presence of mild valvular regurgitation. LVEF is the most important and commonly used marker of ventricular performance and impairment of this indicator would strongly suggest ventricular dysfunction. Although considered to be dependent on loading conditions, LVEF was not affected in this study by pre-load (heart rate, mild valvular regurgitation) or after-load (systolic blood pressure) determinants.

Only 2 previous studies have addressed left ventricular function using CMR as a complement to echocardiography. The first study was conducted by Savolainen *et al*, which did not show a difference in LVEF between children with MFS and controls [Savolainen 1994]. Possible explanations for this negative finding include a small population (22 Marfan patients), use of area-length method to estimate volumes, and an older less accurate cine sequence. In contrast, a more recent work by De Backer *et al* showed reduced mean LVEF in 26 MFS adults when compared with controls [De Backer 2006]. Interestingly, in De Backer's study, echocardiography did not demonstrate a significant difference in LVEF between both groups, supporting previous observations suggesting that CMR requires smaller sample sizes than echocardiography to detect significant changes in ventricular volumes and EF [Grothues 2002, Grothues 2004]. This may also explain why previous echocardiographic studies failed to detect a significant difference in LVEF between Marfan and control groups.

Our observations suggest that Marfan cardiomyopathy is an independent entity. No specific predictors of cardiomyopathy were found when patient demographics, indexed aortic dimensions and presence of valvular disease were analysed. Although the majority of patients have normal LVEF, one quarter of this population have reduced LVEF and impaired systolic function; these patients should therefore be monitored more closely and managed accordingly [Hunt 2009]. The degree of LV involvement should also be evaluated pre- and post-operatively and should be taken into account when deciding the type of aortic root surgery.

5.5.2. Right ventricle

RVEF was significantly reduced in patients with reduced LVEF, suggesting that this cardiomyopathic process is manifested in both ventricles, a pattern previously described in non-ischæmic cardiomyopathies [La Vecchia 2001]. All affected patients had only a mild degree of RV systolic impairment (RVEF <10% below the lower reference value for age and gender in all patients), which parallels the mild degree of LV systolic impairment affecting our cohort of Marfan patients with cardiomyopathy. These findings support a recently published study demonstrating RV impairment in the Marfan population [Kiotsekoglou 2009a].

Of interest was the observation that the RVEF was affected less frequently than the LVEF (10.3% vs. 25.0% of patients, respectively). It is not clear why the LV might be affected in preference to the RV, but potential explanations may lie in the higher haemodynamic systemic workload sustained by the LV.

5.5.3. Aorta

Aortic root dilation is one of the earliest and commonest manifestations of cardiovascular Marfan disease. It would have been intuitive and biologically plausible to suggest that the processes leading to aortic degeneration would be accompanied by similar cardiac deformation, independent of the haemodynamic effects of significant valvular regurgitation. Although absolute proximal aortic dimensions did actually show a marginally significant association with reduced ejection fraction, this association was not present after indexing aortic dimensions to the body surface area. Currently there is no evidence to suggest that it would be productive to routinely measure aortic dimensions in order to predict deterioration in LVEF, or vice versa.

5.5.4. Valves

As with previous studies, we have included patients with mild valvular regurgitation as we would not expect to significantly impact LV performance. Nevertheless, we found that even mild degrees of chronic valvular regurgitation were associated with a statistically significant increase in both end-diastolic and end-systolic LV volumes, together with a non-significant trend towards a decrease in LVEF. We are unsure of the significance of this finding, since we would expect an increase in contractility and LVEF as a result of reduced ventricular afterload in valvular regurgitation. No association was found between MVP and LV systolic dysfunction, suggesting that the pathogenesis behind these two complications is actually diverse.

5.5.5. Medication

Previous studies have suggested that angiotensin receptor antagonists are key disease modifying agents in MFS through their effects on the TGF-beta pathway [Ramirez 2007, Brooke 2008]. Optimal blood pressure control has also been thought to play a role [Brooke 2008]. Our study was unable to provide more than a cross-sectional insight into medication regimes at the time of the scan. Nonetheless, patients on medication had significantly higher LVEF than the ones without ($63.7\% \pm 6.9\%$ vs. $59.7 \pm 6.4\%$, $p=0.02$). This suggests that these agents, primarily used to prevent aortic remodelling, may also have a beneficial effect on ventricular function. Further examination of long term regimes and effects on BP might prove useful.

5.5.6. Limitations

This is a retrospective cohort of patients referred to a tertiary cardiothoracic centre, which may not be entirely representative of the typical Marfan population. Only the initial studies were included for analysis, and no follow-up data is available. Diagnosis was based on the Ghent criteria and genotyping was only performed in cases where the diagnosis was unclear. Further evaluation could be useful to determine who is prone to develop this condition.

Coronary artery disease was not systematically ruled out in these patients by coronary angiography. However, there were no regional wall motion abnormalities in our cohort, or evidence of myocardial infarction in the small group of patient who underwent gadolinium imaging, suggesting that coronary artery disease, if present, did not play a major contributory role to ventricular dysfunction in these patients.

Late gadolinium enhancement imaging for assessment of myocardial fibrosis was not routinely performed as the primary focus was on assessing aortic disease. Within our cohort, late

gadolinium imaging was only performed in 16% (n=11) of patients where clinically indicated. Apart from one patient with mid-wall late gadolinium enhancement suggesting fibrosis, no myocardial enhancement was seen. The true incidence and pathogenesis of any mid-wall fibrosis in Marfan cardiomyopathy remains a focus for future investigation.

5.6. CONCLUSION

Our findings support the existence of a primary cardiomyopathy in a subset of patients with Marfan syndrome. This cardiomyopathy is unrelated with any other cardiovascular manifestations of the disease, and appears to affect the RV as well as the LV.

Cardiac assessment may be of value in the medical and surgical management of this high-risk population with complex multi-system disease. Further studies are needed to assess underlying causes, natural history and prognostic significance of Marfan-related cardiomyopathy. Treatment may need to be tailored not only to prevent further aortic root expansion but also to support myocardial function in these patients.

5.6.1. Acknowledgements

This project was undertaken at the NIHR Cardiovascular Biomedical Research Unit at the Royal Brompton & Harefield NHS Foundation Trust and Imperial College London. We also thank the Marfan Trust and Foyle Foundation for their support.

5.6.2. Publication

These data have been published as: Alpendurada F, Wong J, Kiotsekoglou A, Banya W, Child A, Prasad SK, Pennell DJ, Mohiaddin RH. Evidence for Marfan cardiomyopathy. *Eur J Heart Fail* 2010;12:1085-91.

CHAPTER 6: RELATION OF MYOCARDIAL T2* TO RIGHT VENTRICULAR FUNCTION IN THALASSAEMIA MAJOR

6.1. ABSTRACT

Aims

Myocardial T2* cardiovascular magnetic resonance (CMR) provides a rapid and reproducible measure of cardiac iron loading, and is being increasingly used worldwide for monitoring of transfusion dependent thalassaemia patients. Although myocardial siderosis (T2* <20ms) is associated with impaired left ventricular (LV) function, little is known of its relation with right ventricular (RV) function. The aim of this study was to investigate the relationship between cardiac T2* and RV function.

Methods and results

A retrospective analysis of 319 patients with beta-thalassaemia major presenting for their first CMR scan was performed (45.1% male, mean age 25.6 years). In patients with normal myocardial T2* (>20ms), the RV ejection fraction (EF) was within the normal range in 98% of patients. When myocardial T2* was <20ms, there was a progressive and significant decline in RVEF. There was a linear relationship between RV and LVEF.

Conclusions

Myocardial iron deposition is strongly associated with RV dysfunction, which mirrors the decrease in LV function seen with worsening cardiac iron loading. RV dysfunction may play a significant role in heart failure associated with myocardial siderosis.

6.2. INTRODUCTION

For patients with beta-thalassaemia major, heart failure due to iron overload cardiomyopathy is the main cause of mortality. In developed countries until recently [Modell 2008], it has accounted for up to 71% of all deaths, with up to 50% of these patients dying before 35 years of age, despite iron-chelating therapy [Modell 2000, Borgna-Pignatti 2004]. This form of cardiomyopathy can be reversible if detected early and appropriately treated, but once heart failure develops, prognosis is poor. Conventional techniques to assess iron in the myocardium have either proven to be invasive or unreliable, and frequently the diagnosis is delayed due to the unpredictable nature of cardiac iron loading and the late development of symptoms, which usually only become apparent after significant iron deposition has occurred.

Cardiovascular magnetic resonance (CMR) has emerged as a useful non-invasive tool for evaluating the amount of iron in the heart. The technique relies on the measurement of T2* relaxation from gradient-echo sequences. When the storage capacity of ferritin is exceeded, iron is deposited in the myocardium as particulate hemosiderin, which is a form of ferrihydrite (hydrated iron oxide). This disrupts the local magnetic field homogeneity causing reduced T2* values in inverse relation to iron concentration. T2* CMR is an ideal technique for non-invasive measurement of iron concentration because the acquisition for the validated single slice method requires only a single breath-hold and has good reproducibility making it valuable for serial monitoring over time. Calibration of the T2* technique has been reported in humans [Wood 2005, Ghugre 2006b, Carpenter 2009]. It has been shown that lower myocardial T2* values are associated with an increased likelihood of left ventricular (LV) dysfunction [Anderson 2001], whereas an improvement in myocardial T2* results in improvement in LV ejection fraction (EF) [Anderson 2004]. These findings have been confirmed in observational, prospective and randomised controlled studies of iron chelation in thalassaemia patients [Anderson 2002, Anderson 2004, Pennell 2006, Tanner 2007, Tanner

2008]. However, the relation between myocardial iron loading and right ventricular (RV) function has not been fully addressed. RVEF is an important predictor of outcome in other forms of cardiomyopathy, which is both independent of and incremental to LVEF [Juillière 1997]. Accordingly, the effects of myocardial iron loading on RV function may be important in thalassaemia patients. As CMR is considered to be the most accurate and reproducible technique for assessing RV volumes and EF [Grothues 2002, Grothues 2004], CMR provides an ideal opportunity to correlate myocardial iron loading with RV function. Therefore, the aim of this study was to evaluate the relationship between myocardial T2* and RVEF in patients with thalassaemia major.

6.3. METHODS

6.3.1. Study population

We analysed a database of 323 consecutive patients with beta-thalassaemia major who were referred for their first myocardial T2* scan from 21 UK hematology centres. All the patients included in this analysis were treated with a single iron chelation agent (deferrioxamine) at presentation. They had all received iron chelation therapy since the mid-to-late 1970s or from an early age if born after this. Any patient with suspected pulmonary hypertension (defined as tricuspid regurgitant jet velocity of >3.0 m/sec on transthoracic echocardiogram) or any other known or potential cause of RV abnormality was excluded (eg. congenital heart disease, valve disease, lung disease) [Galiè 2009]. Four patients were excluded from the final analysis due to cardiac or vascular anomalies (one aortic stenosis, one subaortic shelf, one pulmonary artery stenosis, and one repaired tetralogy of Fallot). The residual cohort consisted therefore of 319 patients (144 males and 175 females), with a mean age of 26.5 ± 8.9 years (table 6.1). At the time of their first CMR scan, 21 of the patients were taking medication for LV dysfunction or

heart-failure (diuretics, beta-blockers or angiotensin-converting-enzyme inhibitors). The data collection and analysis associated with this study was approved by Trent NHS Research Ethics Committee.

Table 6.1. Patient demographics and summary of cardiovascular magnetic resonance parameters.

Patient demographics	
Total number of patients	319 (144 male, 175 female)
Age (years)	26.5 ± 8.9
Height (cm)	157 ± 12.8
Weight (kg)	55.1 ± 12.5
Body surface area (m ²)s	1.45 ± 0.41
T2* (geometric mean ± CV%)	
Cardiac T2* (ms)	18.4 ± 11.2%
Liver T2* (ms)	3.2 ± 73.7%
CMR parameters for all patients	
RV ejection fraction (%)	62.9 ± 7.2
LV ejection fraction (%)	66.0 ± 8.3
RV end-systolic volume index (mL/m ²)	31.3 ± 11.1
RV end-diastolic volume index (mL/m ²)	83.2 ± 17.4
RV mass index (g/m ²)	35.4 ± 8.0
Haematological profile	
Serum ferritin (µg/L)	2251 ± 1748
Mean pre-transfusion haemoglobin (g/dL)	10.1 ± 1.2
Annual red cell consumption (mL/kg/year)	162.0 ± 79.6
Clinical profile	
	n (%)
Diabetes	50 (15.7%)
Hypogonadism	133 (41.7%)
Hypothyroidism	28 (8.8%)
Liver fibrosis	8 (2.5%)
Osteoporosis	98 (30.7%)
Splenectomy	131 (41.0%)
Medication use	
	n (%)
Diuretics	5 (1.6%)
ACE-inhibitors	18 (5.6%)
Beta-blockers	7 (2.2%)

Data are presented as mean±SD or number (%), unless otherwise stated.

6.3.2. Magnetic resonance

Patients were scanned with a 1.5T Sonata scanner (Siemens Medical Systems, Erlangen, Germany). Each scan included the measurement of heart T2* (mid-septum) together with left and right ventricular volumes, ejection fraction and mass using previously published techniques [Westwood 2003a, Maceira 2006a, Maceira 2006b]. T2* measured in the mid-ventricular septum is a reliable estimation of cardiac iron loading [Ghugre 2006a, Ghugre 2006b, Pepe 2006a]. Scan duration was approximately 15-20 minutes. For the measurement of myocardial T2*, a single short axis mid-ventricular slice was acquired using a single breath-hold ECG-gated multi-echo technique. This T2* sequence generated a series of 8 images with a range of echo times (TE = 2.54-17.9 ms).

6.3.3. CMR analysis

For T2* analysis, a full-thickness region of interest was defined in the interventricular septum (routinely chosen to avoid T2* artifacts from the cardiac veins, liver and lungs). Myocardial T2* decay was calculated from this region using semi-automated analysis (Thalassaemia-tools, Cardiovascular Imaging Solutions, London, UK). Signal intensity was plotted against echo time for each image and T2* was calculated from the resulting exponential decay curve. To allow for background noise, a truncation method was used as previously described [He 2008]. The normal range for myocardial T2* has been previously published from a series of healthy volunteers (the median normal value is 40ms with a lower cut-off of normality of 20ms) [Anderson 2001]. This value of 20ms is widely accepted in clinical practice and was therefore chosen to define the lower limit of the normal range in this study.

RV and LV volumes were determined from steady-state free precession cines, with contiguous short-axis slices from base to apex as previously described (7mm slice thickness with 3mm gap) [Maceira 2006a, Maceira 2006b]. Ventricular volumes and ejection fraction were

analyzed with CMRtools (Cardiovascular Imaging Solutions, London). Three main steps for volume analysis were performed. Firstly, both RV and LV endocardial and epicardial borders were delineated in all phases of the cardiac cycle in the short-axis slices. Then, valve plane tracking of the tricuspid and mitral valves was used to correct for alteration in volume due to descent of the AV ring towards the apex during systole. Finally, blood pool thresholding was used to delineate the papillary muscles and RV trabeculations (which were excluded from ventricular volume measurements). LV and RV volumes were indexed to body surface area (BSA) [Maceira 2006a, Maceira 2006b]. The normal ranges for LV and RV volumes and function were taken from previously published data with the lower limit of normal for RVEF in healthy subjects being 54% and the lower limit of normal for LVEF in non-iron overloaded thalassaemia patients being 59% [Maceira 2006a, Westwood 2007].

6.3.4. Statistical analysis

All parameters are presented as mean \pm standard deviation, except T2* which is shown as geometric mean (antilog of the mean of the log data) and percent coefficient of variation (CV - equivalent to the variance of the mean in log scale) following log transformation of data to normalize the data distribution. Spearman's rank test was used to assess the correlation between myocardial T2*, ferritin, RV volumes and EF. Analysis of variance (ANOVA) was used to assess differences across different ranges of myocardial T2*. Two sided statistical significance was set at $p < 0.05$. All statistical analysis was performed using Stata 10.1 software (StataCorp, Texas, USA).

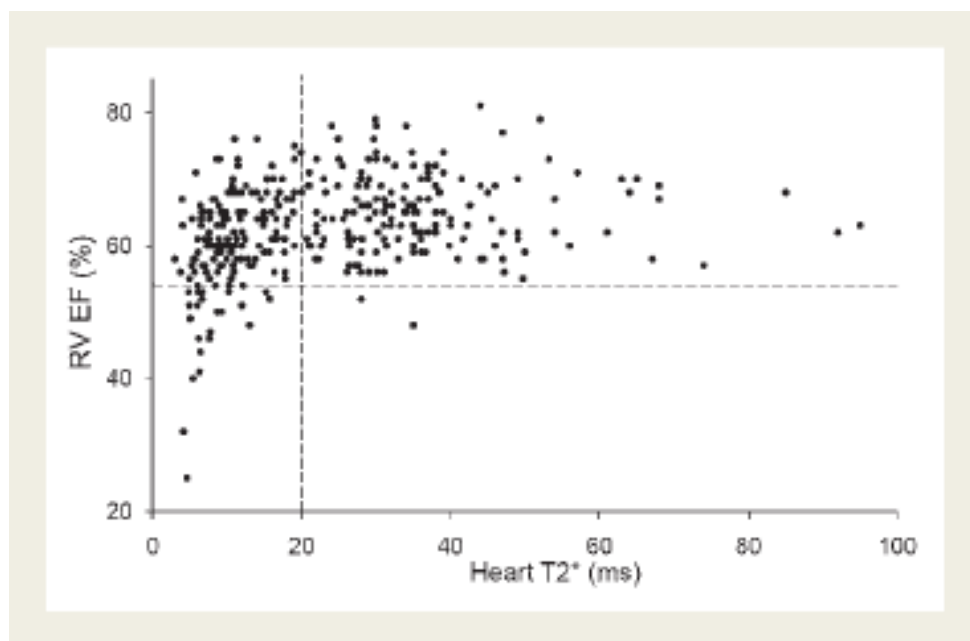


Figure 6.1. The relationship between myocardial T2* and right ventricular ejection fraction (RVEF). The vertical broken line shows the lower limit of the normal range for T2* of 20 ms. The horizontal line shows the lower limit of the normal range for RVEF of 54%.

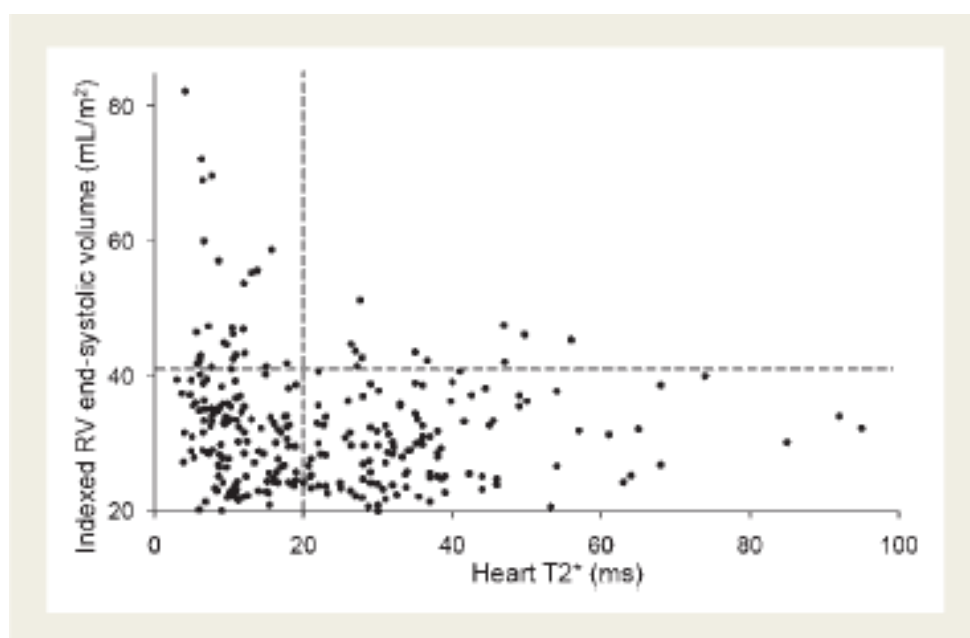


Figure 6.2. The relationship between myocardial T2* and right ventricular end-systolic volume indexed to body surface area. The vertical broken line shows the lower limit of the normal range for T2* of 20 ms. The horizontal line shows the upper limit of the normal range for RV end-systolic volume index of 41 mL/m².

6.4. RESULTS

In thalassaemia patients with a normal myocardial T2* ($>20\text{ms}$), RVEF was $65.0 \pm 6.1\%$, and was distributed within the normal range of expected values in 98% of patients. In patients with myocardial siderosis (T2* $<20\text{ms}$), there was a progressive and significant decline in RVEF ($r=0.43$, $P<0.001$; figure 6.1) and an increase in the RV end-systolic volume ($r=-0.33$, $p<0.001$; figure 6.2). In contrast to ejection fraction and end-systolic volume index, there was no significant correlation of either RV end-diastolic volume index or RV mass index with T2*. Of the 165 patients with myocardial siderosis (T2* $<20\text{ms}$), 23 (14%) were found to have an RVEF below the lower limit of the normal range. Of the patients with impaired RVEF, 82.6% also had an impaired LVEF. There were four patients with T2* $<20\text{ms}$ who had impaired RVEF but a normal LVEF. None of the patients had documented pulmonary hypertension. The mean RVEF for these patients was $49 \pm 1.6\%$ and the mean LVEF was towards the lower limit of the normal range ($62 \pm 3.8\%$). Both RV mass and the pulmonary artery diameter were normal (mean RV mass index $28 \pm 4.6\text{g/m}^2$, mean PA diameter $18 \pm 3.7\text{mm}$). No septal flattening or tricuspid valve regurgitation was seen on cine images. All four patients had severe myocardial iron loading with T2* ranging from 5.0 to 9.2ms (mean T2* $7.0 \pm 2.1\text{ms}$). All were on the same transfusion regime (2 units of packed red cells every four weeks, mean annual red cell consumption 129mL/kg/year), none had undergone previous splenectomy and none had symptoms of heart failure. Apart from hypogonadotrophic hypogonadism in one patient and osteoporosis in another, there were no other complications. Serum ferritin ranged from 723 to $4673\mu\text{g/dl}$ (mean ferritin $1772 \pm 1937\mu\text{g/dl}$).

LVEF was $69.5 \pm 5.2\%$, and was within normal limits in 99% of thalassaemia patients with a normal T2*. Below 20ms, LVEF showed a significant decline with lower T2* values ($r=0.40$, $p<0.001$; figure 6.3). Of patients with myocardial siderosis (T2* $<20\text{ms}$) 47 (28.4%) had reduced LVEF, of which, 19 (40.4%) also had a low RVEF. Linear regression between RVEF and

LVEF showed a significant relation ($r=0.69$, $p<0.001$; figure 6.4). A comparison of two representative patients is shown in figure 6.5, one with severe myocardial iron loading and poor biventricular function and the other with no evidence of myocardial iron loading and normal ventricular function.

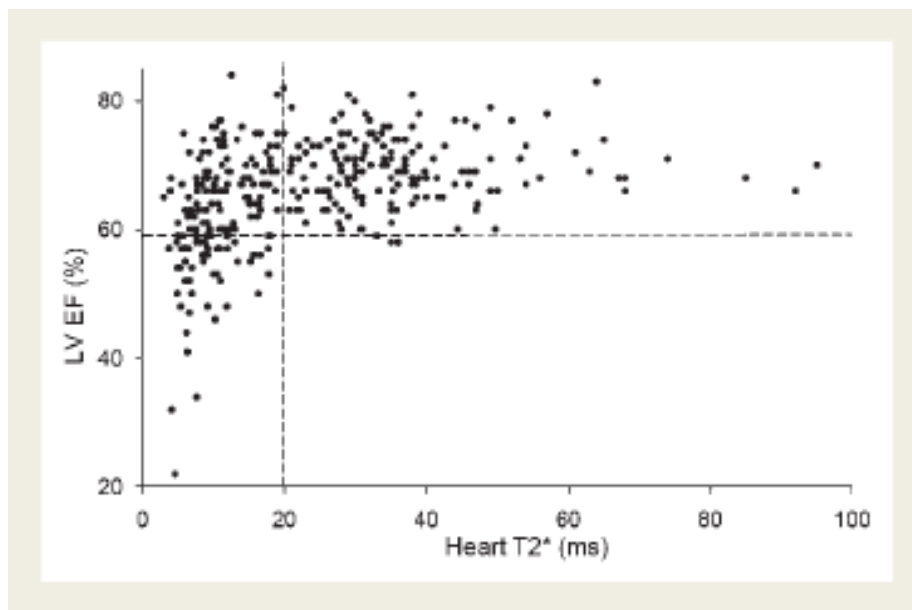


Figure 6.3. The relationship between myocardial T2* and left ventricular ejection fraction (LVEF). The vertical broken line shows the lower limit of the normal range for T2* of 20 ms. The horizontal line shows the lower limit of the normal range for LVEF in thalassaemia major patients of 59%.

A summary of the ventricular and haematological parameters in three different T2* ranges (less than 10ms, 10-20ms and more than 20ms) is shown in table 6.2. Differences between groups were found for RV and LVEF, RV end-systolic volume index and serum ferritin. No difference was found between groups for RV end-diastolic volume index, RV mass index, pre-transfusion haemoglobin, yearly transfusion or total units transfused. No correlation was found between any of the haematological parameters (including ferritin) and RVEF. There was

a weak negative correlation between ferritin and myocardial T2* when the whole patient cohort was considered ($r = -0.22$, $P < 0.001$).

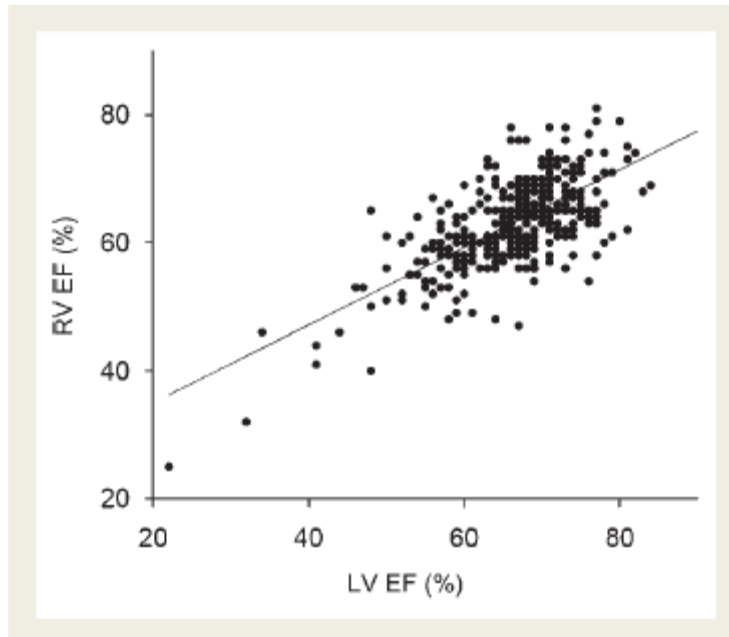


Figure 6.4. The relationship between right ventricular ejection fraction (RVEF) and left ventricular ejection fraction (LVEF).

Table 6.2. Breakdown of CMR parameters for different ranges of T2*.

T2* range	<10 ms	10–20 ms	>20 ms	P-value
Number of patients	75	89	155	—
Male (%)	48.0	41.6	46.8	—
LV ejection fraction (%)	59.1 ± 9.8	65.8 ± 7.6	69.5 ± 5.2	<0.001
RV ejection fraction (%)	57.7 ± 8.4	63.4 ± 6.0	65.1 ± 6.1	<0.001
RV end-systolic volume index (mL/m ²)	36.6 ± 14.0	30.6 ± 9.6	29.2 ± 9.6	<0.001
RV end-diastolic volume index (mL/m ²)	85.1 ± 18.0	82.9 ± 16.4	82.8 ± 17.9	0.63
RV mass index (g/m ²)	36.2 ± 8.3	35.3 ± 8.1	35.1 ± 8.4	0.75
Ferritin (μg/L)	2803 ± 2107	2553 ± 1576	1914 ± 1576	0.001
Pre-transfusion haemoglobin (g/dL)	9.8 ± 0.5	10.0 ± 1.0	10.2 ± 1.4	0.39
Red cell consumption (U/year)	34.2 ± 11.9	35.1 ± 9.8	32.3 ± 11.4	0.15
Total units transfused (U)	888 ± 407	954 ± 396	878 ± 475	0.41

Data are presented as mean ± SD. P-values given are for analysis of variance between groups.

Data are presented as mean+SD. P-values given are for analysis of variance between groups.

6.5. DISCUSSION

Heart failure due to iron-overload cardiomyopathy is the dominant cause of mortality in patients with thalassaemia major. Iron overload in thalassaemia major occurs due to a combination of repeated blood transfusions, with each unit of blood containing 200-250mg of elemental iron, and excessive gastrointestinal absorption. Excess body iron is stored in ferritin and its degradation product hemosiderin. In the heart, this results in impaired function of the mitochondrial respiratory chain, ventricular dysfunction and the potential for progression to heart failure [Hershko 2011]. In this study, we have evaluated the relationship between myocardial iron loading and right ventricular function. Our data show mirror effects on both LV and RV volumes and ejection fraction. We found a normal RVEF in 98% of patients with normal myocardial T2* values, but progressive RV enlargement and dysfunction with increasing myocardial siderosis. The RV and LVEF showed significant correlation. Aside from myocardial iron loading, we did not identify any clinical factors that could explain the observed effects on ventricular function.

In the original validation study by Anderson et al, myocardial T2* values in the normal range were associated with normal LVEF values, but when myocardial T2* fell below 20ms, a progressive deterioration in LVEF was seen [Anderson 2001, Anderson 2002, Tanner 2007, Tanner 2008], and this finding has been reproduced once again in this large cohort. There is limited data examining the relation between cardiac T2* and RV function [Hahalis 2002, Pepe 2006b]. The importance of the right ventricle as an aggravating factor in heart disease and a predictor of adverse cardiac outcomes has often been overlooked in the past. Studies have indicated the importance of RV function in conditions such as congenital heart disease [Gatzoulis 1995, Graham 2000, Roos-Hesselink 2004], dilated cardiomyopathy [Juillière 1997, La Vecchia 2001], chronic systolic dysfunction [Meyer 2010], and ischemic heart failure [Di Salvo 1995, de Groote 1998, Ghio 2001]. In these studies, RV dysfunction was a strong

predictor of mortality and outcomes in heart failure, irrespective of etiology, and independent of the LV function, New York Heart Association (NYHA) functional class of heart failure, or peak oxygen consumption. This suggests that RV function may be a significant contributor to the clinical manifestation of heart failure seen in severe myocardial siderosis.

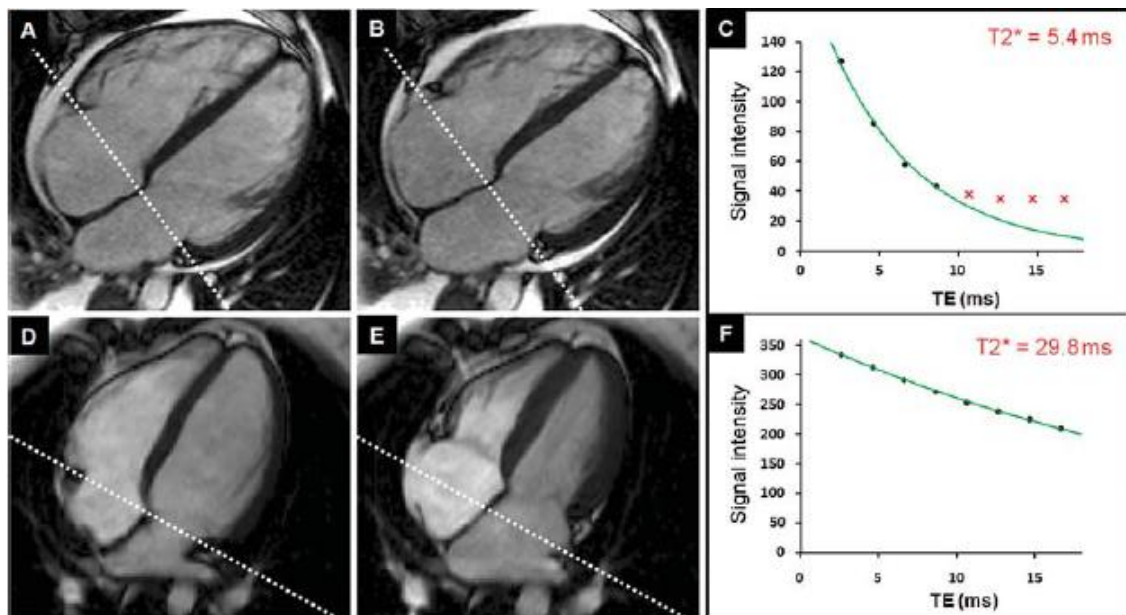


Figure 6.5. Comparison of two patients with different iron loading profiles and ventricular function. The top row of images (A–C) shows a patient with raised right and left ventricular volumes in end-diastole (A) and end-systole (B), poor biventricular ejection fraction (RVEF = 25% and LVEF = 22%) and severe iron overload. Myocardial T2* is 5.4 ms (C). The lower row shows end-diastolic (D) and end-systolic (E) images from a patient with normal biventricular ejection fraction (RVEF = 61% and LVEF = 66%) and no myocardial iron loading [T2* is 29.8 ms (F)]. The dotted line in each case denotes the level of the atrioventricular junction at end-diastole to illustrate the long-axis contraction of the heart in systole. TE, echo time.

The finding of a close correlation between LV and RV function suggests that there is diffuse myocardial toxicity due to excess iron and that this plays an important role in both left and right ventricular dysfunction in this type of cardiomyopathy. This pattern is typical of non-

ischaemic cardiomyopathy, where RV dysfunction is common and more closely parallels LV dysfunction in contrast with the predominant LV impairment seen in ischaemic heart failure. The function of the right ventricle may be affected by pulmonary hypertension (PHT) which can occur as a complication in patients with thalassaemia [Aessopos 2005a]. Initial reports suggested that increased pulmonary systolic pressure was a common finding in thalassaemia major patients but some of these early results were based on a cohort of patients who were under-transfused and poorly chelated [Grisaru 1990, Du 1997]. Subsequent studies in well-treated Italian and Greek patients have not confirmed these findings, with PHT being practically absent in thalassaemia major patients with a high standard of care [Derchi 1999, Aessopos 2004]. In contrast, PHT is a prominent finding in patients with thalassaemia intermedia [Aessopos 2005b]. While beta-thalassaemia major is a severe anemia which presents within the first years of life and requires lifelong transfusions to prolong survival, thalassaemia intermedia is milder with a later clinical onset. In one series of 110 thalassaemia intermedia patients, PHT was found in nearly 60%, causing RV failure in approximately 5% although all patients had preserved LV systolic function [Aessopos 2001]. Despite this, a recent study has shown that patients with thalassaemia intermedia have a higher RVEF than those with TM [Mavrogeni 2008]. The current study included only thalassaemia major patients, all of whom had been transfused from an early age and none had evidence of pulmonary hypertension on transthoracic echocardiography. In the small number of patients where there was isolated RV impairment, all had severe myocardial iron loading with T2* values below 10ms and LVEF was at the lower end of the normal range. None of the patients had known pulmonary hypertension and there were no CMR features to suggest that the RV impairment was related to raised pulmonary artery pressure. It is likely that the RV impairment in these four cases is a precursor to LV impairment secondary to severe iron

loading since T2* values below 10ms are a strong predictor of the development of heart failure [Kirk 2009].

There is limited previous data on RV function in myocardial siderosis. Pepe et al compared patients taking different iron chelating agents and found no correlation between myocardial T2* and RVEF [Pepe 2006]. This may be explained by the small study population and the small proportion of patients with significant myocardial iron loading. In a study of 26 patients with symptomatic heart failure (NYHA class III - IV), LVEF (measured by single plane area-length echocardiography) was compared with RVEF (measured by first-pass radionuclide angiography) [Hahalis 2002]. Our findings not only confirm that RV and LV function are often correlated but also provide evidence that both RV and LV impairment are strongly related to myocardial iron overload. In addition, we have used CMR which is considered to be the gold-standard for the assessment of both right and left ventricular volumes and function [Grothues 2002, Grothues 2004].

6.5.1. Limitations

The data was analysed retrospectively from a prospectively accumulated database. RVEF is highly dependent on loading conditions and may not adequately reflect RV contractility, however it is the most widely available method for assessing RV function. These T2* values only apply at a field strength of 1.5T, and the relaxation parameters will be different at higher field strengths such as 3T which is becoming more widely available for clinical scanning. We measured myocardial T2* in the interventricular septum, using this value to give an assessment of global myocardial iron loading. Although this is an indirect measurement of RV iron, direct measurement of T2* in the right ventricular free wall is not robust as the myocardium is very thin, close to the chest wall and susceptible to artefact. Patients

underwent regular cardiology assessment which included transthoracic echocardiography. We excluded patients with pulmonary hypertension (defined as tricuspid regurgitant jet velocity of >3.0 m/sec on transthoracic echocardiography) but echocardiograms were not performed at the time of the CMR studies. We did not find any significant increase in RV mass index in this cohort (compared with normal reference values for healthy subjects) and there was no significant difference in RV mass between those patients with T2* less than 20ms and those with a T2* of >20 ms. In this study, we did not assess biomarkers (such as brain natriuretic peptide or BNP) or the presence of late enhancement following gadolinium injection, both of which could give further insight into the mechanism of both RV and LV dysfunction in these patients.

6.6. CONCLUSIONS

Increasing myocardial siderosis as assessed by T2* CMR is associated with RV dysfunction, and this may be a significant contributor to heart failure in thalassaemia major. Further studies are required to determine the relative importance of RV function compared with LV function, and to establish whether novel treatment strategies targeted to the RV may prove useful.

6.6.1. Acknowledgements

This work was supported by the NIHR Cardiovascular Biomedical Research Unit at the Royal Brompton and Harefield NHS Foundation Trust and Imperial College London.

6.6.2. Competing interests

DJP is a consultant to Novartis and ApoPharma, and a director of Cardiovascular Imaging Solutions. DJP has received research support and speakers honoraria from Siemens, Novartis and ApoPharma. JPC has received speaker's honoraria from Swedish Orphan and ApoPharma. TH and GCS are consultants to Novartis.

6.6.3. Publication

These data have been published as: Alpendurada F, Carpenter JP, Deac M, Kirk P, Walker JM, Porter JB, Banya W, He T, Smith GC, Pennell DJ. Relation of myocardial T2* to right ventricular function in thalassaemia major. *Eur Heart J* 2010;31:1648-54.

CHAPTER 7: RIGHT VENTRICULAR VOLUMES AND FUNCTION IN THALASSAEMIA MAJOR PATIENTS IN THE ABSENCE OF MYOCARDIAL IRON OVERLOAD

7.1. ABSTRACT

Aim: We aimed to define reference ranges for right ventricular (RV) volumes, ejection fraction (EF) in thalassemia major patients (TM) without myocardial iron overload.

Methods and results: RV volumes, EF and mass were measured in 80 TM patients who had no myocardial iron overload (myocardial T2* > 20 ms by cardiovascular magnetic resonance). All patients were receiving deferoxamine chelation and none had evidence of pulmonary hypertension or other cardiovascular comorbidity. Forty age and sex matched healthy non-anemic volunteers acted as controls. The mean RVEF was higher in TM patients than controls (males $66.2 \pm 4.1\%$ vs. $61.6 \pm 6\%$, $p = 0.0009$; females $66.3 \pm 5.1\%$ vs. $62.6 \pm 6.4\%$, $p = 0.017$), which yielded a raised lower threshold of normality for RVEF in TM patients (males 58.0% vs. 50.0% and females 56.4% vs. 50.1%). RV end-diastolic volume index was higher in male TM patients (mean 98.1 ± 17.3 mL vs. 88.4 ± 11.2 mL/m², $p = 0.027$), with a higher upper limit (132 vs. 110 mL/m²) but this difference was of borderline significance for females (mean 86.5 ± 13.6 mL vs. 80.3 ± 12.8 mL/m², $p = 0.09$, with upper limit of 113 vs. 105 mL/m²). The cardiac index was raised in TM patients (males 4.8 ± 1.0 L/min vs. 3.4 ± 0.7 L/min, $p < 0.0001$; females 4.5 ± 0.8 L/min vs. 3.2 ± 0.8 L/min, $p < 0.0001$). No differences in RV mass index were identified.

Conclusion: The normal ranges for functional RV parameters in TM patients with no evidence of myocardial iron overload differ from healthy non-anemic controls. The new reference RV ranges are important for determining the functional effects of myocardial iron overload in TM patients.

7.2. INTRODUCTION

Patients with beta-thalassemia major (TM) have a severe hereditary anemia which requires lifelong transfusions to prolong survival and allow normal development [Weatherall 2001]. Due to the absence of an effective physiological excretory pathway in humans, the unwanted consequence of these blood transfusions is iron overload, predominantly affecting the heart, liver and endocrine organs. Despite recent improvements in patient care, iron overload cardiomyopathy remains a leading cause of death in TM patients in many centers [Borgna-Pignatti 2004, Modell 2008]. The early detection of iron-induced cardiac toxicity therefore forms a key component of clinical management. The assessment of cardiac iron loading can be performed directly by measurement of myocardial T2* (explicit myocardial iron assessment) or indirectly by the assessment of ventricular volumes and function (examination of effects of myocardial iron on cardiac function).

Previously published data have shown that indices of the left ventricle (LV) such as volumes and ejection fraction (EF) differ in non-cardiac iron loaded TM patients from healthy non-anemic controls, most likely due to chronically increased cardiac output related to the anemia [Westwood 2007, Maceira 2006b]. These differences in the normal range of expected values affect the interpretation of measures of ventricular function from echocardiography and cardiovascular magnetic resonance (CMR). This is important with regard to the early detection of impaired EF because the use of inappropriate reference values may mask the diagnosis of underlying iron-overload cardiomyopathy and this can result in delayed treatment or a preventable episode of heart failure, which places the patient at high hazard [Felker 2000]. Conversely, an apparently dilated heart in a TM patient may be within normal limits for the non-iron overloaded TM population. Although it has been shown that both RV and LV EF are reduced by iron loading [Anderson 2001, Alpendurada 2009b], the normal ranges for RV parameters and function in TM patients who have no evidence of cardiac iron loading are

unknown. The aim of this study therefore was to define the normal reference ranges for RV volumes, ejection fraction and mass in non-iron overloaded transfusion dependent TM patients in comparison with non-anemic healthy controls. CMR was used for this assessment as it is regarded as the gold-standard technique for measurement of both LV and RV volumes and function [Bellenger 2000, Grothues 2002, Grothues 2004], and CMR can also measure myocardial iron loading using myocardial T2*.

7.3. METHODS

7.3.1. Study population

We performed a retrospective analysis of patients with beta-thalassemia major who were referred for their first myocardial T2* scan from 21 UK hematology centres. All patients were regularly transfused (every 3-4 weeks) to maintain pre-transfusion hemoglobin levels of 9-10 g/dl and all had received iron chelation therapy from an early age or from the mid-to-late 1970s if born before this time. To remove any possible effects of different iron chelating agents, only patients taking deferoxamine as a single iron chelator were included. None of the patients had received treatment with either of the oral chelating agents (deferiprone or deferasirox). Forty male and forty female patients over the age of 18 years who had no myocardial iron loading (defined as having cardiac T2* > 20 ms) and no history of any known cardiovascular pathology were identified from the initial target population of 323 patients. The cut-off value for normal T2* was based on the lower limit of normal observed in a cohort of healthy volunteers [Anderson 2001]. Patients with evidence of pulmonary hypertension (defined as tricuspid regurgitant velocity > 3.0 m/s at rest by transthoracic echocardiography) were excluded. Forty age and sex matched healthy non-anemic volunteers formed a control population for comparison. All control subjects were healthy, asymptomatic volunteers with

no cardiovascular risk factors or history of cardiac disease. Each had a normal 12 lead electrocardiogram and no abnormal signs on physical examination. This study was approved by the local NHS Research Ethics Committee. Written informed consent was obtained from all of the volunteers. For the TM patients, the Ethics Committee granted permission for review of clinical and scan data, waiver of informed consent and anonymous publication.

7.3.2. Cardiovascular magnetic resonance

All scans were performed using a 1.5T Sonata scanner (Siemens Medical Systems, Erlangen, Germany). After routine localizer images, each scan comprised of a contiguous set of breath-hold steady state free precession (SSFP) short-axis cines at 10 mm intervals from base to apex (7 mm slice thickness with 3 mm gap) using standardised techniques [Maceira 2006a, Maceira 2006b]. An ECG gated breath-hold bright blood multi-echo sequence was also used to acquire a single short axis mid-ventricular slice for the measurement of myocardial T2* (a gradient echo sequence acquired immediately after the R-wave trigger with flip angle of 35°, matrix of 128 × 256 pixels, field of view (FOV) 40 cm, bandwidth of 810 Hz per pixel and repetition time (TR) of 20 ms between each radiofrequency (RF) pulse). This sequence generated a series of images with a range of equally spaced echo times (TE = 2.6-16.7 ms) [Westwood 2003a].

7.3.3. CMR analysis

Right ventricular volumes and mass were measured from the SSFP cines as previously described [Bellenger 2002, Maceira 2006b], using CMRtools (Cardiovascular Imaging Solutions, London). This involved tracing the endocardial and epicardial borders at end-diastole and end-systole with semi-automated thresholding to delineate the blood pool (figure 7.1).

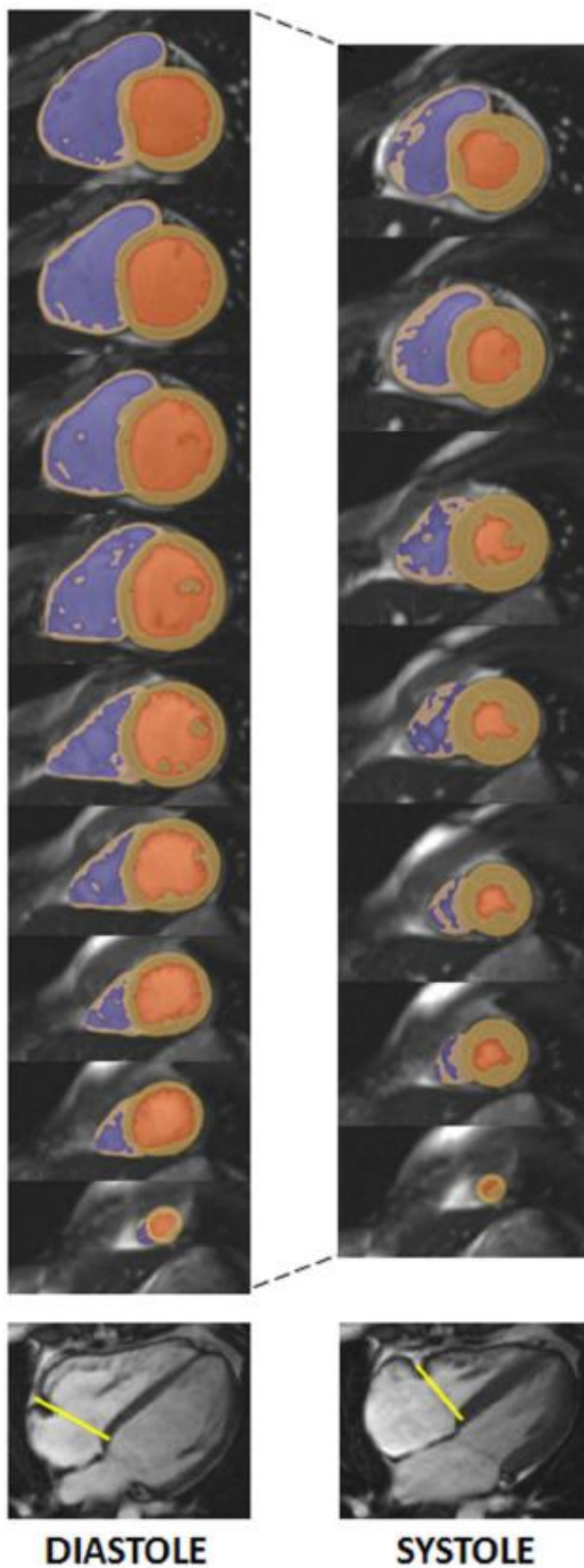


Figure 7.1. Calculation of RV parameters. Delineation of right ventricular endocardial and epicardial borders using semi-automated software, and summing up over all contiguous slices covering the right ventricle allows the calculation of all volume, mass and functional parameters. Representative images are shown for end-diastole and end-systole together with tricuspid valve plane tracking (indicated by the yellow line on the four-chamber view). The RV blood pool is shown in blue, the LV blood pool in orange and the myocardium in beige.

RV trabeculations were excluded from the blood pool volume but included in the RV mass calculation. The tricuspid valve plane was tracked in both systole and diastole to ensure that any blood signal from the right atrium was excluded from the ventricular volume calculation. Any of the blood pool signal above the pulmonary valve was also excluded from the ventricular volume using the endocardial contour definitions. Cardiac output was calculated from the product of right ventricular stroke volume and the mean heart rate recorded at the time of the CMR scan. RV parameters were indexed to body surface area (BSA) which was derived using the Mosteller formula [Maceira 2006b, Mosteller 1987]. Myocardial T2* was measured from a single full thickness region of interest in the septum of the midventricular slice using semi-automated software (Thalassemia-tools, Cardiovascular Imaging Solutions, London, UK). For the analysis of T2*, mean signal intensity was plotted against the echo time for each image in the series. The T2* value was calculated as previously described from the resulting exponential decay curve after truncating the curve to correct for background noise [He 2008].

7.3.4. Hemoglobin measurements

Pre-transfusion hemoglobin measurements were compared with right ventricular parameters. When the interval between the hemoglobin measurement and the index CMR scan exceeded one week, patients were excluded from this part of the analysis.

7.3.5. Statistical analysis

All continuous parameters were found to be normally distributed and are therefore presented as mean \pm standard deviation (SD). An unpaired two-tailed t-test was used to compare TM

patients with the healthy non-anemic volunteers. Separate analysis was performed for males and females due to known gender-specific differences for left and right ventricular parameters. Pearson correlation was used to compare hemoglobin measurements with the RV volumes and function measurements. Statistical significance was set at $p < 0.05$. All statistical analysis was performed using Stata 10.1 software (Stata-Corp, Texas, USA).

Table 7.1. Demographics for TM patients and controls.

	TM patients Mean \pm SD	Controls Mean \pm SD	P value
Males			
Age (years)	30 \pm 8	30 \pm 5	0.94
Height (m)	1.65 \pm 0.1	1.80 \pm 0.09	<0.0001
Weight (kg)	59.1 \pm 8.9	75.8 \pm 9.9	<0.0001
BMI (kg/m ²)	21.9 \pm 3.1	23.6 \pm 3.1	0.048
BSA (m ²)	1.64 \pm 0.16	1.94 \pm 0.15	<0.0001
Heart rate (min ⁻¹)	72.7 \pm 10.4	64.0 \pm 9.5	0.0024
Females			
Age (years)	30 \pm 8	30 \pm 5	0.88
Height (m)	1.54 \pm 8.9	1.67 \pm 9.2	<0.0001
Weight (kg)	53.3 \pm 10.1	61.4 \pm 11.3	0.0064
BMI (kg/m ²)	22.5 \pm 4.5	22.0 \pm 2.8	0.68
BSA (m ²)	1.50 \pm 0.15	1.68 \pm 0.18	0.0001
Heart rate (min ⁻¹)	78.8 \pm 10.1	64.8 \pm 13.6	<0.0001

BSA -- body surface area, BMI -- body mass index.

7.4. RESULTS

7.4.1. Patient population

A summary of the demographics for the patients and the control population is given in table 7.1. Both groups were well matched for age and sex. The body mass index was equivalent in females but was slightly higher in the male control population than the TM patients. However, both male and female TM patients had significantly lower weight, height and body surface

area than the non-anemic controls. Resting heart rate in TM patients was also significantly higher than in the healthy controls.

Table 7.2. Right ventricular parameters for males and females.

	TM patients (mean \pm SD) [95% CI]	Controls (mean \pm SD) [95% CI]	P value
Males			
RVEDVI (mL/m ²)	98.1 \pm 17.3 [64.2 – 132.0]	88.4 \pm 11.2 [66.5 – 110.4]	0.027
RVESVI (mL/m ²)	33.2 \pm 8.0 [17.5 – 48.8]	33.8 \pm 5.0 [24.0 – 43.7]	0.77
RVSVI (mL/m ²)	64.7 \pm 11.2 [42.7 – 86.6]	54.7 \pm 10.3 [34.6 – 74.8]	0.0015
RVEF (%)	66.2 \pm 4.1 [58.0 – 74.3]	61.6 \pm 6.0 [50.0 – 73.3]	0.0009
RVMI (g/m ²)	38.8 \pm 7.9 [23.3 – 54.4]	36.4 \pm 7.8 [21.1 – 51.7]	0.27
CO (L/min)	7.9 \pm 1.9 [4.16 – 11.5]	6.6 \pm 1.6 [3.4 – 9.8]	0.014
CI (L/min/m ²)	4.8 \pm 1.0 [2.9 – 6.7]	3.4 \pm 0.7 [2.0 – 4.8]	<0.0001
Females			
RVEDVI (mL/m ²)	86.5 \pm 13.6 [59.8 – 113.2]	80.3 \pm 12.8 [55.3 – 105.3]	0.093
RVESVI (mL/m ²)	29.2 \pm 7.2 [15.1 – 43.2]	30.3 \pm 8.6 [13.5 – 47.1]	0.58
RVSVI (mL/m ²)	57.4 \pm 9.2 [39.4 – 75.5]	50.0 \pm 7.8 [34.7 – 65.2]	0.0030
RVEF (%)	66.3 \pm 5.1 [56.4 – 76.2]	62.6 \pm 6.4 [50.1 – 75.0]	0.017
RVMI (g/m ²)	34.0 \pm 7.7 [18.8 – 49.1]	30.8 \pm 5.3 [20.5 – 41.1]	0.11
CO (L/min)	6.8 \pm 1.7 [3.5 – 10.1]	5.5 \pm 1.5 [2.5 – 8.4]	0.0033
CI (L/min/m ²)	4.5 \pm 0.8 [2.9 – 6.2]	3.2 \pm 0.8 [1.7 – 4.8]	<0.0001

All values are quoted as mean \pm SD with 95% confidence intervals in square brackets. The table is divided into TM patients with no evidence of cardiac iron overload and age-matched healthy controls.

RVEDVI = right ventricular end-diastolic volume index, RVESVI = right ventricular end-systolic volume index, RVSVI = right ventricular stroke volume index, RVEF = right ventricular ejection fraction, RVMI = right ventricular mass index, CO = cardiac output, CI = cardiac index

7.4.2. Right ventricular parameters

The right ventricular parameters are detailed in table 7.2, and represented graphically in figures 7.2 and 7.3. The mean and upper limit of end-diastolic RV volume were higher in TM patients than controls for males, but this was borderline significant for females ($p = 0.027$ for

males, $p = 0.093$ for females). RV stroke volume and RV ejection fraction were higher in TM patients for both males ($p = 0.0015$ for stroke volume, $p = 0.0009$ for RVEF) and females ($p = 0.0030$ for stroke volume, $p = 0.017$ for RVEF). The lower limit of RVEF was higher in TM patients (males 58.0% vs. 50.0%, females 56.4% vs. 50.1%). The cardiac output was higher in the TM cohort than controls ($p = 0.014$ for males, $p = 0.0033$ for females) and this finding was confirmed when cardiac output was indexed for BSA (cardiac index, $p < 0.0001$). No significant difference was found however between TM patients and controls for either RV end-systolic volume index or RV mass index ($p = 0.11$ to 0.77).

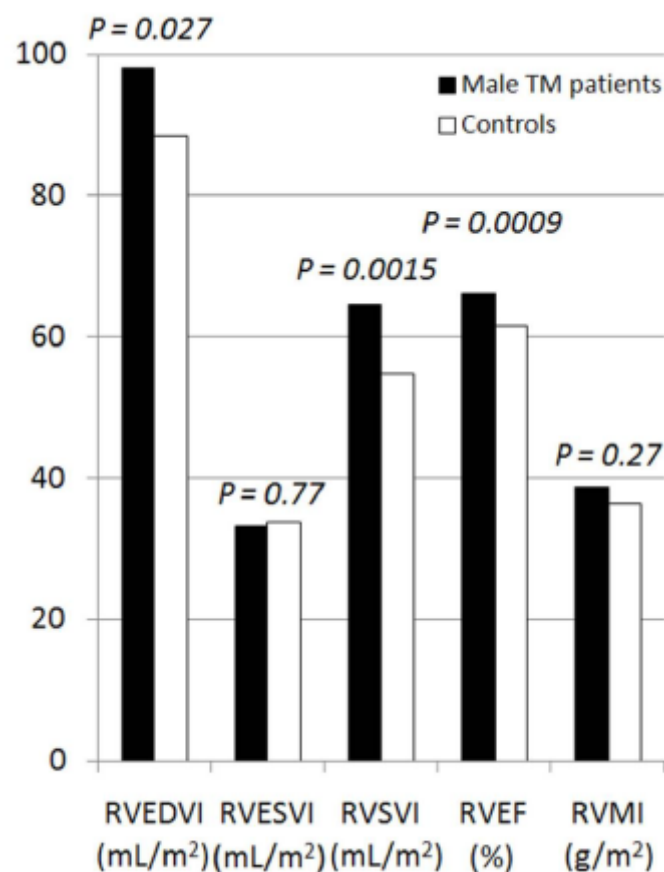


Figure 7.2. Right ventricular volumes and ejection fraction in male TM patients and controls.

RVEDVI = right ventricular end-diastolic volume index, RVESVI = right ventricular end-systolic volume index, RVSVI = right ventricular stroke volume index, RVEF = right ventricular ejection fraction, RVMI = right ventricular mass index.

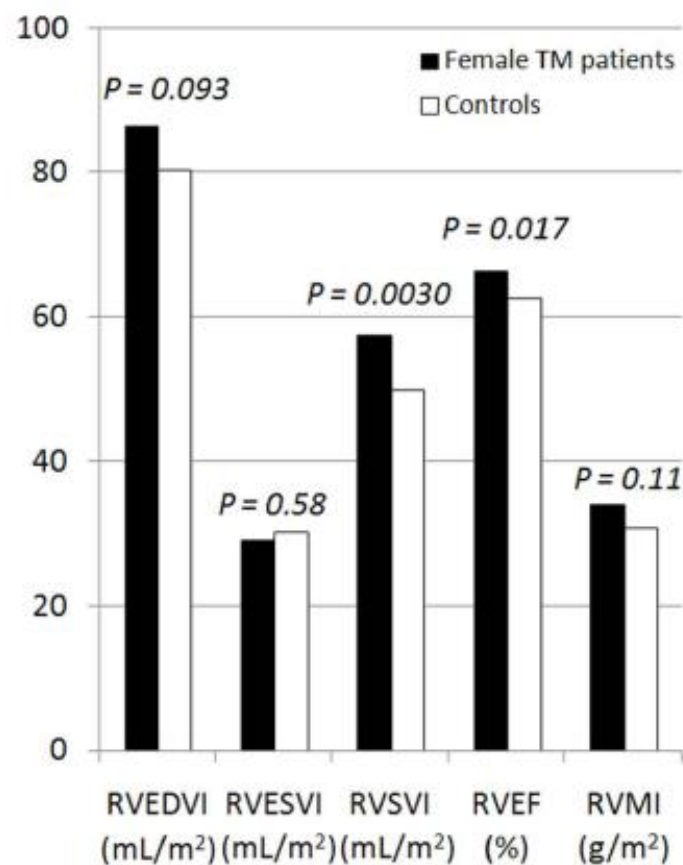


Figure 7.3. Right ventricular volumes and ejection fraction in female TM patients and controls.

Abbreviations as in figure 7.2.

7.4.3. Correlation with hemoglobin levels

Hemoglobin results which coincided with CMR scans (blood tests within one week of the scan) were obtained in 59% of the patients investigated. There was no difference in any of the RV parameters between those patients with hemoglobin results and those in whom the results were unavailable. Mean hemoglobin level was 9.7 ± 1.8 g/ dL for males ($n = 20$) and 10.5 ± 1.4 g/dL for females ($n = 27$). In the female TM patients, no significant correlations existed between hemoglobin concentration and any of the RV parameters. In male TM patients, an inverse correlation was found between cardiac index and haemoglobin ($r = -0.47$, $p = 0.04$). No other significant correlation was found.

7.5. DISCUSSION

Cardiac complications due to myocardial siderosis remain a serious problem for TM patients. Until recently, more than 50% of TM patients died before the age of 35 from cardiac failure [Modell 2000]. The monitoring of cardiac iron using T2* CMR has had a major impact on saving the lives of patients by identifying cardiac iron overload prior to the occurrence of heart failure which therefore allows tailored cardiac chelation [Modell 2008]. However, cardiac T2* is not available in all centers and non-cardiac measures of iron loading are not satisfactory for assessing the risk of heart failure in comparison with cardiac T2* [Kirk 2009]. An indirect approach to assessment of cardiac iron loading is to measure cardiac volumes and function. Although the literature establishing the value of this approach is rather sparse [Davis 2004], it has the merit that techniques for assessment of cardiac function such as echocardiography are widely available and its application is included in some clinical guidelines [Yardumian 2005]. In favor of the use of functional heart measurements is the clear evidence of a correlation with cardiac iron loading that is not present for cross-sectional measures of blood iron (ferritin) or liver iron [Anderson 2001]. Any such approach however, requires that normal values for TM patients who do not have cardiac iron loading are established. Previous data has shown that left ventricular volumes and function in non-cardiac iron loaded TM patients are significantly different from healthy non-anemic controls [Westwood 2007], but there is no data on the normal values of RV volumes and function in non-cardiac iron loaded patients with TM. The right ventricle has consistently been underestimated as an important factor in heart disease and its power to predict adverse cardiac outcomes, which is independent and additional to LV function, has often been overlooked in the past. The balance has been addressed in a number of relatively recent studies of the RV in association with outcomes in heart failure syndromes related to dilated cardiomyopathy [La Vecchia 2001], chronic systolic dysfunction [Meyer 2010], and ischemia

[Di Salvo 1995, de Groote 1998, Ghio 2001], and also in patients with congenital heart disease [Gatzoulis 1995, Graham 2000, Roos-Hesselink 2004]. This suggests that RV function may be a significant contributor to the clinical manifestation of heart failure seen in myocardial iron overload. Therefore in this study, we evaluated RV parameters using CMR in a population of regularly transfused TM patients with no cardiac iron loading or pulmonary hypertension or other cardiac morbidity and have compared the findings to those of healthy non-anemic subjects to established reference ranges that would prove useful to assess the functional effects on the heart of iron overload. Many TM patients have growth retardation with short stature and low body weight. The direct comparison of raw RV indices between TM patients and a cohort of healthy non-anemic subjects therefore requires indexing the RV volumes to body surface area.

Our results show that compared with healthy non-anemic controls, TM patients have a higher RV stroke volume and heart rate, which results in a higher cardiac output. The RVEF is also increased mainly as a result of an increased end-diastolic volume. These results are similar to the observations of LV parameters in TM but the differences in RV parameters appear to be less pronounced than those found for the LV [Westwood 2007]. Our results stress that if functional measurements of the heart are to be made and used clinically to indirectly assess cardiac iron loading, then it is vital to use reference ranges from TM patients with no cardiac iron loading as presented from this study in order to prevent underdiagnosis of cardiac siderosis when using the EF, or its overdiagnosis when using the end-diastolic volume.

No correlation between hemoglobin level and RV parameters was identified in female TM patients but in males, there was an inverse correlation between haemoglobin and cardiac index. It is not evident why male and female patients differ but the result mirrors previous observations [Westwood 2007]. An inverse relationship between haemoglobin and cardiac index is predictable, and indicates a higher output state with a greater degree of anemia.

There was no correlation between hemoglobin and RVEF for either sex, a finding supported by a previous study which found no difference in LVEF using radionuclide ventriculography both before and 24 hours after blood transfusion [Davis 2004]. Pulmonary hypertension (which may depress RV function and cause right heart failure) has been described in thalassemia patients but although it is prominent in those with thalassemia intermedia, it is uncommon in well treated TM patients [Aessopos 2004, Aessopos 2005a, Aessopos 2005b]. Not only have we purposely excluded patients with pulmonary hypertension from this study, but we also found no significant difference in RV mass between cases and controls, a sensitive and specific measure for the diagnosis of pulmonary hypertension using CMR [Saba 2002]. Therefore we believe there is no confounding of our results from pulmonary hypertension.

The right ventricle has a complex anatomical structure in comparison to the LV. Whereas the LV is approximately circular in cross-section, the RV is crescentic, wrapping around the LV with separate inflow and outflow portions, the tricuspid and the pulmonary valves being physically separated by a muscular subpulmonary infundibulum. The RV is thin walled with many trabeculations and there is a moderator band of myocardial tissue towards the apex. All of these features create challenges for modeling RV volumes, making it more difficult to perform reliable measurements using standard echocardiographic techniques. CMR is able to overcome most of these issues and is currently considered the gold standard for the measurement of cardiac volumes and function [Grothues 2004], with well defined normalized values for the RV [Maceira 2006a]. The relative accuracy of echocardiography in relation to CMR must therefore be considered when interpreting results of RV measurements in clinical practice.

There is previously published data regarding RV function in patients with established heart failure due to myocardial siderosis and other studies have reported RV parameters in TM patients across a wide range of iron loading [Hahalis 2002, Pepe 2006b, Mavrogeni 2008].

However, our study focuses only on RV volumes and function in TM patients without evidence of cardiac iron loading.

7.5.1. Limitations

We have restricted our investigation to CMR parameters of RV function and comparisons with RV measurements from other imaging modalities should be interpreted with caution. While RVEF is the most widely available method for assessing RV function, it may not adequately reflect RV contractility and other techniques for the assessment of the RV may provide additional insights. For the haemoglobin correlation, we only used results in a subset of the patients for which the time between the CMR scan and the hemoglobin estimation was less than 1 week. Subset analysis showed no significant differences in any of the RV parameters between patients with and those without hemoglobin results. We did not have reliable information regarding the date of the most recent transfusion prior to the CMR assessment in the TM cohort. While transfusion could potentially affect RV parameters including RVEF, there is only limited data regarding the effects of transfusion on ventricular function. For the LV, no significant difference in LVEF is observed between measurements taken before or 24 hours after blood transfusion [Davis 2004].

7.6. CONCLUSION

Our findings show that the normal ranges for RV parameters differ between TM patients without cardiac iron loading and normal, non-anemic controls. The lower limit of RVEF in TM patients without cardiac iron loading is significantly higher than the lower limit of the normal range in controls which could lead to underdiagnosis of iron-loading cardiomyopathy if this is not appreciated. It is important to use reference ranges which are specific to non-cardiac iron

loaded TM patients when assessing cardiac volumes and function as a surrogate for cardiac iron loading.

7.6.1. Acknowledgements

This work was supported by the National Institutes for Health Research Cardiovascular Biomedical Research Unit, a collaboration between Royal Brompton Hospital and Imperial College London.

7.6.2. Competing interests

DJP is a consultant to Novartis, ApoPharma and Siemens, and is a director of Cardiovascular Imaging Solutions. DJP has received research support and speakers honoraria from Siemens, Novartis and ApoPharma. JPC has received speaker's honoraria from Swedish Orphan and ApoPharma. JBP has received research support from and has performed advisory board work for Novartis.

7.6.3. Publication

These data have been published as: Alpendurada F*, Carpenter JP*, Deac M, Maceira A, Garbowski M, Kirk P, Walker JM, Porter JB, Shah F, Banya W, He T, Smith GC, Pennell DJ. Right ventricular volumes and function in thalassemia major patients in the absence of myocardial iron overload. J Cardiovasc Magn Reson 2010;12:24. (*Joint first author)

CHAPTER 8: EFFECTS OF COMBINED DEFERIPRONE WITH DEFEROXAMINE ON RIGHT VENTRICULAR FUNCTION IN THALASSAEMIA MAJOR

8.1. ABSTRACT

Background: Combination therapy with deferoxamine and oral deferiprone is superior to deferoxamine alone in removing cardiac iron and improving left ventricular ejection fraction (LVEF). The right ventricle (RV) is also affected by the toxic effects of iron and may cause additional cardiovascular perturbation. We assessed the effects of combination therapy on the RV in thalassaemia major (TM) using cardiovascular magnetic resonance (CMR).

Methods: We retrieved imaging data from 2 treatment trials and re-analyzed the data for the RV responses: Trial 1 was a randomized controlled trial (RCT) of 65 TM patients with mild-moderate cardiac siderosis receiving combination therapy or deferoxamine with placebo; Trial 2 was an open label longitudinal trial assessing combination therapy in 15 TM patients with severe iron loading.

Results: In the RCT, combination therapy with deferoxamine and deferiprone was superior to deferoxamine alone for improving RVEF (3.6 vs. 0.7%, $p=0.02$). The increase in RVEF was greater with lower baseline $T2^*$ 8-12ms (4.7 vs. 0.5%, $p=0.01$) than with $T2^*$ 12-20ms (2.2 vs. 0.8%, $p=0.47$). In patients with severe cardiac siderosis, substantial improvement in RVEF was seen with open-label combination therapy ($10.5\% \pm 5.6\%$, $p<0.01$).

Conclusions: In the RCT of mild to moderate cardiac iron loading, combination treatment improved RV function significantly more than deferoxamine alone. Combination treatment also improved RV function in severe cardiac siderosis. Therefore adding deferiprone to deferoxamine has beneficial effects on both RV and LV function in TM patients with cardiac siderosis.

8.2. INTRODUCTION

In transfusion-dependent thalassaemia major (TM) patients, iron chelation therapy is mandatory to prevent or reverse iron accumulation caused by excess intake from transfusional iron and the increased gastrointestinal absorption. Deferoxamine was the first clinically available iron chelating agent, introduced over 40 years ago, and life expectancy in TM increased dramatically with its use [Zurlo 1989, Olivieri 1994]. However, its beneficial effects are tempered by the cumbersome treatment regimes required, which may be a contributor to the frequently observed long term complications of heart failure and cardiac death [Borgna-Pignatti 2004].

Deferiprone is an orally active chelator with a lower molecular weight that is uncharged at physiological pH, and which is both hydrophilic and lipophilic enabling it to readily penetrate myocardial cells. It has been shown to be superior to deferoxamine in removing iron from the myocardium, and is associated with improved cardiac outcomes [Modell 2000, Anderson 2002, Piga 2003, Kolnagou 2006, Borgna-Pignatti 2006, Pennell 2006]. Due to differences in their access to body iron pools, the use of a combination of the two chelators seems to have a synergistic effect on removal of excess iron [Wonke 1998, Kolnagou 2006]. A recent randomised controlled trial comparing combination therapy with subcutaneous deferoxamine and oral deferiprone against deferoxamine monotherapy showed combination treatment to be superior in removing cardiac iron and improving left ventricular ejection fraction (LVEF) [Tanner 2007]. The beneficial effects of combination therapy on LVEF have also been confirmed in patients with TM and severe iron loading [Tanner 2008].

However, despite this success for LV function, the importance of combination therapy on right ventricular (RV) function has not been reported, even though the RV can be affected by the toxic effects of myocardial iron [Hahalis 2002, Alpendurada 2010]. Cardiovascular magnetic resonance (CMR) provides highly reliable and reproducible measurements of RV volumes and

function as well as myocardial iron using the T2* method [Maceira 2006b, Anderson 2001]. We therefore compared the effects of combination treatment (deferoxamine and deferiprone) with deferoxamine monotherapy on RV function in TM patients with cardiac iron overload.

8.3. METHODS

8.3.1. Study population

In order to examine the effects of combination treatment on the RV, we reanalyzed imaging data from 2 previously reported trials. The first was a randomized, double-blind, placebo controlled trial (RCT) comparing combined therapy of deferoxamine with deferiprone against deferoxamine with placebo in mild-moderate myocardial siderosis [Tanner 2007]. The second trial was a longitudinal open-label study of combination treatment (no comparison arm) in patients with severe cardiac siderosis and impaired LV function [Tanner 2008]. Both trials were run simultaneously in Cagliari Italy (figure 8.1). The study protocol was approved by ethics committees in London and Cagliari. Patient information and consent forms were in Italian and all patients gave written informed consent [Tanner 2007, Tanner 2008]. Brief details of the trials are given below.

In the RCT, 167 adult TM patients (75 males, mean age 30 ± 5.3 years) were screened for quantification of myocardial iron loading using myocardial T2*. Inclusion criteria for patient screening were: diagnosis of TM currently maintained on subcutaneous deferoxamine monotherapy; age >18 years; and maintaining pre-transfusion haemoglobin > 9 g/dL. Exclusion criteria were: patients who had received deferiprone for a total of >6 months over the last 5 years; patients with previous reaction to deferiprone; neutropenia (absolute neutrophil count $<1.5 \times 10^9/L$) at screening; thrombocytopenia ($<50 \times 10^9/L$) at screening; liver

enzymes > 3 times upper limit of normal; any condition making CMR impossible or inadvisable. Of the 167 patients screened, 108 had significant myocardial siderosis ($T2^* < 20$ ms), of whom 22 (13%) had severe myocardial loading ($T2^* < 8$ ms). Patients with mild to moderate cardiac iron loading who satisfied the trial entry criteria (myocardial $T2^*$ 8-20 ms, $n=86$) were invited for further detailed assessment by CMR. Of these, 65 were subsequently randomized to receive either deferoxamine plus deferiprone (combined group; $n=32$) or deferoxamine plus placebo (deferoxamine group; $n=33$), and were followed-up for 12 months.

Patients with severe cardiac siderosis ($T2^* < 8$ ms) were excluded from the RCT and it was at the treating clinician's discretion to determine best clinical practice for chelation therapy. Of the 22 patients with severe myocardial siderosis, 15 (9 females, 28.9 ± 4.8 years) received open-label combination therapy according to locally developed protocols, and were followed prospectively over one year. These patients were used in a secondary comparative analysis against patients from the randomised trial who were on combination therapy.

8.3.2. Cardiovascular magnetic resonance

A mobile 1.5 Tesla CMR scanner (Sonata, Siemens Medical Systems, Erlangen, Germany) was transported to Cagliari for this research. Myocardial and hepatic $T2^*$ were assessed using the bright-blood single breath-hold multi-echo technique as previously described [Westwood 2003a]. $T2^*$ analysis was performed using Thalassaemia-Tools (a plug-in of CMRtools, Cardiovascular Imaging Solutions, London, UK) with curve truncation to account for background noise [He 2008]. Right ventricular volumes and ejection fraction were determined at baseline and at 12 months of treatment with steady state free precession cines using contiguous short-axis slices from base to apex [Maceira 2006b]. CMRtools was used for RV

volume analysis. These measurements were performed by observers blinded to the patient's clinical details and chelation regime.

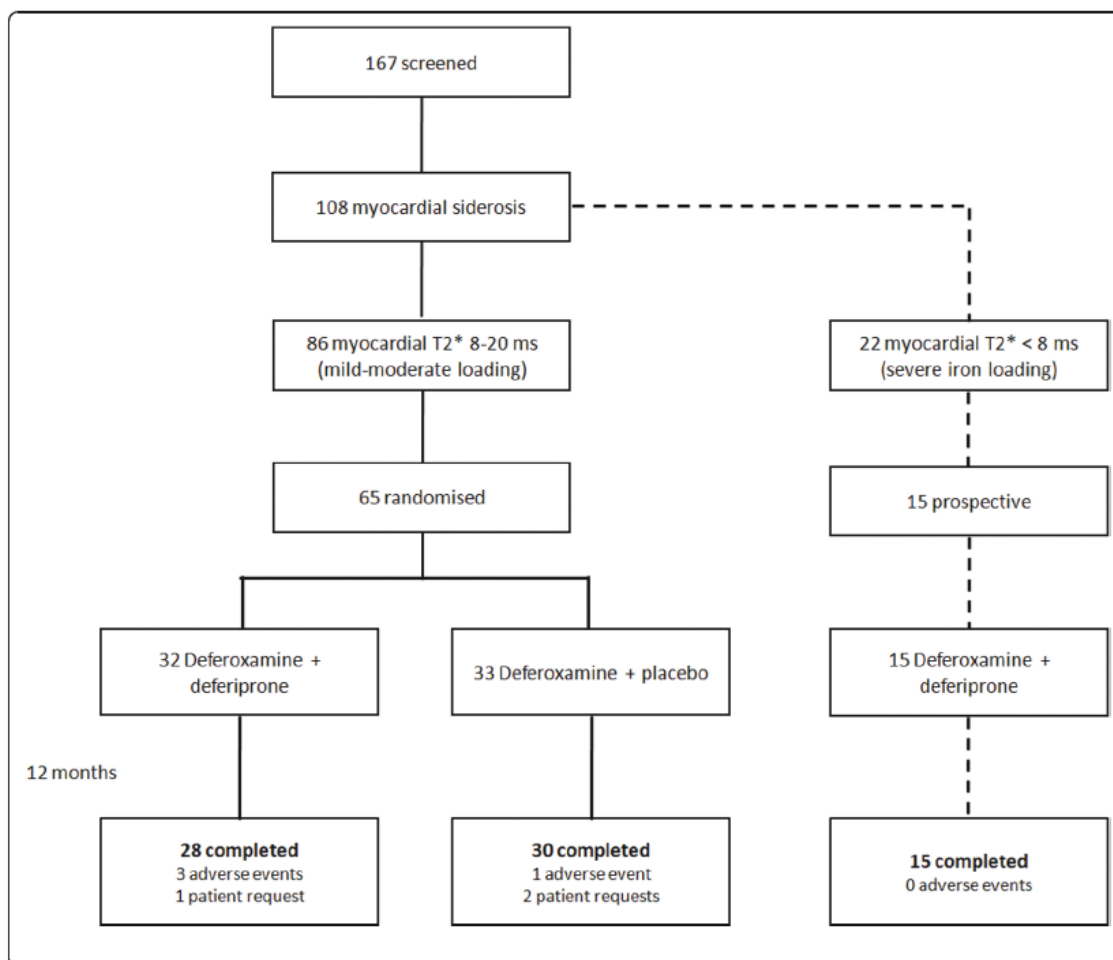


Figure 8.1. Study flow chart.

8.3.3. Echocardiography

Doppler echocardiography studies were performed at baseline and at 12 months to look for pulmonary hypertension. Pulmonary artery systolic pressures (PAP) were determined by peak velocity of the tricuspid regurgitation jet plus estimation of right atrial pressures using standard methodology. Pulmonary hypertension was defined as PAP > 40 mmHg.

8.3.4. Biochemistry

Laboratory measures included weekly full blood count (due to the risk of agranulocytosis with deferiprone), serum ferritin (Abbott AXSYM System), B-type natriuretic peptide (BNP-Biosite Diagnostics Inc, San Diego, California), and liver function tests (alanine aminotransferase-ALT).

8.3.5. Statistical Analysis

Categorical data are presented as frequency and percentage (%). Continuous variables are presented as mean \pm standard deviation (SD), except for BNP, which is displayed in median and interquartile range; and for T2* and ferritin, which use the geometric mean (anti-log of the mean of the log data) \pm coefficient of variation (CV). Baseline characteristics of both treatment groups were compared using an unpaired two-tailed t-test for continuous variables (except for BNP, which was compared by a non-parametric test) and a chi-squared test for categorical variables. Analysis of variance (ANOVA) was used to compare changes in T2* and RVEF over 12 months with treatment and baseline measures entered as covariates. Changes in RVEF over 12 months within individual groups were compared with a paired t-test. Correlations of myocardial T2* with ventricular function were performed using the Spearman's rank test. Subgroup analysis was performed according to severity of myocardial iron loading with cut-offs of 8ms and 12ms used to define patients with mild (T2* 12-20 ms), moderate (T2* 8-12ms) and severe (T2* < 8ms) iron loading. Intraobserver and interobserver variability was assessed using the method of Bland and Altman [Bland 1986]. The coefficient of variability was calculated as the SD of the differences between two sets of measurements divided by the mean value of the parameter under consideration. Statistical significance was set at $p < 0.05$. All statistical analysis was performed using Stata 10.1 software (StataCorp, Texas, USA).

8.4. RESULTS

8.4.1. RCT in mild to moderate cardiac siderosis

The baseline findings and the results of the RCT comparing combination treatment against deferoxamine alone for changes in myocardial T2* and LVEF have been previously published [Tanner 2007], and are briefly summarized here (table 8.1).

Table 8.1. Baseline characteristics of the randomized controlled trial population, according to treatment arm.

	Combined	Deferoxamine	p-value
Number of patients	32	33	-
Age (years)	28.8 ± 4.2	28.7 ± 5.3	0.9
Gender (male)	14 (44%)	13 (39%)	0.5
Body surface area	1.53 ± 0.15	1.56 ± 0.16	0.5
Heart rate	78 ± 10	81 ± 16	0.3
Deferoxamine dose (mg/kg/day)	40.6 ± 13.2 (5 days/week)	40.5 ± 14.0 (5 days/week)	1.0
CMR measures			
Myocardial T2*	11.7 (0.08)	12.4 (0.11)	0.3
Liver T2*	4.9 (0.52)	4.2 (0.62)	0.5
RVEDV (mL)	129.5 ± 30.8	131.8 ± 34.4	0.8
RVESV (mL)	52.5 ± 17.5	52.3 ± 18.5	1.0
RVEF (%)	60.2 ± 7.2	61.0 ± 7.1	0.7
Echo measures			
PAP (mmHg)	22.3 ± 5.0	20.9 ± 5.4	0.4
Blood measures			
Transfusional red blood cell input (mL/kg/year)	133.4 ± 34.9	130.2 ± 38.6	0.7
Haemoglobin (g/L)	106 ± 9.6	102 ± 9.5	0.1
Hepatitis C positive	23 (72%)	26 (79%)	0.4
Serum ferritin (µg/L)	1574 (11)	1379 (10)	0.5
BNP (pmol/L)	13.6 (5.6, 30.1)	15.2 (7.3, 26.2)	0.7
Creatinine (mg/dL)	0.77 ± 0.21	0.74 ± 0.23	0.6
Cardiac medication			
Any	5 (16%)	8 (24%)	0.4
Digoxin	3 (9%)	4 (12%)	0.7
ACEi/ARB	5 (16%)	8 (24%)	0.4
Diuretics	3 (9%)	5 (15%)	0.5

Values are presented as n (%), mean ± SD, geometric mean (coefficient of variation), or as median (25th - 75th percentile). RV = right ventricular; EDV = end-diastolic volume; ESV = end-systolic volume; PAP = pulmonary artery systolic pressure; BNP = B-type natriuretic peptide. ACEi = angiotensin-converting enzyme inhibitors; ARB = angiotensin II receptor blockers.

The patients randomized to combination therapy or deferoxamine alone were evenly matched at baseline. The prescribed dose of deferiprone in the combination arm was 75

mg/kg/day. The average dose of deferoxamine in the deferoxamine alone arm (40.5 mg/kg/day for 5 days/week) was comparable to the combination arm (40.6 mg/kg/day for 5 days/week, $p=1.0$). Four patients in the combination arm withdrew from the study (3 due to adverse events), and 3 patients in the deferoxamine arm withdrew (1 due to an adverse event). Thus, 28 patients in the combination arm and 30 patients in the deferoxamine alone arm completed the study. Over 12 months, the combination treatment group showed superior improvement in myocardial $T2^*$ compared with the deferoxamine group (ratio of change in geometric means 1.50 vs. 1.24, $p=0.02$).

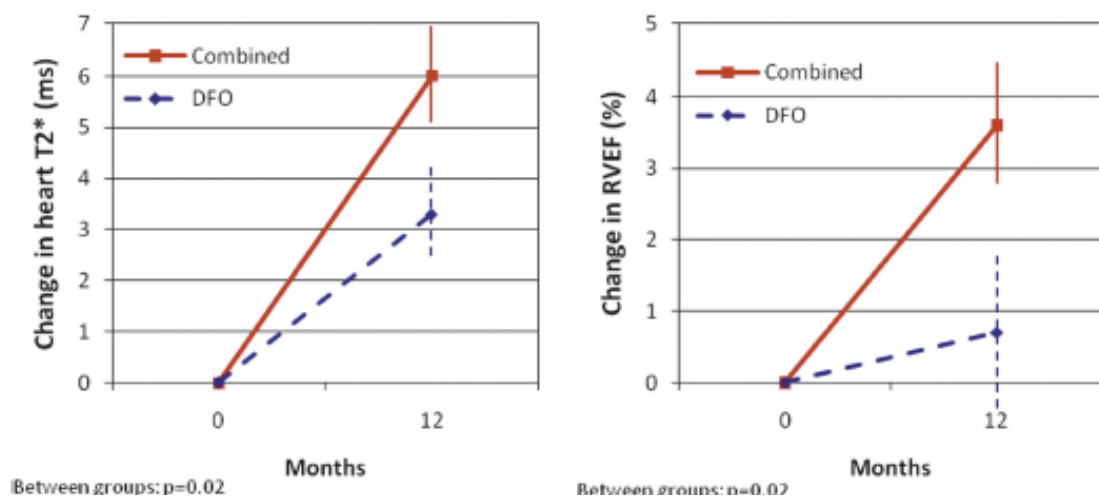


Figure 8.2. Change in myocardial $T2^*$ (left panel) and in RVEF (right panel) over 12 months according to treatment arm. Vertical lines represent standard error.

In the combination group RVEF increased from $60.2 \pm 7.2\%$ at baseline to $63.8 \pm 5.9\%$ at 12 months ($p < 0.01$), whereas in the deferoxamine group RVEF did not change significantly ($61.0 \pm 7.1\%$ at baseline vs. $61.7 \pm 6.4\%$ at 12 months, $p=0.49$). There was a significant difference in the RVEF response between groups favouring combination therapy (3.6 vs. 0.7%, $p=0.02$; figure 8.2). The improvement in RVEF in the combined group was mainly driven by a decrease

in RV end-systolic volumes (52.5 ± 17.5 ml to 46.4 ± 14.9 ml, $p < 0.01$) rather than a change in RV end-diastolic volumes (129.5 ± 30.8 ml to 126.1 ± 29.8 ml, $p = 0.20$). There was no significant change in PAP between the combination vs. the deferoxamine arm from baseline to one year (-1.8 mmHg vs. $+0.3$ mmHg, $p = 0.19$).

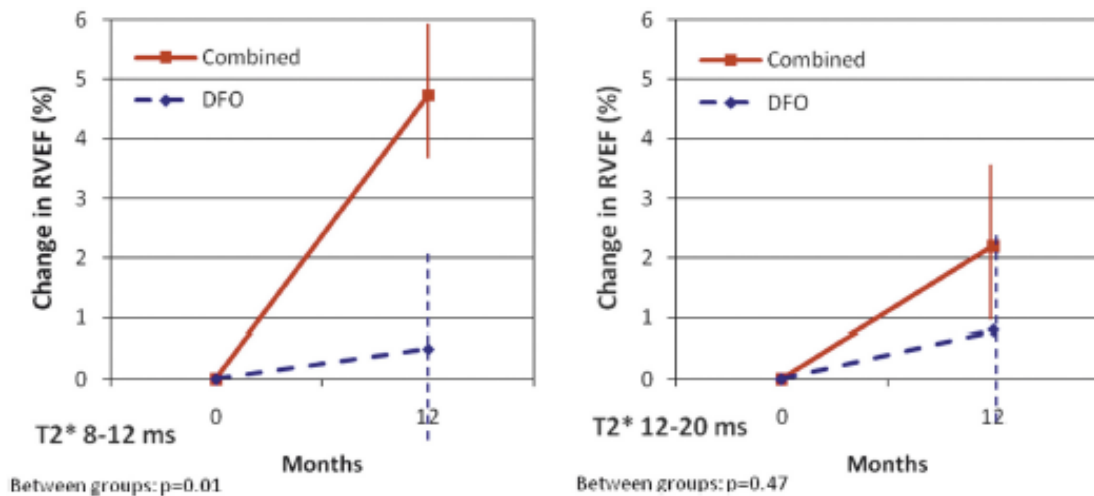


Figure 8.3. Change in RVEF over 12 months according to treatment arm and myocardial T2* at baseline (T2* 8-12 ms on left panel, T2* 12-20 ms on right panel). Vertical lines represent standard error.

The median myocardial T2* in the RCT at baseline was 12.0 ms. This value was used as a cut-off to define patients with mild (myocardial T2* 12-20 ms) and moderate iron loading (myocardial T2* 8-12 ms), and this was in accord with the cut-offs used in the original trials. Both subgroups were then analysed according to the chelation regime. Comparing the individual treatment arms, we observed a significant improvement in RVEF in patients with T2* between 8 and 12 ms on combination therapy ($58.5 \pm 6.9\%$ at baseline vs. $63.3 \pm 6.0\%$ at 12 months, $p < 0.01$), and borderline significant improvement in patients with T2* between 12 and 20 ms ($62.1 \pm 7.3\%$ at baseline vs. $64.3 \pm 6.0\%$ at 12 months, $p = 0.08$). Conversely, patients on deferoxamine alone had no significant improvement in RVEF, whether the baseline T2* was 8-

12ms ($59.3 \pm 6.8\%$ at baseline vs. $59.8 \pm 6.4\%$ at 12 months, $p=0.70$) or 12-20ms ($62.5 \pm 7.2\%$ at baseline vs. $63.3 \pm 6.1\%$ at 12 months, $p=0.58$). Comparison of the between groups effects showed that combination therapy was superior to deferoxamine alone in improving RVEF in patients with baseline $T2^*$ below 12ms (4.7% vs. 0.5%, $p=0.01$) but not in those with $T2^*$ above 12ms (2.2% vs. 0.8%, $p=0.47$; figure 8.3).

Intraobserver and interobserver variability of the right ventricular volumes and ejection fraction was derived from the first 20 subjects participating in the study (table 8.2). The coefficient of variability for the right ventricular measurements was small, in keeping with previous publications on the same area [Grothues 2004, Hudsmith 2005].

Table 8.2. Intraobserver and interobserver reproducibility for the right ventricle.

	Intraobserver		Interobserver	
	Mean difference (\pm SD)	CoV (%)	Mean difference (\pm SD)	CoV (%)
RV end-diastolic volume (mL)	0.6 ± 5.0	3.9	6.7 ± 8.9	7.1
RV end-systolic volume (mL)	-0.1 ± 3.6	6.7	2.0 ± 4.7	8.9
RV ejection fraction (%)	0.5 ± 1.9	3.2	1.0 ± 3.0	5.2

CoV = coefficient of variability; RV = right ventricle.

8.4.2. Longitudinal open-label study in severe cardiac siderosis

The baseline findings and the results of the longitudinal study in the 15 patients with severe iron loading (myocardial $T2^* < 8$ ms) evaluating combination treatment for changes in myocardial $T2^*$ and LVEF have been previously published [Tanner 2008], and are briefly summarized in table 8.3. Two patients were in clinical heart failure, and both had BNP levels >100 pmol/l. The mean prescribed doses of deferoxamine and deferiprone at baseline were 38.0 mg/kg for 5.3 days/week (equivalent to 40.7 mg/kg for 5 days/week) and 73.9 mg/kg/day, respectively. During the trial, doses were reduced to 20.3 mg/kg for 4.5 days/week and 65.7 mg/kg/day respectively, primarily due to reductions in ferritin [Tanner

2008]. All 15 patients received unblinded combination therapy with deferoxamine and deferiprone throughout the study period. Over 12 months, there was a significant improvement in myocardial T2* (ratio of change in geometric means 1.31, $p < 0.01$).

Table 8.3. Baseline characteristics of the randomized controlled trial population (mild and moderate myocardial iron loading) vs. open-label combination therapy population (severe myocardial iron loading).

	Mild-moderate siderosis	Severe siderosis	p- value
	RCT	Longitudinal trial	
Number	65	15	-
Age (years)	28.8 ± 4.7	27.8 ± 4.8	0.5
Gender (male)	27 (41.5%)	6 (40.0%)	0.9
Body surface area	1.55 ± 0.15	1.56 ± 0.13	0.8
Heart rate	79 ± 13	97 ± 18	< 0.01
Deferoxamine (mg/kg/ day)	40.6 ± 13.5 (5 days/week)	40.7 ± 12.0 (5 days/week)	0.9
CMR measures			
Myocardial T2*	12.0 (0.13)	6.0 (0.09)	N/A
Liver T2*	4.5 (0.57)	2.9 (0.67)	0.06
RVEDV (mL)	130.7 ± 32.4	146.7 ± 35.1	0.2
RVESV (mL)	52.4 ± 17.8	76.5 ± 27.6	< 0.01
RVEF (%)	60.6 ± 7.1	49.0 ± 9.4	< 0.01
Echo measures			
PAP (mmHg)	21.6 ± 5.2	22.0 ± 5.9	0.8
Blood measures			
Hepatitis C positive	49 (75%)	11 (73%)	0.9
Serum ferritin (µg/L)	1472 (0.11)	2057 (0.08)	0.1
BNP (pmol/L)	15.0 (7.1, 28.8)	26.0 (15.6, 40.5)	0.01
Cardiac medication			
Any	13 (20%)	7 (47%)	0.03
Digoxin	7 (11%)	4 (27%)	0.1
ACEi/ARB	13 (20%)	7 (47%)	0.03
Diuretics	8 (12%)	4 (27%)	0.2

Values and abbreviations presented as in table 8.1.

In 12 of the 15 patients (80%), the baseline RVEF was low compared to a reference TM population with a normal T2* [Carpenter 2010]. The baseline RVESV was significantly raised and there was a trend for a higher RVEDV, resulting in a significantly reduced mean RVEF ($49.0 \pm 9.4\%$) when compared to the population with less severe iron loading (table 8.3). The open-label group was more frequently medicated for heart failure, particularly angiotensin-converting enzyme inhibitors (ACEi)/angiotensin II receptor blockers (ARB). No patients in the RCT or open-label cohorts were on beta-blockers. Pulmonary artery systolic pressures were similar in both groups (22.0 ± 5.9 mmHg vs. 21.6 ± 5.2 mmHg, $p=0.82$). Over 12 months, there was a significant improvement in RVEF ($10.5 \pm 5.6\%$, $p<0.01$), with no significant change in PAP (22.0 mmHg vs. 24.4 mmHg at 12 months, $p=0.16$). No new cardiac medications were commenced during the study (except for the 2 patients presenting with heart failure, who were asymptomatic by the end of the study). Despite a positive trend, neither cardiac medication as a whole (increase RVEF $12 \pm 6\%$ vs. $9 \pm 5\%$, $p=0.2$), nor individual medications (digoxin: $14 \pm 3\%$ vs. $10 \pm 6\%$, $p=0.2$; ACEi/ARB: $12 \pm 6\%$ vs. $9 \pm 5\%$, $p=0.2$; diuretics: $13 \pm 5\%$ vs. $10 \pm 6\%$, $p=0.4$) were significantly associated with a higher increase in RVEF compared with those without cardiac medication.

When grouping the patients on combination therapy (the 32 patients from the combination arm in the RCT plus the 15 unblinded patients on open-label combined therapy), we found an inverse relation between myocardial T2* at baseline and improvement in RVEF over one year (figure 8.4). Patients with severe iron loading had a greater improvement in RVEF than patients with moderate iron loading (10.5% vs. 4.7% , $p<0.01$).

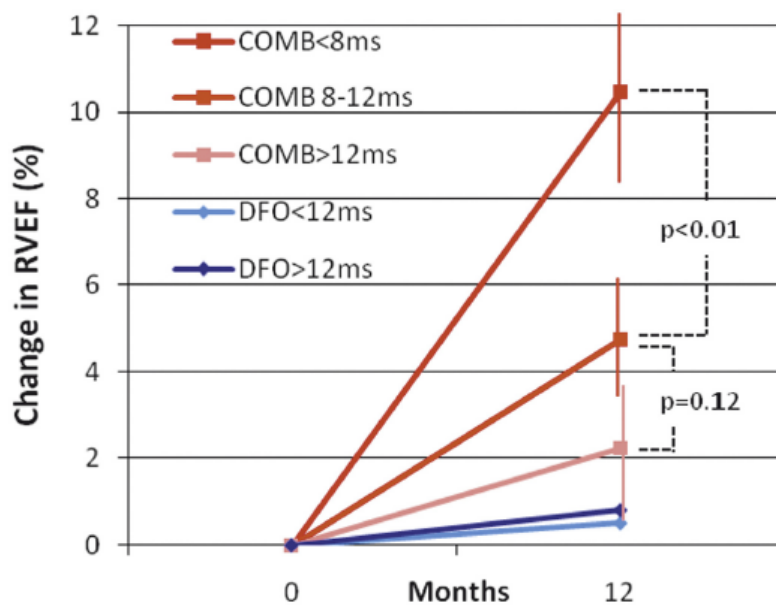


Figure 8.4. Breakdown of improvement in RVEF (%) for different groups according to chelation therapy and myocardial T2* baseline. Vertical lines represent standard error.

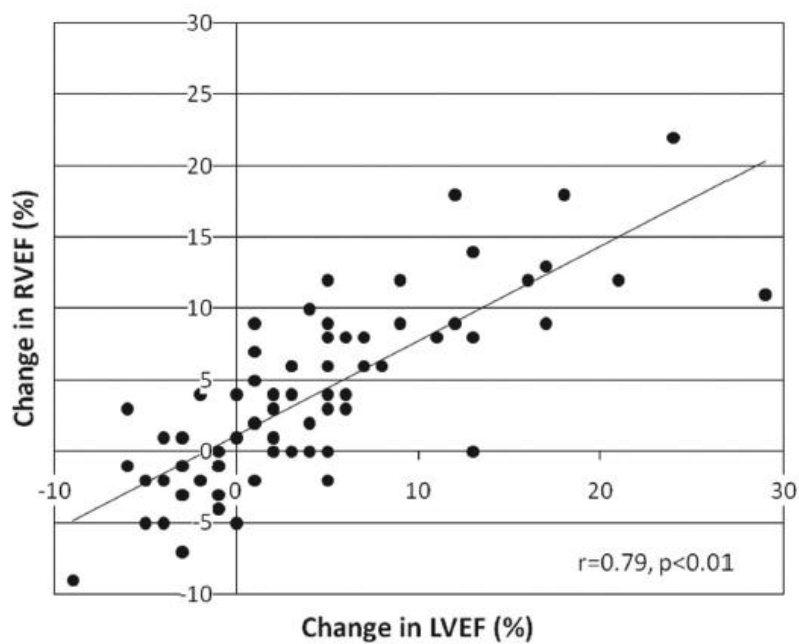


Figure 8.5. Correlation of change in RVEF with change in LVEF over 12 months.

8.4.3. Entire study cohort

In the cohort of 80 patients with myocardial iron loading, a significant correlation was observed between baseline myocardial T2* and baseline RVEF ($r=0.46$, $p<0.01$) and baseline

LVEF ($r=0.50$, $p<0.01$). Accordingly, there was a strong correlation between RVEF and LVEF at baseline ($r=0.82$, $p<0.01$). The improvement in RVEF during the study period also correlated with the improvement in LVEF ($r=0.79$, $p<0.01$; figure 8.5). We also analyzed the change in RVEF with the change in cardiac iron as derived from recent human cardiac iron calibration data from Carpenter et al [Carpenter 2011]. There was a significant inverse correlation between the improvement in myocardial iron concentration and the improvement in RVEF ($r=-0.42$, $p<0.01$).

8.5. DISCUSSION

With the development of the T2* technique, CMR has provided new insights into iron-overload cardiomyopathy, as the myocardial iron concentration and its toxic effect on ventricular function can be assessed at the same time with the same high-fidelity technique. In the first T2* publication by Anderson et al, normal T2* levels were associated with normal LVEF, but when T2* fell below 20ms, there was a progressive fall in LVEF, showing that increasing iron loading is associated with worsening of LV function [Anderson 2001]. Similar observations have recently been made for the RV [Alpendurada 2010], suggesting RV dysfunction may be a contributor to heart failure and cardiac mortality in TM patients, as has been found in other cardiac conditions [Di Salvo 1995, Juillière 1997, Ghio 2001, Larose 2007, Meyer 2010]. However, to date, there has been little published data on the response of the right ventricle to chelation therapy, and no data at all on the most appropriate chelation regime in the presence of right ventricular dysfunction.

Chelation with deferoxamine has been one of the cornerstones for the treatment of TM. It has been extensively studied over the past decades and has shown to decrease the total body iron burden, prevent complications of iron overload and improve survival in TM [Zurlo 1989,

Olivieri 1944, Brittenham 1994]. However, long-term deferoxamine monotherapy has been hampered by poor compliance and failure of long term prevention of myocardial iron deposition, heart failure and cardiac deaths [Modell 2000, Anderson 2002]. Deferiprone is a more recent iron chelator which has a lower molecular weight, is more lipophilic, is uncharged at physiologic pH and consequently appears better able to penetrate cells and organelles than deferoxamine. This may in part explain why deferiprone is superior to deferoxamine for removing iron from the heart [Pennell 2006]. The combined use of these two chelating agents which exploits the relative merits of each drug, has been supported in animal models, and has become an attractive therapeutic option in severe cardiac iron loading or when negative iron balance has not been achieved by other methods [Link 2003, Origa 2005, Tanner 2007]. Observational, prospective and randomised controlled studies have demonstrated the efficacy of combined therapy in removing iron from the liver and heart, improving endothelial function and left ventricular function [Tanner 2007, Tanner 2008], as well as endocrine function [Farmaki 2010]. Our current study compared the effects of combination therapy on RV function in TM patients with myocardial iron loading. Our findings from the RCT show combination therapy to be superior to subcutaneous deferoxamine alone in improving RV function in patients with mild and moderate iron loading. In addition, our data from the longitudinal open-label study show that RV dysfunction is reversible even in patients with severe iron overload. It is of interest that the recovery in RV function was greatest in patients with a more severe degree of myocardial siderosis and RV dysfunction.

It is well recognized that RV performance depends not only on intrinsic contractility but also on RV afterload, which is the resistance that the RV has to overcome during ejection. Increased pulmonary artery pressures reflecting increased pulmonary vascular resistance may thus impair RV function [Shekerdemian 1997]. However, none of the participants in this study had pulmonary hypertension, in line with previous studies suggesting a low prevalence of

pulmonary hypertension in TM [Derchi 1999, Aessopos 2004]. Whilst an improvement in myocardial T2* was associated with an improvement in RVEF, no significant changes in pulmonary artery pressures were observed throughout the study. Therefore, the improvement in RV function seen in this population was independent of pulmonary artery pressure thus eliminating a potential confounding factor for the evaluation of RV function.

Our data are unusual, because reversible RV dysfunction in the setting of a cardiomyopathy is a rarely documented phenomenon. The magnitude of recovery in RV function parallels the recovery in LV function, and this correlates with the response to chelation therapy. This is in keeping with the findings of other studies in non-ischaemic cardiomyopathies, where it has been observed that LV and RV function is usually affected in a similar way and to a similar extent [Juillière 1997, La Vecchia 2001]. The close association seen between RVEF and LVEF and the increase of these parameters over time following successful myocardial iron chelation supports the concept that intrinsic RV myocardial contractility is predominantly affected by intracellular iron and plays a key role in RV performance in this toxic-induced cardiomyopathy model [Alpendurada 2010]. Finally, as right ventricular ejection fraction has incremental prognostic value which is additional to LVEF [Juillière 1997, Di Salvo 1995, Ghio 2001, Larose 2007], it is reasonable to suggest that the improvement in RVEF seen in this study with the combined use of deferiprone and deferoxamine may contribute to improved outcomes.

8.5.1. Limitations

This is a retrospective analysis of 2 trials designed to assess the change on myocardial T2* with iron chelation regimes in which RV parameters were not planned as primary end-points. Nevertheless, all data was prospectively collected and the current RV analysis was blinded to the patients' details and chelation regimes.

8.6. CONCLUSIONS

In the RCT of mild to moderate cardiac iron loading, combination treatment improved RV function significantly more than deferoxamine alone. Combination treatment also improved RV function in severe cardiac siderosis. Therefore adding deferiprone to deferoxamine has beneficial effects on both RV and LV function in TM patients with cardiac siderosis.

8.6.1. Acknowledgements

This project was supported by the NIHR Cardiovascular Biomedical Research Unit at the Royal Brompton & Harefield NHS Foundation Trust and Imperial College London.

8.6.2. Competing interests

FA has received speaker's honoraria from Novartis. GCS is a consultant to Novartis. DJP is a consultant to Novartis and ApoPharma, and a director of Cardiovascular Imaging Solutions. DJP has received research support and speaker's honoraria from Siemens, Novartis, and ApoPharma. JPC has received speaker's honoraria from Swedish Orphan and ApoPharma. SN has received financial assistance from both Novartis and Swedish Orphan for attendance at conferences.

8.6.3. Publication

These data have been published as: Alpendurada F, Smith GC, Carpenter JP, Nair SV, Tanner MA, Banya W, Dessi C, Galanello R, Walker JM, Pennell DJ. Effects of combined deferiprone with deferoxamine on right ventricular function in thalassaemia major. *J Cardiovasc Magn Reson* 2012;14:8.

CHAPTER 9: RIGHT VENTRICULAR DYSFUNCTION IS A PREDICTOR OF NON-RESPONSE AND CLINICAL OUTCOME FOLLOWING CARDIAC RESYNCHRONIZATION THERAPY

9.1. ABSTRACT

Background: Cardiac resynchronization therapy (CRT) is an established treatment in advanced heart failure (HF). However, an important subset does not derive a significant benefit. Despite an established predictive role in HF, the significance of right ventricular (RV) dysfunction in predicting clinical benefit from CRT remains unclear. We investigated the role of RV function, assessed by cardiovascular magnetic resonance (CMR), in predicting response to and major adverse clinical events in HF patients undergoing CRT.

Methods: Sixty consecutive patients were evaluated with CMR prior to CRT implantation in a tertiary cardiac centre. The primary end-point was a composite of death from any cause or unplanned hospitalization for a major cardiovascular event. The secondary end-point was response to therapy, defined as improvement in left ventricular ejection fraction $\geq 5\%$ on echocardiography at one year.

Results: Eighteen patients (30%) met the primary end-point over a median follow-up period of 26 months, and 27 out of 56 patients (48%) were considered responders to CRT. On time-to-event analysis, only atrial fibrillation (HR 2.6, 95% CI 1.02-6.84, $p=0.047$) and RV dysfunction, either by a reduced right ventricular ejection fraction - RVEF (HR 0.96, 95% CI 0.94-0.99, $p=0.006$) or tricuspid annular plane systolic excursion - TAPSE (HR 0.88, 95% CI, 0.80-0.96, $p=0.006$), were significant predictors of adverse events. On logistic regression analysis, preserved RVEF (OR 1.05, 95% CI 1.01-1.09, $p=0.01$) and myocardial scar burden (OR 0.90, 95% CI 0.83-0.96, $p=0.004$) were the sole independent predictors of response to CRT. Patients with marked RV dysfunction ($\text{RVEF} < 30\%$) had a particularly low response rate (18.2%) to CRT.

Conclusions: Right ventricular function is an important predictor of both response to CRT and long-term clinical outcome. Routine assessment of the right ventricle should be considered in the evaluation of patients for CRT.

9.2. INTRODUCTION

Cardiac resynchronisation therapy (CRT) is an established therapeutic option for selected patients with symptomatic heart failure (HF). Amongst its benefits are reduced mortality, improved exercise tolerance and quality of life [Cazeau 2001, Cleland 2005]. However, a proportion of patients do not gain any significant benefit, the reasons for which are unclear. Thus a number of devices are being implanted with no discernible clinical benefit, which has important healthcare costs implications, as well as exposing patients to unnecessary risks. Our current strategy for assessing benefit with CRT is mainly focused on assessing symptomatic or functional response, but it is increasingly clear that this does not necessarily translate into improved clinical outcomes. It is therefore important to refine the selection criteria for device implantation to better identify those who would benefit - both in terms of response and improved clinical outcomes.

Whilst much attention has focused on remodelling of the left ventricle (LV), the role of the right ventricle (RV) in the appropriate selection of patients for CRT remains unclear [Epstein 2008]. Previous studies assessing RV function have utilised echocardiography and radionuclide imaging [Field 2006, Scuteri 2009, Ghio 2009, Burri 2010]. However, accuracy of RV volumes and function by these techniques may be inaccurate due to the anatomical location and complex geometric structure. Cardiovascular magnetic resonance (CMR) imaging offers superior three dimensional representation of the RV, leading to a more accurate and

reproducible assessment of RV function [Hudsmith 2005]. We therefore sought to assess the impact of RV function on outcomes in HF patients undergoing CRT implantation using CMR.

9.3. METHODS

9.3.1. Study population

We studied 60 consecutive patients attending the Royal Brompton Hospital heart failure pacing clinic between January 2005 and March 2010 who fulfilled the following criteria: 1. New York Heart Association (NYHA) class III/IV at the time of CRT implantation; 2. QRS width \geq 120 ms; 3. LVEF \leq 35% by echocardiography, and; 4. CMR study within 3 months before CRT implantation.

These patients were evaluated for clinical (aetiology of heart failure, symptom status and medication, heart rate, blood pressure) and electrocardiographic (rhythm and QRS width) parameters at the time of device implantation. As this study involved review of local patient medical records, individual consent was not required by our Ethics Committee who approved the study.

9.3.2. Imaging

Cardiovascular magnetic resonance studies were performed in 1.5T Sonata or Avanto scanners (Siemens, Erlangen, Germany). A short-axis stack from atrio-ventricular level to the apex was acquired using a steady-state free-precession cine sequence (echo time 1.6 ms, repetition time 3.2 ms, flip angle 60°, slice thickness 7 mm with a 3 mm gap, acquisition time of 8-12 cardiac cycles) to quantify left and right ventricular volumes. Long-axis cines were also acquired to define the valve plane throughout the cardiac cycle. An inversion recovery

gradient echo sequence was used 10 minutes after gadolinium injection (Magnevist® or Gadovist®, 0.1 mmol/kg) to assess myocardial scar. Inversion times were set to null the normal myocardium with images repeated in two stacks of identical short-axis planes but separate phase-encoding directions to exclude artefact.

Left and right ventricular volumes were calculated using semi-automated software (CMR tools, Cardiovascular Imaging Solutions, London, UK), as previously described (figure 9.1) [Maceira 2006a, Maceira 2006b]. The resulting values were then indexed to body surface area and compared to reference values from a control population [Maceira 2006a, Maceira 2006b]. Tricuspid annular plane systolic excursion (TAPSE) was measured from the 4-chamber view (figure 9.2). RV dysfunction was defined as RVEF < 50% or TAPSE < 15 mm; severe RV dysfunction was defined as RVEF < 30% or TAPSE < 10 mm. Peak RV wall thickness was measured from the short-axis slices.

Valvular regurgitation was graded as mild (n=1), moderate (n=2) or severe (n=3) by blinded observers, based on the echocardiographic and CMR findings. LVEF was also calculated by echocardiography before and 1 year after device implantation using the Simpson's method from the 2-chamber and 4-chamber views. Pulmonary artery systolic pressure was determined by echocardiography using standard methodology.

Contrast imaging with gadolinium was performed to assess the aetiology of the heart failure. Assessment of late gadolinium enhancement (LGE) in the left or right ventricle was interpreted by blinded observers. When present, the amount of LGE was quantified in a 16-segment model based on the "full width at half maximum" technique by customized analysis software (MRI-MASS, Medis, Leiden, the Netherlands) [O' Hanlon 2010].

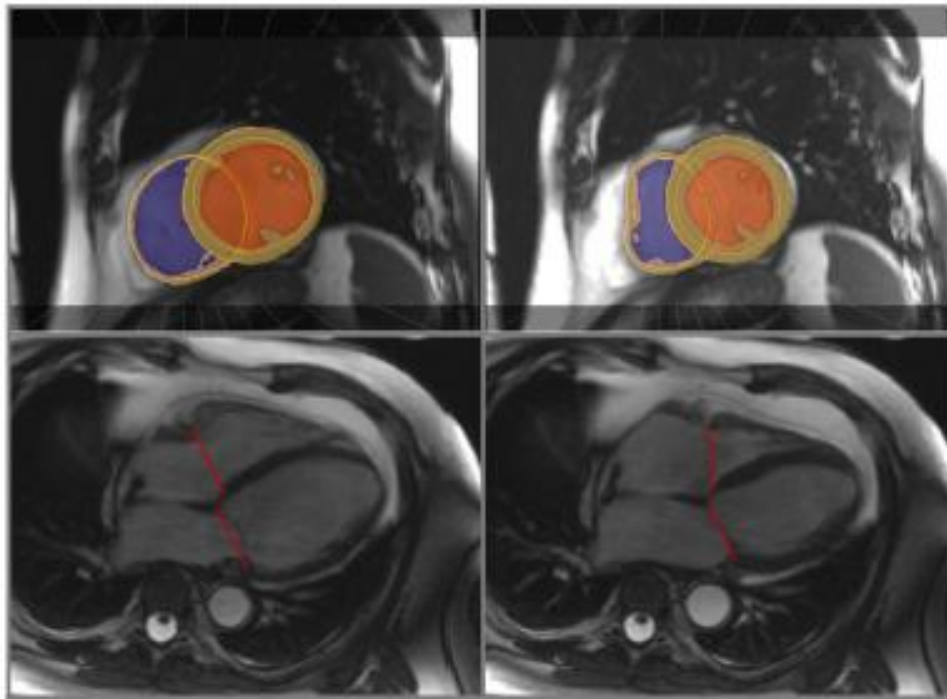


Figure 9.1. Software used for ventricular volumes and mass measurements. Mid-ventricular short-axis (top) and four-chamber views (bottom) at end-diastole (left) and end-systole (right). Coloured areas represent the left and right ventricular cavities and myocardium. Ventricular volumes are generated from a short-axis stack after being confined by the mitral and tricuspid valve planes (red lines).

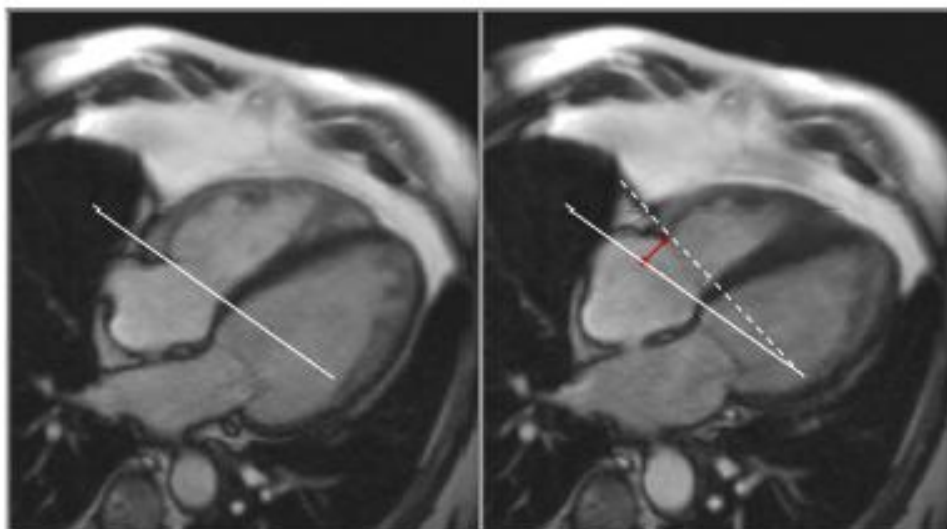


Figure 9.2. Four-chamber view in end-diastole (left panel) and end-systole (right panel). The tricuspid annular plane is marked as a white line in diastole and as a dashed line in systole. The red vector represents the tricuspid annular systolic excursion (TAPSE).

9.3.3. Outcomes

All patients were followed-up in a heart failure clinic and standard medications were adjusted and optimized at these appointments. Data was collected from local hospital records, nationwide summary case records and the Office for National Statistics. The primary end-point was a composite of all-cause mortality or an unplanned hospitalization for a major cardiovascular event; only the first event in each patient was included in this analysis [Cleland 2005]. The secondary end-point was echocardiographic response to CRT, defined as an improvement in LVEF by more than 5% by echocardiography 12 months after CRT implantation [Bax 2003, Bleeker 2006b].

9.3.4. Statistical analysis

Categorical variables are presented as frequency and percentage. Continuous variables are presented as mean \pm standard deviation (SD) if normally distributed, or as median plus interquartile range (IQR) as appropriate. Continuous variables were compared with Student's t-test or the Mann-Whitney test for non-parametric data. Correlation was assessed with Pearson's or Spearman's methods as appropriate.

Time to first event analysis was performed using Cox's proportional hazard models. Log-rank test was used to compare Kaplan-Meier cumulative event curves. Logistic regression was used to assess response to CRT at 12 months. Multivariate logistic regression analysis using a forward stepwise approach was performed on parameters that were significant on univariate analysis.

A two-tailed value of p-value <0.05 was considered significant. All statistical analysis was performed using SPSS 19.0 (IBM, Chicago, Illinois, USA).

9.4. RESULTS

9.4.1. Patients

Patient baseline characteristics are presented in table 9.1. The mean age of the study population was 65.3 ± 12.5 years; most of the patients were male (76.7%). Heart failure was ischaemic in 48.3% of patients, and atrial fibrillation/flutter was found in 23.3% of patients. The mean heart rate was 76 ± 15 bpm, and the mean QRS interval was 156 ± 21 ms (LBBB morphology in 95.0%). The median time between CMR and device implantation was 6 days. Fifty-six out of the 60 CRT (93%) devices were combined with a defibrillator (CRT-D).

Table 9.1. Baseline characteristics of the patients.

Age, years	65.3 ± 12.5
Male gender	46 (76.7%)
Heart failure, aetiology	
Dilated cardiomyopathy	27 (45.0%)
Ischaemic	29 (48.3%)
Valvular	3 (5.0%)
Congenital	1 (1.7%)
Rhythm	
Sinus	46 (76.7%)
Atrial fibrillation	13 (21.7%)
Atrial flutter	1 (1.7%)
Medication	
Beta-blockers	43 (71.7%)
ACE inhibitors/ARB	58 (96.7%)
Aldosterone antagonists	39 (65.0%)
Loop diuretics	52 (86.7%)
Digoxin	12 (20.0%)
Aspirin	23 (38.3%)
Warfarin	19 (31.7%)
Statin	30 (50.0%)

ECG	
QRS width (ms)	156 ± 21
Heart rate	
Beats per minute (bpm)	76 ± 15
Blood pressure	
Systolic (mmHg)	120 ± 20
Diastolic (mmHg)	72 ± 13
Left ventricle	
EDV (mL/m ²)	169 ± 62
ESV (mL/m ²)	124 ± 55
EF (%)	27 ± 8
Mass (g/m ²)	113 ± 30
Right ventricle	
EDV (mL/m ²)	82 (65-123)
ESV (mL/m ²)	38 (27-76)
EF (%)	52 (37-62)
TAPSE (mm)	13.5 ± 5.6
Peak wall thickness (mm)	3.6 ± 0.9
Pulmonary artery pressure (mmHg)	
	38.7 ± 8.7
Late gadolinium enhancement	
Absent	20 (33.3%)
Subendocardial	19 (31.7%)
Subendocardial + mid-wall	6 (10.0%)
Mid-wall	15 (25.0%)
Right ventricle	5 (8.3%)

Data is presented as n (%), mean ± SD, or median (25th – 75th percentile). NYHA = New York Heart Association; ACE = angiotensin-converting enzyme; ARB = angiotensin receptor blocker; BNP = B-type natriuretic peptide; EDV = End-diastolic volume; ESV = End-systolic volume; EF = Ejection fraction; TAPSE = tricuspid annular plane systolic excursion.

9.4.2. Left ventricle

Both mean left ventricular indexed end-diastolic and end-systolic volumes were high (169±62 and 124±55 mL/m², respectively). The indexed left ventricular end-diastolic volume was

increased in 93% of the patients, while the indexed left ventricular end-systolic volume was increased in 99% of the patients compared to normal reference values [Maceira 2006a]. The mean LVEF was $27\pm 8\%$, and the mean mass index was increased at $113\pm 30\text{ g/m}^2$.

Mitral regurgitation was seen in 90% of the patients, and was significant in 25% of patients (18% moderate, 7% severe). Aortic regurgitation was seen in 25% of patients, and was moderate in only one patient.

9.4.3. Right ventricle

Right ventricular indexed volumes and ejection fraction were non-normally distributed, and hence presented as median plus inter-quartile ranges. The median end-diastolic and end-systolic volumes were 82 (65-123) mL/m^2 and 38 (27-76) mL/m^2 , respectively. Right ventricular indexed end-diastolic volume was increased in 38% of patients, while the indexed end-systolic volume was increased in 53% of patients [Maceira 2006b]. The median RVEF was 52% (IQR 37-62%), with 53% of patients having a RVEF $\geq 50\%$.

The mean TAPSE was $13.5\pm 5.6\text{ mm}$, with 40% of patients having values within normal limits when the standard echocardiographic cut-off value of 15mm was considered. The mean peak RV wall thickness was $3.6\pm 0.9\text{ mm}$.

In the 52 patients (87%) in whom it could be measured, the mean PASP was $38.7\pm 8.7\text{ mmHg}$, with 37% of patients having a PASP $> 40\text{ mmHg}$. Tricuspid regurgitation was seen in 57% of the patients, and was significant in 14% of patients (12% moderate, 2% severe). No significant pulmonary regurgitation was identified in any patient.

There was a moderately strong correlation between RVEF with TAPSE ($r=0.58$, $p<0.01$), and a moderate correlation between RVEF and LVEF ($r=0.41$, $p<0.01$). Severity of mitral

regurgitation was associated with a higher PAP ($p=0.01$) and a lower RVEF ($p<0.01$). Modest inverse correlations were observed between RVEF and pulmonary artery pressure ($r=-0.37$, $p<0.01$), RV wall thickness ($r=-0.28$, $p=0.03$) and severity of tricuspid regurgitation ($p=0.03$). TAPSE was inversely related with RV wall thickness ($r=-0.29$, $p=0.03$), but not with pulmonary artery pressure ($r=-0.15$, $p=0.28$) or LVEF ($r=0.09$, $p=0.48$).

RVEF was similar in patients with an ischaemic and non-ischaemic aetiology ($46.9\pm14.8\%$ vs. 49.5 ± 18.9 , $p=0.56$), and in patients with AF compared to those in sinus rhythm ($45.4\pm14.9\%$ vs. $49.2\pm17.8\%$, $p=0.48$).

9.4.4. Myocardial fibrosis

Left ventricular LGE was present in two-thirds of the patients: 19 patients (31.7%) had sub-endocardial enhancement suggesting myocardial infarction, 15 patients (25.0%) had a mid-wall enhancement pattern indicating fibrosis, and the remaining 6 patients (10.0%) had a mixed pattern of myocardial infarction and mid-wall fibrosis. Myocardial infarction was therefore present in 25 patients (41.7%): the septal wall was affected in 11 patients; the inferolateral wall was involved in 15 patients. The median percentage of scar in the myocardium was 4% (IQR 0-18%).

Right ventricular LGE was present in 5 patients (8.3%). All these patients had coronary artery disease with inferior myocardial infarctions of the LV extending to the inferior free wall of the RV.

Table 9.2. Univariate analysis: Primary end-point (time to death from any cause or an unplanned hospitalization for a major cardiovascular event).

	Events (n=18)	No Events (n=42)	HR	95% CI	P value
Age (years)	69.6 ±11.9	63.3 ± 12.3	1.04	0.99-1.09	0.07
Male gender	14 (78%)	32 (76%)	1.14	0.37-3.46	0.82
CAD	10 (56%)	17 (41%)	1.73	0.68-4.38	0.25
Atrial fibrillation	6 (39%)	8 (17%)	2.63	1.02-6.84	0.047
Heart rate (bpm)	79.2 ±19.4	74.1 ± 12.5	1.02	0.99-1.05	0.22
SBP (mmHg)	124 ± 22	118 ± 19	1.01	0.99-1.04	0.36
QRS width (ms)	151 ± 25	158 ± 21	0.99	0.96-1.01	0.23
Left ventricle					
EDV index (mL/m ²)	159 ± 54	173 ± 64	0.99	0.98-1.00	0.09
ESV index (mL/m ²)	120 ± 52	126 ± 56	0.99	0.98-1.00	0.19
EF (%)	26.9 ± 9.5	28.9 ± 7.6	1.00	0.94-1.06	0.93
Mass index (g/m ²)	106 ± 25	115 ± 32	0.98	0.97-1.00	0.08
Mitral regurgitation	1.3 ± 0.6	1.2 ± 0.8	1.33	0.73-2.44	0.35
LGE	13 (72%)	27 (64%)	1.57	0.50-3.98	0.51
LGE (%)	9.5 (0-20)	3 (0-17)	1.01	0.98-1.05	0.54
Myocardial infarction	9 (50%)	16 (38%)	1.57	0.62-3.95	0.34
Right ventricle					
EDV index (mL/m ²)	95 (76-138)	77 (60-103)	1.01	1.00-1.02	0.12
ESV index (mL/m ²)	52 (35-102)	34 (21-66)	1.01	1.00-1.02	0.06
EF (%)	39 (25-54)	55 (43-66)	0.96	0.94-0.99	0.006
TAPSE (mm)	11.0 ± 4.4	14.5 ± 5.9	0.88	0.80-0.96	0.006
Wall thickness (mm)	3.9 ± 1.0	3.5 ± 0.9	1.54	0.93-2.56	0.09
PAP (mmHg)	42.5 ± 8.3	37.5 ± 8.5	1.06	1.00-1.12	0.07

Values are n (%), mean ± SD, or median (25th – 75th percentile). HR = hazard ratio; CI = confidence interval. CAD = Coronary artery disease; SBP = systolic blood pressure; LGE = late gadolinium enhancement; PAP = Pulmonary artery pressure. Other abbreviations as in table 1.

9.4.5. Follow-up

During a median follow-up of 26.1 months (IQR 16.1-39.3 months) after CRT implantation, there were 13 unplanned hospitalizations for a cardiovascular cause (all for heart failure decompensation), and 11 deaths (8 cardiac and 3 non-cardiac deaths). The primary end-point was reached by 18 patients. Atrial fibrillation and RV dysfunction emerged as the only predictors of the primary composite end-point on univariate analysis (table 9.2). Patients in atrial fibrillation or flutter had a HR of 2.6 (95% CI 1.02-6.84, $p=0.047$) for the primary end-point. For each 10% decrease in RVEF, the risk of the primary end-point increased by 40% (HR 0.96, 95% CI 0.94-0.99, $p=0.006$); for each 1 mm decrease in TAPSE, the risk of the primary end-point increased by 12% (HR 0.88, 95% CI 0.80-0.96, $p=0.006$). Kaplan-Meier curves for RV function assessed by RVEF or TAPSE are displayed on figure 9.3.

After documenting AF as a predictor of outcomes, we performed a post-hoc analysis on delivery rate, defined as the percentage of paced left ventricular beats. Data was collected from routine pacing clinic visits during the first year of implantation. Unlike AF, delivery rate was not associated with the primary end-point (HR 0.97, 95% CI 0.88-1.08, $p=0.56$).

9.4.6. Response to therapy

Of the 56 patients (93%) followed-up for over a year, 27 were considered to be responders as they had an increase in LVEF $>5\%$ at one year of follow-up. Thus the response rate using this criterion was 48% (table 9.3). Two sets of closely related parameters were associated with non-response to CRT on univariate analysis: (1) coronary artery disease, associated with myocardial infarction and scar burden (myocardial fibrosis plus infarction relative to LV mass), were predictors of non-response to therapy; (2) right ventricular dysfunction (lower RVEF and TAPSE) and hypertrophy (thicker RV free wall). Myocardial scar burden (OR 0.90, 95% CI 0.83-

0.96, $p=0.004$) and RVEF (OR 1.05, 95% CI 1.01-1.09, $p=0.01$) were the only variables to remain significant on multivariate analysis (table 9.4).

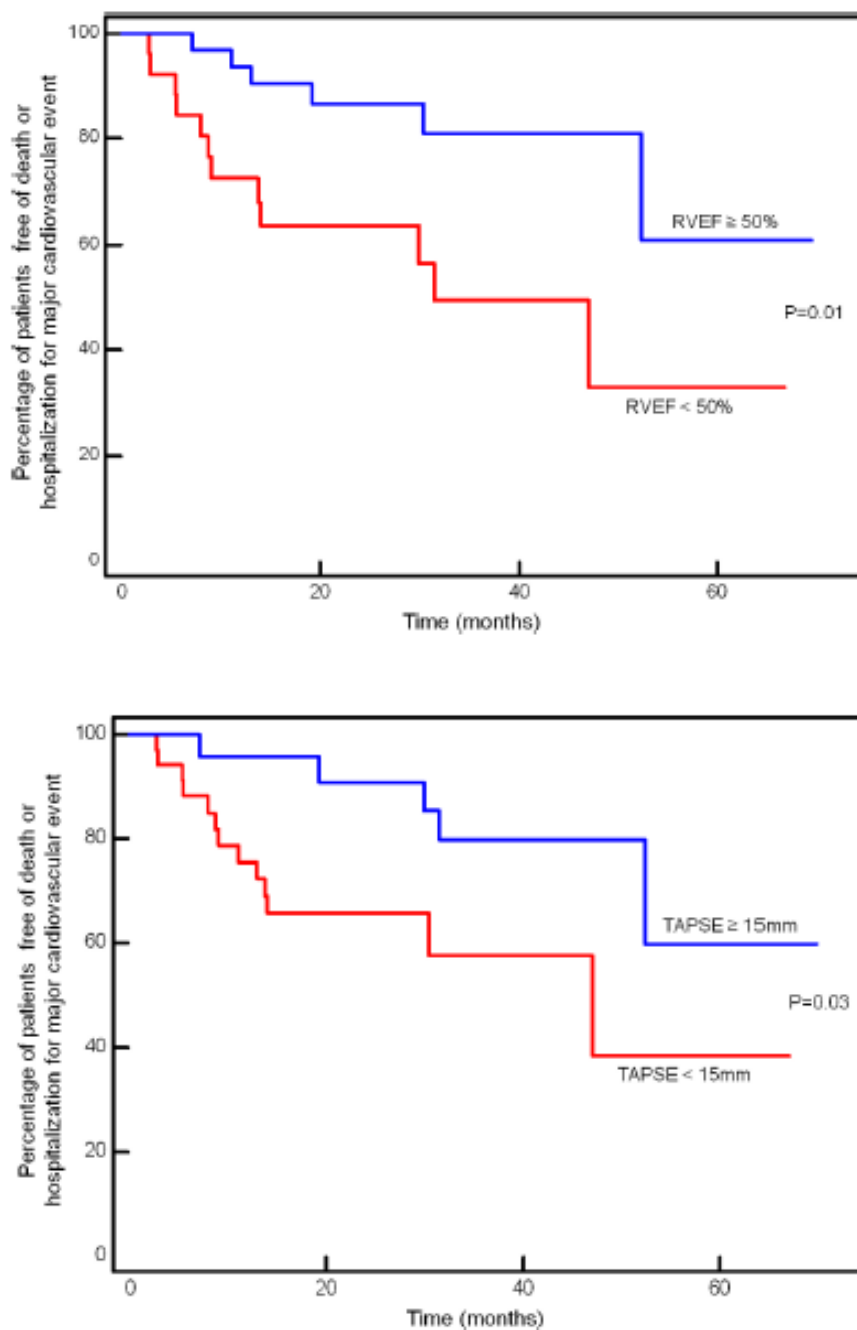


Figure 9.3. Kaplan-Meier estimates of the time to the primary end-point for RVEF (top panel) and TAPSE (bottom panel).

Table 9.3. Response to cardiac resynchronization therapy (improvement of LVEF \geq 5% at one year).

Response	Response (n=27)	No Response (n=29)	OR	95% CI	P value
Age	64.0 \pm 12.2	65.8 \pm 12.2	0.99	0.95-1.03	0.58
Male gender	18 (67%)	25 (86%)	0.32	0.09-1.20	0.09
CAD	7 (26%)	19 (66%)	0.18	0.06-0.58	0.004
Atrial fibrillation	4 (15%)	7 (24%)	0.55	0.14-2.13	0.38
Heart rate (bpm)	76 \pm 15	76 \pm 16	1.00	0.97-1.04	0.89
SBP (mmHg)	120 \pm 20	119 \pm 19	1.00	0.98-1.03	0.76
QRS width (ms)	161 \pm 21	150 \pm 22	1.02	1.00-1.05	0.07
Left ventricle					
EDV index (mL/m ²)	156 \pm 46	177 \pm 71	0.99	0.98-1.00	0.19
ESV index (mL/m ²)	111 \pm 40	133 \pm 63	0.99	0.98-1.00	0.13
EF (%)	30.5 \pm 8.5	26.5 \pm 7.2	1.07	0.99-1.16	0.07
Mass index (g/m ²)	108 \pm 26	118 \pm 34	0.99	0.97-1.01	0.23
Mitral regurgitation	1.1 \pm 0.6	1.3 \pm 0.8	0.58	0.27-1.27	0.17
LGE	13 (48%)	24 (83%)	0.19	0.06-0.66	0.009
LGE (%)	0 (0-7)	13 (3-22)	0.91	0.85-0.97	0.005
Myocardial infarction	6 (22%)	18 (62%)	0.18	0.05-0.57	0.004
Right ventricle					
EDV index (mL/m ²)	77 (67-104)	83 (61-139)	0.99	0.98-1.01	0.28
ESV index (mL/m ²)	36 (23-54)	40 (31-96)	0.99	0.98-1.00	0.10
EF (%)	56 (45-63)	44 (28-61)	1.04	1.01-1.08	0.03
TAPSE (mm)	15.3 \pm 5.8	11.8 \pm 4.2	1.15	1.03-1.29	0.02
Wall thickness (mm)	3.3 \pm 0.7	4.0 \pm 1.0	0.42	0.21-0.84	0.02
PAP (mmHg)	36.9 \pm 8.5	40.5 \pm 9.0	0.95	0.89-1.02	0.16

Values are n (%), mean \pm SD, or median (25th – 75th percentile). OR- odds ratio; CI- confidence interval. Other abbreviations as in tables 1 and 2.

Table 9.4. Multivariate analysis: Response to cardiac resynchronization therapy
(improvement of LVEF \geq 5% at one year).

Response	Response (n=27)	No Response (n=29)	OR	95% CI	P value
LGE (%)	0 (0-7)	13 (3-22)	0.90	0.83-0.96	0.004
RVEF (%)	56 (45-63)	44 (28-61)	1.05	1.01-1.09	0.01

Response to CRT was noted to be lower as RV function deteriorated (figure 9.4). Poor RV function, defined as a RVEF <30% or a TAPSE <10mm, was associated with a particularly low response to CRT (response rates of 18.2% and 26.7%, respectively).

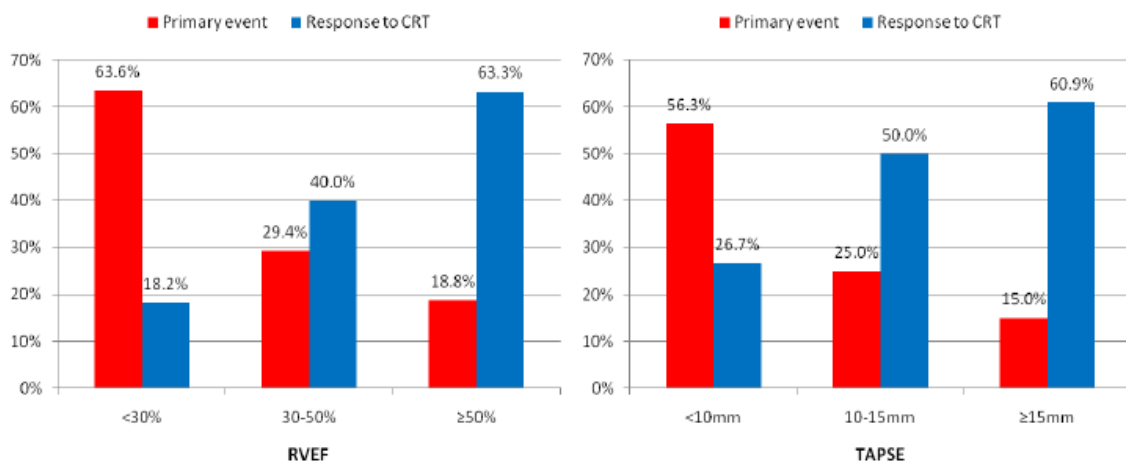


Figure 9.4. Frequency of primary events (red bars) and response to CRT (blue bars) for different ranges of RVEF and TAPSE.

9.5. DISCUSSION

This study shows that RV dysfunction is associated with non-response and adverse outcomes in patients on CRT. Despite meeting the standard criteria for CRT implantation, there was a heterogeneous distribution of RV function in our study population. Since LVEF was narrowly

distributed by accepted indications for CRT, the wide RVEF distribution observed may indeed explain why RV function was an independent discriminator in this population with advanced HF. A lower RVEF was associated with a lower LVEF, more significant mitral regurgitation, and a higher PAP. This suggests that the RV dysfunction may derive from two fundamental mechanisms, the importance of which may vary from patient to patient: 1) an impairment of global biventricular intrinsic contractility; 2) pulmonary hypertension secondary to elevated LV filling pressures and mitral regurgitation.

Adverse RV function may reflect more extensive and severe cardiac disease, to which improving myocardial synchrony has little impact. Of note, the response rate of the subgroup of patients with RVEF < 0.3 was less than 20%. Thus, patients with poor RV function were unlikely to benefit from CRT. This may have implications in stratifying patients for device therapy.

9.5.1. Previous work

Few studies have investigated RV function and dyssynchrony. Previous work has shown that anything up to 20-40% of RV systolic pressure and volume load may originate from contraction from the LV [Santamore 1998]. Conversely, left bundle branch block (LBBB) may interfere with ventricular activation and induce mechanical dyssynchrony. Hence LBBB not only affects LV function but may impair RV function as well.

RV functional indices have been previously evaluated in CRT populations. Initial work by Field et al assessed RV function on adverse outcomes in a population of 77 patients undergoing CRT. This study showed that RV dysfunction measured by the Doppler-derived Tei index was a predictor of the composite end-point of death, transplantation and the implantation of left ventricular assist devices [Field 2006]. More recent work focused on RV function and response

to CRT. In a study of 44 patients undergoing CRT, echocardiographic indices of RV function (TAPSE and RV fractional area change) were significantly worse in non-responders versus responders to CRT [Scuteri 2009]. The value of TAPSE in predicting reverse remodelling was further validated in the CARE-HF population [Ghio 2009]. A further radionuclide imaging study in 44 patients undergoing CRT showed that those with a low baseline RVEF were less likely to improve in NYHA class, and tended to improve less in functional capacity and LVEF [Burri 2010].

The results of our study are in line with the above publications. However, we used CMR as the gold-standard technique for assessment of the RV, and RVEF as the reference marker of RV performance. Along with myocardial infarction, RVEF was an independent predictor of response to CRT. Among an array of established prognostic markers in HF, RVEF and TAPSE emerged as the strongest predictors of events. Our findings correlated response with outcomes over a clinically relevant timeframe, thus supporting the potential of RV function as a predictor of short-term response as well as longer-term outcome following CRT.

9.5.2. Tricuspid annular plane systolic excursion

Although available to all imaging modalities, and despite its validated prognostic value amongst cardiac and pulmonary conditions, RVEF estimation can be challenging as the right ventricle is a complex structure which cannot be modelled with simple geometric assumptions. Therefore, there is some interest in finding simpler ways for assessing RV performance. Of these, tricuspid annular plane systolic excursion (TAPSE) is the most described alternative to RVEF in the literature [Kaul 1984]. This marker of RV longitudinal function is reproducible and easy to obtain, and has shown to be a predictor of adverse outcomes in heart failure, irrespective of NYHA status and LV function [Ghio 2000, Pinedo

2010]. In this study, TAPSE not only identified which patients would respond to CRT, but also the patients more likely to have major adverse events. Thus, TAPSE may be used by CMR as an alternative to RVEF for assessing RV function pre CRT when the latter cannot be estimated.

9.5.3. Pulmonary hypertension

Increased pulmonary artery pressures have shown to be associated with non-response to CRT [Scuteri 2009]. As ejection fraction is influenced by the afterload, it is expected for increasing pulmonary pressures to be associated with decreasing RVEF. A significant negative correlation was indeed observed between PAP and RVEF in our study. However, this correlation was modest and not as strong as other parameters such as LVEF, suggesting that factors other than pulmonary hypertension play a role in RV function. There was a trend for non-response to CRT and adverse outcomes in patients with increased pulmonary pressures, but statistical significance was not reached, probably explained by the smaller study population compared to other studies [Tedrow 2006]. On the other hand, markers of RV function were significantly associated with response and adverse events. This suggests that RV function is more important than pulmonary pressure alone for both mechanical response and long-term prognosis in patients on CRT.

9.5.4. Myocardial fibrosis

Late gadolinium enhancement CMR detects myocardial infarction accurately, with superior histological correlation compared to nuclear techniques [Wagner 2003]. This has become an active area of research in the CRT setting, with several subsequent studies documenting the value of scar burden, location and transmural extent of myocardial infarctions as a predictor of response to CRT [Bleeker 2006c, White 2006, Ypenburg 2007, Chalil 2007a, Marsan 2009].

Consistent with this work, our study showed myocardial infarction and scar burden (as determined by percentage of LGE mass) to portend an adverse response to CRT. Although the amount of septal and lateral scar was associated with non-response to therapy (OR 0.99, 95% CI 0.98-1.00, $p=0.02$; and OR 0.98, 95% CI 0.97-1.00, $p=0.02$, respectively), scar location did not remain significant after including the total amount of scar in a multivariate model.

The lack of response observed with the above parameters did not translate into poorer outcomes. It is possible that this study was underpowered to detect more adverse events, as larger studies have shown ischaemic heart disease and location of myocardial infarction to portend a worse prognosis in CRT [Woo 2005, Zhang 2009, Leyva 2011a].

9.5.5. Atrial fibrillation

Atrial fibrillation was the other predictor of outcomes besides RV dysfunction. This mirrors findings of long term studies of patients on CRT [van Bommel 2010]. It is recognised that AF with a high ventricular rate may impair the delivery of biventricular pacing, and consequently undermine the clinical benefit of CRT [Koplan 2009]. Despite the paucity of data from randomized control trials in AF populations, recent guidelines support the use of CRT in AF patients, although restricted to a slightly wider QRS duration $>130\text{ms}$ [Dickstein 2010]. A recent European registry suggests that around 20% of patients undergoing CRT are actually in permanent AF, which is in keeping with our findings [Dickstein 2009]. Of note, all but one AF patient in this study had QRS $> 130\text{ms}$. Rate control was satisfactory in our AF cohort, the ventricular delivery rate was high (median 97%, IQR 91-99%), and none of the patients underwent AV nodal ablation. Unlike RV dysfunction, AF was not associated with a lower response rate, suggesting that the impact of AF on adverse outcomes was not altered by device implantation.

9.5.6. Response

In addition to the hard clinical endpoints, we assessed the role of RV function on response to CRT. Response is a contentious topic, with various proposed definitions but no consensus amongst different criteria. The response rate varies widely, depending on the study population and the response criteria used. In a recent paper comparing 15 response criteria from the most cited papers, the response rate ranged from 32% to 91%. The same study showed that the agreement between different criteria was poor in 75% of the time, especially between clinical and echocardiographic criteria [Fornwalt 2010]. For our study, we used LVEF to assess response because it is an objective parameter and is also one of the selection criteria for CRT. In keeping with previous work, response for this study was an improvement in LVEF $\geq 5\%$ at 12 months [Bax 2003, Bleeker 2006b]. The response rate observed was relatively low (48%), but still in accordance with the available literature [Fornwalt 2010]. Using this criterion, RV dysfunction predicted a failure of response to CRT in terms of LV remodelling, thus supporting previous echocardiographic and radionuclide studies [Scuteri 2009, Ghio 2009, Burri 2010]. It is possible that significant RV dysfunction marks extensive and irreversible adverse remodelling, preventing reverse remodelling and functional recovery after CRT implantation. Improvement in LVEF $\geq 5\%$ was significantly associated with event-free survival in this cohort of patients (likelihood ratio 4.7, $p=0.01$). Mechanical remodelling thus appears to be a good surrogate marker of response to therapy, in line with a recently published analysis of the MADIT-CRT trial, where it was demonstrated that echocardiographic improvement in LV volumes and ejection fraction was associated with improved outcomes [Solomon 2010].

9.5.7. Limitations

This was a retrospective study with a relatively small number of patients and events limiting multivariate analysis on outcomes. Nonetheless, both RVEF and TAPSE emerged as the most significant prognostic markers, suggesting that RV function as assessed by CMR has a powerful role in advanced HF undergoing CRT.

This was a single centre study in a tertiary referral hospital, but it allowed for consistent CMR scanning protocols, and consistent patient selection for CRT and close follow-up of all patients. To ensure a representative cohort, consecutive patients were identified.

The CRT devices implanted during this time period were non-MRI compatible and hence necessitated an alternative imaging modality for consequent follow-up. The development of CMR-compatible CRT devices could overcome this current limitation and may provide new insights on the response of both left and right ventricle to CRT.

9.6. CONCLUSION

Right ventricular function appears an important predictor of response and major adverse events following CRT implantation. As current selection criteria only include patients with poor LV function, it is reasonable to assume that RV function will act as an important discriminative prognostic marker in patients undergoing CRT. Furthermore, poor RV function appears to identify a subgroup of patients with extensive ventricular remodelling unlikely to change their natural history. Therefore, CRT may be of no benefit in this subgroup of patients. The presence and amount of myocardial fibrosis, by contrast, was a predictor of response but did not predict outcomes.

The results of this study suggest that assessment of RV function can provide valuable information pre CRT implantation. Further work in larger cohorts is required to ascertain the precise role of RV evaluation in the selection of patients for CRT as well as the mechanisms for this dysfunction.

9.6.1. Acknowledgements

This project was supported at the NIHR Cardiovascular Biomedical Research Unit of Royal Brompton & Harefield NHS Foundation Trust and Imperial College London. Research support was also received from the BHF and CORDA.

9.6.2. Competing interests

KG has received support from Biotronik. RS has received honoraria/research grants from Medtronic, Boston Scientific, Biotronik and Servier. DJP is a consultant to Siemens, and a director in Cardiovascular Imaging Solutions. MRC has received research funding from Medtronic, St. Jude Medical and Boston Scientific.

9.6.3. Publication

These data have been published as: Alpendurada F, Guha K, Sharma R, Ismail TF, Clifford A, Banya W, Mohiaddin RH, Pennell DJ, Cowie MR, McDonagh T, Prasad SK. Right ventricular dysfunction is a predictor of non-response and clinical outcome following cardiac resynchronization therapy. *J Cardiovasc Magn Reson* 2011;13:68.

CHAPTER 10: DISCUSSION

Cardiovascular imaging has opened a window of opportunity for cardiac research by enabling direct visualization of the moving heart inside the human body. CMR took longer to establish compared to other imaging modalities, but today is regarded by many as the best imaging tool for the heart. Several features of CMR are especially suited for the study of the RV. The ability for multiplanar imaging permits proper 3D assessment of complex structures like the RV. Excellent image quality allows for perfect delineation of the trabeculations and visualization of the thin RV free wall. Lack of radiation is important from an ethical point of view, enabling follow-up and serial evaluation over time. Finally, the intrinsic faculty to characterize the myocardium without the need for invasive biopsies helps to understand the ultrastructure and nature of the heart disease.

The first CMR study addressing the RV was published in 1985. In this study, it was demonstrated that volume measurements of the LV and RV were both feasible and accurate, as the right to left ventricular stroke volume ratio was very close to the theoretical value of 1 [Longmore 1985]. Since then, RV volumetric analysis has been validated in several scenarios, and is currently used to decide surgical intervention in congenital heart disease and to monitor the response to treatment in pulmonary hypertension [van Wolferen 2006, Oosterhof 2007]. The use of CMR for the RV has expanded from the mere calculation of size and function to combine evaluation of blood vessels and flows, but most importantly, to assess the structure of the myocardium which has hitherto been exclusive to endomyocardial biopsy. Tissue analysis was first shown to help with the diagnosis of ARVC [Molinari 1995], and later on with the diagnosis of RV myocardial infarction [Kumar 2006], where it has shown to predict persistent RV dysfunction and adverse events [Larose 2007]. The study of myocardial fibrosis

was also extended to the field of congenital heart disease, where myocardial fibrosis was found to be associated with symptoms, neuro-hormonal activation, and risk of malignant arrhythmias [Babu-Narayan 2005, Babu-Narayan 2006].

In keeping with the pioneering CMR work, the aim of this thesis was to expand the available knowledge of the RV onto other forms of heart disease. The present work has been published in the form of five papers in different conditions and in different settings. The core of the discussion is in each individual paper. This chapter merely intends to complement the discussion of the individual papers, and will be divided by the pathologies studied in the published works. The discussion herein will comprise a general overview about each disease, the aims behind each project, how the results contributed to the current knowledge, and which potential directions should be sought in the future. A summary of the original contribution to research is presented at the end of this chapter.

10.1. MARFAN SYNDROME

10.1.1. Overview

Marfan syndrome is the commonest inherited connective tissue disease, with an estimated incidence of 1/5.000 individuals [Dietz 1995, Judge 2005, Pearson 2008]. The condition was first described by French paediatrician Antoine Marfan in a girl with striking skeletal abnormalities [Marfan 1896]. Since then different ocular, cardiovascular, pulmonary, cutaneous, and neurological abnormalities have been added to delineate what is now called Marfan syndrome [Cañadas 2010a].

Nearly all cases of Marfan syndrome are caused by mutations in the fibrillin-1 gene on chromosome 15 [Dietz 1991]. Over 1.000 mutations have been described to date, but so far no robust genotype-phenotype correlation has been identified [Faivre 2007, Keane 2008].

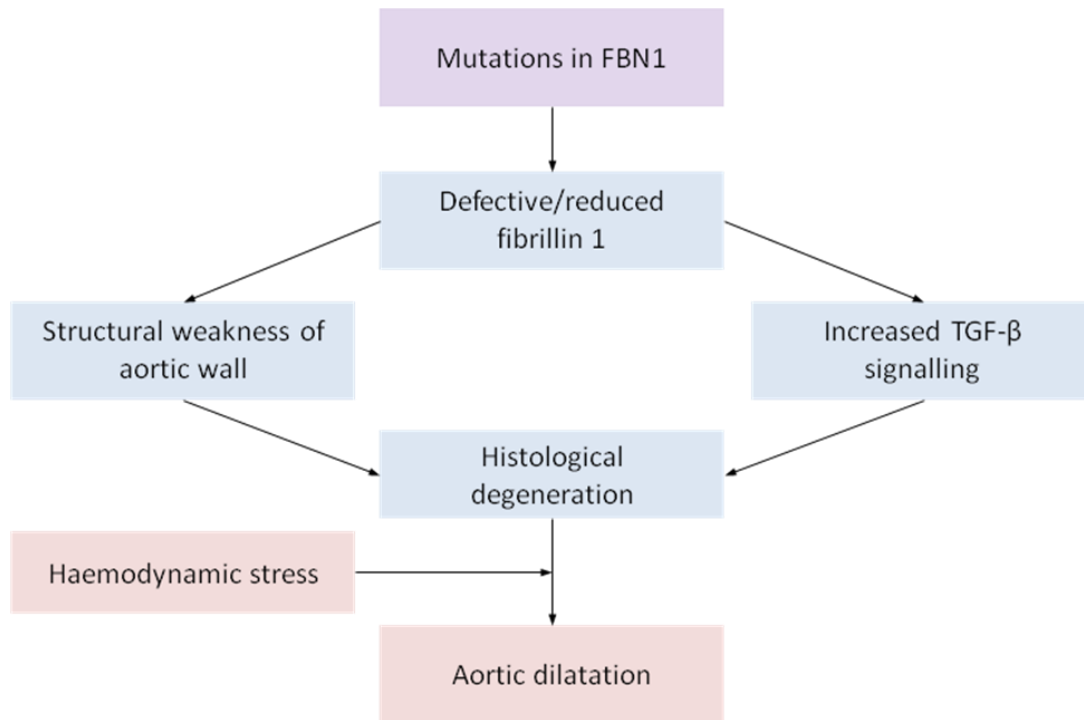


Figure 10.1. Pathogenic model for aortic dilatation. Reproduced with permission from Cañadas 2010b.

These mutations cause reduced or defective production of the extracellular matrix protein fibrillin-1, a key constituent of microfibrils and an important component of the elastic fibres. Marfan syndrome was originally thought to be the result of structural weakness of connective tissues rich in elastic fibres. While this intuitive model would support certain features like aortic dilatation, lens luxation, and joint hyperlaxity, it would not explain other typical features such as long bone overgrowth or myxomatous degeneration of the mitral valve. Over the last decade, studies in animal models suggested an additional regulatory role for fibrillin-1 as a modulator of transforming growth factor (TGF)- β . The lack of fibrillin-1 therefore results in over-expression of the TGF- β signalling pathways, which has been reported to mediate the main histological abnormalities of the disease (figure 10.1) [Neptune 2003, Ng 2004]. The various manifestations of Marfan syndrome are today considered to be the result of abnormal

homeostasis of the extracellular matrix, in which reduced or defective forms of fibrillin-1 lead to alterations of the mechanical properties of tissues, increased TGF- β activity, and loss of cell-matrix interactions [El-Hamamsy 2009, Cañadas 2010a].

Table 10.1. Diagnostic criteria for Marfan syndrome [De Paepe 1996]. Major criteria in two systems plus a minor criterion in a third system are required for diagnosis.

	Major criteria	Minor criteria
Family history	Diagnosis in first degree relative	None
Genetic	Mutation FBN1	None
Cardiovascular	Aortic root dilatation Ascending aorta dissection	Mitral valve prolapse Pulmonary artery dilatation Descending aorta dissection
Ocular	Ectopia lentis	2 of the following: Flat cornea Elongated globe
Skeletal	4 of the following: Pectus carinatum Severe pectus excavatum Pes planus Positive wrist or thumb sign Severe scoliosis Armspan-height ratio>1.05 Protusio acetabulae	2-3 major signs, or 1 major and 2 minor signs: Moderate pectus excavatum High arched palate Typical facies Joint hypermobility
Pulmonary		Spontaneous pneumothorax Apical bulla
Skin		Striae Recurrent or incisional hernia
Nervous system	Lumbosacral dural ectasia	

Despite the advances in the pathogenesis of Marfan syndrome, the diagnosis remains difficult due to the marked phenotypical heterogeneity of the disease. As a result, successive diagnostic criteria have been proposed [Beighton 1988, De Paepe 1996, Loeys 2010], where individual criteria clustered in systems have different weightings according to their relative specificity (table 10.1). Although most manifestations can be disabling, mortality is usually associated with the cardiovascular system. The natural history without medical care is dismal, with 90% patients dying in their third and fourth decades of life due to aortic dissection and related complications [Murdoch 1972]. Aortic root surgery was the important milestone in the management of this condition [Bentall 1968]. Surgical techniques have evolved enormously to accommodate more physiological [Yacoub 1983] and refined procedures [David 1992], which are now employed on a prophylactic basis for patients with high risk of aortic dissection or rupture. Adjunctive pharmacological therapy with beta-blockers appears to slow the progression of aortic dilatation, but so far without clear benefit in preventing aortic dissection or death [Cañadas 2010b]. Angiotensin receptor blockers mitigate the detrimental effects of the TGF- β pathways in animal models [Habashi 2006], and may suppress aortic dilatation as suggested by a small human trial [Brooke 2008]. With early diagnosis, appropriate surveillance and surgical treatment, life expectancy has dramatically increased by 30 years over the past few decades [Silverman 1995b, Pyeritz 2009]. As patients live longer, new features of the disease are emerging. Recent reports suggest that mortality is shifting from aortic disease to ventricular arrhythmias and heart failure [Yeatman 2003, Chan 2008]. Cardiac disease is hence becoming a growing concern in Marfan syndrome.

10.1.2. Present work

The study of cardiovascular manifestations in Marfan syndrome was the stepping stone for the first work of this thesis. CMR is the ideal imaging modality for this purpose because the heart and the great vessels can be reliably assessed at the same time. Initial results showed that aortic root dilatation was the principal manifestation of the disease, in keeping with the available literature [Détaint 2010a]. More distal segments of the thoracic aorta and aortic arch branches were also affected, particularly in the more severe forms of the disease, a finding already known but only documented recently [Yetman 2011]. The heart was frequently involved as aortic regurgitation due to aortic dilatation and mitral regurgitation due to mitral valve prolapse were common findings (around 50% and 20% of patients, respectively). Remarkably, over 40% of patients had increased LV volumes indicating a dilated LV, and up to 30% of patients were found to have reduced LVEF suggesting LV dysfunction [Alpendurada 2008b]. These results prompted a more detailed analysis of the heart.

Revision of the available literature showed conflicting results regarding the presence of a Marfan related cardiomyopathy [Kiotsekoglou 2009b]. Most studies were based on echocardiography and negative for the existence of a cardiomyopathy. CMR is the best technique to diagnose cardiomyopathies, but the two available two studies were small (with 22 and 26 patients, respectively) and showed different results [Savolainen 1994, De Backer 2006]. With 68 patients enrolled, this study was the largest at the time. The main result of the study was that one-quarter of patients had reduced LVEF suggesting LV dysfunction, thus providing the strongest evidence for an underlying cardiomyopathy. A proportion of these patients had reduced RVEF, a novel finding in Marfan syndrome, and a robust indicator for RV dysfunction and biventricular involvement.

When volumetric analysis is the main focus of any study, it is very important to control for any potential confounding factors altering the normal loading conditions. Although significant

aortic and mitral valve regurgitation should be excluded as a cause of increased LV pre-load, it is common to include mild degrees of valvular regurgitation in Marfan related research [Kiotsekoglou 2009b]. In line with previous publications, mild forms of valvular regurgitation were included in our study. Since mild aortic and mitral regurgitation are ubiquitous in Marfan syndrome, exclusion of such patients would have lead to a significant reduction in the sample size and resultant loss of statistical power. Statistical analysis showed that patients with mild regurgitation had slightly higher LV volumes than those without regurgitation, but this did not translate into a significant change in LVEF. Although LVEF was not significantly affected by changing pre-load conditions, mild forms of valvular regurgitation should ideally be excluded from a research setting.

Contrary to the LV, RV measurements were unlikely to be influenced by the loading conditions. As there were no cases of significant right-sided valvular regurgitation, any potential confounding factor affecting pre-load was eliminated. Abnormal after-load in the form of pulmonary hypertension appears uncommon in Marfan syndrome [Kiotsekoglou 2011], but a post-hoc analysis on pulmonary artery pressures (PAPs) was nonetheless performed for the thesis. Of the 54 patients with echocardiographic information, only 43 had available data on PAPs, while in the other 11 patients, PAPs could not be measured by echocardiography because the tricuspid regurgitant jet was too small to determine the pressure gradient between the RV and the RA. The mean PAP of the 43 patients was within the normal range (24.6 ± 4.8 mmHg), and none of the patients had echocardiographic evidence of pulmonary hypertension [Galiè 2009]. Importantly, there was no relationship between PAP and RVEF (Spearman's rank correlation coefficient = -0.22, $p=0.15$). Although these data have not been published in the original paper, it demonstrates that pulmonary hypertension is uncommon in Marfan syndrome and that pulmonary artery pressures did not have any significant effect on RVEF. Therefore RVEF can be used as a reliable marker of RV

function in this cohort because both preload and afterload were not significantly affected. RV measurements may actually have been more reliable than LV measurements because tricuspid valve prolapse was seldom present. Defining valve planes was probably more robust for the tricuspid valve than for the mitral valve, as mitral valve prolapse was a common finding, and a potential challenge when delineating the mitral valve plane.

The presence of RV dysfunction, albeit less common than LV dysfunction, supports the existence of a Marfan cardiomyopathy. Our results were confirmed by a recent study in a large prospective cohort of 144 patients using similar inclusion criteria [De Witte 2011]. Nevertheless, our study analysis was slightly different from the other two positive CMR studies [de Backer 2006, de Witte 2011]. We compared each individual patient with reference ranges in a normal population rather than comparing the entire Marfan cohort as a whole with normal controls also as a whole. Our approach was possible because of the large healthy population available as a control group [Maceira 2006a, Maceira 2006b]. This approach is supported by the bimodal distribution of LVEF, with a large peak in the normal range, and a smaller peak just below the lower limit of normal distribution (figure 6.2). The message of this study is likely more appropriate. Rather than suggesting that Marfan syndrome is associated with worse function than controls, it is more correct to conclude that a subgroup of patients with Marfan syndrome are affected by a primary cardiomyopathy, and such patients should be monitored more closely and treated accordingly.

10.1.3. Future work

With mounting evidence for a primary Marfan cardiomyopathy, future research should integrate the imaging findings with other areas like physiology, biochemistry, histology and genetics. Potential investigations should assess the relationship between ventricular

dysfunction and functional capacity as evaluated by either a simple treadmill exercise test or a more complex cardiopulmonary exercise test. It would also be of interest to see if ventricular dysfunction is associated with neuro-hormonal activation. B-type natriuretic peptide (BNP) could be one of these biochemical markers because it indicates heart failure and hence useful for the diagnostic evaluation of heart disease. Nevertheless, the strongest evidence for a cardiomyopathy would come from histology. A Marfan related cardiomyopathy is biologically plausible since fibrillin-1 has been documented in the myocardium [Vracko 1990]. However, a causative role between reduced expression of fibrillin-1, histological integrity and ventricular impairment is yet to be demonstrated. Histological validation could be possible if myocardial biopsies could be attained at the time of prophylactic aortic root surgery. Furthermore, histological findings could be compared with gadolinium imaging techniques for non-invasive validation. Genetic studies may also be of interest to identify the underlying causes and association with cardiomyopathy, and whether specific loci are more prone to the existence of a cardiomyopathy or to more severe forms of cardiomyopathy.

In addition to the observational studies, longitudinal studies are needed to assess the natural history and prognostic value of a Marfan related cardiomyopathy. Since LV function correlates with RV function in this condition, it would be of interest if the combined analysis of both ventricles would carry additional or incremental information. Pharmacological therapy with beta-blockers and angiotensin receptor blockers could be studied to assess the effects on ventricular remodelling, but performing case-control studies may be unethical because these agents have become standard of care for prevention of aortic remodelling. Several ongoing randomized controlled trials are evaluating the efficacy of medical therapy in Marfan syndrome, and may be helpful to answer some of these pending questions [Lacro 2007, Gambarin 2009, Détaint 2010b, Radonic 2010].

10.2. THALASSAEMIA MAJOR

10.2.1. Overview

The thalassaemias are a family of inherited haemoglobin disorders characterised by reduced synthesis of the globin chains of haemoglobin [Weatherall 1997]. They are thought to be the commonest single gene disorder in humans, affecting close to 100 million people worldwide [Weatherall 1996]. The term is coined from “thallasos” and “emia”, the Greek words for “sea” and “blood”, relative to their original association with the coastal areas of the Mediterranean. However, its endemic distribution stretches far beyond the Mediterranean basin in a broad belt across Africa, the Middle East, and the Indian subcontinent to South-East Asia (figure 10.2). The thalassaemias (like all haemoglobin disorders) are common in regions with a high prevalence of malaria, a mosquito-borne parasitical infectious disease of the red blood cells. There is now evidence that thalassaemia is the result of natural selection and positive gene mutations in areas where malaria is (or was) endemic [Weatherall 1987, Allen 1997]. Minor forms of thalassaemia confer protection to malaria and a survival advantage over those without a defective gene. However, the few who acquire the major forms of thalassaemia will present with severe anaemia and early death. Due to population migration, thalassaemia and other inherited haemoglobin disorders have now become a global disease. In the UK, where malaria has never been a health care issue, there are about one thousand people with thalassaemia major [Modell 2000, Modell 2008].

Oxygen is transported in the red blood cells by haemoglobin, a complex protein made of four haem rings attached to four globin chains. The adult haemoglobin form is a tetramer consisting of two alpha-globin and two beta-globin chains. Normal haemoglobin synthesis relies on the balanced production of alpha and beta globin chains, but in thalassaemia, the production of one type of globin chain is reduced or absent. Thalassaemias are classified

according to which globin chain is affected: alpha-thalassaemia refers to reduced production of alpha globin chains, whereas beta thalassaemia refers to the reduced production of beta globin chains. Over 200 mutations have been described in the beta-like globin domain in chromosome 11, either related to gene control or expression [Olivieri 1999, Rund 2005].

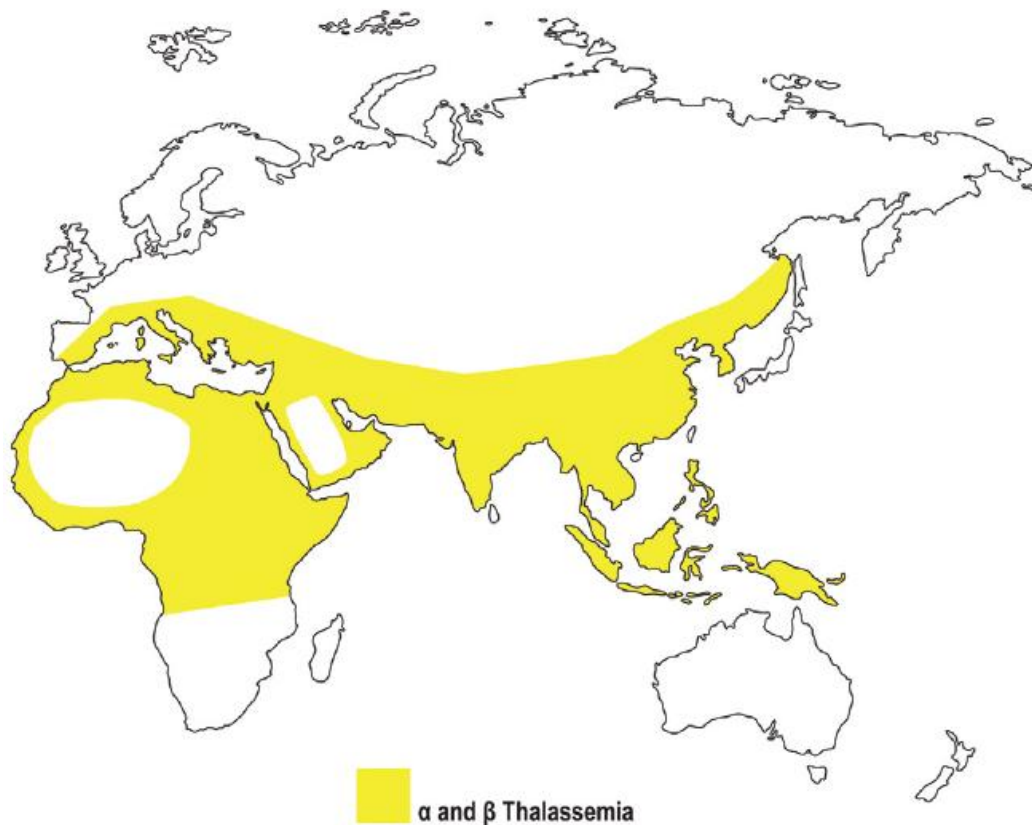


Figure 10.2. Worldwide distribution of thalassaemia. Reproduced with permission from Weatherall 2001.

In beta-thalassaemia, there is an imbalance between alpha and beta chains of haemoglobin in the red blood cells. Excess alpha chains precipitate in the red blood cells, leading to deformation in mild cases, and intravascular haemolysis or destruction in the bone marrow and spleen in severe cases. Anaemia is therefore the result of the excess of alpha chains which

cause destruction of red cells and their precursors [Nathan 1996, Olivieri 1999]. The clinical spectrum of beta-thalassaemia is variable, ranging from asymptomatic patients with no obvious anaemia to patients with life-threatening anaemias. In beta thalassaemia major, haemoglobin production is so impaired that normal growth and survival can be only achieved with regular blood transfusions. Because it is far more prevalent than alpha-thalassaemia major, beta-thalassaemia major is sometimes simply called thalassaemia major (TM) in the medical community.

TM only becomes evident at around 6-12 months of age, when the production of foetal haemoglobin shifts to the adult haemoglobin form. Manifestations include pallor, poor feeding, failure to thrive and frequent infections. The profound anaemia causes compensatory bone marrow expansion and extramedullary haematopoiesis with ineffective erythropoiesis, leading to splenomegaly and skeletal deformities. If left untreated, as it happens in most of the undeveloped countries, the prognosis is dire, with patients dying within the first 2 years of life [Zurlo 1989]. In developed countries, regular blood cell transfusions are standard care in TM, allowing normal development and augmenting life expectancy [Piomelli 1969, Pootrakul 1981]. However, regularly transfused patients developed heart failure and died during adolescence, not because of anaemia, but rather due to dilated cardiomyopathy secondary to iron overload [Engle 1964, Engle 1969, Kremastinos 1995]. The origin for the iron overload was hastily related to the iron contained in the red blood cells packs, as an unfortunate example on how an effective treatment for a disease is responsible for another disease. Patients undergoing regular transfusion programmes receive around 30 times the normal intake of iron, not only due to transfusions but also to increased gastrointestinal absorption secondary to anaemia [Gordeuk 1987]. Since humans are unable to excrete iron, this ultimately leads to iron accumulation and damage to the heart, liver, and endocrine organs (figure 10.3) [Britton 2002].

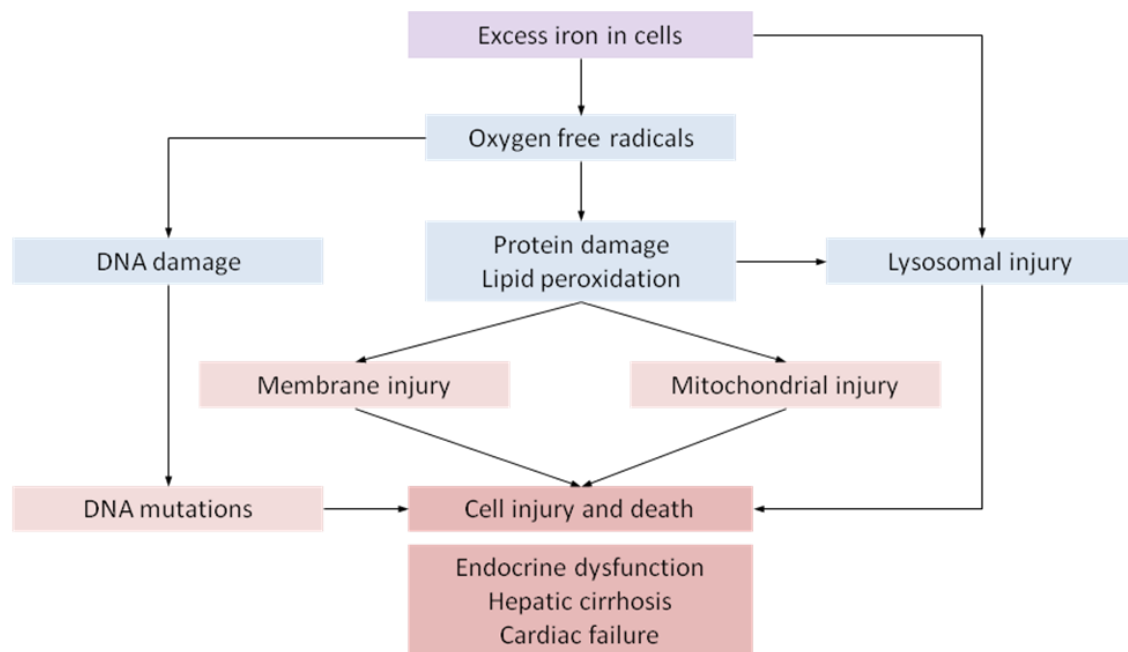


Figure 10.3. Mechanisms of cellular toxicity due to iron overload.

Pharmacological iron chelation therapy naturally became the cornerstone for the treatment of transfusion dependent TM. Deferoxamine, the first available chelator, was introduced in the 1960s, and since then has shown to prevent iron related complications [Hoffbrand 1979, Marcus 1984] and increase survival [Modell 1982, Zurlo 1989, Olivieri 1994, Brittenham 1994]. However, deferoxamine based therapies are hampered by the poor oral absorption and short half life [Callender 1980]. The chelator can only be delivered via parenteral routes, and the cumbersome treatment regimes (around 8-12 hours/day, 5-7 days/week) are responsible for the poor compliance to treatment [Olivieri 1997]. Two newer iron chelators were later introduced in the market. Both can be administered orally, resulting in an increase in patient compliance. Deferiprone was introduced in 1995, and is administered 3 times a day. Deferiprone appears to be the most effective chelator in removing iron from the heart, reducing cardiac complications [Anderson 2002, Piga 2003]. Deferasirox was introduced in 2005, and can be administered once daily. Deferasirox appears effective in removing iron from

the liver and heart [Porter 2010, Pennell 2012], but the long-term experience on outcomes is still limited. Nonetheless, the addition of two iron chelators has substantially increased the management options for TM, especially for those who are intolerant or irresponsive to medication [Berdoukas 2008].

Iron chelation therapy is initiated and titrated according to the amount of iron in the body. Traditionally, the available methods for assessing global iron burden have relied on serial measurements of serum ferritin or liver iron concentration from biopsy, neither of which is representative of the level of iron in the heart [Anderson 2001]. As such, iron cardiomyopathy may develop in patients with apparently good control of their global iron stores [Wood 2009]. Endomyocardial biopsy can directly assess the cardiac iron levels, but this invasive technique is limited to specialized centres, and rarely performed because the size of the specimens is usually too small for reliable quantification [Fitchett 1980, Olson 1987, Wang 2010]. Echocardiography is frequently used to monitor LV function, but measurements are inconsistent and unreliable due to the presence of a high output state. LV dysfunction usually only unravels at the latter stages of the disease, where there is already substantial iron loading and the outlook is poor [Felker 2000, Kremastinos 2001].

Heart failure due to iron overload cardiomyopathy continues to be the leading cause of death in TM patients [Borgna-Pignatti 1998, Li 2002, Borgna-Pignatti 2004]. The key for prevention and successful management of cardiac complications lies with the early detection of iron-overload cardiomyopathy and effective iron chelation therapy. In this respect, CMR has emerged as the technique of choice for evaluating myocardial iron in patients with transfusion-dependent anaemias. Iron quantification relies on the T2* (T2 star) technique, where signal decay over different echo times is used to generate a T2* curve, which is inversely related to the tissue iron concentration [Anderson 2001, Wood 2005]. T2* accurately estimates myocardial iron concentration [Carpenter 2011], and identifies the

patients at risk for heart failure that would otherwise had been undetected by conventional techniques [Kirk 2009]. The technique is reliable and robust [Westwood 2003a], enabling serial follow-up and monitoring treatment over time [Anderson 2002, Tanner 2007]. Since the introduction of T2* CMR in 1999, the number of cardiac deaths in the UK TM population has decreased by over 70% in the space of just 5 years [Modell 2000, Modell 2008]. This dramatic reduction in mortality was due to a combination of wider therapeutic options and implementation of an effective T2* screening programme [Telfer 2009]. The development of the T2* technique is a remarkable example on how translational science can be incorporated into clinical practice and improve outcomes in a short period of time.

10.2.2. Present work

The key papers on T2* CMR have described the relationship between myocardial T2* and the LV in TM. Conversely, little was known about the RV in iron overload cardiomyopathy, until the publication of the 3 papers presented in this thesis. These projects were only possible owing to the large database that has been built in CMR Unit since the development of the T2* technique. The study conception and design was relatively straight-forward, following the core structure of the previous key papers on T2* and LV measurements [Anderson 2001, Westwood 2007, Tanner 2007, Tanner 2008].

The first study of the series refers to the relation of myocardial iron loading with RV function (described in chapter 6). In 319 patients with TM, myocardial T2* was compared to RVEF as estimated by CMR. It was found that in patients with normal myocardial T2*, the RV function was essentially normal. On the other hand, in patients with abnormal T2*, there was a progressive decline in RV function with increasing iron concentrations. Finally, the results of

this observational study showed a strong linear relationship between RV and LV function across the spectrum of myocardial T2*.

The next stage was to define normal reference values for RV volumes and EF in patients with TM (described in chapter 7). The study population comprised 80 TM patients with no myocardial iron overload (defined by a normal T2* >20ms), who were compared to 40 age- and gender-matched controls. RV volumes and EF were higher than controls, whereas RV mass was roughly the same. The new established reference ranges are important in the interpretation of CMR results and in the management of TM. For instance, elevated RV volumes that would apparently suggest an impending cardiomyopathy may well be within physiological limits for the anaemic TM patient. On the other hand, RVEF values originally thought to be towards the lower limit of normal may actually indicate developing RV dysfunction in a TM patient. The new reference ranges thus permit earlier detection of ventricular dysfunction and prompt intensification of chelation therapy that otherwise would have been delayed if the general reference ranges were still in use.

The final of the three studies comprised data from patients who were enrolled in a trial assessing the efficacy of the two different chelation strategies in TM: a conventional scheme using deferoxamine only, and a more intensive scheme using a combination of deferoxamine and deferiprone (described in chapter 8). It was demonstrated that combination therapy was superior to improve RV function compared to conventional therapy, an effect probably mediated by more efficient removal of cardiac iron, as indicated by a significant improvement in myocardial T2*. Moreover, combination therapy appears particularly effective in patients with more severe iron loading, even in the presence of ventricular dysfunction, provided the patient that is compliant to the combination regime. Although the main purpose of the study was to compare the efficacy of two different regimes, the results further support the use of T2* CMR to monitor the response to chelation therapy.

The combined results of the studies above demonstrate a close relationship between LV and RV dynamics relative to the cardiac iron status. Both the LV and RV respond in the same way to the high output states induced by anaemic conditions, and both the LV and RV behave in the same way in iron overload cardiomyopathy, whether to different degrees of iron deposition, or after removal of myocardial iron with different types of chelation regimes. Hence iron overload cardiomyopathy affects the RV in addition to the LV, and usually to the same extent. The biventricular involvement observed in this cardiomyopathy is similar to what has been described in non-ischaemic cardiomyopathies, as opposed to the predominant LV involvement seen in ischaemic cardiomyopathies. By evaluating myocardial T2* in conjunction with the RV and the LV, the present work has completed a chapter on the interaction of cardiac iron with ventricular dynamics.

10.2.3. Future work

Research of the RV in iron overload cardiomyopathy relies on the surrogate T2* measurement of the interventricular septum rather than on direct T2* measurements of the RV. Evaluation of the thin RV free wall by T2* is difficult due to the proximity to the chest wall and susceptibility to artefacts. Therefore it is not currently possible to derive iron concentrations in the RV using standard T2* methodology. When the current work on the RV in TM was completed, an important paper was released on myocardial T2* and iron calibration and distribution. In this study, T2* measurements were validated against 12 ex-vivo hearts of patients with transfusion-dependent anaemias (mostly TM), and calibrated against iron concentration by deriving the formula $[\text{Fe}] = 45.0 \times (\text{T2}^*)^{-1.22}$ [Carpenter 2011]. Moreover, iron was found to be evenly distributed in the LV according to the conventional 16 segment model, though a transmural gradient was found within each segment, with higher concentrations in

the epicardium relative to the mesocardium and endocardium [Carpenter 2011]. The RV free wall was also evaluated, and found to have about 20% lower iron concentration than the LV at 4.69mg/g dry weight. Even when excluding the RV side of the interventricular septum (integrated in the epicardial layer of the LV for practical reasons), the iron concentration of the RV was still ten-fold in excess of the normal reference range [Collins 1987]. These findings do support direct iron cardiotoxicity as the likely pathogenic mechanism for RV dysfunction, with ventricular interdependence playing an additional role.

Myocardial T2* has shown to identify individuals at risk of developing arrhythmias and heart failure [Kirk 2009]. However, the incremental prognostic value of LV and RV function over myocardial T2* is yet to be investigated. Further work is required to address whether the combined assessment of ventricular function can refine the management of patients with iron overload cardiomyopathy.

10.3. CARDIAC RESYNCHRONIZATION THERAPY

10.3.1. Overview

Heart failure is the final common stage of most types of heart disease. The available epidemiological data present heart failure as a major healthcare problem. Its prevalence in the industrialized countries has trebled over the past 3 decades to affect 2-3% of the population [Cowie 1997, Redfield 2003, Dickstein 2008, Lloyd-Jones 2010], and is expected to rise further in the future, due to the ageing population and longer lifespan of heart disease [Levy 2002, Yach 2004, Braunschwig 2011]. Heart failure is the leading cause of hospital admissions over 65 years of age [DeFrances 2008], and a major economic burden to the healthcare systems [Dickstein 2010], consuming around 2% of the UK and US healthcare budgets [Stewart 2002, Lloyd-Jones 2010]. Despite the advances in pharmacological

treatment, prognosis is still poor, with 5 year mortality rates of around 50% [Levy 2002, Bleumink 2004]. It has been reported that survival of patients with heart failure is actually worse than most malignant cancers [Stewart 2001].

Implantable electronic devices have long been used for the treatment of heart disease. Since the implantation of the first cardiac pacemaker in 1958, technology has developed dramatically, with increasingly smaller devices, longer durability, improved programming algorithms, and evolving applications. Implantable cardioverter defibrillators (ICDs) are special type of pacemakers designed to treat ventricular arrhythmias by delivering high-energy electrical shocks [John 2012]. These devices have shown to reduce mortality and are currently used in patients with a high risk of sudden cardiac death [Moss 2002, Bardy 2005]. Cardiac resynchronization therapy (CRT) is also derived from the traditional pacemaker systems (figure 10.4) [Daubert 2012]. Whilst conventional pacemakers pace the right chambers, CRT systems have an additional lead pacing the LV. The proof of concept of CRT (or biventricular pacing) was originally demonstrated on a patient with end-stage failure and a wide QRS complex of left bundle branch block (LBBB) morphology [Cazeau 1994]. LBBB indicates prolonged electrical activation and often results in inefficient LV motion due to delayed mechanical activation of the lateral wall relative to the septal wall (figure 10.5) [Grines 1989]. By stimulating the LV septal and lateral walls at the same time, cardiac synchrony can be restored, resulting in improved LV haemodynamics, energy efficiency and cardiac output [Auricchio 1999, Nelson 2000]. These devices are firmly established for the treatment of refractory heart failure with electrical dyssynchrony (defined as QRS complex >120ms) and severe LV dysfunction (defined as LVEF <35%), where they have shown to reverse ventricular remodelling [Daubert 2009], improve symptom status [Cazeau 2001, Abraham 2002], and reduce cardiovascular morbidity and mortality [Bristow 2004, Cleland 2005, Moss 2009, Tang 2010].

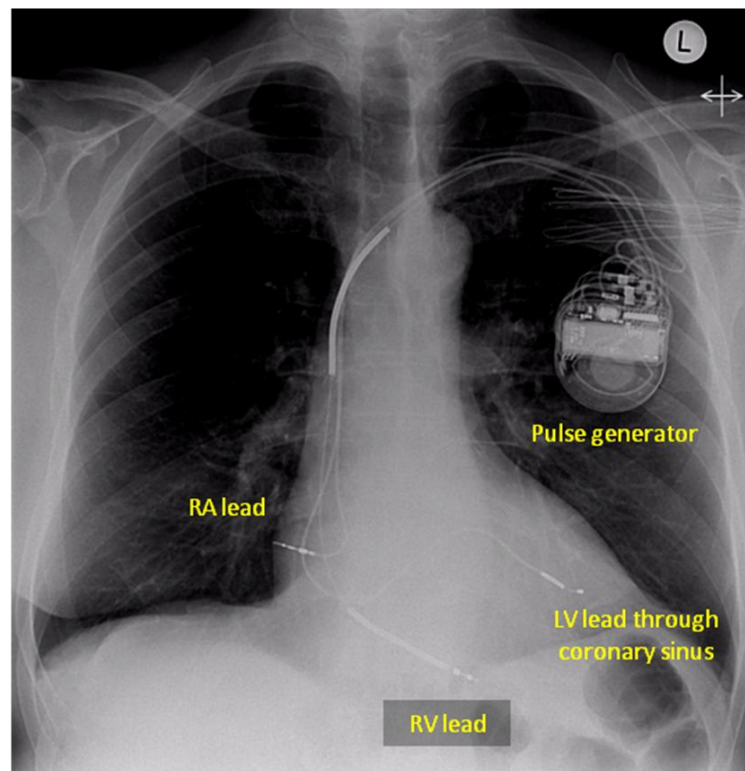


Figure 10.4. Antero-posterior chest X-ray showing a CRT device with leads in the right atrium (RA), right ventricle (RV), and left ventricle (LV) through the coronary sinus. L- Left.

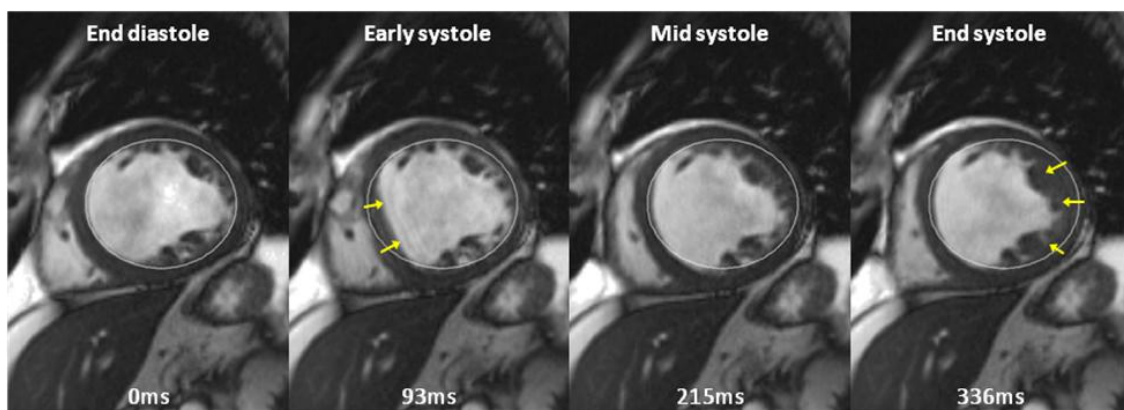


Figure 10.5. Mid-ventricular short-axis slice of a patient with LBBB at different phases of the cardiac cycle. The R-wave is the time reference, and the end-diastolic endocardial border was delineated for comparison. The septum contracts in early systole (arrows) and starts relaxing in mid-systole; the lateral wall only starts contracting at mid-systole, reaching the maximum amplitude at late systole (arrows).

Despite the demonstrable benefits in large populations, it is well known that 30-50% of apparently suitable individuals do not seem to respond to CRT [Nery 2012]. These non-responders remain an important conundrum as they do not appear to benefit from a device which is costly and not devoid of complications. In fact, non-responders have worse prognosis and quality of life than those who respond to CRT [Auricchio 2011, Cleland 2011]. Such observations have driven research to refine patient selection, in order to reduce non-response and increase the effectiveness of this treatment. One of the key initial discoveries was that electrical dyssynchrony (wide QRS) does not always correspond to mechanical dyssynchrony (contraction delay) [Yu 2003, Kass 2008]. It was then speculated that mechanical dyssynchrony could improve patient selection and minimize the number of non-responders to CRT. A multitude of echocardiographic markers of mechanical dyssynchrony then surged, showing promising results on single-centre experience [Pitzalis 2002, Bax 2004, Yu 2005]. However, when tested in randomized controlled or multicentre trials, no single echocardiographic measure of dyssynchrony was found to improve patient selection beyond current guidelines [Beshai 2007, Chung 2008]. These disappointing results were partly attributed to the high variability of the measures of dyssynchrony [Marwick 2008]. Echocardiography has therefore lost momentum since the inconclusive results of the RethinQ and PROSPECT trials [Daubert 2012].

CMR has also an interest in CRT [Leyva 2010]. A small single centre study suggested CMR to be better than echocardiography at discriminating mechanical dyssynchrony [Foley 2009a]. Dyssynchrony indices by CMR appear to predict response to CRT [Bilchick 2008] and adverse events [Chalil 2007b]. However, and despite the potential of CMR to evaluate mechanical dyssynchrony, there are other areas where CMR appears more relevant. The first and foremost CMR study on CRT was published by the Leiden group on the value of myocardial viability in patient selection. They found that the presence and extent of infarction in the LV

lateral wall was associated with lower response to CRT [Bleeker 2006c]. Further studies confirmed that the amount and location of the scar was associated with lower response rates and worse prognosis [White 2006, Ypenburg 2007, Chalil 2007a, Chalil 2007c]. The message of these studies was clear. LV pacing leads should be avoided over scarred areas because they are ineffective and even detrimental by inducing arrhythmias and adverse events [Nazarian 2005, Leyva 2011a]. Thus, the use of LGE CMR to guide LV lead deployment has become standard practice in many centres. Other potential areas of research include visualization of the coronary venous anatomy [Chiribiri 2008], which combined with mechanical dyssynchrony and scar evaluation, can determine the optimal site for LV lead deployment [Helm 2007, Rademakers 2010].

10.3.2. Present work

The study in the present thesis was the first joint collaborative work between the CMR Unit and the Heart Failure Pacing Clinic, as part of a grant application for a single-centre randomized controlled trial of CMR guided management versus conventional management. Hence, this pilot study represented the framework to determine the feasibility of CMR measurements and the most appropriate end-points for a future randomized controlled trial.

Several CMR parameters were evaluated in this study. The LV was measured for volumes, late gadolinium enhancement, and dyssynchrony. Apart from septal to lateral delay, which was marginally significant for response, none of the other markers of dyssynchrony was predictive of any of the proposed end-points. This RV was also evaluated, given the limited evidence by echocardiography and nuclear imaging, and lack of published data by CMR. Besides the conventional RV volumetric variables, evaluation of dyssynchrony as well as longitudinal and radial function was attempted. Whilst longitudinal function determined by tricuspid annular

plane systolic excursion (TAPSE) was easy to acquire and simple to measure, radial function and dyssynchrony was difficult to assess and later abandoned because the measurements appeared unreliable due to the complex RV motion.

To determine benefit to CRT, a hard clinical end-point was chosen instead of a surrogate marker of response, because there is still no consensus on how response should be defined [Foley 2009b, Cleland 2010]. The end-point was a composite of death by any cause plus heart failure hospitalization as defined by the landmark CARE-HF trial [Cleland 2005]. Nonetheless, most of the authors felt that response criteria would add relevant information to the paper. Thus, a functional and a remodelling criterion were initially included for the data collection. Functional improvement was defined as an improvement in New York Heart Association (NYHA) class, a semi-quantitative marker of functional limitation in heart failure that is in use worldwide [Dolgin 1994]. However, improvement in NYHA class was discarded early in the data collection period, not only because it was quite subjective [Raphael 2007], but also because there was poor correlation with the more objective markers of LV remodelling. For assessment of LV remodelling, an improvement in LVEF was chosen as the response criterion, because it is a simple and established parameter, with the additional benefit of being part of the inclusion criteria for CRT.

The main finding of the study was that RV dysfunction was a significant predictor of outcomes in patients undergoing CRT. The results are especially relevant as RV dysfunction remained statistically significant on multivariate analysis when compared to other established prognostic markers in heart failure [Cowburn 1998]. This study confirms RV function as a powerful prognosticator, in keeping with previous publications in heart failure [De Groote 1998, Ghio 2001, Meyer 2010]. For the first time a CRT study demonstrated a link between lack of response and worse outcomes in patients presenting with RV dysfunction. One possible explanation relies on the assumption that RV dysfunction identifies a group of

patients who are too sick to recover. This concept was supported by the fact that patients with RV dysfunction had a lower LVEF, more significant mitral regurgitation, and higher pulmonary artery pressures. Because of the multiple influences affecting the RV due to LV failure, RV dysfunction may constitute a final and irreversible stage in congestive heart failure, where conventional therapy may not have the desired or expected benefit [Voelkel 2006].

Despite widely studied and used by echocardiography in clinical practice, there is only limited information on TAPSE by CMR. The few available studies show good correlation of longitudinal TAPSE with global RVEF, although this 1D parameter appears to be less reproducible than the 3D RVEF [Nijveld 2009, Caudron 2011]. This study was the first to document the prognostic value of TAPSE as evaluated by CMR. Hence TAPSE may be used as a potential alternative to RVEF for assessing RV function in heart failure, particularly whenever the latter cannot be estimated, either due to technical problems or incomplete image acquisition.

10.3.3. Future work

Our findings are novel as RV function remained an independent prognosticator amid other established markers in heart failure, and slightly provocative as the response rate for those with poor RV function was so low (~20%) that CRT might be reconsidered. Because the work was based on a single centre in a relatively small population, larger studies with a multicentre design are required to address whether the RV and other parameters should be considered for patient selection beyond the current consensus criteria. In this regard, CMR should be one of the techniques involved, as part of a comprehensive evaluation of ventricular mechanics and dyssynchrony, aetiology and stage of heart failure, amount of myocardial scar, and optimal site for lead placement, all of which are presumed to determine response to CRT [Marwick 2008].

Despite the reasonable amount of publications on LGE and the LV, there is no available literature on LGE and the RV. In our study, LGE in the RV indicating myocardial infarction was associated with adverse events (HR 5.6, 95% CI 1.8-17.9, $p=0.004$) and a non-significant trend for lack of response (OR 0.24, $p=0.22$). These preliminary data were not published due to the small number of patients with myocardial infarction ($n=5$). A larger cohort may provide more definite evidence about the value, location and extent of RV LGE in CRT. RV mechanical dyssynchrony is another potential area of interest, since CMR can evaluate RV motion in any area and in any plane or direction. Limited studies suggest RV mechanical dyssynchrony to be associated with RV dysfunction and clinical outcomes in pulmonary hypertension and congenital heart disease [Janousek 2009]. However, it is unclear whether RV dyssynchrony is the cause or the consequence of RV dysfunction [Mertens 2010]. Moreover, there is controversy on the usefulness of CRT in patients with predominant RV dyssynchrony [Dubin 2005, Ogunyankin 2010]. Further studies are thus necessary to address these questions.

A major caveat of any research by CMR is that follow-up is not possible after CRT implantation because the available devices are not CMR-compatible. However, development of CMR-compatible CRT devices is currently underway, and expected to be in the market soon, as recently seen with the new generation of CMR-compatible pacemakers and ICDs. Introduction of CMR-compatible CRT devices in the near future will haste new opportunities for research. Studies with CMR-compatible devices will assess the immediate effects of both LV and RV mechanical dyssynchrony and performance, either comparing pre- versus post- implantation, or with the devices switched on and off. Long-term effects of CRT on LV and especially RV remodelling would be reliably assessed by CMR, where the superior accuracy and reproducibility of CMR would ensure smaller sample sizes for meaningful results. CMR would also be in a privileged position to assess whether patients with RV electrical and mechanical dyssynchrony would benefit from CRT, one of the important contentious topics in the field.

With the extension of CMR-compatible technology to CRT devices, it is likely that CMR will play an important role in identifying suboptimal response as well as optimizing the efficacy of the implanted devices [Leyva 2011b].

10.4. ORIGINAL CONTRIBUTION TO RESEARCH

The RV (**chapter 2**) was the focus of the thesis given its increasing recognition in the circulatory system. CMR (**chapter 3**) has emerged as the technique of choice for the study the RV, and the methodology used is arguably the reference standard (**chapter 4**). Marfan syndrome, thalassaemia major and heart failure prior to CRT are all established indications for CMR, and were chosen as the subjects of the thesis, since the role of the RV in these conditions is relatively unknown. This section overviews the key steps involved in the research from a personal perspective, and describes the clinical relevance of the novel findings encountered in this thesis.

10.4.1. Marfan syndrome

The first investigation in this research (**chapter 5**) was undertaken after realising that LV dilatation and dysfunction are prevalent in Marfan syndrome [Alpendurada 2008b]. From the general Marfan database comprehending 150 patients and 383 studies, I selected the study population and defined cardiomyopathy in addition to other cardiovascular parameters. This was the first CMR study to evaluate RV function, and the first to demonstrate RV dilatation and systolic dysfunction. Marfan cardiomyopathy was found to be frequently associated with biventricular involvement. When present, the biventricular dysfunction was usually mild, which explains why this condition is often overlooked by echocardiography. The

cardiomyopathy was also found to be a separate entity and unrelated to the traditional features of the disease. In summary, this work provides compelling evidence for a primary cardiomyopathy, hence raising awareness and highlighting the importance of screening for ventricular dysfunction in patients with Marfan syndrome.

10.4.2. Thalassaemia major

The study of the RV in TM was the next step of the research, as the large TM database in the CMR Unit represented an excellent opportunity to look at the RV in different stages of TM. The work was published in the form of 3 papers, which are briefly commented below.

For the observational study on T2* and RV function (**chapter 6**), I selected the patient population, and eliminated potential confounders such as pulmonary hypertension or associated cardiac conditions. The statistical analysis and data display were also developed by myself. To our knowledge, this was the first study to comprehensively document the relationship between myocardial iron loading and RV function. Progressive RV enlargement and dysfunction occurred with increasing iron loading, a finding likely mediated by direct iron cytotoxicity, as no other factors were found to explain the observed effects on ventricular function. There was a strong agreement between LV and RV function, confirming that iron-overload cardiomyopathy typically presents with biventricular involvement.

For the work on RV reference ranges (**chapter 7**), I collected data on half of the TM patients, and compared the defined variables with an age and gender matched control group. This study showed that RV volumes in TM differ from healthy controls. Thus, the traditional reference ranges for the normal population are inadequate and should be avoided in TM patients. The novel reference ranges for TM can accurately identify RV dilatation or

dysfunction, and infer which patients are most likely to benefit from intensive chelation therapy and heart failure medication.

For the paper on iron chelation and RV function (**chapter 8**), I was responsible for the study design, including the decision to evaluate the open-label cohort alongside the RCT cohort. As a result, the joined cohort offered comprehensive information on RV response to chelation across the entire spectrum of cardiac siderosis. Combination therapy with deferoxamine and deferiprone was found to be most effective, and thus should be regarded as the first-line treatment for patients with cardiac siderosis and ventricular dysfunction. RV dysfunction was noted to be reversible in iron-overload cardiomyopathy, even when there was significant iron loading, where combination therapy actually proved to be most beneficial. Echocardiography-based measurements of pulmonary artery pressures were integrated, thereby excluding any significant influence of pulmonary hypertension. The improvement in RV function paralleled the improvement in LV function, in keeping with the evidence already collected by the observational study.

10.4.3. Cardiac resynchronization therapy

The final work looked at the prognostic role of the RV in CRT (**chapter 9**). After revision of the available literature, I selected the study population and the parameters to be assessed. In keeping with the previous works in the thesis, I decided to explore the RV in detail, and pursued novel methods of measuring RV size, function and synchrony. I defined the cut-offs and chose the end-points including response to therapy. For the first time, RV function was found to be a predictor of both response and outcomes in patients undergoing CRT. These findings are especially relevant as RV function was independent of other well established markers. The RV appears to influence the natural history and hence should be evaluated in

patients under consideration for CRT. Nevertheless, further research is required to assess whether the RV can actually change the management of patients under consideration for CRT.

There was some encouraging feedback during abstract presentations regarding the use of TAPSE, as this became the first CMR study to document the prognostic value of RV longitudinal function in cardiac disease. Because TAPSE is easier to measure than RVEF, this work may reignite the interest on this surrogate marker of RV function, which has been in use by the echocardiographic community for the last 25 years.

CHAPTER 11. CONCLUSION

After decades of neglect, there has been a resurgence of interest in the RV. Most of the renewed awareness derived from advances in cardiovascular imaging, enabling new research opportunities for the evaluation of this complex structure. Among all imaging techniques, CMR is the most adequate one to study the RV. By using CMR as the primary imaging modality, the work in the thesis expanded the available knowledge on the RV in cardiomyopathy and heart failure.

In Marfan syndrome, CMR measurements supported the presence of a primary cardiomyopathy in a subgroup of patients with Marfan syndrome (described in **chapter 5**). This cardiomyopathy is usually mild, asymptomatic, and independent of other cardiovascular manifestations. This was the first study to demonstrate RV systolic dysfunction in Marfan syndrome, a finding that strengthens the existence of a Marfan related cardiomyopathy with biventricular involvement.

The core of the work was on thalassaemia major, where RV measurements were compared to myocardial T2*. Several conclusions can be taken from these studies. Firstly, myocardial iron deposition is associated with RV dysfunction, which mirrors the progressive deterioration in LV function with worsening cardiac iron loading (described in **chapter 6**). Therefore, RV dysfunction may play a role in heart failure associated with myocardial siderosis. Secondly, RV parameters in TM patients without myocardial iron overload differ from healthy controls (described in **chapter 7**). The new proposed reference ranges for RV size and function can therefore be useful for the diagnosis and management of RV dilatation and dysfunction in TM. Thirdly, combination therapy with deferoxamine and deferiprone is superior to standard chelation with deferoxamine alone in improving RV function in iron-overload cardiomyopathy,

and effective when there is severe iron loading (described in **chapter 8**). Improvement in RV function was driven by the removal of iron from the heart and paralleled the improvement in LV function. In summary, the RV shows a similar behaviour to what previously described for the LV, with progressive dysfunction with increasing iron deposition, and improving function with iron removal, reaching the expected high cardiac output dynamics when iron overload is completely eliminated.

Finally, the importance of the RV was demonstrated in heart failure patients undergoing CRT implantation, a condition where the focus is on the LV (described in **chapter 9**). The RV was an independent predictor of both short-term response and long-term clinical outcomes, and should be considered in the routine evaluation of patients for CRT.

In conclusion, the present work supports the recognized value of CMR in the study of the RV, and demonstrates the important role of the RV in the physiology, pathophysiology, diagnosis and prognosis of different cardiac conditions. The RV is therefore an essential component of the circulatory system, and should be evaluated in every patient with cardiopulmonary disease. Future challenges include standardization of RV methodology as CMR is becoming more available, and enrolment of multicentre trials to define more precise management strategies.

CHAPTER 12: APPENDIX**12.1. PUBLICATIONS ARISING FROM THIS WORK****12.1.1. Peer reviewed research papers**

Alpendurada F, Wong J, Kiotsekoglou A, Banya W, Child A, Prasad SK, Pennell DJ, Mohiaddin RH. Evidence for Marfan cardiomyopathy. *Eur J Heart Fail* 2010;12:1085-91.

Alpendurada F, Carpenter JP, Deac M, Kirk P, Walker JM, Porter JB, Banya W, He T, Smith GC, Pennell DJ. Relation of myocardial T2* to right ventricular function in thalassaemia major. *Eur Heart J* 2010;31:1648-54.

Alpendurada F*, Carpenter JP*, Deac M, Maceira A, Garbowski M, Kirk P, Walker JM, Porter JB, Shah F, Banya W, He T, Smith GC, Pennell DJ. Right ventricular volumes and function in thalassemia major patients in the absence of myocardial iron overload. *J Cardiovasc Magn Reson* 2010;12:24. (*Joint first author)

Alpendurada F, Smith GC, Carpenter JP, Nair SV, Tanner MA, Banya W, Dessi C, Galanella R, Walker JM, Pennell DJ. Effects of combined deferiprone with deferoxamine on right ventricular function in thalassaemia major. *J Cardiovasc Magn Reson* 2012;14:8.

Alpendurada F, Guha K, Sharma R, Ismail TF, Clifford A, Banya W, Mohiaddin RH, Pennell DJ, Cowie MR, McDonagh T, Prasad SK. Right ventricular dysfunction is a predictor of non-response and clinical outcome following cardiac resynchronization therapy. *J Cardiovasc Magn Reson* 2011;13:68.

12.1.2. Abstracts

Alpendurada F, Guha K, Sharma R, Prasad SK. Right ventricular dysfunction predicts clinical outcomes following cardiac resynchronization. EuroCMR 2011, Nice, France. *Oral presentation*

Alpendurada F, Smith GC, Carpenter JP, Tanner MA, Banya W, Galanello R, Pennell DJ. Effect of myocardial iron removal on right ventricular function: insights from a randomized, placebo controlled, double-blind trial in thalassaemia major. ESC2010, Stockholm, Sweden. *Poster*

Alpendurada F, Carpenter JP, Smith GC, Tanner MA, Banya W, Galanello R, Pennell DJ. Effect of myocardial iron removal on right ventricular function: insights from a randomized, placebo controlled, double-blind trial in thalassemia major. EuroCMR 2010, Florence, Italy. *Oral presentation*

Alpendurada F, Wong J, Kiotsekoglou A, Banya W, Child A, Prasad SK, Pennell DJ, Mohiaddin RH. Evidence for Marfan cardiomyopathy. Portuguese Society of Cardiology Meeting, Lisbon, Portugal. *Oral presentation*

Carpenter JP, Alpendurada F, Deac M, Kirk P, Maceira A, Walker JM, Porter JB, Banya B, Smith GC, Pennell DJ. Normalized ranges for right ventricular volumes and function in thalassemia major. SCMR 2010. Phoenix, AZ. *Poster*

Alpendurada F, Deac M, Carpenter JP, Kirk P, Smith GC, Pennell DJ. Impact of Myocardial Iron Loading on Right Ventricular Function. ESC2009. Barcelona, Spain. *Poster*

Alpendurada F, Wong J, Kiotsekoglou A, Banya W, Mohiaddin RH. Marfan's cardiomyopathy: a novel entity from a well-known disease? ESC2009. Barcelona, Spain. *Poster*

Kiotsekoglou A, Alpendurada F, Wong J, Kapetanakis V, Child AH, Mohiaddin RH. Assessment of Right Ventricular Function in adults with Marfan syndrome using Cardiovascular Magnetic Resonance. EuroCMR2009. Athens, Greece. *Poster*

Alpendurada F, Wong J, Kiotsekoglou A, Banya W, Mohiaddin RH. Marfan's cardiomyopathy: a novel entity? EuroCMR2009. Athens, Greece. *Poster*

Alpendurada F, Deac M, Carpenter JP, Kirk P, Smith GC, Pennell DJ. Impact of Myocardial Iron Loading on Right Ventricular Function. BSCMR 2009. Oxford, UK. *Poster*

Alpendurada F, Deac M, Carpenter JP, Kirk P, Smith GC, Pennell DJ. Impact of Myocardial Iron Loading on Right Ventricular Function. SCMR 2009, Orlando, FL. *Poster*

Wong J, Alpendurada F, Burman E, Mohiaddin R. Marfan's cardiomyopathy is associated with aortic annular and root dilatation in the absence of significant valvular regurgitation. SCMR 2009, Orlando, FL. *Oral presentation*

Alpendurada F, Mohiaddin R. Evaluation of Marfan syndrome by Cardiovascular Magnetic Resonance. ESC 2008, Munich, Germany. *Poster*

Alpendurada F, Mohiaddin R. Evaluation of left ventricular volumes and mass in a Marfan population by Cardiovascular Magnetic Resonance. EuroCMR 2008, Lisbon, Portugal. *Poster*

Alpendurada F, Mohiaddin R. Evaluation of Marfan syndrome by Cardiovascular Magnetic Resonance. EuroCMR 2008. Lisbon, Portugal. *Poster*

Alpendurada F, Mohiaddin R. Prevalence of cardiovascular manifestations in patients with Marfan syndrome: a Cardiovascular Magnetic Resonance study. SCMR 2008, Los Angeles, CA. *Poster*

12.1.3. Invited presentations

Cardiac volumes and function in thalassaemia major. Novartis Pharma CMR Symposium. London, 5th August 2010

Cardiovascular magnetic resonance in Marfan syndrome. British Heart Foundation Centre of Research Excellence Seminar. London, 25th June 2009

12.2. PERSONAL CONTRIBUTION TO RESEARCH

For the Marfan cardiomyopathy paper, I conceived and designed the study, collected and analysed the data, and drafted the manuscript. For the thalassaemia work on the RV and T2*, I participated in the study design, data collection and analysis, and jointly prepared the manuscript with Dr John-Paul Carpenter. For the study on normal RV reference ranges in TM, I participated in the study design, data collection and analysis, and jointly prepared the manuscript with Dr John-Paul Carpenter. For the paper on the RV and chelation therapy, I participated in the study design, data collection and analysis, and wrote the manuscript in conjunction with Dr Gill Smith. For the cardiac resynchronization therapy paper, I conceived and designed the study, collected and analysed the data, and drafted the manuscript. The statistical analysis was performed with the assistance of Mr Winston Banya (Medical Statistician) at Imperial College.

12.3. CRITICAL DEVELOPMENT REVIEW AS A RESEARCHER

Over the last 4 years, I have been fortunate to be actively engaged in several research projects under the supervision of world-renowned experts in cardiovascular magnetic resonance.

During this period of time, I developed the critical knowledge for creating and developing research projects, as well as re-evaluating the available information and defining the most appropriate directions to pursue. I learned that time is valuable and resources are limited, so I try to focus on the fundamentals, and look for ideas or messages that are potentially relevant for clinical practice. I have acquainted with the Local Ethics Department, and have been involved with applications to the Research Ethics Committees. I improved on creating databases, planning data acquisition, and ensuring consistent data collection. With the help of statistical courses and dedicated professionals, I improved my statistical skills and I am now able to independently perform most the statistical analysis for myself and other members of the Department. I developed skills on medical writing, initially with editorials and reviews articles, and then progressing to original articles. Although there is still room for improvement, I am now reviewing other original articles as a co-author, and case reports as a senior author. I started experiencing the gruesome task of corresponding with Journal editors and especially with the appointed reviewers. As a result, when having the opportunity to review other centres' works for publication, I tend to follow a more constructive approach. Finally, I started participating in grant applications for research funding.

12.4. SUPERVISION

This thesis was supervised by Dr Andrew Tizzard at Middlesex University and by Professor Dudley J Pennell at Imperial College London. Professor Richard Bayford at Middlesex University was the Director of Studies.

12.5. LIST OF ABBREVIATIONS

1D - One-dimensional

2D - Two-dimensional

3D - Three-dimensional

ARVC - Arrhythmogenic right ventricular cardiomyopathy

BSA - Body surface area

BNP - B-type natriuretic peptide

CAD - Coronary artery disease

CE-MRA - Contrast-enhanced magnetic resonance angiography

CHD - Congenital heart disease

CT - Computed tomography

CMR - Cardiovascular magnetic resonance

CRT - Cardiac resynchronization therapy

ECG - Electrocardiogram

EDV - End-diastolic volume

EF - Ejection fraction

ERNA - Equilibrium radionuclide angiography

ESV - End-systolic volume

FID - Free induction decay

FOV - Field of view

FPRNA - First pass radionuclide angiography

GBCA - Gadolinium based contrast agent

GE - Gradient echo

HF - Heart failure

Hz - Hertz

IQR - Interquartile range

LA - Left atrium

LAD - Left anterior descending artery

LBBB - Left bundle branch block

LGE - Late gadolinium enhancement

LV - Left ventricle

MDCT - Multidetector computed tomography

MFS - Marfan syndrome

MR - Magnetic resonance

MRA - Magnetic resonance angiography

MRI - Magnetic resonance imaging

NYHA - New York Heart Association

PAP - Pulmonary artery pressure

PDA - Posterior descending artery

PHT - Pulmonary hypertension

PVR - Pulmonary vascular resistance

RCA - Right coronary artery

ROI - Region of interest

RV - Right ventricle

SD - Standard deviation

SE - Spin echo

SI - Signal intensity

SPECT - Single photon emission computed tomography

SSFP - Steady state free precession

T2* - T2 star

TAPSE - Tricuspid annular plane systolic excursion

T - Tesla

TE - Echo time

TGF- β - Transforming growth factor-beta

TI - Inversion time

TM - Beta thalassaemia major

TR - Repetition time

12.6. REFERENCES**A**

Abraham WT, Fisher WG, Smith AL, Delurgio DB, Leon AR, Loh E, Kocovic DZ, Packer M, Clavell AL, Hayes DL, Ellestad M, Trupp RJ, Underwood J, Pickering F, Truex C, McAtee P, Messenger J; MIRACLE Study Group. Multicenter InSync Randomized Clinical Evaluation. Cardiac resynchronization in chronic heart failure. *N Engl J Med* 2002;346:1845-53.

Abuhid IM, de Rezende NA. Right ventricular wall 'ischemia' findings using a dual isotope protocol. *Clin Nucl Med* 2007;32:652-4.

Adabag AS, Maron BJ, Appelbaum E, Harrigan CJ, Buross JL, Gibson CM, Lesser JR, Hanna CA, Udelson JE, Manning WJ, Maron MS. Occurrence and frequency of arrhythmias in hypertrophic cardiomyopathy in relation to delayed enhancement on cardiovascular magnetic resonance. *J Am Coll Cardiol* 2008;51:1369-74.

Aessopos A, Farmakis D, Karagiorga M, Voskaridou E, Loutradi A, Hatziliambi A, Joussef J, Rombos J, Loukopoulos D. Cardiac involvement in thalassemia intermedia: a multicenter study. *Blood* 2001;97:3411-6.

Aessopos A, Farmakis D, Hatziliambi A, Fragodimitri C, Karabatsos F, Joussef J, Mitileneou E, Diamanti-Kandaraki E, Meletis J, Karagiorga M. Cardiac status in well-treated patients with thalassemia major. *Eur J Haematol* 2004;73:359-66.

Aessopos A, Farmakis D. Pulmonary hypertension in beta-thalassemia. *Ann N Y Acad Sci* 2005a;1054:342-9.

Aessopos A, Farmakis D, Deftereos S, Tsironi M, Tassiopoulos S, Moyssakis I, Karagiorga M. Thalassemia heart disease: a comparative evaluation of thalassemia major and thalassemia intermedia. *Chest* 2005b;127:1523-30.

Alfakih K, Plein S, Bloomer T, Jones T, Ridgway J, Sivananthan M. Comparison of right ventricular volume measurements between axial and short axis orientation using steady-state free precession magnetic resonance imaging. *J Magn Reson Imaging* 2003;18:25-32.

Allen SJ, O'Donnell A, Alexander ND, Alpers MP, Peto TE, Clegg JB, Weatherall DJ. α^+ -Thalassaemia protects children against disease caused by other infections as well as malaria. *Proc Natl Acad Sci USA* 1997;94:14736-41.

Almagro P, Barreiro B, Ochoa de Echaguen A, Quintana S, Rodríguez Carballeira M, Heredia JL, Garau J. Risk factors for hospital readmission in patients with chronic obstructive pulmonary disease. *Respiration* 2006;73:311-7.

Alpendurada F, Pennell DJ. Late gadolinium enhancement in cardiomyopathy. *Int J Cardiovasc Imaging* 2008;24:613-5.

Alpendurada F, Mohiaddin RH. Evaluation of Marfan syndrome by cardiovascular magnetic resonance. *Eur Heart J* 2008b;29(S1):498.

Alpendurada F, Wong J, Pennell DJ. Practical applications of cardiovascular magnetic resonance. *Heart Asia* 2009a;1:31-7.

Alpendurada F, Deac M, Carpenter JP, Kirk P, Pennell DJ. Impact of myocardial iron loading on right ventricular function [abstract]. *J Cardiovasc Magn Reson* 2009b;11(S1):P162.

Alpendurada F, Carpenter JP, Deac M, Kirk P, Walker JM, Porter JB, Banya W, He T, Smith GC, Pennell DJ. Relation of Myocardial T2* to Right Ventricular Function in Thalassaemia Major. *Eur Heart J* 2010;31:1648-54.

Alústiza JM, Artetxe J, Castiella A, Agirre C, Emparanza JI, Otazua P, García-Bengochea M, Barrio J, Mújica F, Recondo JA. MR quantification of hepatic iron concentration. *Radiology* 2004;230:479-84.

Amado LC, Gerber BL, Gupta SN, Rettmann DW, Szarf G, Schock R, Nasir K, Kraitichman DL, Lima JA. Accurate and objective infarct sizing by contrast-enhanced magnetic resonance imaging in a canine myocardial infarction model. *J Am Coll Cardiol* 2004;44:2383-9.

Anderson JL, Adams CD, Antman EM, Bridges CR, Califf RM, Casey DE Jr, Chavey WE 2nd, Fesmire FM, Hochman JS, Levin TN, Lincoff AM, Peterson ED, Theroux P, Wenger NK, Wright RS, Smith SC Jr. 2011 ACCF/AHA Focused Update Incorporated Into the ACC/AHA 2007 Guidelines for the Management of Patients With Unstable Angina/Non-ST-Elevation Myocardial Infarction. *Circulation* 2011;123:e426-579. Erratum in: *Circulation* 2011;123:e627.

Anderson LJ, Holden S, Davis B, Prescott E, Charrier CC, Bunce NH, Firmin DN, Wonke B, Porter J, Walker JM, Pennell DJ. Cardiovascular T2-star (T2*) magnetic resonance for the early diagnosis of myocardial iron overload. *Eur Heart J* 2001;22:2171-9.

Anderson LJ, Wonke B, Prescott E, Holden S, Walker JM, Pennell DJ. Comparison of effects of oral deferiprone and subcutaneous desferrioxamine on myocardial iron concentrations and ventricular function in beta-thalassemia. *Lancet* 2002;360:516-20.

Anderson LJ, Westwood MA, Holden S, Davis B, Prescott E, Wonke B, Porter JB, Walker JM, Pennell DJ. Myocardial iron clearance during reversal of siderotic cardiomyopathy with intravenous desferrioxamine: a prospective study using T2* cardiovascular magnetic resonance. *Br J Haematol* 2004;127:348-55.

Antman EM, Anbe DT, Armstrong PW, Bates ER, Green LA, Hand M, Hochman JS, Krumholz HM, Kushner FG, Lamas GA, Mullany CJ, Ornato JP, Pearle DL, Sloan MA, Smith SC Jr, Alpert JS, Anderson JL, Faxon DP, Fuster V, Gibbons RJ, Gregoratos G, Halperin JL, Hiratzka LF, Hunt SA, Jacobs AK. ACC/AHA guidelines for the management of patients with ST-elevation myocardial infarction. *Circulation* 2004;110:e82-292.

Antman EM, Hand M, Armstrong PW, Bates ER, Green LA, Halasyamani LK, Hochman JS, Krumholz HM, Lamas GA, Mullany CJ, Pearle DL, Sloan MA, Smith SC Jr; 2004 Writing Committee Members, Anbe DT, Kushner FG, Ornato JP, Jacobs AK, Adams CD, Anderson JL, Buller CE, Creager MA, Ettinger SM, Halperin JL, Hunt SA, Lytle BW, Nishimura R, Page RL, Riegel B, Tarkington LG, Yancy CW. 2007 Focused Update of the ACC/AHA 2004 Guidelines for the Management of Patients With ST-Elevation Myocardial Infarction. *Circulation* 2008;117:296-329. Erratum in: *Circulation* 2008;117:e162.

Araoz PA, Gotway MB, Trowbridge RL, Bailey RA, Auerbach AD, Reddy GP, Dawn SK, Webb WR, Higgins CB. Helical CT pulmonary angiography predictors of in-hospital morbidity and mortality in patients with acute pulmonary embolism. *J Thorac Imaging* 2003;18:207-16.

Araoz PA, Gotway MB, Harrington JR, Harmsen WS, Mandrekar JN. Pulmonary embolism: prognostic CT findings. *Radiology* 2007;242:889-97.

Armstrong WF, Ryan T. Physics and instrumentation. In: Feigenbaum's Echocardiography, 7th edition. Philadelphia, PA. Lippincott Williams & Wilkins; 2009:9-38.

Assomull RG, Prasad SK, Lyne J, Smith G, Burman ED, Khan M, Sheppard MN, Poole-Wilson PA, Pennell DJ. Cardiovascular magnetic resonance, fibrosis, and prognosis in dilated cardiomyopathy. *J Am Coll Cardiol* 2006;48:1977-85.

Auricchio A, Stellbrink C, Block M, Sack S, Vogt J, Bakker P, Klein H, Kramer A, Ding J, Salo R, Tockman B, Pochet T, Spinelli J. Effect of pacing chamber and atrioventricular delay on acute systolic function of paced patients with congestive heart failure. *Circulation* 1999;99:2993-3001.

Auricchio A, Prinzen FW. Non-responders to cardiac resynchronization therapy: the magnitude of the problem and the issues. *Circ J* 2011;75:521-7.

B

Babu-Narayan SV, Goktekin O, Moon JC, Broberg CS, Pantely GA, Pennell DJ, Gatzoulis MA, Kilner PJ. Late gadolinium enhancement cardiovascular magnetic resonance of the systemic right ventricle in adults with previous atrial redirection surgery for transposition of the great arteries. *Circulation* 2005;111:2091-8.

Babu-Narayan SV, Kilner PJ, Li W, Moon JC, Goktekin O, Davlouros PA, Khan M, Ho SY, Pennell DJ, Gatzoulis MA. Ventricular fibrosis suggested by cardiovascular magnetic resonance in adults with repaired tetralogy of Fallot and its relationship to adverse markers of clinical outcome. *Circulation* 2006;113:405-13.

Balaban RS, Peters DC. Basic principles of Cardiovascular Magnetic Resonance. In: Manning WJ, Pennell D, editors. *Cardiovascular Magnetic Resonance*, 2nd edition. Philadelphia, PA. Saunders Elsevier; 2010:3-18.

Bardy GH, Lee KL, Mark DB, Poole JE, Packer DL, Boineau R, Domanski M, Troutman C, Anderson J, Johnson G, McNulty SE, Clapp-Channing N, Davidson-Ray LD, Fraulo ES, Fishbein DP, Luceri RM, Ip JH; Sudden Cardiac Death in Heart Failure Trial (SCD-HeFT) Investigators. Amiodarone or an implantable cardioverter-defibrillator for congestive heart failure. *N Engl J Med* 2005;352:225-37.

Basso C, Corrado D, Marcus FI, Nava A, Thiene G. Arrhythmogenic right ventricular cardiomyopathy. *Lancet* 2009;373:1289-300.

Baumgartner H, Bonhoeffer P, De Groot NM, de Haan F, Deanfield JE, Galie N, Gatzoulis MA, Gohlke-Baerwolf C, Kaemmerer H, Kilner P, Meijboom F, Mulder BJ, Oechslin E, Oliver JM,

Serraf A, Szatmari A, Thaulow E, Vouhe PR, Walma E. ESC Guidelines for the management of grown-up congenital heart disease (new version 2010). *Eur Heart J* 2010;31:2915-57.

Bax JJ, Marwick TH, Molhoek SG, Bleeker GB, van Erven L, Boersma E, Steendijk P, van der Wall EE, Schalij MJ. Left ventricular dyssynchrony predicts benefit of cardiac resynchronization therapy in patients with end-stage heart failure before pacemaker implantation. *Am J Cardiol* 2003;92:1238-40.

Bax JJ, Bleeker GB, Marwick TH, Molhoek SG, Boersma E, Steendijk P, Van der Wall EE, Schalij MJ. Left ventricular dyssynchrony predicts response and prognosis after cardiac resynchronization therapy. *J Am Coll Cardiol* 2004;44:1834-40.

Beek AM, Kühl HP, Bondarenko O, Twisk JW, Hofman MB, van Dockum WG, Visser CA, van Rossum AC. Delayed contrast-enhanced magnetic resonance imaging for the prediction of regional functional improvement after acute myocardial infarction. *J Am Coll Cardiol* 2003;42:895-901.

Beighton P, de Paepe A, Danks D, Finidori G, Gedde-Dahl T, Goodman R, Hall JG, Hollister DW, Horton W, McKusick VA, Opitz JM, Pope FM, Pyeritz RE, Rimoin DL, Sillence D, Spranger JW, Thompson E, Tsipouras P, Viljoen D, Winship I, Young I. International Nosology of Heritable Disorders of Connective Tissue, Berlin, 1986. *Am J Med Genet* 1988;29:581-94.

Bellenger NG, Davies LC, Francis JM, Coats AJ, Pennell DJ. Reduction in sample size for studies of remodeling in heart failure by the use of cardiovascular magnetic resonance. *J Cardiovasc Magn Reson* 2000;2:271-8.

Bellenger NG, Pennell DJ. Ventricular function. In: Manning WJ, Pennell D, editors. New York, NY. Churchill Livingstone; 2002:99-111.

Bentall H, De Bono A. A technique for complete replacement of the ascending aorta. *Thorax* 1968;23:338-9.

Berdoukas V, Modell B. Transfusion-dependent thalassaemia: a new era. *Med J Aust* 2008;188:68-9.

Beshai JF, Grimm RA, Nagueh SF, Baker JH 2nd, Beau SL, Greenberg SM, Pires LA, Tchou PJ; RethinQ Study Investigators. Cardiac-resynchronization therapy in heart failure with narrow QRS complexes. *N Engl J Med* 2007;357:2461-71.

Bilchick KC, Dimaano V, Wu KC, Helm RH, Weiss RG, Lima JA, Berger RD, Tomaselli GF, Bluemke DA, Halperin HR, Abraham T, Kass DA, Lardo AC. Cardiac magnetic resonance assessment of dyssynchrony and myocardial scar predicts function class improvement following cardiac resynchronization therapy. *JACC Cardiovasc Imaging* 2008;1:561-8.

Bland JM, Altman DG. Statistical methods for assessing agreement between two methods of clinical measurement. *Lancet* 1986;1:307-10.

Bleeker GB, Steendijk P, Holman ER, Yu CM, Breithardt OA, Kaandorp TA, Schalij MJ, van der Wall EE, Nihoyannopoulos P, Bax JJ. Assessing right ventricular function: the role of echocardiography and complementary technologies. *Heart* 2006a;92:i19-i26.

Bleeker GB, Bax JJ, Fung JW, van der Wall EE, Zhang Q, Schalij MJ, Chan JY, Yu CM. Clinical versus echocardiographic parameters to assess response to cardiac resynchronization therapy. *Am J Cardiol* 2006b;97:260-3.

Bleeker GB, Kaandorp TA, Lamb HJ, Boersma E, Steendijk P, de Roos A, van der Wall EE, Schalij MJ, Bax JJ. Effect of posterolateral scar tissue on clinical and echocardiographic improvement after cardiac resynchronization therapy. *Circulation* 2006c;113:969-76.

Bleumink GS, Knetsch AM, Sturkenboom MC, Straus SM, Hofman A, Deckers JW, Witteman JC, Stricker BH. Quantifying the heart failure epidemic: prevalence, incidence rate, lifetime risk and prognosis of heart failure. The Rotterdam Study. *Eur Heart J* 2004;25:1614-9.

Bijnens BH, Cikes M, Claus P, Sutherland GR. Velocity and deformation imaging for the assessment of myocardial dysfunction. *Eur J Echocardiogr* 2009;10:216-26.

Bogaard HJ, Abe K, Vonk Noordegraaf A, Voelkel NF. The right ventricle under pressure: cellular and molecular mechanisms of right-heart failure in pulmonary hypertension. *Chest* 2009;135:794-804.

Bogaert J, Meyns B, Rademakers FE, Bosmans H, Verschakelen J, Flameng W, Marchal G, Baert AL. Follow-up of aortic dissection: contribution of MR angiography for evaluation of the abdominal aorta and its branches. *Eur Radiol* 1997;7:695-702.

Bogren HG, Klipstein RH, Mohiaddin RH, Firmin DN, Underwood SR, Rees RS, Longmore DB. Pulmonary artery distensibility and blood flow patterns: a magnetic resonance study of

normal subjects and of patients with pulmonary arterial hypertension. *Am Heart J* 1989;118:990-9.

Bolger AP, Sharma R, Li W, Leenarts M, Kalra PR, Kemp M, Coats AJ, Anker SD, Gatzoulis MA. Neurohormonal activation and the chronic heart failure syndrome in adults with congenital heart disease. *Circulation* 2002;106:92-99.

Bonow RO, Carabello BA, Chatterjee K, de Leon AC Jr, Faxon DP, Freed MD, Gaasch WH, Lytle BW, Nishimura RA, O'Gara PT, O'Rourke RA, Otto CM, Shah PM, Shanewise JS. 2008 Focused update incorporated into the ACC/AHA 2006 guidelines for the management of patients with valvular heart disease. *Circulation* 2008;118:e523-661.

Borgna-Pignatti C, Rugolotto S, De Stefano P, Piga A, Di Gregorio F, Gamberini MR, Sabato V, Melevendi C, Cappellini MD, Verlato G. Survival and disease complications in thalassemia major. *Ann N Y Acad Sci* 1998;850:227-31.

Borgna-Pignatti C, Rugolotto S, De Stefano P, Zhao H, Cappellini MD, Del Vecchio GC, Romeo MA, Forni GL, Gamberini MR, Ghilardi R, Piga A, Cnaan A. Survival and complications in patients with thalassemia major treated with transfusion and deferoxamine. *Haematologica* 2004;89:1187-93.

Borgna-Pignatti C, Cappellini MD, De Stefano P, Del Vecchio GC, Forni GL, Gamberini MR, Ghilardi R, Piga A, Romeo MA, Zhao H, Cnaan A. Cardiac morbidity and mortality in deferoxamine- or deferiprone-treated patients with thalassemia major. *Blood* 2006;107:3733-7.

Botnar RM, Stuber M, Danias PGP, Kissinger KV, Manning WJ. Improved coronary artery definition with T2-weighted, free-breathing, threedimensional coronary MRA. *Circulation* 1999;99:3139-48.

Bowers TR, O'Neill WW, Pica M, Goldstein JA. Patterns of coronary compromise resulting in acute right ventricular ischemic dysfunction. *Circulation* 2002;106:1104-9.

Bourantas CV, Loh HP, Bragadeesh T, Rigby AS, Lukaschuk EI, Garg S, Tweddel AC, Alamgir FM, Nikitin NP, Clark AL, Cleland JG. Relationship between right ventricular volumes measured by cardiac magnetic resonance imaging and prognosis in patients with chronic heart failure. *Eur J Heart Fail* 2011;13:52-60.

Bowers TR, O'Neill WW, Grines C, Pica MC, Safian RD, Goldstein JA. Effect of reperfusion on biventricular function and survival after right ventricular infarction. *N Engl J Med* 1998;338:933-40.

Boyle GE, Cooke J, Sheehy NP, Meaney JF. An interactive taxonomy of MR imaging sequences. *Radiographics* 2006;26:e24.

Bradlow WM, Hughes ML, Keenan NG, Bucciarelli-Ducci C, Assomull R, Gibbs JS, Mohiaddin RH. Measuring the heart in pulmonary arterial hypertension (PAH): implications for trial study size. *J Magn Reson Imaging* 2010;31:117-24.

Bradlow WM, Gibbs JS, Mohiaddin RH. Cardiovascular magnetic resonance in pulmonary hypertension. *J Cardiovasc Magn Reson* 2012;14:6.

Braunschweig F, Cowie MR, Auricchio A. What are the costs of heart failure? *Europace* 2011;13(S2):ii13-7.

Bristow MR, Saxon LA, Boehmer J, Krueger S, Kass DA, De Marco T, Carson P, DiCarlo L, DeMets D, White BG, DeVries DW, Feldman AM; Comparison of Medical Therapy, Pacing, and Defibrillation in Heart Failure (COMPANION) Investigators. Cardiac-resynchronization therapy with or without an implantable defibrillator in advanced chronic heart failure. *N Engl J Med* 2004;350:2140-50.

Brittenham GM, Griffith PM, Nienhuis AW, McLaren CE, Young NS, Tucker EE, Allen CJ, Farrell DE, Harris JW. Efficacy of deferoxamine in preventing complications of iron overload in patients with thalassemia major. *N Engl J Med* 1994;331:567-73.

Britton RS, Leicester KL, Bacon BR. Iron toxicity and chelation therapy. *Int J Hematol* 2002;76:219-28.

Brooke BS, Habashi JP, Judge DP, Patel N, Loeys B, Dietz HC. Angiotensin II blockade and aortic-root dilation in Marfan's syndrome. *N Engl J Med* 2008;358:2787-95.

Brookes C, Ravn H, White P, Moeldrup U, Oldershaw P, Redington A. Acute right ventricular dilatation in response to ischemia significantly impairs left ventricular systolic performance. *Circulation* 1999;100:761-7.

Bruzzi JF, Rémy-Jardin M, Delhay D, Teisseire A, Khalil C, Rémy J. When, why, and how to examine the heart during thoracic CT. Part 1. Basic principles. *AJR Am J Roentgenol* 2006a; 186:324-32.

Bruzzi JF, Rémy-Jardin M, Delhay D, Teisseire A, Khalil C, Rémy J. When, why, and how to examine the heart during thoracic CT. Part 2. Clinical applications. *AJR Am J Roentgenol* 2006b;186:333-41.

Buechel ER, Dave HH, Kellenberger CJ, Dodge-Khatami A, Pretre R, Berger F, Bauersfeld U. Remodelling of the right ventricle after early pulmonary valve replacement in children with repaired tetralogy of Fallot: assessment by cardiovascular magnetic resonance. *Eur Heart J* 2005;26:2721-27.

Bueno H, Lopez-Palop R, Bermejo J, Lopez-Sendon JL, Delcan JL. In-hospital outcome of elderly patients with acute inferior myocardial infarction and right ventricular involvement. *Circulation* 1997;96:436-41.

Burke A, Jeudy J Jr, Virmani R. Cardiac tumours: an update: Cardiac tumours. *Heart* 2008;94:117-23.

Burman ED, Keegan J, Kilner PJ. Aortic root measurement by cardiovascular magnetic resonance: specification of planes and lines of measurement and corresponding normal values. *Circ Cardiovasc Imaging* 2008;1:104-13.

Burri H, Domenichini G, Sunthorn H, Fleury E, Stettler C, Foulkes I, Shah D. Right ventricular systolic function and cardiac resynchronization therapy. *Europace* 2010;12:389-94.

Butany J, Nair V, Naseemuddin A, Nair GM, Catton C, Yau T. Cardiac tumours: diagnosis and management. *Lancet Oncol* 2005;6:219-28.

C

Callender ST, Weatherall DJ. Iron chelation with oral desferrioxamine. *Lancet* 1980;2:689.

Cañadas V, Vilacosta I, Bruna I, Fuster V. Marfan syndrome. Part 1: pathophysiology and diagnosis. *Nat Rev Cardiol* 2010a;7:256-65.

Cañadas V, Vilacosta I, Bruna I, Fuster V. Marfan syndrome. Part 2: treatment and management of patients. *Nat Rev Cardiol* 2010b;7:266-76.

Carabello BA. Evolution of the study of left ventricular function: everything old is new again. *Circulation* 2002;105:2701-3.

Carpenter JP, He T, Kirk P, Anderson LJ, Porter JB, Wood J, Galanella R, Forni G, Catani G, Fucharoen S, Fleming A, House M, Black G, Firmin DN, St Pierre TG, Pennell DJ. Calibration of myocardial iron concentration against T2-star cardiovascular magnetic resonance (abstract). *J Cardiovasc Magn Reson* 2009;11(S1):P224.

Carpenter JP, Alpendurada F, Deac M, Maceira A, Garbowski M, Kirk P, Walker JM, Porter JB, Shah F, Banya W, He T, Smith GC, Pennell DJ. Right ventricular volumes and function in thalassemia major patients in the absence of myocardial iron overload. *J Cardiovasc Magn Reson* 2010;12:24.

Carpenter JP, He T, Kirk P, Roughton M, Anderson LJ, de Noronha SV, Sheppard MN, Porter JB, Walker JM, Wood JC, Galanella R, Forni G, Catani G, Matta G, Fucharoen S, Fleming A, House MJ, Black G, Firmin DN, St Pierre TG, Pennell DJ. On T2* magnetic resonance and cardiac iron. *Circulation* 2011;123:1519-28.

Caruthers SD, Lin SJ, Brown P, Watkins MP, Williams TA, Lehr KA, Wickline SA. Practical value of cardiac magnetic resonance imaging for clinical quantification of aortic valve stenosis: comparison with echocardiography. *Circulation* 2003;108:2236-43.

Casolo G, Minneci S, Manta R, Sulla A, Del Meglio J, Rega L, Gensini G. Identification of the ischemic etiology of heart failure by cardiovascular magnetic resonance imaging: Diagnostic accuracy of late gadolinium enhancement. *Am Heart J* 2006;151:101-8.

Caudron J, Fares J, Vivier PH, Lefebvre V, Petitjean C, Dacher JN. Diagnostic accuracy and variability of three semi-quantitative methods for assessing right ventricular systolic function from cardiac MRI in patients with acquired heart disease. *Eur Radiol* 2011;21:2111-20.

Caudron J, Fares J, Lefebvre V, Vivier PH, Petitjean C, Dacher JN. Cardiac MRI assessment of right ventricular function in acquired heart disease: factors of variability. *Acad Radiol* 2012;19:991-1002.

Cawley PJ, Maki JH, Otto CM. Cardiovascular magnetic resonance imaging for valvular heart disease: technique and validation. *Circulation* 2009;119:468-78.

Cazeau S, Ritter P, Bakdach S, Lazarus A, Limousin M, Henao L, Mundler O, Daubert JC, Mugica J. Four chamber pacing in dilated cardiomyopathy. *Pacing Clin Electrophysiol* 1994;17:1974-9.

Cazeau S, Leclercq C, Lavergne T, Walker S, Varma C, Linde C, Garrigue S, Kappenberger L, Haywood GA, Santini M, Bailleul C, Daubert JC. Effects of multisite biventricular pacing in patients with heart failure and intraventricular conduction delay. *N Engl J Med* 2001;344:873-80.

Chai P, Mohiaddin R. How we perform cardiovascular magnetic resonance flow assessment using phase-contrast velocity mapping. *J Cardiovasc Magn Reson* 2005;7:705-16.

Chalil S, Foley PW, Muhyaldeen SA, Patel KC, Yousef ZR, Smith RE, Frenneaux MP, Leyva F. Late gadolinium enhancement-cardiovascular magnetic resonance as a predictor of response to cardiac resynchronization therapy in patients with ischaemic cardiomyopathy. *Europace* 2007a;9:1031-7.

Chalil S, Stegemann B, Muhyaldeen S, Khadjooi K, Smith R, Jordan P, Leyva F. Intraventricular Dyssynchrony Predicts Mortality and Morbidity Following Cardiac Resynchronization Therapy: A Study Using Cardiovascular Magnetic Resonance Tissue Synchronization Imaging. *J Am Coll Cardiol* 2007b;50:243-52.

Chalil S, Stegemann B, Muhyaldeen SA, Khadjooi K, Foley PW, Smith RE, Leyva F. Effect of posterolateral left ventricular scar on mortality and morbidity following cardiac resynchronization therapy. *Pacing Clin Electrophysiol* 2007c;30:1201-9.

Champion HC, Michelakis ED, Hassoun PM. Comprehensive invasive and noninvasive approach to the right ventricle-pulmonary circulation unit: state of the art and clinical and research implications. *Circulation* 2009;120:992-1007.

Chan KM, Wage R, Symmonds K, Rahman-Haley S, Mohiaddin RH, Firmin DN, Pepper JR, Pennell DJ, Kilner PJ. Towards comprehensive assessment of mitral regurgitation using cardiovascular magnetic resonance. *J Cardiovasc Magn Reson* 2008;10:61.

Chan YC, Ting CW, Ho P, Poon JT, Cheung GC, Cheng SW. Ten-year epidemiological review of in-hospital patients with Marfan syndrome. *Ann Vasc Surg* 2008;22:608-12.

Channick RN, Simonneau G, Sitbon O, Robbins IM, Frost A, Tapson VF, Badesch DB, Roux S, Rainisio M, Bodin F, Rubin LJ. Effects of the dual endothelin-receptor antagonist bosentan in

patients with pulmonary hypertension: a randomised placebo-controlled study. *Lancet* 2001;358:1119-23.

Chatrath R, Beauchesne LM, Connolly HM, Michels VV, Driscoll DJ. Left Ventricular Function in the Marfan Syndrome Without Significant Valvular Regurgitation. *Am J Cardiol* 2003;91:914-6.

Chavhan GB, Babyn PS, Thomas B, Shroff MM, Haacke EM. Principles, techniques, and applications of T2*-based MR imaging and its special applications. *Radiographics* 2009;29:1433-49.

Chin KM, Kim NH, Rubin LJ. The right ventricle in pulmonary hypertension. *Coron Artery Dis* 2005;16:13-8.

Chiribiri A, Kelle S, Götze S, Kriatselis C, Thouet T, Tangcharoen T, Paetsch I, Schnackenburg B, Fleck E, Nagel E. Visualization of the cardiac venous system using cardiac magnetic resonance. *Am J Cardiol* 2008;101:407-12.

Chiribiri A, Ishida M, Nagel E, Botnar RM. Coronary imaging with cardiovascular magnetic resonance: current state of the art. *Prog Cardiovasc Dis* 2011;54:240-52.

Chockalingam A, Gnanavelu G, Subramaniam T, Dorairajan S, Chockalingam V. Right ventricular myocardial infarction: presentation and acute outcomes. *Angiology* 2005;56:371-6.

Choe YH, Kim DK, Koh EM, Do YS, Lee WR. Takayasu arteritis: diagnosis with MR imaging and MR angiography in acute and chronic active stages. *J Magn Reson Imaging* 1999;10:751-7.

Christiansen JP, Karamitsos TD, Myerson SG. Assessment of valvular heart disease by cardiovascular magnetic resonance imaging: a review. *Heart Lung Circ* 2011;20:73-82.

Chung ES, Leon AR, Tavazzi L, Sun JP, Nihoyannopoulos P, Merlino J, Abraham WT, Ghio S, Leclercq C, Bax JJ, Yu CM, Gorcsan J 3rd, St John Sutton M, De Sutter J, Murillo J. Results of the Predictors of Response to CRT (PROSPECT) trial. *Circulation* 2008;117:2608-16.

Cigarroa JE, Isselbacher EM, DeSanctis RW, Eagle KA. Diagnostic imaging in the evaluation of suspected aortic dissection. Old standards and new directions. *N Engl J Med* 1993;328:35-43.

Cleland JG, Daubert JC, Erdmann E, Freemantle N, Gras D, Kappenberger L, Tavazzi L; Cardiac Resynchronization-Heart Failure (CARE-HF) Study Investigators. The effect of cardiac resynchronization on morbidity and mortality in heart failure. *N Engl J Med* 2005;352:1539-49.

Cleland JG, Tageldien A, Buga L, Wong K, Gorcsan J 3rd. Should we be trying to define responders to cardiac resynchronization therapy? *JACC Cardiovasc Imaging* 2010;3:541-9.

Coche E, Vlassenbroek A, Roelants V, D'Hoore W, Verschuren F, Goncette L, Maldague B. Evaluation of biventricular ejection fraction with ECG-gated 16-slice CT: preliminary findings in acute pulmonary embolism in comparison with radionuclide ventriculography. *Eur Radiol* 2005;15:1432-40.

Colletti PM. Evaluation of intracardiac shunts with cardiac magnetic resonance. *Curr Cardiol Rep* 2005;7:52-8.

Collins W, Taylor WH. Determination of iron in cardiac and liver tissues by plasma emission spectroscopy. *Ann Clin Biochem* 1987;24:482-7.

Contractor S, Maldjian PD, Sharma VK, Gor DM. Role of helical CT in detecting right ventricular dysfunction secondary to acute pulmonary embolism. *J Comput Assist Tomogr* 2002;26:587-91.

Corbett JR, Akinboboye OO, Bacharach SL, Borer JS, Botvinick EH, DePuey EG, Ficaro EP, Hansen CL, Henzlova MJ, Van Kriekinge S. Equilibrium radionuclide angiocardiology. *J Nucl Cardiol* 2006;13:e56-79.

Constable RT, Anderson AW, Zhong J, Gore JC. Factors influencing contrast in fast spin-echo MR imaging. *Magn Reson Imaging* 1992;10:497-511.

Cowburn PJ, Cleland JG, Coats AJ, Komajda M. Risk stratification in chronic heart failure. *Eur Heart J* 1998;19:696-710.

Cowie MR, Mosterd A, Wood DA, Deckers JW, Poole-Wilson PA, Sutton GC, Grobbee DE. The epidemiology of heart failure. *Eur Heart J* 1997;18:208-25.

D

D'Alonzo GE, Barst RJ, Ayres SM, Bergofsky EH, Brundage BH, Detre KM, Fishman AP, Goldring RM, Groves BM, Kernis JT, Levy PS, Pietra GG, Reid LM, Reeves JT, Rich S, Vreim CE, Williams GW, Wu M. Survival in patients with primary pulmonary hypertension. Results from a national prospective registry. *Ann Intern Med* 1991;115:343-9.

D'Hooge J, Heimdal A, Jamal F, Kukulski T, Bijnens B, Rademakers F, Hatle L, Suetens P, Sutherland GR. Regional strain and strain rate measurements by cardiac ultrasound: principles, implementation and limitations. *Eur J Echocardiogr* 2000;1:154-70.

Damiano RJ Jr, La Follette P Jr, Cox JL, Lowe JE, Santamore WP. Significant left ventricular contribution to right ventricular systolic function. *Am J Physiol* 1991;261:H1514-24.

Daou D, Van Kriekinge SD, Coaguila C, Lebtahi R, Fourme T, Sitbon O, Parent F, Slama M, Le Guludec D, Simonneau G. Automatic quantification of right ventricular function with gated blood pool SPECT. *J Nucl Cardiol* 2004;11:293-304.

Daou D, Coaguila C, Vilain D. Electrocardiograph-gated single photon emission computed tomography radionuclide angiography presents good interstudy reproducibility for the quantification of global systolic right ventricular function. *Nucl Med Commun* 2007;28:391-9.

Das BB, Taylor AL, Yetman AT. Left Ventricular Diastolic Dysfunction in Children and Young Adults with Marfan Syndrome. *Pediatr Cardiol* 2006;27:256-8.

Daubert C, Gold MR, Abraham WT, Ghio S, Hassager C, Goode G, Szili-Török T, Linde C; REVERSE Study Group. Prevention of disease progression by cardiac resynchronization therapy in patients with asymptomatic or mildly symptomatic left ventricular dysfunction. *J Am Coll Cardiol* 2009;54:1837-46.

Daubert C, Cazeau S, Ritter P, Leclercq C. Past, present and future of cardiac resynchronization. *Arch Cardiovasc Dis* 2012;105:291-9.

David TE, Feindel M. An aortic valve-sparing operation for patients with aortic incompetence and aneurysm of the ascending aorta. *J Thorac Cardiovasc Surg* 1992;103:617-22.

Davis BA, O'Sullivan C, Jarritt PH, Porter JB. Value of sequential monitoring of left ventricular ejection fraction in the management of thalassemia major. *Blood* 2004;104:263-69.

Davlouros PA, Niwa K, Webb G, Gatzoulis MA. The right ventricle in congenital heart disease. *Heart* 2006;92:i27-38.

Dawson D, Mohiaddin R. Assessment of pericardial diseases and cardiac masses with cardiovascular magnetic resonance. *Prog Cardiovasc Dis* 2011;54:305-19.

De Backer JF, Devos D, Segers P, Matthys D, François K, Gillebert TC, De Paepe AM, De Sutter J. Primary impairment of left ventricular function in Marfan syndrome. *Int J Cardiol* 2006;112:353-8.

de Groote P, Millaire A, Foucher-Hossein C, Nague O, Marchandise X, Ducloux G, Lablanche JM. Right ventricular ejection fraction is an independent predictor of survival in patients with moderate heart failure. *J Am Coll Cardiol* 1998;32:948-54.

De Paepe A, Devereux RB, Dietz HC, Hennekam RC, Pyeritz RE. Revised diagnostic criteria for the Marfan syndrome. *Am J Med Genet* 1996;62:417-26.

de Witte P, Aalberts JJ, Radonic T, Timmermans J, Scholte AJ, Zwinderman AH, Mulder BJ, Groenink M, van den Berg MP. Intrinsic biventricular dysfunction in Marfan syndrome. *Heart* 2011;97:2063-8.

Debl K, Djavidani B, Buchner S, Heinicke N, Fredersdorf S, Haimerl J, Poschenrieder F, Feuerbach S, Riegger GA, Luchner A. Assessment of the anatomic regurgitant orifice in aortic regurgitation: a clinical magnetic resonance imaging study. *Heart* 2008;94:e8.

DeFrances CJ, Lucas CA, Buie VC, Golosinskiy A. 2006 National Hospital Discharge Survey. *Natl Health Stat Report*. 2008;5:1-20.

Dell'Italia LJ, Walsh RA. Acute determinants of the hangout interval in the pulmonary circulation. *Am Heart J* 1988a;116:1289-97.

Dell'Italia LJ, Walsh RA. Application of a time varying elastance model to right ventricular performance in man. *Cardiovasc Res* 1988b;22:864-74.

Dell'Italia LJ. Mechanism of postextrasystolic potentiation in the right ventricle. *Am J Cardiol* 1990;65:736-41.

Dell'Italia LJ. The right ventricle: anatomy, physiology, and clinical importance. *Curr Probl Cardiol* 1991;16:653-720.

DePuey EG, Jones ME, Garcia EV. Evaluation of right ventricular regional perfusion with technetium-99m-sestamibi SPECT. *J Nucl Med* 1991;32:1199-205.

Derchi G, Fonti A, Forni GL, Galliera EO, Cappellini MD, Turati F, Policlinico OM. Pulmonary hypertension in patients with thalassemia major. *Am Heart J* 1999;138:384.

Détaint D, Faivre L, Collod-Beroud G, Child AH, Loeys BL, Binquet C, Gautier E, Arbustini E, Mayer K, Arslan-Kirchner M, Stheneur C, Halliday D, Beroud C, Bonithon-Kopp C, Claustres M, Plauchu H, Robinson PN, Kiotsekoglou A, De Backer J, Adès L, Francke U, De Paepe A, Boileau C, Jondeau G. Cardiovascular manifestations in men and women carrying a FBN1 mutation. *Eur Heart J* 2010a;31:2223-9.

Détaint D, Aegerter P, Tubach F, Hoffman I, Plauchu H, Dulac Y, Faivre LO, Delrue MA, Collignon P, Odent S, Tchitchinadze M, Bouffard C, Arnoult F, Gautier M, Boileau C, Jondeau G. Rationale and design of a randomized clinical trial (Marfan Sartan) of angiotensin II receptor blocker therapy versus placebo in individuals with Marfan syndrome. *Arch Cardiovasc Dis* 2010b;103:317-25.

Di Salvo TG, Mathier M, Semigran MJ, Dec GW. Preserved right ventricular ejection fraction predicts exercise capacity and survival in advanced heart failure. *J Am Coll Cardiol* 1995;25:1143-53.

Dias CA, Assad RS, Caneo LF, Abduch MC, Aiello VD, Dias AR, Marcial MB, Oliveira SA. Reversible pulmonary trunk banding. II. An experimental model for rapid pulmonary ventricular hypertrophy. *J Thorac Cardiovasc Surg* 2002;124:999-1006.

Dickstein K, Cohen-Solal A, Filippatos G, McMurray JJ, Ponikowski P, Poole-Wilson PA, Strömberg A, van Veldhuisen DJ, Atar D, Hoes AW, Keren A, Mebazaa A, Nieminen M, Priori SG, Swedberg K. ESC guidelines for the diagnosis and treatment of acute and chronic heart failure 2008. *Eur Heart J* 2008;29:2388-442.

Dickstein K, Bogale N, Priori S, Auricchio A, Cleland JG, Gitt A, Limbourg T, Linde C, van Veldhuisen DJ, Brugada J. The European cardiac resynchronization therapy survey. *Eur Heart J* 2009;30:2450-60.

Dickstein K, Vardas PE, Auricchio A, Daubert JC, Linde C, McMurray J, Ponikowski P, Priori SG, Sutton R, van Veldhuisen DJ. 2010 Focused Update of ESC Guidelines on device therapy in heart failure. *Europace* 2010;12:1526-36.

Dietz HC, Cutting GR, Pyeritz RE, Maslen CL, Sakai LY, Corson GM, Puffenberger EG, Hamosh A, Nanthakumar EJ, Curristin SM, Stetten G, Meyers DA, Francomano C. Marfan syndrome caused by a recurrent de novo missense mutation in the fibrillin gene. *Nature* 1991;352:337-9.

Dietz HC, Pyeritz RE. Mutations in human gene for fibrillin-1 in the Marfan syndrome and related disorders. *Hum Mol Genet* 1995;4:1799-809.

Djavidani B, Debl K, Lenhart M, Seitz J, Paetzel C, Schmid FX, Nitz WR, Feuerbach S, Riegger G, Luchner A. Planimetry of mitral valve stenosis by magnetic resonance imaging. *J Am Coll Cardiol* 2005;45:2048-53.

Doğan H, Kroft LJ, Bax JJ, Schuijf JD, van der Geest RJ, Doornbos J, de Roos A. MDCT assessment of right ventricular systolic function. *AJR Am J Roentgenol* 2006;186(S2):S366-70.

Dolgin M. Nomenclature and Criteria for Diagnosis of Diseases of the Heart and Great Vessels, 9th edition. Boston, MA. Little Brown & Co 1994.

Du ZD, Roguin N, Milgram E, Saab K, Koren A. Pulmonary hypertension in patients with thalassemia major. *Am Heart J* 1997;134:532-7.

Dubin AM, Janousek J, Rhee E, Strieper MJ, Cecchin F, Law IH, Shannon KM, Temple J, Rosenthal E, Zimmerman FJ, Davis A, Karpawich PP, Al Ahmad A, Vetter VL, Kertesz NJ, Shah M, Snyder C, Stephenson E, Emmel M, Sanatani S, Kanter R, Batra A, Collins KK. Resynchronization therapy in pediatric and congenital heart disease patients: an international multicenter study. *J Am Coll Cardiol* 2005;46:2277-83.

Dupont MV, Drăgean CA, Coche EE. Right ventricle function assessment by MDCT. *AJR Am J Roentgenol* 2011;196:77-86.

Dymarkowski S, Bosmans H. Cardiac MRI physics. In: Bogaert J, Dymarkowski S, Taylor AM, editors. *Clinical Cardiac MRI*. Heidelberg, Germany. Springer; 2005:1-31.

E

Edelman RR, Mattle HP, Atkinson DJ, Hoogewoud HM. MR angiography. *AJR Am J Roentgenol* 1990;154:937-46.

El-Hamamsy I, Yacoub MH. Cellular and molecular mechanisms of thoracic aortic aneurysms. *Nat Rev Cardiol* 2009;6:771-86.

Elliott P, Andersson B, Arbustini E, Bilinska Z, Cecchi F, Charron P, Dubourg O, Kühl U, Maisch B, McKenna WJ, Monserrat L, Pankuweit S, Rapezzi C, Seferovic P, Tavazzi L, Keren A. Classification of the cardiomyopathies: a position statement from the European Society Of Cardiology Working Group on Myocardial and Pericardial Diseases. *Eur Heart J* 2008;29:270-6.

Engle MA, Erlandson M, Smith CH. Late cardiac complications of chronic, severe, refractory anemia with hemochromatosis. *Circulation* 1964;30:698-705.

Engle MA. Cardiac involvement in Cooley's anemia. *Ann N Y Acad Sci.* 1969;119:694-702.

Epstein AE, Dimarco JP, Ellenbogen KA, Estes NA 3rd, Freedman RA, Gettes LS, Gillinov AM, Gregoratos G, Hammill SC, Hayes DL, Hlatky MA, Newby LK, Page RL, Schoenfeld MH, Silka MJ, Stevenson LW, Sweeney MO. ACC/AHA/HRS 2008 guidelines for Device-Based Therapy of Cardiac Rhythm Abnormalities: executive summary. *Heart Rhythm* 2008;5:934-55.

F

Faber TL, Chen J, Garcia EV. Single-Photon Emission Computed Tomography Processing, Quantification and Display. In: Zaret BL, Beller GA, editors. *Clinical Nuclear Cardiology: State of the Art and Future Direction*, 4th edition. Philadelphia, PA. Elsevier; 2010:53-71.

Faivre L, Collod-Beroud G, Loeys BL, Child A, Binquet C, Gautier E, Callewaert B, Arbustini E, Mayer K, Arslan-Kirchner M, Kiotsekoglou A, Comeglio P, Marziliano N, Dietz HC, Halliday D, Beroud C, Bonithon-Kopp C, Claustres M, Muti C, Plauchu H, Robinson PN, Adès LC, Biggin A, Benetts B, Brett M, Holman KJ, De Backer J, Coucke P, Francke U, De Paepe A, Jondeau G, Boileau C. Effect of mutation type and location on clinical outcome in 1,013 probands with Marfan syndrome or related phenotypes and FBN1 mutations: an international study. *Am J Hum Genet* 2007;81:454-66.

Fan TH, Liang CS, Kawashima S, Banerjee SP. Alterations in cardiac beta-adrenoceptor responsiveness and adenylate cyclase system by congestive heart failure in dogs. *Eur J Pharmacol* 1987;140:123-132.

Farb A, Burke AP, Virmani R. Anatomy and pathology of the right ventricle (including acquired tricuspid and pulmonic valve disease. *Cardiol Clin* 1992;10:1-21.

Farmaki K, Tzoumari I, Pappa C, Chouliaras G, Berdoukas V. Normalisation of total body iron load with very intensive combined chelation reverses cardiac and endocrine complications of thalassaemia major. *Br J Haematol* 2010;148:466-75.

Farrer-Brown G. Vascular pattern of myocardium of right ventricle of human heart. *Br Heart J* 1968;30:679-86.

Feldt RH, Driscoll DJ, Offord KP, Cha RH, Perrault J, Schaff HV, Puga FJ, Danielson GK. Protein-losing enteropathy after the Fontan operation. *J Thorac Cardiovasc Surg* 1996;112:672-80.

Felker GM, Thompson RE, Hare JM, Hruban RH, Clemetson DE, Howard DL, Baughman KL, Kasper EK. Underlying causes and long-term survival in patients with initially unexplained cardiomyopathy. *N Engl J Med* 2000;342:1077-84.

Feneley MP, Gavaghan TP, Baron DW, Branson JA, Roy PR, Morgan JJ. Contribution of left ventricular contraction to the generation of right ventricular systolic pressure in the human heart. *Circulation* 1985;71:473-80.

Feng D, Glockner J, Kim K, Martinez M, Syed IS, Araoz P, Breen J, Espinosa RE, Sundt T, Schaff HV, Oh JK. Cardiac magnetic resonance imaging pericardial late gadolinium enhancement and elevated inflammatory markers can predict the reversibility of constrictive pericarditis after antiinflammatory medical therapy: a pilot study. *Circulation* 2011;124:1830-7.

Field ME, Solomon SD, Lewis EF, Kramer DB, Baughman KL, Stevenson LW, Tedrow UB. Right ventricular dysfunction and adverse outcome in patients with advanced heart failure. *J Card Fail* 2006;12:616-20.

Fieno DS, Saouaf R, Thomson LE, Abidov A, Friedman JD, Berman DS. Cardiovascular magnetic resonance of primary tumors of the heart: A review. *J Cardiovasc Magn Reson* 2006;8:839-53.

Firmin DN, Nayler GL, Klipstein RH, Underwood SR, Rees RS, Longmore DB. In vivo validation of MR velocity imaging. *J Comput Assist Tomogr* 1987;11:751-6.

Firmin D. Blood flow velocity assessment. In: Manning WJ, Pennell D, editors. *Cardiovascular Magnetic Resonance*, 2nd edition. Philadelphia, PA. Saunders Elsevier; 2010:91-9.

Fischbach R, Juergens KU, Ozgun M, Maintz D, Grude M, Seifarth H, Heindel W, Wichter T. Assessment of regional left ventricular function with multidetector-row computed tomography versus magnetic resonance imaging. *Eur Radiol* 2007;17:1009-17.

Fitchett DH, Coltart DJ, Littler WA, Leyland MJ, Trueman T, Gozzard DI, Peters TJ. Cardiac involvement in secondary haemochromatosis: a catheter biopsy study and analysis of myocardium. *Cardiovasc Res* 1980;14:719-24.

Foale R, Nihoyannopoulos P, McKenna W, Kleinebenne A, Nadazdin A, Rowland E, Smith G. Echocardiographic measurement of the normal adult right ventricle. *Br Heart J* 1986;56:33-44.

Foley PW, Khadjooi K, Ward JA, Smith RE, Stegemann B, Frenneaux MP, Leyva F. Radial dyssynchrony assessed by cardiovascular magnetic resonance in relation to left ventricular function, myocardial scarring and QRS duration in patients with heart failure. *J Cardiovasc Magn Reson* 2009;11:50-6.

Foley PW, Leyva F, Frenneaux MP. What is treatment success in cardiac resynchronization therapy? *Europace* 2009b;11(S5):v58-65.

Forman MB, Wilson BH, Sheller JR, Kopelman HA, Vaughn WK, Virmani R, Friesinger GC. Right ventricular hypertrophy is an important determinant of right ventricular infarction complicating acute inferior left ventricular infarction. *J Am Coll Cardiol* 1987;10:1180-7.

Fornwalt BK, Sprague WW, BeDell P, Suever JD, Gerritse B, Merlino JD, Fyfe DA, León AR, Oshinski JN. Agreement is poor among current criteria used to define response to cardiac resynchronization therapy. *Circulation* 2010;121:1985-91.

Francis JM, Pennell DJ. Treatment of claustrophobia for cardiovascular magnetic resonance: use and effectiveness of mild sedation. *J Cardiovasc Magn Reson* 2000;2:139-41.

Fratz S, Schuhbaeck A, Buchner C, Busch R, Meierhofer C, Martinoff S, Hess J, Stern H. Comparison of accuracy of axial slices versus short-axis slices for measuring ventricular volumes by cardiac magnetic resonance in patients with corrected tetralogy of Fallot. *Am J Cardiol* 2009;103:1764-9.

Friedman JD, Berman DS, Borges-Neto S, Hayes SW, Johnson LL, Nichols KJ, Pagnanelli RA, Port SC. First-pass radionuclide angiography. *J Nucl Cardiol* 2006;13:e42-55.

Fujiseki Y, Okuno K, Tanaka M, Shimada M, Takahashi M, Kawanishi K. Myocardial involvement in the Marfan syndrome. *Jpn Heart J* 1985;26:1043-50.

Fussen S, De Boeck BW, Zellweger MJ, Bremerich J, Goetschalckx K, Zuber M, Buser PT. Cardiovascular magnetic resonance imaging for diagnosis and clinical management of suspected cardiac masses and tumours. *Eur Heart J* 2011;32:1551-60.

G

Gaasch WH, Cole JS, Quinones MA, Alexander JK. Dynamic determinants of left ventricular diastolic pressure-volume relations in man. *Circulation* 1975;51:317-323.

Galiè N, Hoesper MM, Humbert M, Torbicki A, Vachiery JL, Barbera JA, Beghetti M, Corris P, Gaine S, Gibbs JS, Gomez-Sanchez MA, Jondeau G, Klepetko W, Opitz C, Peacock A, Rubin L, Zellweger M, Simonneau G. Guidelines for the diagnosis and treatment of pulmonary hypertension. *Eur Heart J* 2009;30:2493-537.

Gambarin FI, Favalli V, Serio A, Regazzi M, Pasotti M, Klersy C, Dore R, Mannarino S, Viganò M, Odero A, Amato S, Tavazzi L, Arbustini E. Rationale and design of a trial evaluating the effects of losartan vs. nebivolol vs. the association of both on the progression of aortic root dilation in Marfan syndrome with FBN1 gene mutations. *J Cardiovasc Med (Hagerstown)* 2009;10:354-62.

Gao Y, Du X, Liang L, Cao L, Yang Q, Li K. Evaluation of right ventricular function by 64-row CT in patients with chronic obstructive pulmonary disease and cor pulmonale. *Eur J Radiol* 2012;81:345-53.

Gatehouse PD, Keegan J, Crowe LA, Masood S, Mohiaddin RH, Kreitner KF, Firmin DN. Applications of phase-contrast flow and velocity imaging in cardiovascular MRI. *Eur Radiol* 2005;15:2172-84.

Gatzoulis MA, Clark AL, Cullen S, Newman CG, Redington AN. Right ventricular diastolic function 15 to 35 years after repair of tetralogy of Fallot. Restrictive physiology predicts superior exercise performance. *Circulation* 1995;91:1775-81.

Geleijns J, Kroft LJM, Bax JJ, Lamb HJ, de Roos A. Techniques for cardiovascular computed tomography. In: Higgins CB, de Roos A, editors. *MRI and CT of the Cardiovascular System*, 2nd edition. Philadelphia, PA. Lippincott Williams & Wilkins; 2005:37-52.

Gelfand EV, Hughes S, Hauser TH, Yeon SB, Goepfert L, Kissinger KV, Rofsky NM, Manning WJ. Severity of mitral and aortic regurgitation as assessed by cardiovascular magnetic resonance: optimizing correlation with Doppler echocardiography. *J Cardiovasc Magn Reson* 2006;8:503-7.

Ghio S, Recusani F, Klersy C, Sebastiani R, Laudisa ML, Campana C, Gavazzi A, Tavazzi L. Prognostic usefulness of the tricuspid annular plane systolic excursion in patients with congestive heart failure secondary to idiopathic or ischemic dilated cardiomyopathy. *Am J Cardiol* 2000;85:837-42.

Ghio S, Gavazzi A, Campana C, Inserra C, Klersy C, Sebastiani R, Arbustini E, Recusani F, Tavazzi L. Independent and additive prognostic value of right ventricular systolic function and

pulmonary artery pressure in patients with chronic heart failure. *J Am Coll Cardiol* 2001;37:183-8.

Ghio S, Freemantle N, Scelsi L, Serio A, Magrini G, Pasotti M, Shankar A, Cleland JG, Tavazzi L. Long-term left ventricular reverse remodelling with cardiac resynchronization therapy: results from the CARE-HF trial. *Eur J Heart Fail* 2009;11:480-8.

Ghio S, Klersy C, Magrini G, D'Armini AM, Scelsi L, Raineri C, Pasotti M, Serio A, Campana C, Viganò M. Prognostic relevance of the echocardiographic assessment of right ventricular function in patients with idiopathic pulmonary arterial hypertension. *Int J Cardiol* 2010;140:272-8.

Ghugre NR, Enriquez CM, Gonzalez I, Nelson MD Jr, Coates TD, Wood JC. MRI detects myocardial iron in the human heart. *Magn Reson Med* 2006a;56:681-6.

Ghugre NR, Enriquez CM, Coates TD, Nelson MD Jr, Wood JC. Improved R2* measurements in myocardial iron overload. *J Magn Reson Imaging* 2006b;23:9-16.

Giorgi B, Mollet NR, Dymarkowski S, Rademakers FE, Bogaert J. Clinically suspected constrictive pericarditis: MR imaging assessment of ventricular septal motion and configuration in patients and healthy subjects. *Radiology* 2003;228:417-24.

Glockner JF, Hu HH, Stanley DW, Angelos L, King K. Parallel MR imaging: a user's guide. *Radiographics* 2005;25:1279-97.

Goldstein JA, Vlahakes GJ, Verrier ED, Schiller NB, Tyberg JV, Ports TA, Parmley WW, Chatterjee K. The role of right ventricular systolic dysfunction and elevated intrapericardial pressure in the genesis of low output in experimental right ventricular infarction. *Circulation* 1982;65:513-22.

Goldstein JA, Barzilai B, Rosamond TL, Eisenberg PR, Jaffe AS. Determinants of hemodynamic compromise with severe right ventricular infarction. *Circulation* 1990;82:359-68.

Goldstein JA. Pathophysiology and management of right heart ischemia. *J Am Coll Cardiol* 2002;40:841-53.

Gomez A, Bialostozky D, Zajarias A, Santos E, Palomar A, Martínez ML, Sandoval J. Right ventricular ischemia in patients with primary pulmonary hypertension. *J Am Coll Cardiol* 2001;38:1137-42.

Goor DA, Lillehei CW. In: Goor DA, Lillehei CW, editors. Congenital malformations of the heart. New York, NY. Grune and Stratton; 1975:1-37.

Gordeuk VR, Bacon BR, Brittenham GM. Iron overload: causes and consequences. *Annu Rev Nutr* 1987;7:485-508.

Gossuin Y, Muller RN, Gillis P. Relaxation induced by ferritin: a better understanding for an improved MRI iron quantification. *NMR Biomed* 2004;17:427-32.

Graham TP Jr, Bernard YD, Mellen BG, Celermajor D, Baumgartner H, Cetta F, Connolly HM, Davidson WR, Dellborg M, Foster E, Gersony WM, Gessner IH, Hurwitz RA, Kaemmerer H, Kugler JD, Murphy DJ, Noonan JA, Morris C, Perloff JK, Sanders SP, Sutherland JL. Long-term outcome in congenitally corrected transposition of the great arteries: a multi-institutional study. *J Am Coll Cardiol* 2000;36:255-61.

Grapsa J, O'Regan DP, Pavlopoulos H, Durighel G, Dawson D, Nihoyannopoulos P. Right ventricular remodelling in pulmonary arterial hypertension with three-dimensional echocardiography: comparison with cardiac magnetic resonance imaging. *Eur J Echocardiogr* 2010;11:64-73.

Greenwood JP, Maredia N, Younger JF, Brown JM, Nixon J, Everett CC, Bijsterveld P, Ridgway JP, Radjenovic A, Dickinson CJ, Ball SG, Plein S. Cardiovascular magnetic resonance and single-photon emission computed tomography for diagnosis of coronary heart disease (CE-MARC): a prospective trial. *Lancet* 2012;379:453-60.

Greil GF, Boettger T, Germann S, Klumpp B, Baltes C, Kozerke S, Bialkowski A, Urschitz MS, Miller S, Wolf I, Meinzer HP, Sieverding L. Quantitative assessment of ventricular function using three-dimensional SSFP magnetic resonance angiography. *J Magn Reson Imaging* 2007;26:288-95.

Grines CL, Bashore TM, Boudoulas H, Olson S, Shafer P, Wooley CF. Functional abnormalities in isolated left bundle branch block. The effect of interventricular asynchrony. *Circulation* 1989;79:845-53.

Grisaru D, Rachmilewitz EA, Mosseri M, Gotsman M, Lafair JS, Okon E, Goldfarb A, Hasin Y. Cardiopulmonary assessment in beta-thalassemia major. *Chest* 1990;98:1138-42.

Grothoff M, Elpert C, Hoffmann J, Zachrau J, Lehmkuhl L, de Waha S, Desch S, Eitel I, Mende M, Thiele H, Gutberlet M. Right ventricular injury in ST-elevation myocardial infarction: risk stratification by visualization of wall motion, edema, and delayed-enhancement cardiac magnetic resonance. *Circ Cardiovasc Imaging* 2012;5:60-8.

Grothues F, Smith GC, Moon JC, Bellenger NG, Collins P, Klein HU, Pennell DJ. Comparison of interstudy reproducibility of cardiovascular magnetic resonance with two-dimensional echocardiography in normal subjects and in patients with heart failure or left ventricular hypertrophy. *Am J Cardiol* 2002;90:29-34.

Grothues F, Moon JC, Bellenger NG, Smith GS, Klein HU, Pennell DJ. Interstudy reproducibility of right ventricular volumes, function, and mass with cardiovascular magnetic resonance. *Am Heart J* 2004;147:218-23.

Grün S, Schumm J, Greulich S, Wagner A, Schneider S, Bruder O, Kispert EM, Hill S, Ong P, Klingel K, Kandolf R, Sechtem U, Mahrholdt H. Long-term follow-up of biopsy-proven viral myocarditis: predictors of mortality and incomplete recovery. *J Am Coll Cardiol* 2012;59:1604-15.

Guo YK, Gao HL, Zhang XC, Wang QL, Yang ZG, Ma ES. Accuracy and reproducibility of assessing right ventricular function with 64-section multi-detector row CT: comparison with magnetic resonance imaging. *Int J Cardiol* 2010;139:254-62.

Gupta A, Frazer CK, Ferguson JM, Kumar AB, Davis SJ, Fallon MJ, Morris IT, Drury PJ, Cala LA. Acute pulmonary embolism: diagnosis with MR angiography. *Radiology* 1999;210:353-9.

Gutberlet M, Fröhlich M, Mehl S, Amthauer H, Hausmann H, Meyer R, Siniawski H, Ruf J, Plotkin M, Denecke T, Schnackenburg B, Hetzer R, Felix R. Myocardial viability assessment in patients with highly impaired left ventricular function: comparison of delayed enhancement, dobutamine stress MRI, end-diastolic wall thickness, and Tl201-SPECT with functional recovery after revascularization. *Eur Radiol* 2005;15:872-80.

H

Habashi JP, Judge DP, Holm TM, Cohn RD, Loeys BL, Cooper TK, Myers L, Klein EC, Liu G, Calvi C, Podowski M, Neptune ER, Halushka MK, Bedja D, Gabrielson K, Rifkin DB, Carta L, Ramirez F, Huso DL, Dietz HC. Losartan, an AT1 antagonist, prevents aortic aneurysm in a mouse model of Marfan syndrome. *Science* 2006;312:117-21.

Halliburton S, Arbab-Zadeh A, Dey D, Einstein AJ, Gentry R, George RT, Gerber T, Mahesh M, Weigold WG. State-of-the-art in CT hardware and scan modes for cardiovascular CT. *J Cardiovasc Comput Tomogr* 2012;6:154-63.

Haddad F, Hunt SA, Rosenthal DN, Murphy DJ. Right ventricular function in cardiovascular disease, part I: Anatomy, physiology, aging, and functional assessment of the right ventricle. *Circulation* 2008a;117:1436-48.

Haddad F, Doyle R, Murphy DJ, Hunt SA. Right ventricular function in cardiovascular disease, part II: pathophysiology, clinical importance, and management of right ventricular failure. *Circulation* 2008b;117:1717-31.

Hahalis G, Manolis AS, Apostolopoulos D, Alexopoulos D, Vagenakis AG, Zoumbos NC. Right ventricular cardiomyopathy in beta-thalassaemia major. *Eur Heart J* 2002;23:147-56.

Hamdan A, Asbach P, Wellnhofer E, Klein C, Gebker R, Kelle S, Kilian H, Huppertz A, Fleck E. A prospective study for comparison of MR and CT imaging for detection of coronary artery stenosis. *JACC Cardiovasc Imaging* 2011;4:50-61.

Hamon M, Agostini D, Le Page O, Riddell JW, Hamon M. Prognostic impact of right ventricular involvement in patients with acute myocardial infarction: meta-analysis. *Crit Care Med* 2008;36:2023-33.

Hamon M, Fau G, Née G, Ehtisham J, Morello R, Hamon M. Meta-analysis of the diagnostic performance of stress perfusion cardiovascular magnetic resonance for detection of coronary artery disease. *J Cardiovasc Magn Reson* 2010;12:29.

Haupt HM, Hutchins GM, Moore GW. Right ventricular infarction: role of the moderator band artery in determining infarct size. *Circulation* 1983;67:1268-72.

He T, Gatehouse PD, Kirk P, Tanner MA, Smith GC, Keegan J, Mohiaddin RH, Pennell DJ, Firmin DN. Black-blood T2* technique for myocardial iron measurement in thalassemia. *J Magn Reson Imaging* 2007;25:1205-9.

He T, Gatehouse PD, Smith GC, Mohiaddin RH, Pennell DJ, Firmin DN. Myocardial T2* measurements in iron-overloaded thalassemia: An in vivo study to investigate optimal methods of quantification. *Magn Reson Med* 2008;60:1082-9.

Hein M, Roehl AB, Baumert JH, Rossaint R, Steendijk P. Continuous right ventricular volumetry by fast-response thermodilution during right ventricular ischemia: head-to-head comparison with conductance catheter measurements. *Crit Care Med* 2009;37:2962-7.

Helbing WA, Bosch HG, Maliepaard C, Rebergen SA, van der Geest RJ, Hansen B, Ottenkamp J, Reiber JH, de Roos A. Comparison of echocardiographic methods with magnetic resonance imaging for assessment of right ventricular function in children. *Am J Cardiol* 1995;76:589-94.

Helm RH, Byrne M, Helm PA, Daya SK, Osman NF, Tunin R, Halperin HR, Berger RD, Kass DA, Lardo AC. Three-dimensional mapping of optimal left ventricular pacing site for cardiac resynchronization. *Circulation* 2007;115:953-61.

Hennig J, Nauerth A, Friedburg H. RARE imaging: a fast imaging method for clinical MR. *Magn Reson Med* 1986;3:823-33.

Herfkens RJ, Higgins CB, Hricak H, Lipton MJ, Crooks LE, Lanzer P, Botvinick E, Brundage B, Sheldon PE, Kaufman L. Nuclear magnetic resonance imaging of the cardiovascular system: Normal and pathologic findings. *Radiology* 1983;147:749-59.

Hershko C, Link G, Cabantchik I. Pathophysiology of iron overload. *Ann NY Acad Sci* 1998;850:191-201.

Heusch A, Koch JA, Krogmann ON, Korbmacher B, Bourgeois M. Volumetric analysis of the right and left ventricle in a porcine heart model: comparison of three-dimensional echocardiography, magnetic resonance imaging and angiocardiology. *Eur J Ultrasound* 1999;9:245-55.

Ho SY, Nihoyannopoulos P. Anatomy, echocardiography, and normal right ventricular dimensions. *Heart* 2006;92(S1):i2-i13.

Hoch DH, Rosenfeld LE. Tachycardias of right ventricular origin. *Cardiol Clin* 1992;10:151-64.

Hoeper MM, Barberà JA, Channick RN, Hassoun PM, Lang IM, Manes A, Martinez FJ, Naeije R, Olschewski H, Pepke-Zaba J, Redfield MM, Robbins IM, Souza R, Torbicki A, McGoon M. Diagnosis, assessment, and treatment of non-pulmonary arterial hypertension pulmonary hypertension. *J Am Coll Cardiol* 2009;54:S85-96.

Hoffbrand AV, Gorman A, Laulicht M, Garidi M, Economidou J, Georgipoulou P, Hussain MA, Flynn DM. Improvement in iron status and liver function in patients with transfusional iron overload with long-term subcutaneous desferrioxamine. *Lancet* 1979;1:947-9.

Hoffman D, Sisto D, Frater RW, Nikolic SD. Left-to-right ventricular interaction with a noncontracting right ventricle. *J Thorac Cardiovasc Surg* 1994;107:1496-502.

Hoffmann R, von Bardeleben S, ten Cate F, Borges AC, Kasprzak J, Firschke C, Lafitte S, Al-Saadi N, Kuntz-Hehner S, Engelhardt M, Becher H, Vanoverschelde JL. Assessment of systolic left ventricular function: a multi-centre comparison of cineventriculography, cardiac magnetic resonance imaging, unenhanced and contrast-enhanced echocardiography. *Eur Heart J* 2005;26:607-16.

Hoffmann U, Globits S, Schima W, Loewe C, Puig S, Oberhuber G, Frank H. Usefulness of Magnetic Resonance Imaging of cardiac and paracardiac masses. *Am J Cardiol* 2003;92:890-5.

Hogan MC, Petersen SE, Hudsmith LE, Francis JM, Neubauer S, Robson MD. Effects of steady state free precession parameters on cardiac mass, function, and volumes. *Int J Cardiovasc Imaging* 2007;23:583-9.

Hopkins WE, Waggoner AD. Severe pulmonary hypertension without right ventricular failure: the unique hearts of patients with Eisenmenger syndrome. *Am J Cardiol* 2002;89:34-8.

Hopkins WE. The remarkable right ventricle of patients with Eisenmenger syndrome. *Coron Artery Dis* 2005;16:19-25.

Horton KD, Meece RW, Hill JC. Assessment of the right ventricle by echocardiography: a primer for cardiac sonographers. *J Am Soc Echocardiogr* 2009;22:776-92.

Hudsmith LE, Petersen SE, Francis JM, Robson MD, Neubauer S. Normal human left and right ventricular and left atrial dimensions using steady state free precession magnetic resonance imaging. *J Cardiovasc Magn Reson* 2005;7:775-82.

Hundley WG, Li HF, Willard JE, Landau C, Lange RA, Meshack BM, Hillis LD, Peshock RM. Magnetic resonance imaging assessment of the severity of mitral regurgitation. *Circulation* 1995;92:1151-8.

Hundley WG, Bluemke DA, Finn JP, Flamm SD, Fogel MA, Friedrich MG, Ho VB, Jerosch-Herold M, Kramer CM, Manning WJ, Patel M, Pohost GM, Stillman AE, White RD, Woodard PK.

ACCF/ACR/AHA/NASCI/SCMR 2010 expert consensus document on cardiovascular magnetic resonance. *Circulation* 2010;121:2462-508.

Hunt SA, Abraham WT, Chin MH, Feldman AM, Francis GS, Ganiats TG, Jessup M, Konstam MA, Mancini DM, Michl K, Oates JA, Rahko PS, Silver MA, Stevenson LW, Yancy CW. 2009 focused update incorporated into the ACC/AHA 2005 Guidelines for the Diagnosis and Management of Heart Failure in Adults. *Circulation* 2009;119:e391-479.

I

Ibrahim T, Bülow HP, Hackl T, Hörnke M, Nekolla SG, Breuer M, Schömig A, Schwaiger M. Diagnostic value of contrast-enhanced magnetic resonance imaging and single-photon emission computed tomography for detection of myocardial necrosis early after acute myocardial infarction. *J Am Coll Cardiol* 2007;49:208-16.

Iles L, Pfluger H, Lefkovits L, Butler MJ, Kistler PM, Kaye DM, Taylor AJ. Myocardial fibrosis predicts appropriate device therapy in patients with implantable cardioverter-defibrillators for primary prevention of sudden cardiac death. *J Am Coll Cardiol* 2011;57:821-8.

Ingkanisorn WP, Kwong RY, Bohme NS, Geller NL, Rhoads KL, Dyke CK, Paterson DI, Syed MA, Aletras AH, Arai AE. Prognosis of negative adenosine stress magnetic resonance in patients presenting to an emergency department with chest pain. *J Am Coll Cardiol* 2006;47:1427-32.

J

Jahnke C, Nagel E, Gebker R, Kokocinski T, Kelle S, Manka R, Fleck E, Paetsch I. Prognostic value of cardiac magnetic resonance stress tests: adenosine stress perfusion and dobutamine stress wall motion imaging. *Circulation*. 2007a;115:1769-76.

Jahnke C, Nagel E, Gebker R, Bornstedt A, Schnackenburg B, Kozerke S, Fleck E, Paetsch I. Four-dimensional single breathhold magnetic resonance imaging using kt-BLAST enables reliable assessment of left- and right-ventricular volumes and mass. *J Magn Reson Imaging* 2007b;25:737-42.

Jain D, Zaret BL. Assessment of right ventricular function: role of nuclear imaging techniques. *Cardiol Clin* 1992;10:23-39.

Janousek J. Cardiac resynchronisation in congenital heart disease. *Heart* 2009;95:940-7.

Jauhiainen T, Järvinen VM, Hekali PE, Poutanen VP, Penttilä A, Kupari M. MR gradient echo volumetric analysis of human cardiac casts: focus on the right ventricle. *J Comput Assist Tomogr* 1998;22:899-903.

Jiang L. Right ventricle. In: Weyman AE, editor. *Principle and Practice of Echocardiography*. Philadelphia, PA. Lippincott Williams & Wilkins; 1994:901-21.

John RM, Tedrow UB, Koplan BA, Albert CM, Epstein LM, Sweeney MO, Miller AL, Michaud GF, Stevenson WG. Ventricular arrhythmias and sudden cardiac death. *Lancet* 2012;380:1520-9.

Johnson LL, McCarthy DM, Sciacca RR, Cannon PJ. Right ventricular ejection fraction during exercise in patients with coronary artery disease. *Circulation* 1979;60:1284-91.

Johnson LL, Lawson MA, Blackwell GG, Tauxe EL, Russell K, Dell'Italia LJ. Optimizing the method to calculate right ventricular ejection fraction from first-pass data acquired with a multicrystal camera. *J Nucl Cardiol* 1995;2:372-9.

Judge DP, Dietz HC. Marfan's syndrome. *Lancet* 2005;366:1965-76.

Juillière Y, Barbier G, Feldmann L, Grentzinger A, Danchin N, Cherrier F. Additional predictive value of both left and right ventricular ejection fractions on long-term survival in idiopathic dilated cardiomyopathy. *Eur Heart J* 1997;18:276-80.

Jurcut R, Giusca S, La Gerche A, Vasile S, Ginhina C, Voigt JU. The echocardiographic assessment of the right ventricle: what to do in 2010? *Eur J Echocardiogr* 2010;11:81-96.

K

Kagan A. Dynamic responses of the right ventricle following extensive damage by cauterization. *Circulation* 1952;5:816-23.

Kakouros N, Cokkinos DV. Right ventricular myocardial infarction: pathophysiology, diagnosis, and management. *Postgrad Med J* 2010;86:719-28.

Kasimir MT, Seebacher G, Jaksch P, Winkler G, Schmid K, Marta GM, Simon P, Klepetko W. Reverse cardiac remodelling in patients with primary pulmonary hypertension after isolated lung transplantation. *Eur J Cardiothorac Surg* 2004;26:776-81.

Kass DA, Maughan WL. From "Emax" to pressure-volume relations: a broader view. *Circulation* 1988;77:1203-12.

Kass D. An epidemic of dyssynchrony. *J Am Coll Cardiol* 2008;51:12-7.

Kato S, Kitagawa K, Ishida N, Ishida M, Nagata M, Ichikawa Y, Katahira K, Matsumoto Y, Seo K, Ochiai R, Kobayashi Y, Sakuma H. Assessment of coronary artery disease using magnetic resonance coronary angiography: a national multicenter trial. *J Am Coll Cardiol* 2010;56:983-91.

Katz J, Whang J, Boxt LM, Barst RJ. Estimation of right ventricular mass in normal subjects and in patients with primary pulmonary hypertension by nuclear magnetic resonance imaging. *J Am Coll Cardiol* 1993;21:1475-81.

Kaufman BD, Desai M, Reddy S, Osorio JC, Chen JM, Mosca RS, Ferrante AW, Mital S. Genomic profiling of left and right ventricular hypertrophy in congenital heart disease. *J Card Fail* 2008;14:760-7.

Kaul S, Tei C, Hopkins JM, Shah PM. Assessment of right ventricular function using two-dimensional echocardiography. *Am Heart J* 1984;107:526-31.

Kawut SM, Horn EM, Berekashvili KK, Garofano RP, Goldsmith RL, Widlitz AC, Rosenzweig EB, Kerstein D, Barst RJ. New predictors of outcome in idiopathic pulmonary arterial hypertension. *Am J Cardiol* 2005;95:199-203.

Kawut SM, Lima JA, Barr RG, Chahal H, Jain A, Tandri H, Praestgaard A, Bagiella E, Kizer JR, Johnson WC, Kronmal RA, Bluemke DA. Sex and race differences in right ventricular structure and function: the multi-ethnic study of atherosclerosis-right ventricle study. *Circulation* 2011;123:2542-51.

Keane, MG, Pyeritz RE. Medical management of Marfan syndrome. *Circulation* 2008;117:2802-13.

Kellman P, Arai AE. Imaging sequences for first pass perfusion --a review. *J Cardiovasc Magn Reson* 2007;9:525-37.

Khaja F, Alam M, Goldstein S, Anbe DT, Marks DS. Diagnostic value of visualization of the right ventricle using thallium-201 myocardial imaging. *Circulation* 1979;59:182-8.

Khoo NS, Young A, Occleshaw C, Cowan B, Zeng IS, Gentles TL. Assessments of right ventricular volume and function using three-dimensional echocardiography in older children

and adults with congenital heart disease: comparison with cardiac magnetic resonance imaging. *J Am Soc Echocardiogr* 2009;22:1279-88.

Kiely DG, Cargill RI, Lipworth BJ. Angiotensin II receptor blockade and effects on pulmonary hemodynamics and hypoxic pulmonary vasoconstriction in humans. *Chest* 1996;110:698-703.

Kilner PJ, Gatehouse PD, Firmin DN. Flow measurement by magnetic resonance: a unique asset worth optimising. *J Cardiovasc Magn Reson* 2007;9:723-8.

Kim RJ, Fieno DS, Parrish TB, Harris K, Chen EL, Simonetti O, Bundy J, Finn JP, Klocke FJ, Judd RM. Relationship of MRI delayed contrast enhancement to irreversible injury, infarct age, and contractile function. *Circulation* 1999;100:1992-2002.

Kim RJ, Wu E, Rafael A, Chen EL, Parker MA, Simonetti O, Klocke FJ, Bonow RO, Judd RM. The use of contrast-enhanced magnetic resonance imaging to identify reversible myocardial dysfunction. *N Engl J Med* 2000;343:1445-53.

Kim RJ, Choi KM, Judd RM. Assessment of myocardial viability by contrast enhancement. In: Higgins CB, de Roos A, editors. *Cardiovascular MRI and MRA*. Philadelphia, PA. Lippincott Williams and Wilkins; 2003:209-37.

Kim TH, Ryu YH, Hur J, Kim SJ, Kim HS, Choi BW, Kim Y, Kim HJ. Evaluation of right ventricular volume and mass using retrospective ECG-gated cardiac multidetector computed tomography: comparison with first-pass radionuclide angiography. *Eur Radiol* 2005;15:1987-93.

Kim WY, Danias PG, Stuber M, Flamm SD, Plein S, Nagel E, Langerak SE, Weber OM, Pedersen EM, Schmidt M, Botnar RM, Manning WJ. Coronary magnetic resonance angiography for the detection of coronary stenoses. *N Engl J Med* 2001;345:1863-9.

Kinch JW, Ryan TJ. Right ventricular infarction. *N Engl J Med* 1994;330:1211-7.

Kiotsekoglou A, Sutherland GR, Moggridge JC, Kapetanakis V, Bajpai A, Bunce N, Mullen MJ, Louridas G, Nassiri DK, Camm J, Child AH. Early impairment of left ventricular long-axis systolic function demonstrated by reduced atrioventricular plane displacement in patients with Marfan syndrome. *Eur J Echocardiogr* 2008;9:605-13.

Kiotsekoglou A, Moggridge JC, Bijnens BH, Kapetanakis V, Alpendurada F, Mullen MJ, Saha S, Nassiri DK, Camm J, Sutherland GR, Child AH. Biventricular and atrial diastolic function

assessment using conventional echocardiography and tissue-Doppler imaging in adults with Marfan syndrome. *Eur J Echocardiogr* 2009a;10:947-55.

Kiotsekoglou A, Sutherland GR, Moggridge JC, Nassiri DK, Camm AJ, Child AH. The unravelling of primary myocardial impairment in Marfan syndrome by modern echocardiography. *Heart* 2009b;95:1561-6.

Kiotsekoglou A, Saha S, Moggridge JC, Kapetanakis V, Govindan M, Alpendurada F, Mullen MJ, Nassiri DK, Camm J, Sutherland GR, Bijnsens BH, Child A. Impaired biventricular deformation in Marfan syndrome: a strain and strain rate study in adult unoperated patients. *Echocardiography* 2011;28:416-30.

Kirk P, Roughton M, Porter JB, Walker JM, Tanner MA, Patel J, Wu D, Taylor J, Westwood MA, Anderson LJ, Pennell DJ. Cardiac T2* magnetic resonance for prediction of cardiac complications in thalassemia major. *Circulation* 2009;120:1961-8.

Kirk P, He T, Anderson LJ, Roughton M, Tanner MA, Lam WW, Au WY, Chu WC, Chan G, Galanello R, Matta G, Fogel M, Cohen AR, Tan RS, Chen K, Ng I, Lai A, Fucharoen S, Laothamata J, Chuncharunee S, Jongjirasiri S, Firmin DN, Smith GC, Pennell DJ. International reproducibility of single breathhold T2* MR for cardiac and liver iron assessment among five thalassemia centers. *J Magn Reson Imaging* 2010;32:315-9.

Kirk P, Carpenter JP, Tanner MA, Pennell DJ. Low prevalence of fibrosis in thalassemia major assessed by late gadolinium enhancement cardiovascular magnetic resonance. *J Cardiovasc Magn Reson* 2011;13:8.

Kjaergaard J, Petersen CL, Kjaer A, Schaadt BK, Oh JK, Hassager C. Evaluation of right ventricular volume and function by 2D and 3D echocardiography compared to MRI. *Eur J Echocardiogr* 2006;7:430-8.

Klein C, Nekolla SG, Bengel FM, Momose M, Sammer A, Haas F, Schnackenburg B, Delius W, Mudra H, Wolfram D, Schwaiger M. Assessment of myocardial viability with contrast-enhanced magnetic resonance imaging: comparison with positron emission tomography. *Circulation* 2002;105:162-7.

Kojima S, Yamada N, Goto Y. Diagnosis of constrictive pericarditis by tagged cine magnetic resonance imaging. *N Engl J Med* 1999;341:373-4.

Kolnagou A, Kontoghiorghes GJ. Effective combination therapy of deferiprone and deferoxamine for the rapid clearance of excess cardiac iron and the prevention of heart disease in thalassemia. The Protocol of the International Committee on Oral Chelators. Hemoglobin 2006;30:239-49.

Kon MW, Myerson SG, Moat NE, Pennell DJ. Quantification of regurgitant fraction in mitral regurgitation by cardiovascular magnetic resonance: comparison of techniques. J Heart Valve Dis 2004;13:600-7.

Kondo C, Caputo GR, Semelka R, Foster E, Shimakawa A, Higgins CB. Right and left ventricular stroke volume measurements with velocity-encoded cine MR imaging: in vitro and in vivo validation. Am J Roentgenol 1991;157:9-16.

Kondo C, Caputo GR, Masui T, Foster E, O'Sullivan M, Stulbarg MS, Golden J, Catterjee K, Higgins CB. Pulmonary hypertension: pulmonary flow quantification and flow profile analysis with velocity-encoded cine MR imaging. Radiology 1992;183:751-8.

Kopelman HA, Forman MB, Wilson BH, Anbe DT, Marks DS. Right ventricular myocardial infarction in patients with chronic lung disease: possible role of right ventricular hypertrophy. J Am Coll Cardiol 1985;5:1302-7.

Koplan BA, Kaplan AJ, Weiner S, Jones PW, Seth M, Christman SA. Heart failure decompensation and all-cause mortality in relation to percent biventricular pacing in patients with heart failure: is a goal of 100% biventricular pacing necessary? J Am Coll Cardiol 2009;53:355-60.

Kreit JW. The impact of right ventricular dysfunction on the prognosis and therapy of normotensive patients with pulmonary embolism. Chest 2004;125:1539-45.

Kremastinos DT, Tiniakos G, Theodorakis GN, Katritsis DG, Toutouzas PK. Myocarditis in β -thalassemia major. A cause of heart failure. Circulation 1995;91:66-71.

Kremastinos DT, Tsetsos GA, Tsiapras DP, Karavolias GK, Ladis VA, Kattamis CA. Heart failure in β -thalassemia: a 5-year follow-up study. Am J Med 2001;111:349-54.

Kühl HP, Lipke CS, Krombach GA, Katoh M, Battenberg TF, Nowak B, Heussen N, Buecker A, Schaefer WM. Assessment of reversible myocardial dysfunction in chronic ischaemic heart disease: comparison of contrast-enhanced cardiovascular magnetic resonance and a

combined positron emission tomography-single photon emission computed tomography imaging protocol. *Eur Heart J* 2006;27:846-53.

Kukulski T, Hübbert L, Arnold M, Wranne B, Hatle L, Sutherland GR. Normal regional right ventricular function and its change with age: a Doppler myocardial imaging study. *J Am Soc Echocardiogr* 2000;13:194-204.

Kumar A, Abdel-Aty H, Kriedemann I, Schulz-Menger J, Gross CM, Dietz R, Friedrich MG. Contrast-enhanced cardiovascular magnetic resonance imaging of right ventricular infarction. *J Am Coll Cardiol* 2006;48:1969-76.

Kupfahl C, Honold M, Meinhardt G, Vogelsberg H, Wagner A, Mahrholdt H, Sechtem U. Evaluation of aortic stenosis by cardiovascular magnetic resonance imaging: comparison with established routine clinical techniques. *Heart* 2004;90:893-901.

Kusachi S, Nishiyama O, Yasuhara K, Saito D, Haraoka S, Nagashima H. Right and left ventricular oxygen metabolism in open-chest dogs. *Am J Physiol* 1982;243:H761-6.

Kwong RY, Chan AK, Brown KA, Chan CW, Reynolds HG, Tsang S, Davis RB. Impact of unrecognized myocardial scar detected by cardiac magnetic resonance imaging on event-free survival in patients presenting with signs or symptoms of coronary artery disease. *Circulation* 2006;113:2733-43.

L

La Gerche A, Jurcut R, Voigt JU. Right ventricular function by strain echocardiography. *Curr Opin Cardiol* 2010;25:430-6.

La Vecchia L, Paccanaro M, Bonanno C, Varotto L, Ometto R, Vincenzi M. Left ventricular versus biventricular dysfunction in idiopathic dilated cardiomyopathy. *Am J Cardiol* 1999;83:120-2.

La Vecchia L, Varotto L, Zanolli L, Spadaro GL, Fontanelli A. Reduced right ventricular ejection fraction as a marker for idiopathic dilated cardiomyopathy compared with ischemic left ventricular dysfunction. *Am Heart J* 2001;142:181-9.

Lacro RV, Dietz HC, Wruck LM, Bradley TJ, Colan SD, Devereux RB, Klein GL, Li JS, Minich LL, Paridon SM, Pearson GD, Printz BF, Pyeritz RE, Radojewski E, Roman MJ, Saul JP, Stylianou MP, Mahony L. Rationale and design of a randomized clinical trial of beta-blocker therapy

(atenolol) versus angiotensin II receptor blocker therapy (losartan) in individuals with Marfan syndrome. *Am Heart J* 2007;154:624-31.

Laffon E, Laurent F, Bernard V, De Boucaud L, Ducassou D, Marthan R. Noninvasive assessment of pulmonary arterial hypertension by MR phase-mapping method. *J Appl Physiol* 2001;90:2197-202.

Lanzer P, Barta C, Botvinick EH, Wiesendanger HUD, Modin G, Higgins CB. ECG-synchronised cardiac MR imaging: Method and evaluation. *Radiology* 1985;155:681-86.

Larose E, Ganz P, Reynolds HG, Dorbala S, Di Carli MF, Brown KA, Kwong RY. Right ventricular dysfunction assessed by cardiovascular magnetic resonance imaging predicts poor prognosis late after myocardial infarction. *J Am Coll Cardiol* 2007;49:855-62.

Laster SB, Shelton TJ, Barzilai B, Goldstein JA. Determinants of the recovery of right ventricular performance following experimental chronic right coronary artery occlusion. *Circulation* 1993;88:696-708.

Lee FA. Hemodynamics of the right ventricle in normal and disease states. *Cardiol Clin* 1992;10:59-67.

Lee KS, Abbas AE, Khandheria BK, Lester SJ. Echocardiographic assessment of right heart hemodynamic parameters. *J Am Soc Echocardiogr* 2007;20:773-82.

Lee VS, Resnick D, Bundy JM, Simonetti OP, Lee P, Weinreb JC. Cardiac function. MR evaluation in one breath hold with real-time true fast imaging with steady-state precession. *Radiology* 2002;222:835-42.

Leibundgut G, Rohner A, Grize L, Bernheim A, Kessel-Schaefer A, Bremerich J, Zellweger M, Buser P, Handke M. Dynamic assessment of right ventricular volumes and function by real-time three-dimensional echocardiography: a comparison study with magnetic resonance imaging in 100 adult patients. *J Am Soc Echocardiogr* 2010;23:116-26.

Lenz GW, Haacke EM, White RD. Retrospective cardiac gating: a review of technical aspects and future directions. *Magn Reson Imaging* 1989;7:445-55.

Levine GN, Gomes AS, Arai AE, Bluemke DA, Flamm SD, Kanal E, Manning WJ, Martin ET, Smith JM, Wilke N, Shellock FS. Safety of magnetic resonance imaging in patients with cardiovascular devices: an American Heart Association scientific statement from the Committee on

Diagnostic and Interventional Cardiac Catheterization, Council on Clinical Cardiology, and the Council on Cardiovascular Radiology and Intervention. *Circulation* 2007;116:2878-91.

Leyton RA, Sonnenblick EH. The sarcomere as the basis of Starling's law of the heart in the left and right ventricles. *Methods Achiev Exp Pathol* 1971;5:22-59.

Levy D, Kenchiah S, Larson MG, Benjamin EJ, Kupka MJ, Ho KK, Murabito JM, Vasan RS. Long-term trends in the incidence of and survival with heart failure. *N Engl J Med* 2002;347:1397-1402.

Leyva F. Cardiac resynchronization therapy guided by cardiovascular magnetic resonance. *J Cardiovasc Magn Reson* 2010;12:64.

Leyva F, Foley PW, Chalil S, Ratib K, Smith RE, Prinzen F, Auricchio A. Cardiac resynchronization therapy guided by late gadolinium-enhancement cardiovascular magnetic resonance. *J Cardiovasc Magn Reson* 2011a;13:29.

Leyva F, Foley PW. Current and future role of cardiovascular magnetic resonance in cardiac resynchronization therapy. *Heart Fail Rev* 2011b;16:251-62.

Li CK, Luk CW, Ling SC, Chik KW, Yuen HL, Li CK, Shing MM, Chang KO, Yuen PM. Morbidity and mortality patterns of thalassaemia major patients in Hong Kong: retrospective study. *Hong Kong Med J* 2002;8:255-60.

Lin SJ, Brown PA, Watkins MP, Williams TA, Lehr KA, Liu W, Lanza GM, Wickline SA, Caruthers SD. Quantification of stenotic mitral valve area with magnetic resonance imaging and comparison with Doppler ultrasound. *J Am Coll Cardiol* 2004;44:133-7.

Lindström L, Wilkenshoff UM, Larsson H, Wranne B. Echocardiographic assessment of arrhythmogenic right ventricular cardiomyopathy. *Heart* 2001;86:31-8.

Link G, Ponka P, Konijn AM, Breuer W, Cabantchik ZI, Herskho C. Effects of combined chelation treatment with pyridoxal isonicotinoyl hydrazone analogs and deferoxamine in hypertransfused rats and in iron-loaded rat heart cells. *Blood* 2003;101:4172-9.

Listerud J, Einstein S, Outwater E, Kressel HY. First principles of fast spin echo. *Magn Reson Q* 1992;8:199-244.

Lloyd-Jones D, Adams RJ, Brown TM, Carnethon M, Dai S, De Simone G, Ferguson TB, Ford E, Furie K, Gillespie C, Go A, Greenlund K, Haase N, Hailpern S, Ho PM, Howard V, Kissela B, Kittner S, Lackland D, Lisabeth L, Marelli A, McDermott MM, Meigs J, Mozaffarian D, Mussolino M, Nichol G, Roger VL, Rosamond W, Sacco R, Sorlie P, Roger VL, Thom T, Wasserthiel-Smoller S, Wong ND, Wylie-Rosett J. Heart disease and stroke statistics – 2010 update: a report from the American Heart Association. *Circulation* 2010;121:e46-215.

Lockie T, Ishida M, Perera D, Chiribiri A, De Silva K, Kozerke S, Marber M, Nagel E, Rezavi R, Redwood S, Plein S. High-resolution magnetic resonance myocardial perfusion imaging at 3.0-Tesla to detect hemodynamically significant coronary stenoses as determined by fractional flow reserve. *J Am Coll Cardiol* 2011;57:70-5.

Loeys BL, Dietz HC, Braverman AC, Callewaert BL, De Backer J, Devereux RB, Hilhorst-Hofstee Y, Jondeau G, Faivre L, Milewicz DM, Pyeritz RE, Sponseller PD, Wordsworth P, De Paepe AM. The revised Ghent nosology for the Marfan syndrome. *J Med Genet* 2010; 47:476-485.

Longmore DB, Klipstein RH, Underwood SR, Firmin DN, Hounsfield GN, Watanabe M, Bland C, Fox K, Poole-Wilson PA, Rees RS. Dimensional accuracy of magnetic resonance in studies of the heart. *Lancet* 1985;1:1360-2.

Lorenz CH, Walker ES, Morgan VL, Klein SS, Graham TP Jr. Normal human right and left ventricular mass, systolic function, and gender differences by cine magnetic resonance imaging. *J Cardiovasc Magn Reson* 1999;1:7-21.

Louie EK, Lin SS, Reynertson SI, Brundage BH, Levitsky S, Rich S. Pressure and volume loading of the right ventricle have opposite effects on left ventricular ejection fraction. *Circulation* 1995;92:819-24.

Lyons AS, Keiner M. The seventeenth century. In: Lyons AS, Petrucelli RJ II, editors. *Medicine: an illustrated history*, 2nd edition. New York, NY. Abradale Press; 1987:427-59.

M

Maceira AM, Joshi J, Prasad SK, Moon JC, Perugini E, Harding I, Sheppard MN, Poole-Wilson PA, Hawkins PN, Pennell DJ. Cardiovascular magnetic resonance in cardiac amyloidosis. *Circulation* 2005;111:186-93.

Maceira AM, Prasad SK, Khan M, Pennell DJ. Reference right ventricular systolic and diastolic function normalized to age, gender and body surface area from steady-state free precession cardiovascular magnetic resonance. *Eur Heart J* 2006a;27:2879-88.

Maceira AM, Prasad SK, Khan M, Pennell DJ. Normalized left ventricular systolic and diastolic function by steady state free precession cardiovascular magnetic resonance. *J Cardiovasc Magn Reson* 2006b;8:417-26.

MacNee W. Pathophysiology of cor pulmonale in chronic obstructive pulmonary disease. Part One. *Am J Respir Crit Care Med* 1994;150:833-52.

Maddahi J, Berman DS, Matsuoka DT, Waxman AD, Stankus KE, Forrester JS, Swan HJ. A new technique for assessing right ventricular ejection fraction using rapid multiple-gated equilibrium cardiac blood pool scintigraphy. Description, validation and findings in chronic coronary artery disease. *Circulation* 1979;60:581-9.

Maffei E, Messalli G, Martini C, Nieman K, Catalano O, Rossi A, Seitun S, Guaricci AI, Tedeschi C, Mollet NR, Cademartiri F. Left and right ventricle assessment with Cardiac CT: validation study vs. Cardiac MR. *Eur Radiol* 2012;22:1041-9.

Mahrholdt H, Wagner A, Holly TA, Elliott MD, Bonow RO, Kim RJ, Judd RM. Reproducibility of chronic infarct size measurement by contrast-enhanced magnetic resonance imaging. *Circulation* 2002;106:2322-7.

Mahrholdt H, Goedecke C, Wagner A, Meinhardt G, Athanasiadis A, Vogelsberg H, Fritz P, Klingel K, Kandolf R, Sechtem U. Cardiovascular magnetic resonance assessment of human myocarditis: A comparison to histology and molecular pathology. *Circulation* 2004;109:1250-8.

Mahrholdt H, Wagner A, Judd RM, Sechtem U, Kim RJ. Delayed enhancement cardiovascular magnetic resonance assessment of non-ischaemic cardiomyopathies. *Eur Heart J* 2005;26:1461-74.

Mahrholdt H, Wagner A, Deluigi CC, Kispert E, Hager S, Meinhardt G, Vogelsberg H, Fritz P, Dippón J, Bock CT, Klingel K, Kandolf R, Sechtem U. Presentation, patterns of myocardial damage, and clinical course of viral myocarditis. *Circulation* 2006;114:1581-90.

Mangion JR. Right ventricular imaging by two-dimensional and three-dimensional echocardiography. *Curr Opin Cardiol* 2010;25:423-9.

Manning WJ, Atkinson DJ, Grossman W, Paulin S, Edelman RR. First-pass nuclear magnetic resonance imaging studies using gadolinium-DTPA in patients with coronary artery disease. *J Am Coll Cardiol* 1991;18:959-65.

Marcus RE, Davies SC, Bantock HM, Underwood SR, Walton S, Huehns ER. Desferrioxamine to improve cardiac function in iron-overloaded patients with thalassemia major. *Lancet* 1984;1:392-3.

Marfan, A. Un cas de déformation congénital des quatre membres, plus prononcée aux extrémités, caractérisée par l'allongement des os avec un certain degré d'amincissement [French]. *Bull. Mem. Soc. Med. Hop (Paris)* 1896;13:220-6.

Maron MS, Hauser TH, Dubrow E, Horst TA, Kissinger KV, Udelson JE, Manning WJ. Right ventricular involvement in hypertrophic cardiomyopathy. *Am J Cardiol* 2007;100:1293-8.

Marsan NA, Westenberg JJ, Ypenburg C, van Bommel RJ, Roes S, Delgado V, Tops LF, van der Geest RJ, Boersma E, de Roos A, Schalij MJ, Bax JJ. Magnetic resonance imaging and response to cardiac resynchronization therapy: relative merits of left ventricular dyssynchrony and scar tissue. *Eur Heart J* 2009;30:2360-7.

Marwick TH. Hype and hope in the use of echocardiography for selection for cardiac resynchronization therapy: the Tower of Babel revisited. *Circulation* 2008;117:2573-6.

Masci PG, Dymarkowski S, Bogaert J. Valvular heart disease: what does cardiovascular MRI add? *Eur Radiol* 2008;18:197-208.

Masci PG, Francone M, Desmet W, Ganame J, Todiere G, Donato R, Siciliano V, Carbone I, Mangia M, Strata E, Catalano C, Lombardi M, Agati L, Janssens S, Bogaert J. Right ventricular ischemic injury in patients with acute ST-segment elevation myocardial infarction: characterization with cardiovascular magnetic resonance. *Circulation* 2010;122:1405-12.

Maurer G. Aortic regurgitation. *Heart* 2006;92:994-1000.

Mavrogeni S, Gotsis E, Ladis V, Berdousis E, Verganelakis D, Toulas P, Cokkinos DV. Magnetic resonance evaluation of liver and myocardial iron deposition in thalassemia intermedia and b-thalassemia major. *Int J Cardiovasc Imaging* 2008;24:849-54.

McCrohon JA, Moon JC, Prasad SK, McKenna WJ, Lorenz CH, Coats AJ, Pennell DJ. Differentiation of heart failure related to dilated cardiomyopathy and coronary artery disease using gadolinium-enhanced cardiovascular magnetic resonance. *Circulation* 2003;108:54-9.

McGill HC Jr, Brown BW, Gore I, McMillan GC, Pollak OJ, Robbins S, Roberts JC Jr, Wissler RW. Report of Committee on Grading Lesions, Council on Arteriosclerosis, American Heart Association. Grading stenosis in the right coronary artery. *Circulation* 1968;37:460-8.

McLaughlin VV, Sitbon O, Badesch DB, Barst RJ, Black C, Galiè N, Rainisio M, Simonneau G, Rubin LJ. Survival with first-line bosentan in patients with primary pulmonary hypertension. *Eur Respir J* 2005;25:244-9.

McMurray JJ, Adamopoulos S, Anker SD, Auricchio A, Böhm M, Dickstein K, Falk V, Filippatos G, Fonseca C, Gomez-Sanchez MA, Jaarsma T, Køber L, Lip GY, Maggioni AP, Parkhomenko A, Pieske BM, Popescu BA, Rønnevik PK, Rutten FH, Schwitter J, Seferovic P, Stepinska J, Trindade PT, Voors AA, Zannad F, Zeiher A. ESC Guidelines for the diagnosis and treatment of acute and chronic heart failure 2012. *Eur Heart J* 2012;33:1787-847.

Marino TA, Kent RL, Uboh CE, Fernandez E, Thompson EW, Cooper G 4th. Structural analysis of pressure versus volume overload hypertrophy of cat right ventricle. *Am J Physiol* 1985;249:H371-9.

Marti S, Munoz X, Rios J, Morell F, Ferrer J. Body weight and comorbidity predict mortality in COPD patients treated with oxygen therapy. *Eur Respir J* 2006;27:689-96.

Mehta SR, Eikelboom JW, Natarajan MK, Diaz R, Yi C, Gibbons RJ, Yusuf S. Impact of right ventricular involvement on mortality and morbidity in patients with inferior myocardial infarction. *J Am Coll Cardiol* 2001;37:37-43.

Meijboom LJ, Timmermans J, van Tintelen JP, Nollen GJ, De Backer J, van den Berg MP, Boers GH, Mulder BJ. Evaluation of Left Ventricular Dimensions and Function in Marfan's Syndrome without Significant Valvular Regurgitation. *Am J Cardiol* 2005;95:795-7.

Meris A, Faletra F, Conca C, Klersy C, Regoli F, Klimusina J, Penco M, Pasotti E, Pedrazzini GB, Moccetti T, Auricchio A. Timing and magnitude of regional right ventricular function: a speckle tracking-derived strain study of normal subjects and patients with right ventricular dysfunction. *J Am Soc Echocardiogr* 2010;23:823-31.

Mertens LL, Friedberg MK. Imaging the right ventricle-current state of the art. *Nat Rev Cardiol* 2010;7:551-63.

Messika-Zeitoun D, Thomson H, Bellamy M, Scott C, Tribouilloy C, Dearani J, Tajik AJ, Schaff H, Enriquez-Sarano M. J Medical and surgical outcome of tricuspid regurgitation caused by flail leaflets. *Thorac Cardiovasc Surg* 2004;128:296-302.

Meyer P, Filippatos GS, Ahmed MI, Iskandrian AE, Bittner V, Gilbert J, Perry GJ, White M, Aban IB, Mujib M, Dell'Italia LJ, Ahmed A. Effects of right ventricular ejection fraction on outcomes in chronic systolic heart failure. *Circulation* 2010;121:252-8.

Mezrich R. A perspective on k-space. *Radiology* 1995;195:297-315.

Miller D, Farah MG, Liner A, Fox K, Schluchter M, Hoit BD. The relation between quantitative right ventricular ejection fraction and indices of tricuspid annular motion and myocardial performance. *J Am Soc Echocardiogr* 2004;17:443-7.

Miszalski-Jamka T, Klimeczek P, Tomala M, Krupiński M, Zawadowski G, Noelting J, Lada M, Sip K, Banyś R, Mazur W, Kereiakes DJ, Zmudka K, Pasowicz M. Extent of RV dysfunction and myocardial infarction assessed by CMR are independent outcome predictors early after STEMI treated with primary angioplasty. *JACC Cardiovasc Imaging* 2010;3:1237-46.

Mital S. Right ventricle in congenital heart disease: is it just a "weaker" left ventricle? *Arch Mal Coeur Vaiss* 2006;99:1244-51.

Modell B, Letsky EA, Flynn DM, Peto R, Weatherall DJ. Survival and desferrioxamine in thalassaemia major. *BMJ* 1982;284:1081-4.

Modell B, Khan M, Darlison M. Survival in beta-thalassaemia major in the UK: data from the UK Thalassaemia Register. *Lancet* 2000;355:2051-2.

Modell B, Khan M, Darlison M, Westwood MA, Ingram D, Pennell DJ. Improved survival of thalassaemia major in the UK and relation to T2* cardiovascular magnetic resonance. *J Cardiovasc Magn Reson* 2008;10:42.

Mogelvang J, Stubgaard M, Thomsen C, Henriksen O. Evaluation of right ventricular volumes measured by magnetic resonance imaging. *Eur Heart J* 1988;9:529-33.

Mohiaddin RH, Yang GZ, Kilner PJ. Visualization of flow by vector analysis of multidirectional cine MR velocity mapping. *J Comput Assist Tomogr* 1994;18:383-92.

Molinari G, Sardanelli F, Gaita F, Ottonello C, Richiardi E, Parodi RC, Masperone MA, Caponnetto S. Right ventricular dysplasia as a generalized cardiomyopathy? findings on magnetic resonance imaging. *Eur Heart J* 1995;16:1619-24.

Moon JC, McKenna WJ, McCrohon JA, Elliott PM, Smith GC, Pennell DJ. Toward clinical risk assessment in hypertrophic cardiomyopathy with gadolinium cardiovascular magnetic resonance. *J Am Coll Cardiol* 2003;41:1561-7.

Moon JC, Sachdev B, Elkington AG, McKenna WJ, Mehta A, Pennell DJ, Leed PJ, Elliott PM. Gadolinium enhanced cardiovascular magnetic resonance in Anderson-Fabry disease. Evidence for a disease specific abnormality of the myocardial interstitium. *Eur Heart J* 2003b;24:2151-5.

Moon JC, Fisher NG, McKenna WJ, Pennell DJ. Detection of apical hypertrophic cardiomyopathy by cardiovascular magnetic resonance in patients with nondiagnostic echocardiography. *Heart* 2004; 90:645-9.

Morcos P, Vick GW 3rd, Sahn DJ, Jerosch-Herold M, Shurman A, Sheehan FH. Correlation of right ventricular ejection fraction and tricuspid annular plane systolic excursion in tetralogy of Fallot by magnetic resonance imaging. *Int J Cardiovasc Imaging* 2009;25:263-70.

Mosteller RD. Simplified calculation of body surface area. *N Engl J Med* 1987;317:1098.

Moss AJ, Zareba W, Hall WJ, Klein H, Wilber DJ, Cannom DS, Daubert JP, Higgins SL, Brown MW, Andrews ML; Multicenter Automatic Defibrillator Implantation Trial II Investigators. Prophylactic implantation of a defibrillator in patients with myocardial infarction and reduced ejection fraction. *N Engl J Med* 2002;346:877-83.

Moss AJ, Hall WJ, Cannom DS, Klein H, Brown MW, Daubert JP, Estes NA 3rd, Foster E, Greenberg H, Higgins SL, Pfeffer MA, Solomon SD, Wilber D, Zareba W; MADIT-CRT Trial Investigators. Cardiac resynchronization therapy for the prevention of heart failure events. *N Engl J Med* 2009;361:1329-38.

Mousseaux E, Tasu JP, Jolivet O, Simonneau G, Bittoun J, Gaux JC. Pulmonary arterial resistance: noninvasive measurement with indexes of pulmonary flow estimated at velocity-encoded MR imaging—preliminary experience. *Radiology* 1999;212:896-902.

Mulder P, Richard V, Derumeaux G, Hogie M, Henry JP, Lallemand F, Compagnon P, Mace B, Comoy E, Letac B, Thuillez C. Role of endogenous endothelin in chronic heart failure: effect of long-term treatment with an endothelin antagonist on survival, hemodynamics, and cardiac remodeling. *Circulation* 1997;96:1976-82.

Murdoch JL, Walker BA, Halpern BL, Kuzma JW, McKusick VA. Life expectancy and causes of death in the Marfan syndrome. *N Engl J Med* 1972;286:804-8.

Myerson SG. Heart valve disease: investigation by cardiovascular magnetic resonance. *J Cardiovasc Magn Reson* 2012;14:7.

N

Naehle CP, Strach K, Thomas D, Meyer C, Linhart M, Bitaraf S, Litt H, Schwab JO, Schild H, Sommer T. Magnetic resonance imaging at 1.5-T in patients with implantable cardioverter-defibrillators. *J Am Coll Cardiol* 2009;54:549-55.

Nagaya N, Nishikimi T, Uematsu M, Satoh T, Kyotani S, Sakamaki F, Kakishita M, Fukushima K, Okano Y, Nakanishi N, Miyatake K, Kangawa K. Plasma brain natriuretic peptide as a prognostic indicator in patients with primary pulmonary hypertension. *Circulation* 2000;102:865-70.

Nagel E, Lehmkuhl HB, Bocksch W, Klein C, Vogel U, Frantz E, Ellmer A, Dreyse S, Fleck E. Noninvasive diagnosis of ischemia-induced wall motion abnormalities with the use of high-dose dobutamine stress MRI: comparison with dobutamine stress echocardiography. *Circulation* 1999;99:763-70.

Nandalur KR, Dwamena BA, Choudhri AF, Nandalur MR, Carlos RC. Diagnostic performance of stress cardiac magnetic resonance imaging in the detection of coronary artery disease: a meta-analysis. *J Am Coll Cardiol* 2007;50:1343-53.

Nathan DG, Gunn RB. Thalassemia: the consequences of unbalanced hemoglobin synthesis. *Am J Med* 1966;41:815-30.

Nayler GL, Firmin DN, Longmore DB. Blood flow imaging by cine magnetic resonance. *J Comput Assist Tomogr* 1986;10:715-22.

Nazarian S, Roguin A, Zviman MM, Lardo AC, Dickfeld TL, Calkins H, Weiss RG, Berger RD, Bluemke DA, Halperin HR. Clinical utility and safety of a protocol for noncardiac and cardiac magnetic resonance imaging of patients with permanent pacemakers and implantable-cardioverter defibrillators at 1.5 tesla. *Circulation* 2006;114:1277-84.

Neimatallah MA, Ho VB, Dong Q, Williams D, Patel S, Song JH, Prince MR. Gadolinium-enhanced 3D magnetic resonance angiography of the thoracic vessels. *J Magn Reson Imaging* 1999;10:758-70.

Nelson GS, Berger RD, Fetters BJ, Talbot M, Spinelli JC, Hare JM, Kass DA. Left ventricular or biventricular pacing improves cardiac function at diminished energy cost in patients with dilated cardiomyopathy and left bundle branch block. *Circulation* 2000;102:3053-9.

Neptune ER, Frischmeyer PA, Arking DE, Myers L, Bunton TE, Gayraud B, Ramirez F, Sakai LY, Dietz HC. Dysregulation of TGF-beta activation contributes to pathogenesis in Marfan syndrome. *Nat Genet* 2003;33:407-11.

Nery PB, Keren A, Birnie DH. Cardiac resynchronization therapy: expanding clinical indications and refining patient selection. *Curr Opin Cardiol* 2012;27:137-42.

Ng CM, Cheng A, Myers LA, Martinez-Murillo F, Jie C, Bedja D, Gabrielson KL, Hausladen JM, Mecham RP, Judge DP, Dietz HC. TGF-beta-dependent pathogenesis of mitral valve prolapse in a mouse model of Marfan syndrome. *J Clin Invest* 2004;114:1586-92.

Nichols K, Saouaf R, Ababneh AA, Barst RJ, Rosenbaum MS, Groch MW, Shoyeb AH, Bergmann SR. Validation of SPECT equilibrium radionuclide angiographic right ventricular parameters by cardiac magnetic resonance imaging. *J Nucl Cardiol* 2002;9:153-60.

Nicol ED, Kafka H, Stirrup J, Padley SP, Rubens MB, Kilner PJ, Gatzoulis MA. A single, comprehensive non-invasive cardiovascular assessment in pulmonary arterial hypertension: combined computed tomography pulmonary and coronary angiography. *Int J Cardiol* 2009;136:278-88.

Niemann PS, Pinho L, Balbach T, Galuschky C, Blankenhagen M, Silberbach M, Broberg C, Jerosch-Herold M, Sahn DJ. Anatomically oriented right ventricular volume measurements

with dynamic three-dimensional echocardiography validated by 3-Tesla magnetic resonance imaging. *J Am Coll Cardiol* 2007;50:1668-76.

Nienaber CA, Sievers HH. Intramural hematoma in acute aortic syndrome: more than one variant of dissection? *Circulation* 2002;106:284-5.

Nienaber CA, von Kodolitsch Y, Nicolas V, Siglow V, Piepho A, Brockhoff C, Koschyk DH, Spielmann RP. The diagnosis of thoracic aortic dissection by noninvasive imaging procedures. *N Engl J Med* 1993;328:1-9.

Nijveldt R, Germans T, McCann GP, Beek AM, van Rossum AC. Semi-quantitative assessment of right ventricular function in comparison to a 3D volumetric approach: a cardiovascular magnetic resonance study. *Eur Radiol* 2008;18:2399-405.

Nitz WR, Reimer P. Contrast mechanisms in MR imaging. *Eur Radiol* 1999;9:1032-46.

Nogami M, Ohno Y, Koyama H, Kono A, Takenaka D, Kataoka T, Kawai H, Kawamitsu H, Onishi Y, Matsumoto K, Matsumoto S, Sugimura K. Utility of phase contrast MR imaging for assessment of pulmonary flow and pressure estimation in patients with pulmonary hypertension: comparison with right heart catheterization and echocardiography. *J Magn Reson Imaging* 2009;30:973-80.

O

O'Hanlon R, Grasso A, Roughton M, Moon JC, Clark S, Wage R, Webb J, Kulkarni M, Dawson D, Sulaibeekh L, Chandrasekaran B, Bucciarelli-Ducci C, Pasquale F, Cowie MR, McKenna WJ, Sheppard MN, Elliott PM, Pennell DJ, Prasad SK. Prognostic significance of myocardial fibrosis in hypertrophic cardiomyopathy. *J Am Coll Cardiol* 2010;56:867-74.

O'Rourke RA, Dell'Italia LJ. Diagnosis and management of right ventricular myocardial infarction. *Curr Probl Cardiol* 2004;29:6-47.

Ogunyankin KO, Puthumana JJ. Effect of cardiac resynchronization therapy on right ventricular function. *Curr Opin Cardiol* 2010;25:464-8.

Olivieri NF, Nathan DG, MacMillan JH, Wayne AS, Liu PP, McGee A, Martin M, Koren G, Cohen AR. Survival in medically treated patients with homozygous beta-thalassemia. *N Engl J Med* 1994;331:574-8.

Olivieri NF, Brittenham GM. Iron-chelating therapy and the treatment of thalassemia. *Blood* 1997;89:739-61.

Olivieri NF. The beta-thalassemias. *N Engl J Med* 1999;341:99-109.

Olivotto I, Maron MS, Autore C, Lesser JR, Rega L, Casolo G, De Santis M, Quarta G, Nistri S, Cecchi F, Salton CJ, Udelson JE, Manning WJ, Maron BJ. Assessment and significance of left ventricular mass by cardiovascular magnetic resonance in hypertrophic cardiomyopathy. *J Am Coll Cardiol* 2008;52:559-66.

Olson LJ, Edwards WD, McCall JT, Ilstrup DM, Gersh BJ. Cardiac iron deposition in idiopathic hemochromatosis: histologic and analytic assessment of 14 hearts from autopsy. *J Am Coll Cardiol* 1987;10:1239-43.

Oosterhof T, van Straten A, Vliegen HW, Meijboom FJ, van Dijk AP, Spijkerboer AM, Bouma BJ, Zwinderman AH, Hazekamp MG, de Roos A, Mulder BJ. Preoperative thresholds for pulmonary valve replacement in patients with corrected tetralogy of Fallot using cardiovascular magnetic resonance. *Circulation* 2007;116:545-51.

Origa R, Bina P, Agus A, Crobu G, Defraia E, Dessì C, Leoni G, Muroli PP, Galanello R. Combined therapy with deferiprone and desferrioxamine in thalassemia major. *Haematologica* 2005;90:1309-14.

Orlov MV, Ansari MM, Akrivakis ST, Jadidi A, Nijhof N, Natan SR, Wylie JV, Hicks A, Armstrong J, Jais P. First experience with rotational angiography of the right ventricle to guide ventricular tachycardia ablation. *Heart Rhythm* 2011;8:207-11.

P

Paelinck BP, Lamb HJ, Bax JJ, Van der Wall EE, de Roos A. Assessment of diastolic function by cardiovascular magnetic resonance. *Am Heart J* 2002;144:198-205.

Pearson GD, Devereux R, Loeys B, Maslen C, Milewicz D, Pyeritz R, Ramirez F, Rifkin D, Sakai L, Svensson L, Wessels A, Van Eyk J, Dietz HC. Report of the National Heart, Lung, and Blood Institute and National Marfan Foundation Working Group on research in Marfan syndrome and related disorders. *Circulation* 2008;118:785-91.

Pennell DJ, Berdoukas V, Karagiorga M, Ladis V, Piga A, Aessopos A, Gotsis ED, Tanner MA, Smith GC, Westwood MA, Wonke B, Galanello R. Randomised controlled trial of deferiprone

or deferoxamine in beta-thalassemia major patients with asymptomatic myocardial siderosis. *Blood* 2006;107:3738-44.

Pennell DJ. Cardiovascular magnetic resonance. *Circulation* 2010;121:692-705.

Pennell DJ, Porter JB, Cappellini MD, Chan LL, El-Beshlawy A, Aydinok Y, Ibrahim H, Li CK, Viprakasit V, Elalfy MS, Kattamis A, Smith G, Habr D, Domokos G, Roubert B, Taher A. Deferasirox for up to 3 years leads to continued improvement of myocardial T2* in patients with β -thalassemia major. *Haematologica* 2012;97:842-8.

Pepe A, Positano V, Santarelli MF, Sorrentino F, Cracolici E, De Marchi D, Maggio A, Midiri M, Landini L, Lombardi M. Multislice multiecho T2* cardiovascular magnetic resonance for detection of the heterogeneous distribution of myocardial iron overload. *J Magn Reson Imaging* 2006a;23:662-8.

Pepe A, Lombardi M, Positano V, Cracolici E, Capra M, Malizia R, Prossomariti L, De Marchi D, Midiri M, Maggio A. Evaluation of the efficacy of oral deferiprone in beta-thalassemia major by multislice multiecho T2*. *Eur J Haematol* 2006b;76:183-92.

Peters DC, Wylie JV, Hauser TH, Nezafat R, Han Y, Woo JJ, Taclas J, Kissinger KV, Goddu B, Josephson ME, Manning WJ. Recurrence of atrial fibrillation correlates with the extent of post-procedural late gadolinium enhancement: a pilot study. *JACC Cardiovasc Imaging* 2009;2:308-16.

Petersen SE, Jerosch-Herold M, Hudsmith LE, Robson MD, Francis JM, Doll HA, Selvanayagam JB, Neubauer S, Watkins H. Evidence for microvascular dysfunction in hypertrophic cardiomyopathy: new insights from multiparametric magnetic resonance imaging. *Circulation* 2007;115:2418-25.

Petitjean C, Rougon N, Cluzel P. Assessment of myocardial function: a review of quantification methods and results using tagged MRI. *J Cardiovasc Magn Reson* 2005;7:501-16.

Perazella MA, Reilly RF. Nephrogenic Systemic Fibrosis: Recommendations for Gadolinium-Based Contrast Use in Patients with Kidney Disease. *Seminars in Dialysis* 2008;21:171-3.

Petersen SE, Voigtlander T, Kreitner KF, Kalden P, Wittlinger T, Scharhag J, Horstick G, Becker D, Hommel G, Thelen M, Meyer J. Quantification of shunt volumes in congenital heart

diseases using a breath-hold MR phase contrast technique-comparison with oximetry. *Int J Cardiovasc Imaging* 2002;18:53-60.

Pfisterer M, Emmenegger H, Solèr M, Burkart F. Prognostic significance of right ventricular ejection fraction for persistent complex ventricular arrhythmias and/or sudden cardiac death after first myocardial infarction: relation to infarct location, size and left ventricular function. *Eur Heart J* 1986;7:289-98.

Pflugler HB, Maeder MT, LaGerche A, Taylor AJ. One- and two dimensional estimation of right and left ventricular size and function-comparison with cardiac magnetic resonance imaging volumetric analysis. *Heart Lung Circ* 2010;19:541-8.

Piga A, Caglioti C, Fogliacco E, Tricta F. Comparative effects of deferiprone and deferoxamine on survival and cardiac disease in patients with thalassemia major: a retrospective analysis. *Haematologica* 2003;88:489-96.

Pyeritz RE. Marfan syndrome: 30 years of research equals 30 years of additional life expectancy. *Heart* 2009;95:173-5.

Piga A, Caglioti C, Fogliacco E, Tricta F. Comparative effects of deferiprone and deferoxamine on survival and cardiac disease in patients with thalassaemia major: a retrospective analysis. *Haematologica* 2003;88:489-96.

Pinedo M, Villacorta E, Tapia C, Arnold R, López J, Revilla A, Gómez I, Fulquet E, San Román JA. Inter- and intra-observer variability in the echocardiographic evaluation of right ventricular function. *Rev Esp Cardiol* 2010;63:802-9.

Piomelli S, Danoff SJ, Becker MH, Lipera MJ, Travis SF. Prevention of bone malformations and cardiomegaly in Cooley's anemia by early hypertransfusion regimen. *Ann N Y Acad Sci* 1969;165:427-36.

Pitzalis MV, Iacoviello M, Romito R, Guida P, De Tomasi E, Luzzi G, Anaclerio M, Forleo C, Rizzon P. Cardiac resynchronization therapy tailored by echocardiographic evaluation of ventricular asynchrony. *J Am Col Cardiol* 2002;40:1615-22.

Plein S, Smith WH, Ridgway JP, Kassner A, Beacock DJ, Bloomer TN, Sivananthan MU. Qualitative and quantitative analysis of regional left ventricular wall dynamics using real-time

magnetic resonance imaging: comparison with conventional breath-hold gradient echo acquisition in volunteers and patients. *J Magn Reson Imaging* 2001;14:23-30.

Plumhans C, Mühlenbruch G, Rapae A, Sim KH, Seyfarth T, Günther RW, Mahnken AH. Assessment of global right ventricular function on 64-MDCT compared with MRI. *AJR Am J Roentgenol* 2008;190:1358-61.

Polak JF, Holman BL, Wynne J, Colucci WS. Right ventricular ejection fraction: an indicator of increased mortality in patients with congestive heart failure associated with coronary artery disease. *J Am Coll Cardiol* 1983;2:217-24.

Pootrakul P, Hungsprenges S, Fucharoen S, Baylink D, Thompson E, English E, Lee M, Burnell J, Finch C. Relation between erythropoiesis and bone metabolism in thalassemia. *N Engl J Med* 1981;304:1470-3.

Porter JB. Deferasirox - current knowledge and future challenges. *Ann N Y Acad Sci* 2010;1202:87-93.

Positano V, Pepe A, Santarelli MF, Ramazzotti A, Meloni A, De Marchi D, Favilli B, Cracolici E, Midiri M, Spasiano A, Lombardi M, Landini L. Multislice multiecho T2* cardiac magnetic resonance for the detection of heterogeneous myocardial iron distribution in thalassaemia patients. *NMR Biomed* 2009;22:707-15.

Prince MR, Yucel EK, Kaufman JA, Harrison DC, Geller SC. Dynamic gadolinium-enhanced three-dimensional abdominal MR arteriography. *J Magn Reson Imaging* 1993;3:877-81.

Pyeritz RE, McKusick VA. The Marfan syndrome: diagnosis and management. *N Engl J Med* 1979;300:772-7.

Q

Quiroz R, Kucher N, Schoepf UJ, Kipfmüller F, Solomon SD, Costello P, Goldhaber SZ. Right ventricular enlargement on chest computed tomography: prognostic role in acute pulmonary embolism. *Circulation* 2004;109:2401-4.

R

Rabinovitch M, Fischer KC, Treves S. Quantitative thallium-201 myocardial imaging in assessing right ventricular pressure in patients with congenital heart defects. *Br Heart J* 1981; 45:198-205.

Rademakers LM, van Kerckhoven R, van Deursen CJ, Strik M, van Hunnik A, Kuiper M, Lampert A, Klersy C, Leyva F, Auricchio A, Maessen JG, Prinzen FW. Myocardial infarction does not preclude electrical and hemodynamic benefits of cardiac resynchronization therapy in dyssynchronous canine hearts. *Circ Arrhythm Electrophysiol* 2010;3:361-8.

Radonic T, de Witte P, Baars MJ, Zwinderman AH, Mulder BJ, Groenink M. Losartan therapy in adults with Marfan syndrome: study protocol of the multi-center randomized controlled COMPARE trial. *Trials* 2010;11:3.

Ramani GV, Gurm G, Dilsizian V, Park MH. Noninvasive assessment of right ventricular function: will there be resurgence in radionuclide imaging techniques? *Curr Cardiol Rep* 2010;12:162-9.

Ramirez F, Dietz HC. Marfan syndrome: from molecular pathogenesis to clinical treatment. *Curr Opin Genet Dev* 2007;17:252-8.

Raphael C, Briscoe C, Davies J, Ian Whinnett Z, Manisty C, Sutton R, Mayet J, Francis DP. Limitations of the New York Heart Association functional classification system and self-reported walking distances in chronic heart failure. *Heart* 2007;93:476-82.

Rathi VK, Doyle M, Yamrozik J, Williams RB, Caruppannan K, Truman C, Vido D, Biederman RW. Routine evaluation of left ventricular diastolic function by cardiovascular magnetic resonance: a practical approach. *J Cardiovasc Magn Reson* 2008;10:36.

Reant P, Lederlin M, Lafitte S, Serri K, Montaudon M, Corneloup O, Roudaut R, Laurent F. Absolute assessment of aortic valve stenosis by planimetry using cardiovascular magnetic resonance imaging: comparison with transesophageal echocardiography, transthoracic echocardiography, and cardiac catheterisation. *Eur J Radiol* 2006;59:276-83.

Rebergen SA, Chin JGL, Ottenkamp J, Vander wall EE, De Roos A. Pulmonary regurgitation in the late post-operative follow-up of tetralogy of Fallot: volumetric quantification by nuclear magnetic resonance velocity mapping. *Circulation* 1993;88:2257-66.

Redfield MM, Jacobsen SJ, Burnett JC Jr, Mahoney DW, Bailey KR, Rodeheffer RJ. Burden of systolic and diastolic ventricular dysfunction in the community: appreciating the scope of the heart failure epidemic. *JAMA* 2003;289:194-202.

Redington AN, Gray HH, Hodson ME, Rigby ML, Oldershaw PJ. Characterisation of the normal right ventricular pressure-volume relation by biplane angiography and simultaneous micromanometer pressure measurements. *Br Heart J* 1988;59:23-30.

Reduto LA, Berger HJ, Cohen LS, Gottschalk A, Zaret BL. Sequential radionuclide assessment of left and right ventricular performance after acute transmural myocardial infarction. *Ann Intern Med* 1978;89:441-47.

Reeder SB, Faranesh AZ. Ultrafast Pulse Sequence Techniques for Cardiac Magnetic Resonance Imaging. *Top Magn Reson Imaging* 2000;11:312-30.

Reesink HJ, Marcus JT, Tulevski II, Jamieson S, Kloek JJ, Vonk Noordegraaf A, Bresser P. Reverse right ventricular remodeling after pulmonary endarterectomy in patients with chronic thromboembolic pulmonary hypertension: utility of magnetic resonance imaging to demonstrate restoration of the right ventricle. *J Thorac Cardiovasc Surg* 2007;133:58-64.

Rehr RB, Malloy CR, Filipchuk NG, Peshock RM. Left ventricular volumes measured by MR imaging. *Radiology* 1985;156:717-9.

Reiter G, Reiter U, Kovacs G, Kainz B, Schmidt K, Maier R, Olschewski H, Rienmueller R. Magnetic resonance derived 3-dimensional blood flow patterns in the main pulmonary artery as a marker of pulmonary hypertension and a measure of elevated mean pulmonary arterial pressures. *Circ Cardiovasc Imaging* 2008;1:23-30.

Rezai K, Weiss R, Stanford W, Preslar J, Marcus M, Kirchner P. Relative accuracy of three scintigraphic methods for determination of right ventricular ejection fraction: a correlative study with ultrafast computed tomography. *J Nucl Med* 1991;32:429-35.

Rich JD, Ward RP. Right-ventricular function by nuclear cardiology. *Curr Opin Cardiol* 2010;25:445-50.

Rickers C, Wilke NM, Jerosch-Herold M, Casey SA, Panse P, Panse N, Weil J, Zenovich AG, Maron BJ. Utility of cardiac magnetic resonance imaging in the diagnosis of hypertrophic cardiomyopathy. *Circulation* 2005;112:855-61.

Ridgway JP. Cardiovascular magnetic resonance physics for clinicians: part I. *J Cardiovasc Magn Reson* 2010;12:71.

Rieber J, Huber A, Erhard I, Mueller S, Schweyer M, Koenig A, Schiele TM, Theisen K, Siebert U, Schoenberg SO, Reiser M, Klauss V. Cardiac magnetic resonance perfusion imaging for the functional assessment of coronary artery disease: a comparison with coronary angiography and fractional flow reserve. *Eur Heart J* 2006;27:1465-71.

Rochais F, Mesbah K, Kelly RG. Signaling pathways controlling second heart field development. *Circ Res* 2009;104:933-42.

Rochitte CE, Oliveira PF, Andrade JM, Ianni BM, Parga JR, Avila LF, Kalil-Filho R, Mady C, Meneghetti JC, Lima JA, Ramires JA. Myocardial delayed enhancement by magnetic resonance imaging in patients with Chagas' disease: A marker of disease severity. *J Am Coll Cardiol* 2005;46:1553-8.

Roeleveld RJ, Vonk-Noordegraaf A, Marcus JT, Bronzwaer JG, Marques KM, Postmus PE, Boonstra A. Effects of epoprostenol on right ventricular hypertrophy and dilatation in pulmonary hypertension. *Chest* 2004;125:572-9.

Roeleveld RJ, Marcus JT, Boonstra A, Postmus PE, Marques KM, Bronzwaer JG, Vonk-Noordegraaf A. A comparison of noninvasive MRI based methods of estimating pulmonary artery pressure in pulmonary hypertension. *J Magn Reson Imaging* 2005;22:67-72.

Roman MJ, Devereux RB, Kramer-Fox R, Spitzer MC. Comparison of Cardiovascular and Skeletal Features of Primary Mitral Valve Prolapse and Marfan Syndrome. *Am J Cardiol* 1989;63:317-21.

Roos-Hesselink JW, Meijboom FJ, Spitaels SE, van Domburg R, van Rijen EH, Utens EM, McGhie J, Bos E, Bogers AJ, Simoons ML. Decline in ventricular function and clinical condition after Mustard repair for transposition of the great arteries (a prospective study of 22-29 years). *Eur Heart J* 2004;25:1264-70.

Rouleau JL, Kapuku G, Pelletier S, Gosselin H, Adam A, Gagnon C, Lambert C, Meloche S. Cardioprotective effects of ramipril and losartan in right ventricular pressure overload in the rabbit: importance of kinins and influence on angiotensin II type 1 receptor signalling pathway. *Circulation* 2001;104:939-44.

Rudolph AM. The changes in the circulation after birth: their importance in congenital heart disease. *Circulation* 1970;41:343-59.

Rudolph AM. Congenital cardiovascular malformations and the fetal circulation. *Arch Dis Child Fetal Neonatal Ed* 2010;95:F132-6.

Rudski LG, Lai WW, Afilalo J, Hua L, Handschumacher MD, Chandrasekaran K, Solomon SD, Louie EK, Schiller NB. Guidelines for the echocardiographic assessment of the right heart in adults. *J Am Soc Echocardiogr* 2010;23:685-713.

Rund D, Rachmilewitz E. Beta-thalassemia. *N Engl J Med* 2005;353:1135-46.

Rybczynski M, Koschyk DH, Aydin MA, Robinson PN, Brinken T, Franzen O, Berger J, Hofmann T, Meinertz T, von Kodolitsch Y. Tissue Doppler Imaging Identifies Myocardial Dysfunction in Adults with Marfan Syndrome. *Clin Cardiol* 2007;30:19-24.

S

Saba TS, Foster J, Cockburn M, Cowan M, Peacock AJ. Ventricular mass index using magnetic resonance imaging accurately estimates pulmonary artery pressure. *Eur Respir J* 2002;20:1519-24.

Sakuma H, Ichikawa Y, Chino S, Hirano T, Makino K, Takeda K. Detection of coronary artery stenosis with whole-heart coronary magnetic resonance angiography. *J Am Coll Cardiol* 2006;48:1946-50.

Sandoval J, Bauerle O, Palomar A, Gómez A, Martínez-Guerra ML, Beltrán M, Guerrero ML. Survival in primary pulmonary hypertension. Validation of a prognostic equation. *Circulation* 1994;89:1733-44.

Sandstede J, Lipke C, Beer M, Hofmann S, Pabst T, Kenn W, Neubauer S, Hahn D. Age- and gender-specific differences in left and right ventricular cardiac function and mass determined by cine magnetic resonance imaging. *Eur Radiol* 2000;10:438-42.

Santamore WP, Dell'Italia LJ. Ventricular interdependence: significant left ventricular contributions to right ventricular systolic function. *Prog Cardiovasc Dis* 1998;40:289-308.

Sato H, Murakami Y, Shimada T, Ochiai K, Kitamura J, Sano K, Morioka S. Detection of right ventricular infarction by gadolinium DTPA-enhanced magnetic resonance imaging. *Eur Heart J* 1995;16:1195-9.

Savolainen A, Nisula L, Keto P, Hekali P, Viitasalo M, Kaitila I, Kupari M. Left ventricular function in children with the Marfan syndrome. *Eur Heart J* 1994;15:625-30.

Scheffler K, Lehnhardt S. Principles and applications of balanced SSFP techniques. *Eur Radiol* 2003;13:2409-18.

Schild HH. *Magnetic Resonance Imaging made easy*. Berlin, Germany. Heenemann GmbH & Co; 1990.

Schoepf UJ, Kucher N, Kipfmüller F, Quiroz R, Costello P, Goldhaber SZ. Right ventricular enlargement on chest computed tomography: a predictor of early death in acute pulmonary embolism. *Circulation* 2004;110:3276-80.

Schwittler J, Wacker CM, van Rossum AC, Lombardi M, Al-Saadi N, Ahlstrom H, Dill T, Larsson HB, Flamm SD, Marquardt M, Johansson L. MR-IMPACT: comparison of perfusion-cardiac magnetic resonance with single-photon emission computed tomography for the detection of coronary artery disease in a multicentre, multivendor, randomized trial. *Eur Heart J* 2008;29:480-9.

Schwittler J, Wacker CM, Wilke N, Al-Saadi N, Sauer E, Huettler K, Schönberg SO, Luchner A, Strohm O, Ahlstrom H, Dill T, Hoebel N, Simor T. MR-IMPACT II: Magnetic Resonance Imaging for Myocardial Perfusion Assessment in Coronary artery disease Trial: perfusion-cardiac magnetic resonance vs. single-photon emission computed tomography for the detection of coronary artery disease: a comparative multicentre, multivendor trial. *Eur Heart J* 2012a [Epub ahead of print]

Schwittler J, Wacker CM, Wilke N, Al-Saadi N, Sauer E, Huettler K, Schönberg SO, Debl K, Strohm O, Ahlstrom H, Dill T, Hoebel N, Simor T; MR-IMPACT investigators. Superior diagnostic performance of perfusion-cardiovascular magnetic resonance versus SPECT to detect coronary artery disease. *J Cardiovasc Magn Reson* 2012b;14:61.

Scuteri L, Rordorf R, Marsan NA, Landolina M, Magrini G, Klersy C, Frattini F, Petracci B, Vicentini A, Campana C, Tavazzi L, Ghio S. Relevance of echocardiographic evaluation of right ventricular function in patients undergoing cardiac resynchronization therapy. *Pacing Clin Electrophysiol* 2009;32:1040-9.

Selton-Suty C, Juillière Y. Non-invasive investigations of the right heart: how and why? *Arch Cardiovasc Dis* 2009;102:219-32.

Sen-Chowdhry S, Lowe MD, Sporton SC, McKenna WJ. Arrhythmogenic right ventricular cardiomyopathy: clinical presentation, diagnosis, and management. *Am J Med* 2004;117:685-95.

Sen-Chowdhry S, Prasad SK, Syrris P, Wage R, Ward D, Merrifield R, Smith GC, Firmin DN, Pennell DJ, McKenna WJ. Cardiovascular magnetic resonance in arrhythmogenic right ventricular cardiomyopathy revisited: comparison with task force criteria and genotype. *J Am Coll Cardiol* 2006;48:2132-40.

Sen-Chowdhry S, Syrris P, Ward D, Asimaki A, Sevdalis E, McKenna WJ. Clinical and genetic characterization of families with arrhythmogenic right ventricular dysplasia/cardiomyopathy provides novel insights into patterns of disease expression. *Circulation* 2007;115:1710-20.

Sen-Chowdhry S, Syrris P, Prasad SK, Hughes SE, Merrifield R, Ward D, Pennell DJ, McKenna WJ. Left-dominant arrhythmogenic cardiomyopathy: an under-recognized clinical entity. *J Am Coll Cardiol* 2008;52:2175-87.

Sengupta PP, Korinek J, Belohlavek M, Narula J, Vannan MA, Jahangir A, Khandheria BK. Left ventricular structure and function: basic science for cardiac imaging. *J Am Coll Cardiol* 2006;48:1988-2001.

Setser RM, Fischer SE, Lorenz CH. Quantification of left ventricular function with magnetic resonance images acquired in realtime. *J Magn Reson Imaging* 2000;12:430-8.

Shah PK, Maddahi J, Staniloff HM, Ellrodt AG, Pichler M, Swan HJ, Berman DS. Variable spectrum and prognostic implications of left and right ventricular ejection fractions in patients with and without clinical heart failure after acute myocardial infarction. *Am J Cardiol* 1986;58:387-93.

Sheehan FH, Bolson EL. Measurement of right ventricular volume from contrast ventriculograms: in vitro validation by cast and 3 dimensional echo. *Cathet Cardiovas Intervention* 2004;62:46-51.

Sheehan F, Redington A. The right ventricle: anatomy, physiology and clinical imaging. *Heart* 2008;94:1510-5.

Shekerdemian LS, Bush A, Lincoln C, Shore DF, Petros AJ, Redington AN. Cardiopulmonary interactions in healthy children and children after simple cardiac surgery: the effects of positive and negative pressure ventilation. *Heart* 1997;78:587-93.

Shimada YJ, Shiota M, Siegel RJ, Shiota T. Accuracy of right ventricular volumes and function determined by three-dimensional echocardiography in comparison with magnetic resonance imaging: a meta-analysis study. *J Am Soc Echocardiogr* 2010;23:943-53.

Sibille L, Bouallegue FB, Bourdon A, Micheau A, Vernhet-Kovacsik H, Mariano-Goulart D. Comparative values of gated blood-pool SPECT and CMR for ejection fraction and volume estimation. *Nucl Med Commun* 2011;32:121-8.

Silva MC, Meira ZM, Gurgel Giannetti J, da Silva MM, Campos AF, Barbosa Mde M, Starling Filho GM, Ferreira Rde A, Zatz M, Rochitte CE. Myocardial delayed enhancement by magnetic resonance imaging in patients with muscular dystrophy. *J Am Coll Cardiol* 2007;49:1874-9.

Silverman DI, Burton KJ, Gray J, Bosner MS, Kouchoukos NT, Roman MJ, Boxer M, Devereux RB, Tsipouras P. Family history of severe cardiovascular disease in Marfan syndrome is associated with increased aortic diameter and decreased survival. *J Am Coll Cardiol* 1995a;26:1062-7.

Silverman DI, Burton KJ, Gray J, Bosner MS, Kouchoukos NT, Roman MJ, Boxer M, Devereux RB, Tsipouras P. Life expectancy in the Marfan syndrome. *Am J Cardiol* 1995b;75:157-60.

Simonetti OP, Finn JP, White RD, Laub G, Henry DA. "Black Blood" T2-weighted inversion recovery MR imaging of the heart. *Radiology* 1996;199:49-57.

Simonetti OP, Kim RJ, Fieno DS, Hillenbrand HB, Wu E, Bundy JM, Finn JP, Judd RM. An improved MR imaging technique for the visualization of myocardial infarction. *Radiology* 2001;218:215-23.

Simonneau G, Robbins IM, Beghetti M, Channick RN, Delcroix M, Denton CP, Elliott CG, Gaine SP, Gladwin MT, Jing ZC, Krowka MJ, Langleben D, Nakanishi N, Souza R. Updated clinical classification of pulmonary hypertension. *J Am Coll Cardiol* 2009;54(S1):S43-54.

Sitbon O, Humbert M, Nunes H, Parent F, Garcia G, Hervé P, Rainisio M, Simonneau G. Long-term intravenous epoprostenol infusion in primary pulmonary hypertension: prognostic factors and survival. *J Am Coll Cardiol* 2002;40:780-8.

Sivananthan UM, Ridgway JP, Bann K, Verma SP, Cullingworth J, Ward J, Rees MR. Fast magnetic resonance angiography using turbo-FLASH sequences in advanced aortoiliac disease. *Br J Radiol* 1993;66:1103-10.

Slart RH, Poot L, Piers DA, van Veldhuisen DJ, Jager PL. Evaluation of right ventricular function by NuSMUGA software: gated blood-pool SPECT vs. first-pass radionuclide angiography. *Int J Cardiovasc Imaging* 2003;19:401-7.

Smedema JP, Snoep G, van Kroonenburgh MP, van Geuns RJ, Dassen WR, Gorgels AP, Crijns HJ. Evaluation of the accuracy of gadolinium-enhanced cardiovascular magnetic resonance in the diagnosis of cardiac sarcoidosis. *J Am Coll Cardiol* 2005;45:1683-90.

Snellen HA. History of Cardiology: a brief outline of the 350 years' prelude to an explosive growth. Rotterdam, Netherlands. Donker Academic Publications; 1984.

Solomon SD, Foster E, Bourgoun M, Shah A, Vilorio E, Brown MW, Hall WJ, Pfeffer MA, Moss AJ. Effect of cardiac resynchronization therapy on reverse remodeling and relation to outcome: multicenter automatic defibrillator implantation trial: cardiac resynchronization therapy. *Circulation* 2010;122:985-92.

Soriano CJ, Ridocci F, Estornell J, Jimenez J, Martinez V, De Velasco JA. Noninvasive diagnosis of coronary artery disease in patients with heart failure and systolic dysfunction of uncertain etiology, using late gadolinium-enhanced cardiovascular magnetic resonance. *J Am Coll Cardiol* 2005;45:743-8.

Srichai MB, Junor C, Rodriguez LL, Stillman AE, Grimm RA, Lieber ML, Weaver JA, Smedira NG, White RD. Clinical, imaging, and pathological characteristics of left ventricular thrombus: a comparison of contrast-enhanced magnetic resonance imaging, transthoracic echocardiography, and transesophageal echocardiography with surgical or pathological validation. *Am Heart J* 2006;152:75-84.

Stark DD. Hepatic iron overload: paramagnetic pathology. *Radiology* 1991;179:333-5.

Starling MR, Walsh RA, Dell'Italia LJ, Mancini GB, Lasher JC, Lancaster JL. The relationship of various measures of end-systole to left ventricular maximum time-varying elastance in man. *Circulation* 1987;76:32-43.

Starr I, Jeffers WA, Meade RH. The absence of conspicuous increments of venous pressure after severe damage to the RV of the dog, with discussion of the relation between clinical congestive heart failure and heart disease. *Am Heart J* 1943;26:291-301.

Stewart S, MacIntyre K, Hole DJ, Capewell S, McMurray JJ. More 'malignant' than cancer? Five-year survival following a first admission for heart failure. *Eur J Heart Fail* 2001;3:315-22.

Stewart S, Jenkins A, Buchan S, McGuire A, Capewell S, McMurray JJ. The current cost of heart failure to the National Health Service in the UK. *Eur J Heart Fail* 2002;4:361-71.

Stuber M, Botnar RM, Danias PG, Sodickson DK, Kissinger KV, Van Cauteren M, De Becker J, Manning WJ. Double-oblique free-breathing high resolution three-dimensional coronary magnetic resonance angiography. *J Am Coll Cardiol* 1999;34:524-31.

Strugnell WE, Slaughter RE, Riley RA, Trotter AJ, Bartlett H. Modified RV short axis series-a new method for cardiac MRI measurement of right ventricular volumes. *J Cardiovasc Magn Reson* 2005;7:769-74.

Sugeng L, Mor-Avi V, Weinert L, Niel J, Ebner C, Steringer-Mascherbauer R, Bartolles R, Baumann R, Schummers G, Lang RM, Nesser HJ. Multimodality comparison of quantitative volumetric analysis of the right ventricle. *JACC Cardiovasc Imaging* 2010;3:10-8.

T

Tandri H, Calkins H, Nasir K, Bomma C, Castillo E, Rutberg J, Tichnell C, Lima JA, Bluemke DA. Magnetic resonance imaging findings in patients meeting task force criteria for arrhythmogenic right ventricular dysplasia. *J Cardiovasc Electrophysiol* 2003;14:476-82.

Tandri H, Saranathan M, Rodriguez ER, Martinez C, Bomma C, Nasir K, Rosen B, Lima JA, Calkins H, Bluemke DA. Noninvasive detection of myocardial fibrosis in arrhythmogenic right ventricular cardiomyopathy using delayed-enhancement magnetic resonance imaging. *J Am Coll Cardiol* 2005;45:98-103.

Tang AS, Wells GA, Talajic M, Arnold MO, Sheldon R, Connolly S, Hohnloser SH, Nichol G, Birnie DH, Sapp JL, Yee R, Healey JS, Rouleau JL; Resynchronization-Defibrillation for Ambulatory Heart Failure Trial Investigators. Cardiac resynchronization therapy for mild-to-moderate heart failure. *N Engl J Med* 2010;363:2385-95.

Tanner MA, Porter JB, Westwood MA, Nair SV, Anderson LJ, Walker JM, Pennell DJ. Myocardial T2* in patients with cardiac failure secondary to iron overload. *Blood* 2005;106:406. Abstract.

Tanner MA, He T, Westwood MA, Firmin DN, Pennell DJ; Thalassemia International Federation Heart T2* Investigators. Multi-center validation of the transferability of the magnetic resonance T2* technique for the quantification of tissue iron. *Haematologica* 2006;91:1388-91.

Tanner MA, Galanello R, Dessi C, Smith GC, Westwood MA, Agus A, Roughton M, Assomull R, Nair SV, Walker JM, Pennell DJ. A randomized, placebo-controlled, double-blind trial of the effect of combined therapy with deferoxamine and deferiprone on myocardial iron in thalassemia major using cardiovascular magnetic resonance. *Circulation* 2007;115:1876-84.

Tanner MA, Galanello R, Dessi C, Smith GC, Westwood MA, Agus A, Pibiri M, Nair SV, Walker JM, Pennell DJ. Combined chelation therapy in thalassaemia major for the treatment of severe myocardial siderosis with left ventricular dysfunction. *J Cardiovasc Magn Reson* 2008;10:12.

Taylor AM, Dymarkowski S, Verbeken EK, Bogaert J. Detection of pericardial inflammation with late-enhancement cardiac magnetic resonance imaging: initial results. *Eur Radiol* 2006;16:569-574.

Taylor RR, Covell JW, Sonnenblick EH, Ross J Jr. Dependence of ventricular distensibility on filling of the opposite ventricle. *Am J Physiol* 1967;213:711-8.

Tedrow UB, Kramer DB, Stevenson LW, Stevenson WG, Baughman KL, Epstein LM, Lewis EF. Relation of right ventricular peak systolic pressure to major adverse events in patients undergoing cardiac resynchronization therapy. *Am J Cardiol* 2006;97:1737-40.

Tei C. New non-invasive index for combined systolic and diastolic ventricular function. *J Cardiol* 1995;26:135-6.

Telfer P. Update on survival in thalassemia major. *Hemoglobin* 2009;33:S76-80.

Therrien J, Siu SC, Harris L, Dore A, Niwa K, Janousek J, Williams WG, Webb G, Gatzoulis MA. Impact of pulmonary valve replacement on arrhythmia propensity late after repair of tetralogy of Fallot. *Circulation* 2001;103:2489-94.

Tongers J, Schwerdtfeger B, Klein G, Kempf T, Schaefer A, Knapp JM, Niehaus M, Korte T, Hoepfer MM. Am Incidence and clinical relevance of supraventricular tachyarrhythmias in pulmonary hypertension. *Am Heart J* 2007;153:127-32.

U

Ueno M, Miyauchi T, Sakai S, Kobayashi T, Goto K, Yamaguchi I. Effects of physiological or pathological pressure load in vivo on myocardial expression of ET-1 and receptors. *Am J Physiol* 1999;277:R1321-R1330.

Underwood SR, Firmin DN, Klipstein RH, Rees RS, Longmore DB. Magnetic resonance velocity mapping: clinical application of a new technique. *Br Heart J* 1987;57:404-12.

Urashima T, Zhao M, Wagner R, Fajardo G, Farahani S, Quertermous T, Bernstein D. Molecular and physiological characterization of RV remodeling in a murine model of pulmonary stenosis. *Am J Physiol Heart Circ Physiol* 2008;295:H1351-H1368.

V

van Bommel RJ, Borleffs CJ, Ypenburg C, Marsan NA, Delgado V, Bertini M, van der Wall EE, Schalij MJ, Bax JJ. Morbidity and mortality in heart failure patients treated with cardiac resynchronization therapy: influence of pre-implantation characteristics on long-term outcome. *Eur Heart J* 2010;31:2783-90.

van den Brink JS, Watanabe Y, Kuhl CK, Chung T, Muthupillai R, Van Cauteren M, Yamada K, Dymarkowski S, Bogaert J, Maki JH, Matos C, Casselman JW, Hoogeveen RM. Implications of SENSE MR in routine clinical practice. *Eur J Radiol* 2003;46:3-27.

van der Zwaan HB, Helbing WA, McGhie JS, Geleijnse ML, Luijnenburg SE, Roos-Hesselink JW, Meijboom FJ. Clinical value of real-time three-dimensional echocardiography for right ventricular quantification in congenital heart disease: validation with cardiac magnetic resonance imaging. *Am Soc Echocardiogr* 2010;23:134-40.

van der Zwaan HB, Geleijnse ML, McGhie JS, Boersma E, Helbing WA, Meijboom FJ, Roos-Hesselink JW. Right ventricular quantification in clinical practice: two-dimensional vs. three-dimensional echocardiography compared with cardiac magnetic resonance imaging. *Eur J Echocardiogr* 2011;12:656-64.

van Wolferen SA, Boonstra A, Marcus JT, Marques KM, Bronzwaer JG, Postmus PE, Vonk-Noordegraaf A. Right ventricular reverse remodeling after sildenafil in pulmonary arterial hypertension. *Heart* 2006;92:1860-1.

van Wolferen SA, Marcus JT, Boonstra A, Marques KM, Bronzwaer JG, Spreeuwenberg MD, Postmus PE, Vonk-Noordegraaf A. Prognostic value of right ventricular mass, volume, and function in idiopathic pulmonary arterial hypertension. *Eur Heart J* 2007;28:1250-7.

Vermes E, Childs H, Carbone I, Barckow P, Friedrich MG. Auto-Threshold quantification of late gadolinium enhancement in patients with acute heart disease. *J Magn Reson Imaging* 2013;37:382-90.

Voelkel NF, Quaife RA, Leinwand LA, Barst RJ, McGoon MD, Meldrum DR, Dupuis J, Long CS, Rubin LJ, Smart FW, Suzuki YJ, Gladwin M, Denholm EM, Gail DB. Right ventricular function and failure: report of a National Heart, Lung, and Blood Institute working group on cellular and molecular mechanisms of right heart failure. *Circulation* 2006;114:1883-91.

Vogel M, Schmidt MR, Kristiansen SB, Cheung M, White PA, Sorensen K, Redington AN. Validation of myocardial acceleration during isovolumic contraction as a novel noninvasive index of right ventricular contractility: comparison with ventricular pressure-volume relations in an animal model. *Circulation* 2002;105:1693-99.

Vogelsberg H, Mahrholdt H, Deluigi CC, Yilmaz A, Kispert EM, Greulich S, Klingel K, Kandolf R, Sechtem U. Cardiovascular magnetic resonance in clinically suspected cardiac amyloidosis: noninvasive imaging compared to endomyocardial biopsy. *J Am Coll Cardiol* 2008;51:1022-30.

Vracko R, Thorning D, Frederickson RG. Spatial arrangements of microfibrils in myocardial scars: application of antibody to fibrillin. *J Mol Cell Cardiol* 1990;22:749-57.

W

Wagner A, Mahrholdt H, Holly TA, Elliott MD, Regenfus M, Parker M, Klocke FJ, Bonow RO, Kim RJ, Judd RM. Contrast-enhanced MRI and routine single photon emission computed tomography (SPECT) perfusion imaging for detection of subendocardial myocardial infarcts: an imaging study. *Lancet* 2003;361:374-9.

Walsh EP, Cecchin F. Arrhythmias in adult patients with congenital heart disease. *Circulation* 2007;115:534-45.

Wang ZJ, Fischer R, Chu Z, Mahoney DH Jr, Mueller BU, Muthupillai R, James EB, Krishnamurthy R, Chung T, Padua E, Vichinsky E, Harmatz P. Assessment of cardiac iron by MRI susceptometry and R2* in patients with thalassemia. *Magn Reson Imaging* 2010;28:363-71.

Warnes CA, Williams RG, Bashore TM, Child JS, Connolly HM, Dearani JA, del Nido P, Fasules JW, Graham TP Jr, Hijazi ZM, Hunt SA, King ME, Landzberg MJ, Miner PD, Radford MJ, Walsh EP, Webb GD. ACC/AHA 2008 Guidelines for the Management of Adults with Congenital Heart Disease. *Circulation* 2008;118:e714-833.

Warnes CA. Adult congenital heart disease importance of the right ventricle. *J Am Coll Cardiol* 2009;54:1903-10.

Watkins S, McGeoch R, Lyne J, Steedman T, Good R, McLaughlin MJ, Cunningham T, Bezlyak V, Ford I, Dargie HJ, Oldroyd KG. Validation of magnetic resonance myocardial perfusion imaging with fractional flow reserve for the detection of significant coronary heart disease. *Circulation* 2009;120:2207-13.

Weatherall DJ. The thalassaemias. *BMJ* 1997;314:1675-8.

Weatherall DJ, Clegg JB. Thalassaemia - a global public health problem. *Nat Med* 1996;2:847-9.

Weatherall DJ. Common genetic disorders of the red cell and the "malaria hypothesis." *Ann Trop Med Parasitol* 1987;81:539-48.

Weatherall DJ, Clegg JB. The Thalassaemia syndromes. 4th edition. Oxford, England. Blackwell Science; 2001.

Weber OM, Martin AJ, Higgins CB. Whole-heart steady-state free precession coronary artery magnetic resonance angiography. *Magn Reson Med* 2003;50:1223-8.

Welinder A, Hakacova N, Martin T, Engblom H. Importance of standardized assessment of late gadolinium enhancement for quantification of infarct size by cardiac magnetic resonance: implications for comparison with electrocardiogram. *J Electrocardiol* 2011;44:538-43.

Westbrook C, Roth CK, Talbot J. MRI in practice, 3rd edition. Oxford, England. Blackwell Science; 2005.

Westwood M, Anderson LJ, Firmin DN, Gatehouse PD, Charrier CC, Wonke B, Pennell DJ. A single breath-hold multiecho T2* cardiovascular magnetic resonance technique for diagnosis of myocardial iron overload. *J Magn Reson Imaging* 2003a;18:33-9.

Westwood MA, Anderson LJ, Firmin DN, Gatehouse PD, Lorenz CH, Wonke B, Pennell DJ. Interscanner reproducibility of cardiovascular magnetic resonance T2* measurements of tissue iron in thalassemia. *J Magn Reson Imaging* 2003b;18:616-20.

Westwood MA, Anderson LJ, Maceira AM, Shah FT, Prescott E, Porter JB, Wonke B, Walker JM, Pennell DJ. Normalized left ventricular volumes and function in thalassemia major patients with normal myocardial iron. *J Magn Reson Imaging* 2007;25:1147-51.

White JA, Yee R, Yuan X, Krahn A, Skanes A, Parker M, Klein G, Drangova M. Delayed enhancement magnetic resonance imaging predicts response to cardiac resynchronization therapy in patients with intraventricular dyssynchrony. *J Am Coll Cardiol* 2006;48:1953-60.

Winter MM, Bernink FJ, Groenink M, Bouma BJ, van Dijk AP, Helbing WA, Tijssen JG, Mulder BJ. Evaluating the systemic right ventricle by CMR: the importance of consistent and reproducible delineation of the cavity. *J Cardiovasc Magn Reson* 2008;10:40.

Wonke B, Wright C, Hoffbrand AV. Combined therapy with deferiprone and desferrioxamine. *Br J Haematol* 1998;103:361-4.

Woo GW, Petersen-Stejskal S, Johnson JW, Conti JB, Aranda JA Jr, Curtis AB. Ventricular reverse remodeling and 6-month outcomes in patients receiving cardiac resynchronization therapy: analysis of the MIRACLE study. *J Interv Card Electrophysiol* 2005;12:107-13.

Wood JC, Otto-Duessel M, Aguilar M, Nick H, Nelson MD, Coates TD, Pollack H, Moats R. Cardiac iron determines cardiac T2*, T2, and T1 in the gerbil model of iron cardiomyopathy. *Circulation* 2005;112:535-43.

Wood JC, Ghugre N. MRI assessment of excess iron in thalassemia, sickle cell disease and other iron overload diseases. *Hemoglobin* 2008;32:85-96.

Wood JC. History and current impact of cardiac magnetic resonance imaging on the management of iron overload. *Circulation* 2009;120:1937-9.

Wu KC, Weiss RG, Thiemann DR, Kitagawa K, Schmidt A, Dalal D, Lai S, Bluemke DA, Gerstenblith G, Marbán E, Tomaselli GF, Lima JA. Late gadolinium enhancement by cardiovascular magnetic resonance heralds an adverse prognosis in nonischemic cardiomyopathy. *J Am Coll Cardiol* 2008;51:2414-21.

Y

Yach D, Hawkes C, Gould CL, Hofman KJ. The global burden of chronic diseases: overcoming impediments to prevention and control. *JAMA* 2004;291:2616-22.

Yacoub MH, Fagan A, Stessano P, Radley-Smith R. Results of valve conserving operations for aortic regurgitation. *Circulation* 1983;68:311.

Yang HS, Mookadam F, Warsame TA, Khandheria BK, Tajik JA, Chandrasekaran K. Evaluation of right ventricular global and regional function during stress echocardiography using novel velocity vector imaging. *Eur J Echocardiogr* 2010;11:157-64.

Yardumian A, Telfer P, Darbyshire P. Standards for the clinical care of children and adults with thalassaemia in the UK. United Kingdom Thalassaemia Society 2005. ISBN 978-1-900254-19-9.

Yasuda T, Okada RD, Leinbach RC, Gold HK, Phillips H, McKusick KA, Glover DK, Boucher CA, Strauss HW. Serial evaluation of right ventricular dysfunction associated with acute inferior myocardial infarction. *Am Heart J* 1990;119:816-22.

Yetman AT, Bornemeier RA, McCrindle BW. Long-term outcome in patients with Marfan syndrome: is aortic dissection the only cause of sudden death? *J Am Coll Cardiol* 2003;41:329-32.

Yetman AT, Roosevelt GE, Veit N, Everitt MD. Distal aortic and peripheral arterial aneurysms in patients with Marfan syndrome. *J Am Coll Cardiol* 2011;58:2544-5.

Yeo TC, Dujardin KS, Tei C, Mahoney DW, McGoon MD, Seward JB. Value of a Doppler-derived index combining systolic and diastolic time intervals in predicting outcome in primary pulmonary hypertension. *Am J Cardiol* 1998;81:1157-61.

Ypenburg C, Roes SD, Bleeker GB, Kaandorp TA, de Roos A, Schalij MJ, van der Wall EE, Bax JJ. Effect of total scar burden on contrast-enhanced magnetic resonance imaging on response to cardiac resynchronization therapy. *Am J Cardiol* 2007;99:657-60.

Yu CM, Sanderson JE, Chan S, Yeung L, Hung YT, Woo KS. Right ventricular diastolic dysfunction in heart failure. *Circulation* 1996;93:1509-14.

Yu CM, Lin H, Zhang Q, Sanderson JE. High prevalence of left ventricular systolic and diastolic asynchrony in patients with congestive heart failure and normal QRS duration. *Heart* 2003;89:54-60.

Yu CM, Abraham WT, Bax J, Chung E, Fedewa M, Ghio S, Leclercq C, Leon AR, Merlino J, Nihoyannopoulos P, Notabartolo D, Sun JP, Tavazzi L, for the PROSPECT Investigators. Predictors of Response to Cardiac Resynchronization Therapy (PROSPECT): study design. *Am Heart J* 2005;149:600-5.

Z

Zaffran S, Kelly RG. New developments in the second heart field. *Differentiation* 2012;84:17-24.

Zehender M, Kasper W, Kauder E, Schönthaler M, Geibel A, Olschewski M, Just H. Right ventricular infarction as an independent predictor of prognosis after acute inferior myocardial infarction. *N Engl J Med* 1993;328:981-8.

Zhang Q, Fung JW, Chan JY, Yip G, Lam YY, Liang YJ, Yu CM. Difference in long-term clinical outcome after cardiac resynchronisation therapy between ischaemic and non-ischaemic aetiologies of heart failure. *Heart* 2009;95:113-8.

Zornoff LA, Skali H, Pfeffer MA, St John Sutton M, Rouleau JL, Lamas GA, Plappert T, Rouleau JR, Moyé LA, Lewis SJ, Braunwald E, Solomon SD. Right ventricular dysfunction and risk of heart failure and mortality after myocardial infarction. *J Am Coll Cardiol* 2002;39:1450-5.

Zur Y, Wood ML, Neuringer LJ. Spoiling of transverse magnetization in steady-state sequences. *Magn Reson Med* 1991;21:251-63.

Zurlo MG, De Stefano P, Borgna-Pignatti C, Di Palma A, Piga A, Melevendi C, Di Gregorio F, Burattini MG, Terzoli S. Survival and causes of death in thalassaemia major. *Lancet* 1989;2:27-30.